Oral Delivery of Therapeutic Peptides Using GCPQ Nanoparticles

Preethi Marimuthu

A thesis submitted in partial fulfillment of the requirements for the degree of Doctor of Philosophy

2016

Department of Pharmaceutics
UCL School of Pharmacy
29 – 39 Brunswick Square
London WC1N 1AX
United Kingdom

This thesis describes research conducted in the UCL School of Pharmacy, under the supervision of Professor Andreas Schatzlein. I certify that the research described is original and that I have written all the text herein and have clearly indicated by suitable citation any part of this dissertation that has already appeared in publication.

Preethi Marimuthu ....28.02.2017...

Signature Date

The research leading to these results has received funding from the European Union Seventh Framework Programme (FP7/2007-2013) under grant agreement n° 281035.

Abstract

Oral delivery of therapeutic peptides poses serious challenges in the field of drug delivery. The main concerns in developing an oral formulation of therapeutic peptide is that the peptide can be susceptible to enzymes in the gastrointestinal tract, poor solubility, short circulation time in plasma and fast renal clearance. This study focuses on improving the oral availability of therapeutic peptide by its encapsulation in a biodegradable polymer called GCPQ. GCPQ has been reported previously to solubilize small molecular weight hydrophobic drugs and peptides. GCPQ also demonstrated to improve their oral bioavailability.

In the present study, two therapeutic peptides, Methionine enkephalin (anti-cancer peptide) and Labyrinthopeptin (anti-noiciceptive peptide) was characterized and formulated with GCPQ nanoparticles. Labyrinthopeptin, a hydrophobic peptide having poor solubility was solubilized using GCPQ nanoparticles and their oral uptake was evaluated *in vivo.* Anti-noiciceptive activity of Laby GCPQ B2 formulation was evaluated in rat CFA model and compared against Laby glycofurol formulation. Therapeutic effect of Laby GCPQ B2 oral and nasal formulation was found to be significantly higher to control at time points 240 min and 40 min respectively as demonstrated in rat CFA model. Laby glycofurol formulation also showed significant therapeutic effect (40 and 60 min) after nasal administration as a result of permeation enhancing property of glycofurol itself. Concentrations of Laby in plasma were observed to be higher for Laby GCPQ B3 oral and nasal formulation compared to Laby glycofural formulation, suggesting that GCPQ improves oral uptake of Laby peptide. However, concentrations of Laby in plasma for Laby GCPQ B1 formulation were lower than that it was observed for Laby GCPQ B3 and Laby glycofural formulation, suggesting that the characteristics of GCPQ can be modified to control the uptake of Laby peptide.

Similarly, Methionine enkephalin, a peptide having poor stability in the gut was formulated with GCPQ B1 & B2 and characterized *in vitro* and *in vivo.* Their therapeutic effect was evaluated in nude mice tumor xenograft model. Significant reduction in tumor volume for mice treated with MENK-GCPQ B2 oral formulation was observed compared to MENK formulation and control. The concentration of MENK following oral administration of MENK GCPQ B2 formulation (100 mg/kg)

were variable and at nanogram levels. However, this concentration could be sufficient to cause therapeutic effect in mice xenograft model.

The concentrations of MENK in plasma were observed to be at nanogram levels (298 ng/mL), 180 min after administration of MENK-GCPQ B1 IV formulation. Following administration of MENK IV formulation, the concentrations of MENK in mice plasma were not detectable after 5 min. This result also suggests that only a fraction of MENK was encapsulated in MENK GCPQ B1 formulation. Although, there were significant differences in pharmacokinetic effect between MENK and MENK GCPQ B1 IV formulations, the therapeutic effect of MENK-GCPQ B1 IV formulation in tumor xenograft model was only significant to that of control but insignificant to that of MENK IV formulation. Excess MENK concentration resulting from MENK-GCPQ B1 IV formulation may not have improved the therapeutic effect due to saturation of OGFr receptor and clearance from the system. An alternative mode of MENK-GCPQ administration such as sub-cutaneous or intra-peritoneal could delay MENK release in the systemic circulation and thereby enhancing the therapeutic effect compared to MENK only formulation.

Acknowledgements

It is my pleasure to acknowledge my profound indebtedness to Prof. Andreas Schatzlein, for giving me the opportunity to work under his supervision. I wish to express my deep sense of gratitude for his encouragement and learned guidance. His amicable behaviour shall be cherished by me for long.

I am grateful to my co-supervisor, Prof. Ijeoma Uchegbu, for her constant indispensable guidance, support and trust during the course of the study.

I am also extremely grateful to EU-Transint and Overseas Research Studentship for their generous funding.

I would also like to thank the members of the Nanomedicine group at UCL School of Pharmacy, past and present especially, Funmi, Era for their friendship throughout the time spent with the group. A special thanks for Ramesh, Vicky, Lisa and Fionn, guiding me with the experiments.

And finally I would like to dedicate this work to my family for all their support they have given during the course of this thesis. Without them this work would not have materialized.

Table of Contents

List of Abbreviations

ABC	ATP-binding casette
ATP	Adenosine triphosphate
AUC	Area under the curve
$CaCl_2$	Calcium chloride
CAGR	Compound annual growth rate
CD	Cluster of differentiation
CDK-2	Cyclin-dependent protein kinases
CFA	Complete Freund's adjuvant
Cmax	Concentration maximum
CMC	Critical micellar concentration
CNS	Central nervous system
CV	Coefficient of variation
CW-NMR	Continuous wave – nuclear magnetic resonance
DC	Dendritic cells
DGC	Degraded glycol chitosan
DLS	Dynamic light scattering
DMSO	Dimethyl sulfoxide
dRI	Differential refractometer
EDTA	Ethylenediaminetetraacetic acid
EIA	Enzyme immunoassay
EMV	Electron multiplier voltage
EPR	Enhanced permeability and retention effect
eV	Electronvolt
FA	Formic acid
FaSSGF	Fasted-state simulated gastric fluid
FaSSIF	Fasted-state simulated intestinal fluid
FDA	Food and Drug Administration
FeSSIF	Fed-state simulated intestinal fluid
FID	Free induction decay
FITC	Fluorescein isothiocyanate
FT-NMR	Fourier-transform nuclear magnetic resonance
GALT	Gut-associated lymphoid tissue

GCPQ	Quaternary ammonium palmitoyl glycol chitosan
GHRH	Growth hormone-releasing hormone
GI	Gastrointestinal
GLP-1	Glucagon-like peptide-1
GPC	Gel permeation chromatography
h	Hour
HA	Hyaluronic acid
HBSS	Hank's Balanced Salt Solution
HCl	Hydrochloric acid
HPLC	High-performance liquid chromatography
HRP	Horseradish peroxidase
IASP	International Association for the Study of Pain
IFN	Interferon
IgG	Immunoglobulin G
IL	Interleukin
IS	Internal standard
ITC	Isothermal titration calorimetry
IV	Intravenous
KDa	Kilodalton
kg	Kilogram
L	Litre
LABY	Labyrinthopeptin
LCMS-QQQ	Triple quadrupole liquid chromatography mass spectrometry
LENK	Leu-enkephalin
LLOQ	Lower limit of quantification
LLOD	Lower limit of detection
LS	Light scattering
MALLS	Multi-angle laser light scattering
MENK	Met-enkephalin
mg	Milligram
MHz	Megahertz
min	Minute

mL	Millilitre
mM	Millimolar
MRP2	Multidrug resistance-associated protein 2
ms	Millisecond
mV	Millivolt
MWCO	Molecular weight cut-off
NaCl	Sodium chloride
NaOH	Sodium hydroxide
NCE	New chemical entity
ng	Nanogram
nm	Nanometer
NSAIDS	Nonsteroidal anti-inflammatory drug
ºC	Degree Celsius
OGFr	Opioid growth factor receptor
P-gp	P-glycoprotein
PBS	Phosphate-buffered saline
PDI	Polydispersity index
PEG	Polyethylene glycol
PLA	Poly-lactic acid
PLGA	Poly-lactic-co-glycolic acid
PNS	N-(Palmitoyloxy)succinimide
psi	Pound per square inch
QELS	Quasi-elastic light scattering
Rb	Retinoblastoma
RF	Radio frequency
RPM	Revolutions per minute
RSD	Relative standard deviation
SEDDS	Self-emulsifying drug delivery systems
SGF	Simulated gastric fluid
SIF	Simulated intestinal fluid
SLC	Solute carrier
SLN	Solid lipid nanoparticles
TEM	Transmission electron microscopy

TFA	Trifluoroacetic acid
Tg	Glass-transition temperature
Tmax	Temperature maximum
TMB	Tetramethylbenzidine
VFH	Von Frey hair
µg	Microgram
µL	Microlitre

List of Tables

List of Figures

1 Introduction

1.1 Therapeutic peptides - Growth, Scope and Market

Peptides are chains of amino acids ranging between 2 and 50 residues and linked by peptide bonds. Chemically, peptide can be placed between small molecules, for their size and proteins, for their composition. Peptides act as regulatory or signaling molecules with physiological roles in defense, stress, immunity, growth, homeostasis and reproduction. With the advent of the modern drug era came several therapeutic peptides such as; opioids, cyclic peptides, penicillin and insulin. However, due to lack of peptide screening and large-scale production technologies at the beginning of twentieth century, the scope for marketing of therapeutic peptides were limited. Moreover, peptides lack stability due to poor physiochemical properties resulting in poor pharmacological profile for clinical use. This has led the pharmaceutical industry to focus more on small molecules for their perceived advantages such as stability, superior pharmacodynamics profile, suitability for oral administration and overall low production cost. In the past decades, small molecules have suffered higher attrition rates due to several reasons, such as, inability to prove improved efficacy over existing drugs and side effects due to lack of specificity. The success rate of small molecules produced by conventional method has been less than 12 % and the average time scale required for a drug to enter market is between 8 and 15 years. Moreover, an average cost for new drug development is $ 2.6 billion [1]. In order to overcome the high cost associated with drug development, the pharmaceutical industry has shifted its paradigm to repurposed or orphan drugs. In the year 2015, FDA has approved 45 new medicines of which 47% are to treat rare diseases [2]. Human genome project has identified 30,000 genes of which only 10% are likely to be susceptible to small molecules [3]. With fewer drugs making into the market and patent expiry of successful drug, an alternative chemical entity such as peptide could be promising.

Peptide research and development have been gaining increased attention in the past decade for its potential ability to improve efficacy, safety and tolerability compared to small molecules. Peptides are typically highly selective and effective at low concentrations. The simple chemical composition allows researchers to predict the metabolism. Unlike antibodies, some peptides can penetrate the cell membrane, which opens window for identifying novel target and drug development. With the

advent of molecular biology and improvements in synthetic chemistry, overall production costs are cheaper, compared to proteins. The success rate of peptides entering clinical trials between 1984 and 2000 were reported to be 23 to 26% [4]. The average time scale required for clinical development and US approval of peptides during the year 2012 was 9 and 2.1 years with medium phase length of 7.8 and 0.9 years respectively [5]. There are 60 peptide drugs in the market, 140 in clinical development and around 500 at the preclinical development stage. Lupron™, anti-cancer peptide marketed by Abbott technologies, reached a global sale of US $ 2.3 billion dollars in 2011. Similarly, Lantus™, insulin glargin marketed by Sanofi, reached a global sale of US $ 7.9 billion in 2013 [5]. The projected sale for peptide drug is expected to increase from US $ 14 billion in the year 2011 to US $ 25 billion in the year 2018. Peptides currently in development have various therapeutic applications (Figure 1-1) in metabolic disorders, cancer and as orphan drugs for rare diseases, inflammation and infectious diseases [6].

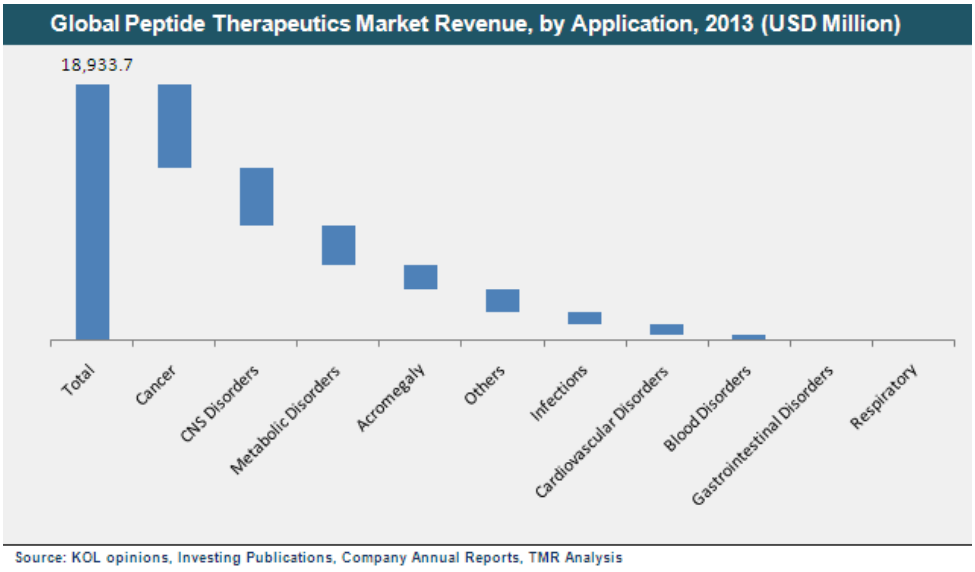

Figure 1-1 Therapeutic peptide market revenue by application [7]

Most therapeutic peptides (> 75%) are administered via the parenteral route. According to transparency market research analysis, the projected market share (2018) for injectable peptides was the largest. However, compound annual growth rate % (CAGR) of peptides administered by non-invasive routes exceeds that of the injectable peptide formulations [7]. An invasive method of drug administration is inconvenient to the patient, particularly for chronic conditions, and requires stringent manufacturing procedures in order to maintain sterile conditions. Non-invasive route of peptide administration can circumvent the aforementioned constraints. Although

oral route is the most favored, the oral delivery of peptides are hampered due to poor physiochemical properties and the physiological barriers that limit peptide absorption from the gastrointestinal tract. In this review, a brief description of nature of peptides and its physiochemical properties, physiological factor affecting oral peptide delivery and current strategies to overcome biological barrier will be discussed.

1.2 Anatomy and physiology of the Gastrointestinal tract

The gastrointestinal tract comprises of oral mucosa, the stomach, the small intestine and the large intestine.

1.2.1 Oral mucosa

The oral cavity is lined by oral mucosa, which has keratinized, or non-keratinized squamous epithelium, lamina propia or connective tissue beneath the oral epithelium, sub mucosa and bone. The function of oral mucosa is to secrete saliva, thermal regulation, protection against microbes and sensation. The oral cavity is exposed to mucus and saliva that has enzymes like esterases, oxidases and reductase from buccal epithelium and phosphatases and carbohydrases in saliva [8]. The oral cavity has relatively smaller surface area (214 cm^2) [9] compared to small intestine. The drug absorption that occurs through mucosa reaches the systemic circulation bypassing first pass metabolism. Drug absorbed through oral cavity also avoids gastrointestinal content. However, the efficacy of drug absorption is altered by constant movement of drug facilitated by saliva and mucus, which leads to swallowing [10].

1.2.2 Gastrointestinal mucosa

The mucosal lining of the gastrointestinal tract facilitates absorption of nutrients and water as well as act as a protective barrier from external environment. The upper gastrointestinal tract consists of mouth, oesophagus and stomach. The food in the mouth is chewed to form bolus that is carried via the oesophagus to the stomach.

1.2.2.1 The Stomach

In the stomach, the bolus is partially digested by acid and enzymes secreted by the gastric mucosa. The stomach is divided in to the fundus, the body and the pyrolic region [11]. The stomach wall has series of ridges called rugae, which expands when the food is consumed and allows mechanical degradation of food.

The gastric mucosa has indentation that leads to tubular shaped gastric glands. The gastric glands are composed of parietal cells that secrete HCl in to the stomach; chief cells that release zymogen, a precursor to pepsin, foveolar cells that produce mucus, G cells that secretes gastrin which in turn stimulate the release of histamine and enterochromaffin-like cells that produces histamine in the presence of excess acid [11, 12]. The histamine promotes the production and release of bicarbonate ions from the parietal cells. The mucus protects the gastric mucosa from acid by trapping the bicarbonate ions secreted by the parietal cells to neutralize any back diffusion of hydrogen ions from the lumen [13]. The volume of the stomach typically ranges from 200-300 mL in fasted state to 1400 mL after a meal. Hormones such as GLP-1 regulate the gastric emptying [14].

1.2.2.2 The Small Intestine

The partially digested semi fluid food in the stomach called chyme empties in to the small intestine. Small intestine is the major site of food and drug absorption and is divided in to duodenum, jejunum and ileum [15]. It constitutes 81% of the total surface area of the GI tract [16]. The small intestine has circular folds of mucosa or *plicae circularis* (Figure 1-2) that increases the surface area three fold. The *plicae circularis* further has finger like villi increasing the surface area 30 fold (Figure 1-3). The villi, in turn, are covered by microvilli, which increase the surface area a further 600 fold. The intestinal wall has single layer of specialized epithelial cells and has mucus producing goblet cells and follicle-associated epithelium interspersed between epithelial cells [16]. In addition to gut lining, the digestive juice aids in digestion of food. Bile juice that contains bile acids and derivatives solubilizes lipids in the food by forming micelles. The micelles have larger surface area and absorbed by brush border membrane of jejunum. From the ileum 95% of the bile acids are reabsorbed and recycled in the liver. 2-5% of bile acids are further reabsorbed in large intestine after metabolic transformation by intestinal bacteria [17]. Pancreas secretes pancreatic juice, which neutralizes the acidic chyme by producing bicarbonates. In addition, the pancreatic juices also contain various enzymes such as lipases and proteases that aids in break down of lipids and proteins. Once the food constituents are broke down by digestive juices they are then absorbed by active or passive mechanism through the enterocytes [16].

In addition to digestive and absorption function, intestine is also functionalized to offer protection against harmful pathogens. The immune system associated with intestinal mucosa is called gut-associated lymphoid tissue (GALT). GALT are composed of Peyer's patch in the ileum and intraepithelial lymphocytes basolateral spaces between luminal epithelial cells and lamina propia lymphocytes in lamina propia of mucosa [15]. Peyer's patch are involved in immune surveillance of the contents in intestinal lumen and facilitates immune response. M-cells covers Peyer's patch that are know uptake antigen by endocytosis and elicit immune response by activating T-cells [15, 16].

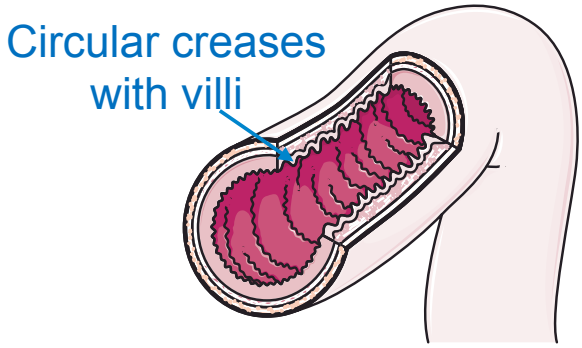

Figure 1-2 Vertical section of small intestine- plicae cirvularis [18]

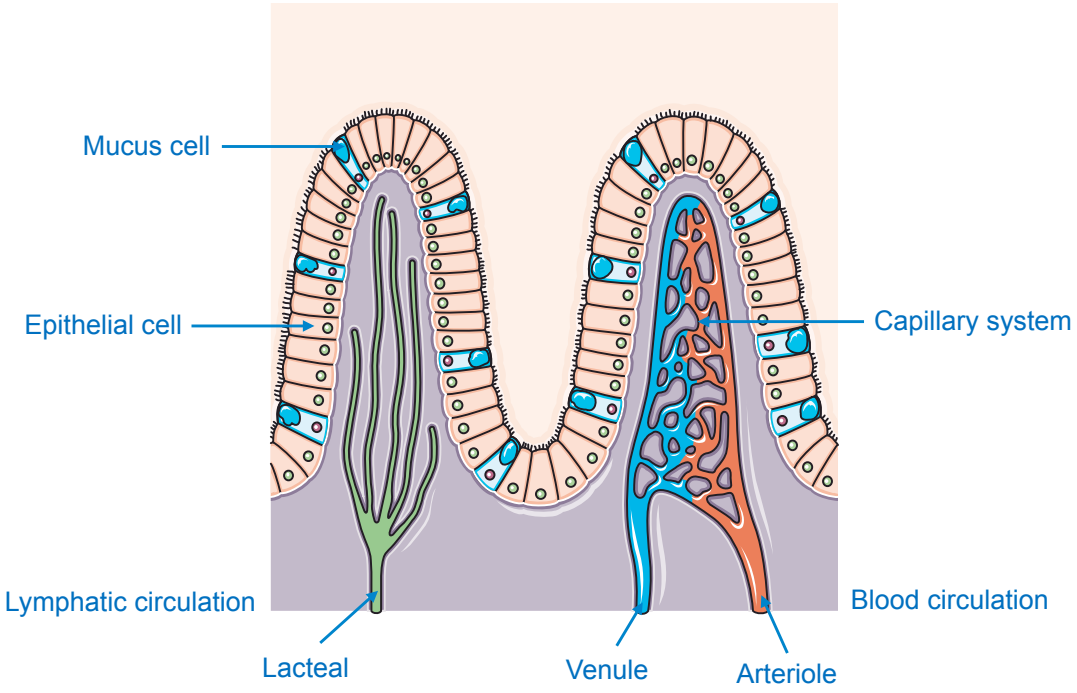

Figure 1-3 Villi in small intestine [18]

1.2.2.3 The large Intestine

The large intestine extends from ileocaecal junction to the anus. The large intestine consists of caecum, colon (ascending, transverse, descending and sigmoid), rectum and anus. The main function of large intestine is absorption of water, electrolytes, secretion of mucus, formation of faeces and defecation [16]. Large intestine also has bacterial flora at an estimated population of 10^{10}-10^{12} cfu/g that break down complex material as well as produce nutrients that are absorbed in the colon [19]. Compared to small intestine, large intestine lacks villi resulting in reduced surface area for nutrient or drug absorption. Also drug absorbed via large intestine avoid first pass effect of liver. The mucosa also lacks most endogenous enzymes and P-gp that can reduce the bioavailability of certain drugs [8].

1.3 Factors affecting the oral delivery of peptides

Several factors limit the oral bioavailability of peptides. Peptides in the gastrointestinal tract are affected by their solubility in the GI medium, their susceptibility to enzymes, and their uptake across the enterocytes. The barriers that limit the oral uptake of peptides in the gut are discussed in the following sub sections.

1.3.1 Peptide solubility

To achieve systemic delivery via the oral route of administration, an ideal therapeutic drug has to be soluble in the gastrointestinal tract as well as permeable through the gut in order to reach the site of action. The pH varies along the length of the gastro-intestinal tract, with acidic in the stomach, neutral in the duodenum, alkaline in the distal portion of the small intestine and again acidic in the large intestine due to the presence of bacteria. The pH at the absorption site and the extent of ionization has an effect on solubility and permeability of peptide of interest.

The physiochemical properties of the peptide, such as the pKa, isoelectric point, log P and water solubility determine the bioavailability and efficacy of therapeutic peptides. Dissolution is a stepwise process where a solid drug first dissociates from the bulk form and accommodates within the water molecules. The rate of dissolution (dw/dt) is represented using Noyes-whitney equation that depends on saturation solubility of drug in dissolution layer (C_s), diffusion coefficient of the dissolved solute (D), thickness of dissolution layer (H) and surface area of the solid (A) [20].

$dw/dt = D*A*C_s/H$

In a solvent system containing two immiscible solvents, a drug in solution partitions into different phases based on their affinity for each phase. This is represented as partition coefficient P, where hydrophobicity of a molecule is determined by the ratio of concentration of drug in the hydrophobic phase to the concentration of drug in the aqueous phase. The log P provides some estimate of the bioavailability of a drug molecule. The higher the log P value the more lipophilic is the drug molecule and vice versa [21]. For a drug to be orally bioavailable, a drug molecule has to be hydrophilic to be solubilized in the gut as well as possess lipophilicity for cellular uptake [22].

1.3.2 Enzymes in the Oral and Gastro-intestinal tract

The therapeutic peptide first encounters the enzymes in the oral cavity. The major enzymes present in the mouth are amylases and lipases that degrade starch [23]. Thus, therapeutic proteins or peptides are not degraded in the oral cavity. Following that is the gastric medium, which contains pepsin; an enzyme that breaks down polypeptides to peptides, cleaving bond at phenylalanine, methionine, leucine, tryptophan and other hydrophobic residues to give short chains of amino acids [24]. The therapeutic peptide further follows through the small intestine where it encounters pancreatic enzyme. Pancreas secretes enzymes (Table 1-1) as non-active precursor molecules (zymogens) that are only activated when they come into contact with the intestinal wall. Enzymes in the brush border membrane (Table 1-2) such as; enteropeptidases are released into the lumen that convert the precursor trypsinogen to active trypsin, which in turn activates other pancreatic enzymes like chymotrypsin, elastase carboxypeptidase A & B. Here, large proteins and peptides are completely degraded to small fragments (tripeptides and dipeptides) [25] [26]. However, some small peptides can resist the action of pancreatic enzymes; in particular cyclic hepta-, octa- and decapeptides of *Amanita* mushrooms [27], synthetic hexa- and octapeptide analogue of somatostatin [28], vasopressin [29] or cyclosporine A [30].

At the mucosa, brush border enzymes like endo and exopeptidases are produced which further degrades the di, -tri- and tetra peptide into individual amino acids. Any peptide that escapes the pancreatic and brush border peptidase is likely to be digested by lysosomal enzyme after uptake into enterocytes. The degraded peptides, when being internalized into the epithelial cells, pass through endocytotic

pathway, fuse with the lysosomes and undergo intracellular hydrolysis. Furthermore, when the epithelial cells slough off, lysosomal enzymes are released in to the lumen and may digest the therapeutic proteins. However, lysosomal enzymes are less active in the intestinal lumen as their optimum activity is only between pH 5-5.5 [31].

Table 1-1 Pancreatic enzymes and their site of action [31]

Enzyme	Bond Hydrolysed
Trypsin	-❍-◉⬇❍-❍- Arginine, lysine
Chymotrypsin	-❍-◉⬇❍-❍- Phenylalanine, tyrosine (leucine, methionine, aspartic acid, glutamine, tryptophan)
Elastase	-❍-◉⬇❍-❍- Alanine, glycine, leucine, valine, isoleucine
Carboxypeptidase A	❍-❍-❍-❍⬇◉ Phenylalanine, tyrosine, isoleucine (threonine, glutamic acid, histidine, alanine)
Carboxypeptidase A	❍-❍-❍-❍⬇◉ Lysine, arginine, hydroxylysine, ornithine

Table 1-2 Brush border enzymes and their site of action [31]

Brush Border Enzymes	Bond hydrolysed
Endopeptidases	
Endopeptidase 24.11	-❍-❍-❍⬇◉-❍-❍- hydrophobic amino acids
Endopeptidase 24.18	-❍-❍-❍⬇◉⬇-❍-❍- Aromatic amino acids
Exopeptidases: Amino terminus	
Aminopeptidase N	◉⬇❍-❍-❍-❍- Many different amino acids
Aminopeptidase A	◉⬇❍-❍-❍-❍- aspartic acid, glutamic acid
Aminopeptidase P	◉⬇❍-❍-❍-❍- Proline
Aminopeptidase W	◉⬇❍-❍-❍-❍- Tryptophan,tyrosine, phenylalanine
γ-Glutamyl transpeptidase	◉⬇❍-❍-❍-❍- γ-Glutamic acid
Dipeptidyl peptidase	❍-◉⬇❍-❍-❍-❍- Proline, alanine
Exopeptidases: carboxy terminus	
Carboxypeptidase P	-❍-❍-❍-❍⬇◉ Proline, glycine, alanine
Carboxypeptidase M	-❍-❍-❍-❍⬇◉ Lysine, arginine
Peptidyl dipeptidase A	-❍-❍-❍-❍⬇◉-⚬ histidine-leucine
γ-Glutamyl carboxypeptidase	-❍-❍-❍-❍⬇◉ $(\gamma\text{-Glutamic acid})_n$

1.3.3 Mucosal Barrier

Mucus lines the small intestine and act as a physical barrier to drug absorption. Mucus enables exchange of nutrients, water, gases, odorants and hormones while being impermeant to bacteria and many pathogens. The mucus is a complex hydrogel composed of proteins, carbohydrates, lipids, salts, antibodies, bacteria and cellular debris [32]. The thickness of the barrier varies along the length of the GI tract with the least thickness observed in the jejunum and greatest in the colon (Figure 1-5).

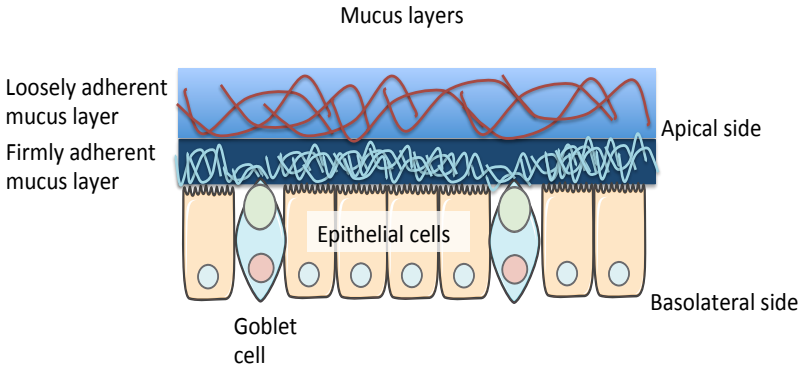

Figure 1-4 Mucus layers showing loosely and firmly adherent mucus layer on epithelial cells

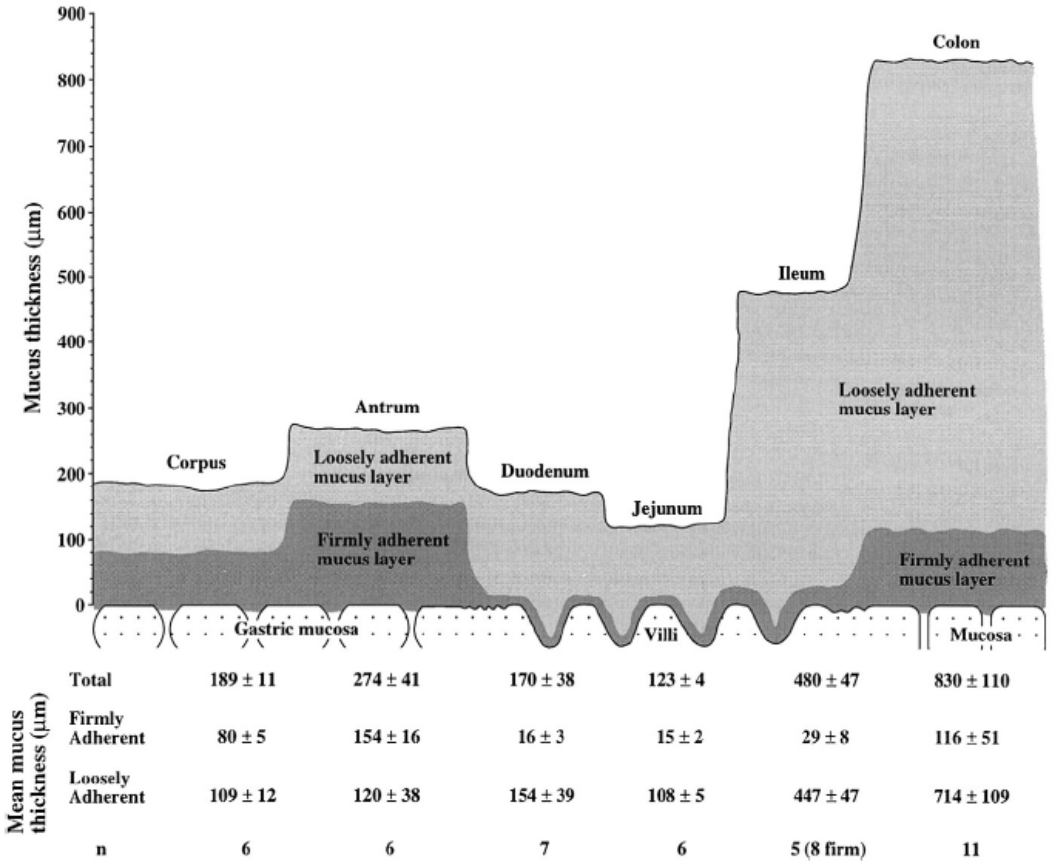

Mean mucus thickness (μm)

Total	189 ± 11	274 ± 41	170 ± 38	123 ± 4	480 ± 47	830 ± 110
Firmly Adherent	80 ± 5	154 ± 16	16 ± 3	15 ± 2	29 ± 8	116 ± 51
Loosely Adherent	109 ± 12	120 ± 38	154 ± 39	108 ± 5	447 ± 47	714 ± 109
n	6	6	7	6	5 (8 firm)	11

Figure 1-5 Thickness of the rat mucus along the Gastro-intestinal tract [33]

The mucus barrier consists of two layers: an outer sloppy layer that slips away with the movement of the chyme and an inner unstirred adherent layer that is entangled firmly with the enterocytes (Figure 1-4). The outer layer is constantly renewed. The quicker the peptide reaches the unstirred adherent layer the less it is removed from the GI tract together with the loose mucus [34] [35]. It must be noted that the jejunum has the thinnest layer of loosely adherent mucus, followed by the corpus, antrum, duodenum, ileum and colon (Figure 1-5). The main component of mucus is mucin, which is composed of a protein backbone linked to

oligosaccharides. The mucin monomers entangle and cross-link adhesively and reversibly forming a viscoelastic gel. Mucus gel entanglement creates a sieve (400 nm) that limits the penetration of large particles [32]. Viscoelastic properties of the mucus are important for its protective and lubricating properties. The viscoelasticity of mucus is regulated by water, lipid and ion content. The mucus viscoelasticity is regulated for exclusion of particulates and molecules in gastrointestinal tract, lungs and vagina. In the lungs, the mucus loosens its viscoelasticity to enable its movement towards trachea. In the vagina, the mucus viscoelasticity is regulated between ovulation and non-ovulation phase. Thickness of the mucus during non-ovulation phase is higher creating a barrier for the penetration of sperms and vice versa. [36].

More than 20% of the mucus is composed of lipids that can cause hydrophobic interaction with foreign particles and pathogens [37]. The glycosylated portion of mucin is also capable of forming non-specific hydrogen bonding and electrostatic interaction [38].

Peptides that have poor mucosal permeability and cellular uptake are likely to be affected by intestinal transit time. The oral absorption of a drug across the GI tract is determined by its residence time in the gut and its absorption in each GIT segment. Gastric retention time (Table 1-3) is only 1.5 h after which the drug traverses the stomach. The human small intestine has a faster velocity between its proximal and distal end with an intestinal transit time around ∾ 3-4h. The intestinal transit time is relatively independent of feeding conditions and the physical composition of intestinal component [39].

Table 1-3 Surface area and physical characteristics of different segments of Gastro-Intestinal tract in humans [31]

Segment	Surface	Segment	Residence time	pH of the segment	Catabolic activity
Oral cavity	100cm^2	-	Seconds to minutes	6.5	Polysaccharides
Esophagus	200cm^2	23-25cm	Seconds		
Stomach	3.5m^2	0.25cm	1.5 h	1-2	Proteases, lipases
Duodenum	1.9m^2	0.35m	0.5-0.75 h	4-5.5	Polysaccharides, oligosaccharides, proteases, peptidases, lipases and nucleases
Jejunum	184m^2	2.8m	1.5-2 h	5.5-7	Oligosaccharides, peptidases and lipases
Illeum	276m^2	4.2m	5-7 h	7.0-7.5	Oligosaccharides, peptidases, lipases, nucleases and nucleotidases
Colon and rectum	1.3m^2	1.5m	1-60 h (35 h average)	7.0 -7.5	Bacterial enzymes

1.3.4 Peptide uptake across the enterocytes

1.3.4.1 Passive transport

Once the peptide crosses the mucosal barrier, absorption can take place by two ways i.e. passive diffusion or trans cellular pathway (Figure 1-6). In passive absorption, molecules diffuse along their concentration gradients from apical (lumen) to basolateral membrane (blood). It is an energy-independent process, and physiochemical and diffusive properties such as electrostatic charge, ionization, dissociation constant, hydrophilic-lipophillic balance and hydrodynamic size play a significant role in passive absorption. Passive diffusion of drug molecules can be paracellular (between the cells) or transcellular (through the cell membrane). In the paracellular pathway, only hydrophilic molecules smaller than 250Da can diffuse through the intercellular spaces. Tight junctions obstruct the transport of large peptides by regulating the intercellular spaces. The paracellular route of drug absorption accounts for less than 0.01% of total surface area of intestinal membrane [40] [41].

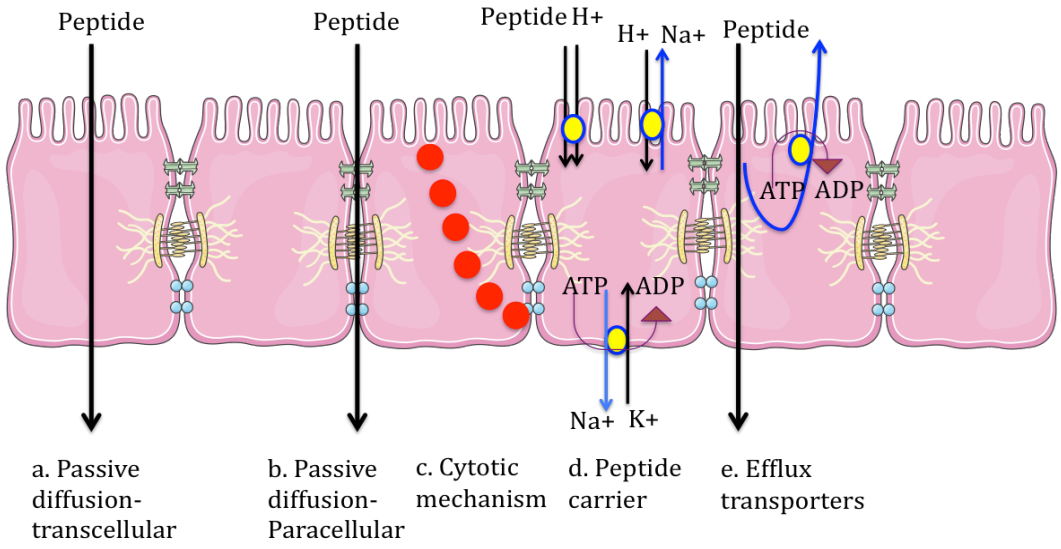

Figure 1-6 Mechanism of intestinal peptide absorption (a) Passive diffusion through enterocytes; (b) Passive diffusion via paracellular pathway; (c) Cytotic mechanism; (d) Peptide transporters; (e) Efflux transporters

The transcellular pathway (Figure 1-6) is the major route of absorption for most drug molecules. Physiochemical properties such as size (>300Da), lipophilicity and hydrogen bonding capacity determine the rate of transport across the apical cell membrane. Peptides form hydrogen bonds with water molecules, and for transcellular absorption; peptides must desolvate to interact with cell membrane. For an optimum transcellular uptake, the energy required to break peptide-water bond should be minimal and therefore degree of hydrogen bonding is inversely proportional to transcellular absorption. Due to low lipid solubility and large size, only break down products of proteins and peptides such as tripeptides, dipeptides and amino acids are absorbed through this mechanism [42] [43].

1.3.4.2 Active transport

Active absorption is an energy-dependent and ion gradient driven process that utilizes carriers such as transporters to cross the cellular barrier. Physiochemical properties of proteins/peptides are determinants of active absorption. The enterocytes express transporters on the apical and basolateral membranes for the influx and efflux of endogenous substances and xenobiotics. These transporters broadly belong to adenosine triphosphate (ATP) binding cassette (ABC) superfamily (those transporters that utilizes ATP for transport) and solute carrier (SLC) super families (transporters that utilizes ion gradient). PepT1 transporters are H+ dependent di-peptide

transporters predominantly localized in duodenum. It uses H+ gradient and inside negative membrane potential as a driving force for substrate translocation [44] [45].

1.3.4.3 Transporters that reduces peptide transport – Efflux transporters

Efflux transporters belong to the family of ABC transporters, which efflux not only endogenous substrates and toxic components, but also therapeutic peptides out of the cell against the concentration gradient. The major groups of efflux transporters in the intestinal epithelium are P-glycoprotein (P-gp) [46], Multidrug resistance-associated protein 2 (MRP2) [47] and breast cancer resistance protein (BCRP) [48]. P-gp and MRP2 are located in the apical membrane of enterocytes [49]. Peptides such as Metkephamid and D-Ala-leucine enkephalin are substrates for the above mentioned efflux pumps [50]. Different strategies are employed to prevent efflux action such as, efflux inhibitors, pro-drug modifications, antisense targeting and avoiding exposure to intestinal efflux pumps. Efflux inhibitors modulate the efflux pump by one of the three mechanisms,

a. By blocking the drug binding site allosterically or competitively
b. By interfering with ATP hydrolysis
c. By altering the integrity of cell membrane lipids.

1.3.5 Bile

Bile, stored in the gall bladder is released in to the intestine at a rate of 2-22 mL/kg/day. Bile causes emulsification of fat and increases its absorption through the intestine. The bile salts can also form ionic interaction with the peptide and re-circulate between the intestine and hepatocytes enhancing oral absorption [51]. Insulin encapsulated in liposomes was observed to be susceptible to bile salts. However, surface coating of liposomes were observed to be stable against bile salts and improved the oral bioavailability of insulin [52]. Radiolabeled GCPQ polymeric nanoparticles were reported to recirculate between gall bladder and small intestine via bile and with which, it was hypothesized to show improved absorption [53].

1.3.6 Lymphatic circulation

Nutrients absorbed through the villi of intestinal mucosa pass through to either blood capillaries or the lymphatic circulation. Peptides that are carried through capillary network are subjective to degradation by hepatic first pass metabolism. This could be circumvented if the peptide drugs are carried via lymphatic circulation.

Although it has been reported in the past that peptides can be carried through to the lymphatic circulation via Peyer's patches in the ileum, approaches to target lymphatic circulation has not yet been successfully exploited [51].

1.4 Strategies to improve oral bioavailability of peptides

The strategies to improve oral bioavailability of peptides can be broadly classified in to three types, such as; structural modification of therapeutic peptides, addition of auxiliary agents and drug carrier system.

1.4.1 Structural modification of therapeutic peptides

By natural selection, peptides of biological origin are prone to enzymes in the digestive system. Inherently, these biological entities exist as propeptides, an inactive protein that undergo post-translational modification to become functionally active. Propeptides have a specific role in signaling, by providing steric hindrance that provides protection against enzymes and in facilitating transport across all membranes. This property has been exploited to modify therapeutic peptides, and thus to protect them from enzymatic hydrolysis and to increase their cellular uptake.

The Peptide structure can be modified to protect them from proteolytic enzymes in number of ways. This includes replacement of susceptible amino acids, protecting the N or C terminal by attaching a functional group, cyclization of linear peptide and conjugation to macromolecules such as PEG (Polyethylene glycol) or albumin. Examples in (Table 1-4) provide a detailed summary of different types of approaches used to improve the oral bioavailability of therapeutic peptides. However there is a key limitation in using this strategy, as the modification should not affect the activity of a peptide. From regulatory point of view, synthetic peptides are classified as new chemical entity (NCE), which require more trials to achieve stringent regulatory approval.

Table 1-4 Strategies to reduce enzyme degradation in biological fluids

Mechanism	Protection against	Examples	Therapeutic benefit
Structural Modification of peptide			
N-acetylation	Weakly inhibiting trypsin	Salmon calcitonin [54]	Improved oral bioavailability
Attachment of moiety	exopeptidases	Tesamorelin contains a hexenoyl group attached to N-terminal tyrosine amino acid of growth hormone releasing hormone (GHRH) [55]	Tesamorelin is resistant to the action of dipeptidyl aminopeptidase IV. Improves half-life of GHRH from 6.8 min to 1 h
Replacement of L-amino acids with D-amino acids	Trypsin	Desmopression has L-Arg replaced by D-Arg, an analogue of vasopressin	Improves half-life from 10 – 35 min [56] to 3.7 h .
	Endopeptidases	Octreotide an analogue of somatostatin [57]	Improves half-life from few min to 1.5 h
Replacement of susceptible amino acids	Serum enzymes	Ipamorelin, a growth hormone secretagogue in which alanine is replaced with 2-aminoisobutyric acid	Improves terminal half-life around 2 h [58] , [59]
Cyclization by lactamization/ lactonization/ sulphide bridges	Serum enzymes	ALRN-5281, GHRH peptide for treating orphan endocrine disorder [60]	97% of the ALRN-5281 peptide remain pharmacologically active after 24 h of incubation in rat plasma compared to sermorelin, a GHRH analogue which completely degrades in 13 h [61].
Conjugation of macromolecules (PEG, albumin)	Dipeptidyl peptidase and neutral endopeptidase	Liraglutide analog of GLP-1 can bind to albumin	Increased serum half life from few min to 8 h [62] Also reduce renal clearance.

1.4.2 Addition of pH modulators

Co-administration of pH modulators is one of the methods to enhance oral peptide delivery. Auxillary agents are small molecules that either bind with the proteolytic enzymes (protease inhibitors) or interact with the cell structure to facilitate cellular uptake (permeation enhancer). Most of the carriers currently in clinical development are based on protease inhibitors and permeation enhancers. However, it should be noted that peptides are susceptible to different classes of enzymes and may require more than one protease inhibitors. Also, some of the permeation enhancers and protease inhibitors are surfactants, which when used at higher concentrations can be toxic. However, reducing the concentrations to non-

toxic levels may not provide sufficient therapeutic benefit. The Table 1-5 describes the list of protease inhibitors and permeation enhancers in preclinical development.

Table 1-5 Strategies to enhance oral delivery of peptide by co-administration of auxiliary agents

Addition of Auxiliary agents			
Function	**Target molecule**	**Example**	**Benefit**
As protease inhibitors	Chymotrypsin	Soybean trypsin inhibitor	Enhanced oral bioavailability of insulin [63]
	Trypsin, chymotrypsin and plasmin	Aprotonin	Insulin - Better pharmacokinetic results [64]
	serine and metallopeptidases	Puromycin	Better stability of leucine enkephalin [65]
	Trypsin, pepsin and aminopeptidase N	Bacitracin	Insulin, met-kephamid and buserelin [66] [67] [68]
As permeation enhancers	Tight junction	Fatty acids- Sodium caprate [69]	D-decapeptide and sodium caprate were directly delivered (non invasively) to rat lumen of the terminal rectum. Bioavailability of D-decapeptide improved from 2 to 11% in rat model.
	Uptake via trans-cellular route	Surfactants -DS1, a modified *Quillaja* saponin [70]	Increases uptake of D-decapeptide (model peptide) in a dose dependant manner (*in vitro* Caco-2 model)
	Interacts with membrane lipids and proteins	C_8/C_{10} Mono-/di glycerides [71] Progesterone [72]	Co-administration of C_8/C_{10} Mono-/di glycerides enhanced absorption of calcein (fluorescent complex) following intradudonal administration in rat model
	Opens tight junctions	Zonula occludens toxin-Insulin [73]	10 fold increase in insulin absorption in rabbit
	Transcytosis	Insulin-TAT conjugate [74]	5-8 times better permeation than native insulin

1.4.3 Drug carrier system

Nanomaterials have gained attention over the past 40 years in the pharmaceutical field for their remarkable potential to improve the poor characteristics of therapeutic drugs, thereby helping to meet clinical needs. These materials, apart from their size, have unique characteristics, such as their shape and surface-to-volume ratio, which give them unique electrical, optical, thermodynamic, mechanical and chemical properties. The nanomaterials, due to their larger surface area facilitate higher concentrations of therapeutic drug to be entrapped, adsorbed or covalently attached [75]. The high loading efficiency of nanoparticles and their improved solubility allow drug-nanoparticle systems to be pharmacologically active

at their very low concentrations. Their smaller sizes enable drug accessibility to cancer cells, inflamed tissue etc. through enhanced permeation and retention effect (EPR) [76]. Nanoparticles are formed by top-down approach where larger particles are broken down to nano-sized particles or bottom-up approach where small molecules undergo controlled assembly to form nanoparticles [77]. An ideal drug delivery nanoparticulate system should be biocompatible and safe, improve the solubility of a drug, should protect the drug from proteolysis in the gut, liver and serum, improve the drug circulation time in plasma and prevent drug loss due to renal clearance.

The nanomaterials used in the pharmaceutical field can be broadly classified as self assembled polymers, polymer drug conjugates, polymeric nanoparticles, carbon nanotubes, porous silicon nanoparticles, drug nanocrystals, nanoemulsions, liposomes, niosomes, low molecular weight micelles, solid lipid nanoparticles and polymersomes. Few examples of therapeutic peptide for enhancing oral bioavailability of therapeutic peptides are mentioned in Table 1-6.

Polymeric nanoparticles are versatile structure that can be functionalized to enhance the bioavailability of the peptide. Natural and synthetic polymers such as; chitosan, dextran, PLA, PLGA were reported to have been modified with conjugates that increase the stability of peptide in gastric fluid [78] [79], increased permeation by para cellular uptake [80] [81] and trans cellular uptake [82].

Polymers such as; chitosan [83], thiolated polymers [84], lectins [85], hydrogels [86], poly acrylic acid derivatives [87] are reported to have mucoadhesive properties. The advantage of using polymeric nanoparticles for encapsulating small molecular drugs, proteins and peptides is that their surface characteristics can be optimized to enhance mucoadhesion and mucopenetration. An ideal polymer should be able to rapidly adhere and interact with mucin epithelial tissue. The polymer's physical properties, such as wettability, swelling and spread ability, along with its chemical characteristics, such as polymer chain interpenetration, electrostatic, hydrophobic and van der waals interactions, are important determinants of mucoadhesion [88]. Mucoadhesive properties of nanoparticles increase their residence time in the gut and ideally should be optimal enough to allow the nanoparticles to traverse the mucosal barrier without being trapped in the mucus. Other than polymers, mucoadhesive patch system (GI-MAPS) has also been designed for enhancing oral bioavailability. The patch system consists of drug and

additives sandwiched between an enteric pH sensitive top layer and insoluble ethyl cellulose bottom layer. In GI tract, the top layer dissolves leaving the drug layer to tightly adhere to mucus wall. The concentration gradient between the patch and the enterocytes enhances drug uptake [89].

Liposomes are vesicular structure that can accommodate drugs within the phospholipid bilayer and enhance bioavailability of therapeutic peptide. Liposomes are transported via peyer's patch [90]. However, liposomes are characterized by poor stability in the gastrointestinal tract an as effect of bile salts, pancreatic lipase and gastric pH. Other report suggests that surface coating of liposome can improve its stability in the GI tract [52].

Hydrogels are hydrophilic polymeric network known to stabilize peptide in gastric medium. Hydrogels swell and accommodate water depending on the pH and ionic strength of the medium. In gastric medium the network for hydrogen bonding and protect the peptide whereas in intestinal medium the beads swell due to ionic repulsion and release the peptide in the intestine [91].

Solid lipid nanoparticles are formulation that can accommodate drug in solid lipid core matrix stabilized by emulsifiers. SLNs have better stability in the gastrointestinal tract and cross the epithelium by endocytosis. However, their ability to cross mucus still remains a challenge due to electrostatic repulsion between carrier and mucin. It was previously reported that CSK peptide ligand has affinity for goblet cells [92] [93]. Fan et al reported an increase in the oral bioavailability of calcitonin when SLNs are conjugated with peptide ligand CSK [94].

Self-emulsifying drug delivery system (SEDDS) is composed of oil, non-ionic surfactants and co-surfactant coated with hard or soft gel capsules. This system is known to solubilize hydrophobic drug until absorption. The SEDDS formulation spontaneously forms emulsion in the gastrointestinal tract due to gastric mobility and agitation in the intestine. Moreover, the system also promotes absorption across intestinal epithelium [95]. Sandimmune™, an oral cyclosporine SEDDS formulation shown to improve bioavailability of the respective peptide. However, absorption is drastic leading to liver and kidney toxicity. Neoral™, a modified SEDDS formulation shows better oral bioavailability than sandimmune™. The toxicity of Sandimmune™ is explained by the formation of polydisperse macroemulsion in aqueous solution leading to irregular absorption. However, Neoral™ when dispersed in an aqueous solution spontaneously forms microemulsion of particle size less than

100 nm. The small and monodisperse size of the neoral formulation results in consistent absorption of cyclosporine leading to greater systemic exposure [96].

Table 1-6 Drug carrier system for enhancing oral delivery of therapeutic peptides

Drug carrier system for enhancing oral delivery of peptide					
Strategies	**Carrier**	**Example**	**Contributing factors for improved therapeutic benefit**		
			Proteolytic stability	**Mucoadhesive**	**Permeation enhancer**
Polymeric Nanoparticles	PLGA-polyanhydride nanoparticles	Zinc insulin [97]	-	mucoadhesive	Can cross intestinal epithelium within 1 to 6 h of oral administration [98]
	PLGA/RS-HP55 (hydroxypropyl methylcellulose phthalate) [99]	Insulin	Delayed release in SGF due to HP-55 coating	mucoadhesive	Eudragit RS Opens tight junction
	Quaternary ammonium palmitoyl glycol chitosan (GCPQ) nanoparticles	Leucine enkephalin	Stable in SGF and SIF	mucoadhesive	transcellular uptake
	Dextran- Vitamin B12 nanoparticles	Insulin	Stable in SIF [100]	-	Complexation with intrinsic factor and uptake via intrinsic factor receptor
	PLA-PEG-IgG Fc nanoparticles [101]	Insulin	Stable in SGF [102]	mucoadhesive	Receptor mediated uptake via Fc receptor
Hydrogels	Poly[methacrylic acid-grafted-poly(ethylene glycol)]	Insulin	Against trypsin and ∝ chymotrypsin [103]	Mucoadhesive [104]	Permeability increased from 0.77 to 1.16 × 10^{-8} cm/s [105]
Lipid based drug delivery system	PEGlyated Liposome	Insulin	Stable against trypsin and ∝ chymotrypsin in GI tract [52]	Mucoadhesive - [106]	No permeability – modest hypoglycemic activity [52]
	Liposomes coated with Chitosan aprotonin conjugate [107]	Calcitonin	Stable against trypsin	Mucoadhesive	-

	Dry powder of Proliposomes made with egg lecithin, lactose and chremophor EL [108]	Cyclosporine	-	-	Improved absorption
Solid lipid nanoparticles	Stearic acid and tripalmitin [109]	Calcitonin (13% bioavailability)	Stable in GI tract	-	Clathrin and caveolae dependant endocytosis
	Cetyl palmitate and poloxamer [110]	Insulin	Prevents aggregation in gastric medium	-	Transcytosis pathway
Self emulsifying drug delivery system	Phospholipid, oil phase, surfactant and co surfactant 407	LXT-101 [111]	Stable in GI tract	mucoadhesive	Predicted to show para cellular uptake due to presence of permeation enhancers like fatty acids and phospholipids and transcytosis by microemulsion
Nano composites	Silica-chitosan nanocomposites containing TAT cell penetrating peptide [112]	Insulin	Stable in GI medium	Mucoadhesive (in vitro)	Permeable

1.5 Therapeutic Peptides in clinical development

Peptides currently under clinical development are mostly formulated using permeation enhancers while remaining systems use peptide drug conjugates and liposomal formulation (Table 1-7). However, in conditions where the drug concentrations have to be increased to achieve therapeutic benefit, permeation enhancers may cause dose limiting toxicity [113]. This is also one of the reasons why formulation like Eligen® fail in clinical development.

In the Table 1-7, comprehensive examples technologies currently being used by different pharmaceutical companies for oral delivery of therapeutic peptides, their outcomes and development phase are summarized as follows.

Table 1-7 Peptides under clinical development

Peptide under clinical development					
Company	**Product name**	**Therapeutic peptide**	**Technology**	**Benefit**	**Development phase**
Biocon (trials in partnership with Bristol-myers Squibb)	Insulin Tregopil (formerly referred as IN-105)	Oral Insulin for Diabetes	Insulin –amphiphilic oligomer conjugate (methoxy PEG derivative conjugated to LysB (29) of human insulin	Enhanced transcellular transportation, enzyme stability [114] Rapid insulization of liver and lower propensity to cause post prandial hypoglycemia [115]	Completed Phase I
Tarsa Therapeutics, Inc.	TBRIA™ (once daily)	Salmon Calcitonin for oesteoporosis	Peptelligence™ technology enteric coated formulation consisting of citric acid (pH lowering agent) and acyl carnitine (permeation enhancer) [116]	Ca+2 chelator, Permeation through tight junction, Positive effect on bone mineral density at lumbar spine [117]	NDA filed for review [118]
Chiasma, Inc.	Mycapssa™	Octreotide for orphan disease acromegaly	Transient permeability enhancer (TPE®) – sodium caprylate (C8)	Temporary opening of the tight junctions	NDA filed for review [119]
Generex Biotechnology Corp.	Oral-lyn™ [120]	Insulin (pre prandial) Type I and Type II	Rapid-mist™ device Aerosol type device (propellant penetration enhancer and stabilizer)	Permeates across buccal epithelium and reaches blood circulation [121] Fast absorption better than sub cutaneous formulation	Phase III
Diabetology	Capsulin	Insulin (Type I)	Axcess™ oral delivery system (Penetration enhancers, solubilizer) [122]	Onset of action within 30 min and duration of action up to 4-6 h [123]	Phase II

Diasome Pharmaceuticals, Inc.	Oral HDV Insulin [124]	Insulin (Pre prandial) (Type I and II)	Liposomal insulin made of hepatocyte-targeting molecule - biotin-phosphatidylethanolamine in phospholipid bilayer	Stable against intestinal enzymes, selective targeted delivery of insulin to hepatocytes	Phase II
Oramed Pharmaceuticals	ORMD-0801	Insulin (Type I and II)	Enteric coated capsule (SNAC, RDTA, Aprotonin, soybean trypsin inhibitor, omega 3 fatty acid)	Stable in GI tract and permeable across the enterocytes, Effectively reduced glycemia throughout the day in type I diabetes patients [125]	Phase II

Alternatively, drug carrier system particularly polymeric nanoparticles; pose an attractive tool for peptide delivery because of its safety, biocompatibility and limited toxicity profile. Despite their advantages, the majority of these materials are still under pre-clinical development. Several constraints such as loading efficiency, controlled release, stability and accumulation in non-target organs still remain a challenge in achieving desired therapeutic benefit [126]. However, preclinical studies also suggest these polymeric nanoparticles can be functionalized by several mechanisms (Table 1-6). Thus there is scope for improving oral bioavailability with carrier materials that is safe for clinical use. The following review focuses on polymeric nanoparticles for improving drug delivery.

1.6 Polymeric nanoparticles

The polymeric nanomaterial are biodegradable and biocompatible that over 60% of the nanoparticles in preclinical testing and on going clinical trials are derived from polymers. Polymers of natural, semi-synthetic or synthetic origin can be fabricated to form nanoparticles that improves poor characteristics of therapeutic drugs such as solubility, stability, permeability and release in order to attain its target and specific activity at a predetermined rate and time. Polymeric nanoparticles are

prepared from amphiphilic polymers, hydrophobic polymers and hydrophilic polymers.

Amphiphilic polymers are self-assembling polymers that have hydrophobic and hydrophilic functional groups, and are widely used for the preparation of polymeric nanoparticles. Depending on the nature of the solvent, these amphiphilic polymers produce regular micelles or reverse micelles. The polymers aggregate in solutions due to the hydrophobic effect. They offer a dual advantage, by solubilizing hydrophobic drugs as regular micelles and by protecting hydrophilic drugs against physiological barrier as reverse micelles. Few examples of amphiphilic polymers are quaternary ammonium palmitoyl glycol chitosan (GCPQ) [127] , poly(vinyl-co-ester) [128] and amphiphilic hyper-branched core shell polymers with foliate moieties [129] etc.

1.6.1 Characteristics of Polymeric nanoparticles

The advantages of using polymers are that the polymers can be fabricated to desired size, hydrophobicity and molecular weight. The size of the polymeric nanoparticles increases with increase in molecular weight as seen in chitosan [130] and PLGA [131] nanoparticles. Fabricating hydrophobicity of the polymer gives different forms such as polymeric micelles and polymeric bilayer vesicles [132]. Polymeric micelles are made up of hydrophobic core and hydrophilic shells that can encapsulate drugs in the core. Polymeric bilayer vesicles can accommodate hydrophobic drugs within the bilayer and hydrophilic drugs in the core (Figure 1-7).

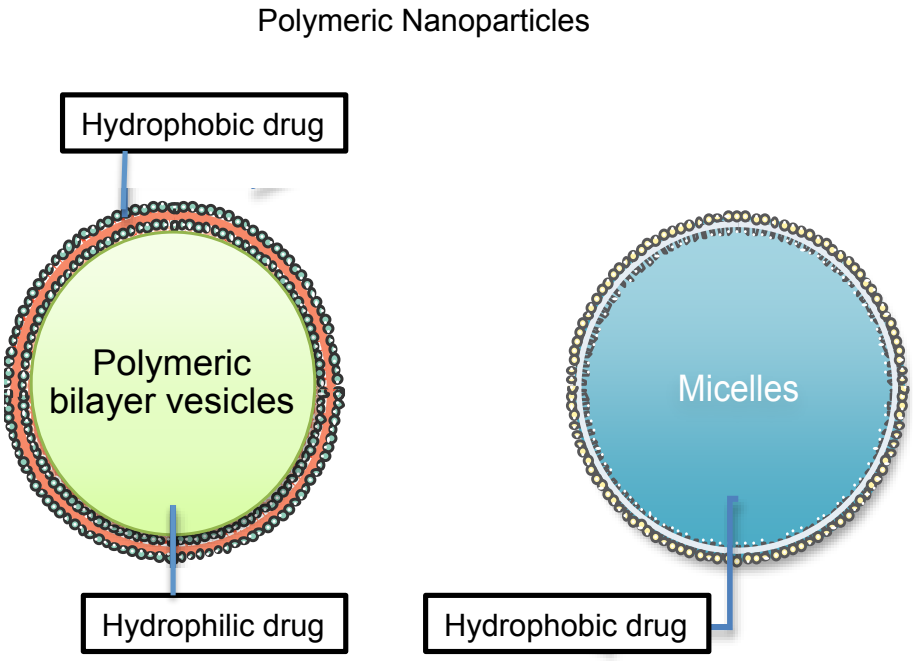

Figure 1-7 Schematics of Polymeric nanoparticles showing polymeric bilayer vesicles on the left and micelles on the right.

For example, the amphiphilic variants forming polymeric micelles or polymeric bilayer vesicles are based on the hydrophobicity of the polymer. For N-cetyl-poly(ethylenimine), an amphiphile with greater than 58% hydrophobic content yield dense sphere, 45-58% molar hydrophobic content yields vesicles and less that 45% hydrophobic content yields polymeric micelles [133].

This is represented as vesicle formation index (F)

$$F = H/L\sqrt{DP}$$

Where H= mol % of underivatized polymer monomers; L = mol % of hydrophobic unit derivatized monomers; and DP = degree of polymerization of polymer backbone. An F value greater than 0.11 indicates the formation of vesicles in N-cetyl-poly(ethylenimine) [133] .The hydrophobicity not only gives different forms but also determines the drug loading efficiency of the polymer. For example, GCPQ [134] and N-cetyl N-trimethyl, N-dimethyl, N-monomethyl-poly(ehtylenimine) [135] polymers with high hydrophobicity exhibits high drug loading efficiency.

The polymer self assembles at its critical micellar concentration (CMC). The CMC determines the stability of the amphiphilic aggregates and therefore the drug loading efficiency of the polymeric nanoparticles. Below the CMC, the amphiphiles

exist as molecular entities and only aggregate above the CMC [136]. Lower the CMC of a polymeric nanoparticles higher its stability in physiological medium.

Depending on the nature of the polymers, polymeric nanoparticles can be prepared by dispersion of preformed polymers in aqueous solution [134], precipitation of hydrophobic polymers in aqueous solution [137] and stabilization with surface active agents or ionic gelation/ coacervation of hydrophilic polymers[138], [139]. The method used for preparing nanoparticles formulation should be less toxic, and easy to scale up, with good drug loading efficiency and yield. Synthetic polymers are prepared by conventional dispersion methods that include nano-precipitation [140] [141], solvent evaporation [142] [143], salting out [144], emulsification/solvent diffusion and dialysis [145]. All these techniques involve usage of solvents, which could be a disadvantage in producing pure nanoparticles. A solvent free simple preparation method was reported using amphiphillic polymer GCPQ [146] and poly (allyl) amine grafted with palmitoyl and quaternary ammonium group [147] where the drug encapsulation was achieved by suspension of drug and the respective polymer in aqueous solution.

Polymeric nanoparticles have been used to deliver drugs via oral, intravenous, nasal, topical and oral routes. Drug-encapsulating polymeric nanoparticles have been shown to enhance drug delivery to tumours and across the blood brain barrier following oral administration, while also extending plasma half-life, increasing residence time within ocular tissue, augmenting the oral bioavailability of gut-liable peptides and reducing side effects. Selected examples of how polymeric nanoparticles have been used to improve the physiochemical properties of a drug overcoming biological barriers and site specific targeting are listed in Table 1-8.

Table 1-8 Applications of polymeric nanoparticles

Application	Nanoparticles-Drug	Advantage
Tumour targeting	Abraxane- Nanocrystalline paclitaxel stabilized by albumin [148]	Tumour targeting (binds to secreted protein and rich in cysteine) and improved solubility. Reduced side effect compared to excipient (Cremophor EL) based formulation
	PLGA-Vitamin E – Paclitaxel [137]	High AUC compared to cremophor based formulation
	Chitosan amphiphile-octreotide [149]	Tumor targeting via somatostain receptor on tumour cells.
	Hyaluronic acid based amphiphile [150]	Tumor targeting (CD44 receptor)

	Poly (ethylene oxide)-block (benzyl-L-aspartate- Doxorubicin [151]	Increased blood residence time
Blood brain barrier	Poly (ethylene glycol)-b-poly(lactic acid) nanoparticles – Paclitaxel [143]	Conjugation of F3 peptide (target-neurolipin-1 expressed on tumours)
	TP-LENK and LENK –GCPQ nanoparticles [53]	Stable in plasma and increased uptake in brain
Oral delivery	LENK nanoparticles [53]	Stable against enzymatic degradation in the gut
	Eudragit nanoparticles- Insulin [152]	Promoted mucoadhesion
Hydrophobic drug solubilization	Cyclosporin A-GCPQ [153]	Increased drug solubilization and absorption in the gut

1.6.2 Chitosan polymers

Chitosan is a linear polysaccharide consisting of β-(1-4)-linked D-glucosamine and N-aetyl-D-glucosamine. The polymer's reactive functional group such as amino group, primary hydroxyl and secondary hydroxyl group can be chemically modified to obtain chitosan-based derivatives for drug delivery application [154]. The amino group of chitosan is protonated and remains soluble at acidic conditions but insoluble at neutral pH as the pKa of D-glucosamine is 6.5 [155]. This cationic property of chitosan is exploited for its ability to bind with negatively charged mucus in the gut wall [156]. Glycol chitosan is chitosan with 6-O-linked glycol unit, which is soluble at neutral pH with a pKa 5.99 [157].

1.7 Quaternary Ammonium Palmitoyl Glycol Chitosan (GCPQ)

1.7.1 GCPQ molecular architecture

GCPQ is a self-assembling amphiphilic polymer previously reported to solubilize hydrophobic drugs [146], [153]. GCPQ is a pendant shaped amphiphilic derivative of glycol chitosan with palmitoyl chain and quaternary ammonium group (Figure 1-8). Some amino groups of glycol chitosan backbone are modified by palmitoyl chain and the degree of substitution of palmitoyl chain called as the degree of palmitoylation (DP) determines the hydrophobicity of the polymer. Similarly, in addition to palmitoyl chain, the amino groups of glycol chitosan were also substituted with quaternary ammonium group. Here, the degree of substitution of quaternary ammonium group to the glycol chitosan backbone called the degree of quaternization (DQ) determines the solubility of GCPQ in an aqueous solution. Quaternary ammonium group remains charged above neutral pH and increases the solubility of GCPQ in aqueous solution up to a pH of 9 [157].

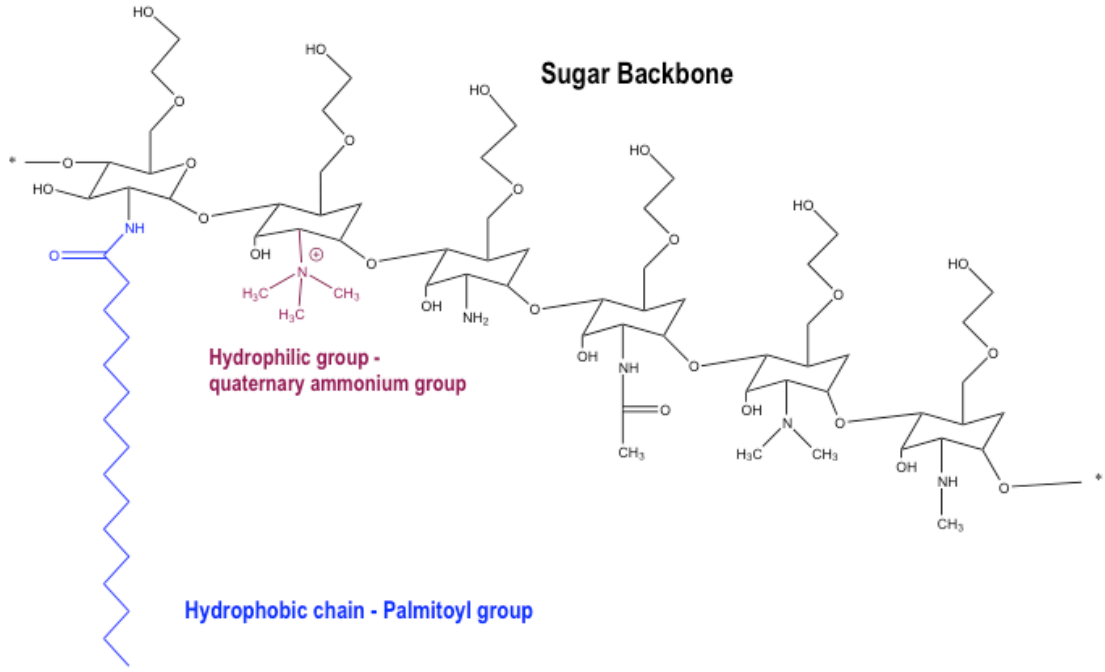

Figure 1-8 2-D structure of GCPQ with glycol chitosan chain in black color, palmitoyl group shown in blue color and quaternization ammonium group in magenta color

1.7.2 GCPQ micelle formation

The polymer in an aqueous environment favors the association of hydrophobic pendant group and liberation of water molecules to form micelles of size around 20-40 nm [134]. During the process of micellization, hydrophobic drugs can be solubilized or directly added to GCPQ solution, where the GCPQ accommodate lipophilic drugs in its hydrophobic core. The amount of hydrophobic drug incorporation depends on the hydrophobicity of GCPQ polymer. Drug loading levels up to 40% are achievable with GCPQ [134]. The CMC of GCPQ is very low (19µM) compared to block copolymer amphiphiles [134], meaning that upon dilution in physiological condition, the drug solubilizing property may not be lost.

1.7.3 GCPQ - Physical characteristics

GCPQ of molecular weight 19.9 KDa with palmitoylation 23 % and quaternization 10 % were characterized for its physical properties. The polymer is glass at room temperature with Tg of 164.4 ± 8.5 °C and decomposes at 218 ± 4 °C. GCPQ is a weak base with a pKa 5.99 ± 0.15. It was also observed that GCPQ forms micellar network and exhibit viscoelastic properties at a concentration of 90 mg/mL in water. GCPQ also show Newtonian rheological behavior below a concentration of 70 mg/mL. However, at higher concentrations, GCPQ undergoes sheer thinning

because of chain disentanglement due to high shear rates. The storage stability of GCPQ was also observed to be lasting for 18 months at room temperature [158].

1.7.4 GCPQ - *in vitro*

GCPQ is considered as safe for preclinical evaluation. GCPQ below a concentration of 0.1 mg/mL show no cytotoxic effect in A431 and A549 cancer cell lines. The GCPQ also shows no haemolysis at a concentration of 1 mg/mL and less than 20% haemolysis at a concentration of 10 mg/mL [127]. Preliminary experiments in vitro cell culture model shows that the polymer is transported via transcellular pathway but the exact mechanism is not known. GCPQ neither inhibits the efflux activity of the P-glycoprotein efflux pump nor paracellularly transported [146].

1.7.5 GCPQ – *in vivo*

GCPQ nanoparticle has been reported to enhance the delivery of hydrophobic drugs via oral, intravenous, intranasal and ocular route [146], [53], [159], [134], [153], [135]. Orally delivered GCPQ nanoparticle has been shown to improve dissolution of hydrophobic drug in gastrointestinal tract and promotes drug absorption via interaction with the intestinal mucosa [146]. *Ex vivo* imaging of small intestine shows that GCPQ traverses the mucosal barrier by adhering to the mucosal surface of the villi. GCPQ nanoparticles are observed at the boundary of sub mucosa, in the muscularis propia below the base of the villi and within the hepatocytes [160]. It is also hypothesized, based on the uptake of radiolabelled GCPQ-LENK nanoparticles, that the high molecular weight GCPQ nanoparticles shows better plasma stability. Approximately 1-2% of orally administered nanoparticles are found in the blood within 15 min, with 2-3% in the liver and gall bladder [53]. Radiolabelling experiments have reported that GCPQ accumulates in gall bladder two h after oral administration. It has also been hypothesized from this observation that the GCPQ nanoparticles could be absorbed in the GI tract via enterocytes in the villi, pass into the blood stream and are transported to the hepatocytes and hepatocellular spaces of the liver, and then recirculated via bile in the gall bladder to small intestine [160]. GCPQ improved oral bioavailability of amphotericin B (24%), a nephrotoxic drug. The polymer protected the peptide from gastrointestinal degradation, enhanced drug bioavailability of the drug to target organs such as lung, liver and spleen and reduced exposure to kidney [161].

GCPQ coating on pro-drug peptide (palmitoyl leucine enkephalin) was reported to improve the enzymatic stability of peptide in plasma, increasing the plasma half-life by 520% [162]. The polymer does not accumulate in liver following intravenous administration. GCPQ coating also promotes its absorption to the luminal vasculature surfaces of the brain [160]. This action enhances the uptake of prodrug peptide across the blood brain barrier thereby increasing therapeutic effect [162]. GCPQ was also shown to promote nasal delivery of hydrophilic peptide (leucine enkephalin). The peptide-GCPQ nanoparticles, following nasal administration, crossed blood brain barrier and improved anti nociceptive activity in rats CFA pain model [163].

GCPQ was also used to enhance the ocular delivery of cyclosporine A. GCPQ polymer improved the mucoadhesion of the peptide that resulted in increase in its ocular residence time. GCPQ was also observed to promote ocular absorption and thereby increasing the bioavailability of cyclosporine A formulation [164].

Aim and Objective

Aim

The potential of therapeutic peptides has been exploited in various disease conditions. With the increasing demand, possibilities for non-invasive route of peptide administration are of great importance, particularly in chronic conditions, where drugs require frequent administration and patient non-compliance frequently experienced with invasive methods becomes a challenge. Several excipients and carrier materials have been reported to enhance the oral bioavailability of peptides by different mechanisms. This study focuses on two therapeutic peptides, Methionine enkephalin, an anti-cancer peptide for the treatment of pancreatic cancer and Labyrinthopeptin, an anti-nociceptive peptide for chronic pain treatment. Both the peptides have previously demonstrated significant therapeutic effect after intravenous administration [165], [166], [167]. However, their non-invasive and in particular oral administrations are hampered due to poor bioavailability and in the case of MENK also poor stability. The aim of the current project is to test the hypothesis that it might be possible to enhance the oral bioavailability of therapeutic peptides using GCPQ nanoparticles.

Objective

- Synthesis of GCPQ by two methods and characterize their molecular weight and degree of substitution on the polymer backbone.
- Characterize GCPQ micelles for their size and polydispersity and study their colloidal stability under simulated conditions.
- Formulate peptides (Laby and MENK) with GCPQ; characterize the peptide GCPQ nanoparticles for their size, PDI, surface charge, encapsulation efficiency and colloidal stability in simulated medium.
- Validate method for quantification of the peptides *in vivo* by LCMS.
- Evaluate *in vivo* pharmacokinetic of the peptides following oral and nasal administration of Laby-GCPQ formulations and oral and intravenous administration of MENK GCPQ formulations.
- Study the anti-nociceptive activity of Laby-GCPQ formulation following oral and nasal administration and compare its efficacy with control (Laby glycofural formulation).
- Study the effect of MENK GCPQ IV and oral formulation on mice tumour xenograft models.

2 GCPQ polymer synthesis

2.1 Objective

Objective of this chapter is to,

1. Synthesize of GCPQ by old and new methods.
2. Evaluate the synthesis methods by comparing the molecular characteristics of GCPQs such as their molecular weights, polydispersity indices and surface modifications.
3. Evaluate the colloidal stability of GCPQ B2 in water, sodium chloride solutions of different concentrations, simulated gastric and intestinal fluids in fasted and fed states.

2.2 Introduction -Polymer Characterization methods

2.2.1 Structure prediction of polymer by H^1 NMR

Nuclear magnetic resonance spectroscopy is a tool for predicting molecular structure based on the magnetic properties of certain nuclei. NMR works by measuring the emitting radio frequency from a sample, which is inside a constant magnetic field [168]. The underlying principle of NMR is that some nuclei exist in specific spin states in an applied external magnetic field. NMR measures the transition between the spin states that are specific to particular nuclei and nuclei's chemical environment[169].

Theory

Certain nuclei experience charged spin, creating a magnetic moment that allows chemist to predict structure, using NMR [169]. The nuclei spin could be no spin for those nuclei that have an even number of both protons and neutrons, an integer spin for those nuclei that have an odd number of both protons and neutrons, or a half integer spin when the number of proton and neutron of nuclei sums up to an odd number. These nuclei have a random orientation in the absence of a magnetic field [169]. However, when an external magnetic field is applied, the nuclei can either experience alpha spin state or beta spin state. In alpha-spin state, the nuclei having low energy orient parallel with the applied magnetic field, whereas; nuclei with beta-spin state having higher energy orient anti parallel to the applied magnetic field [170]. The energy difference ($\triangle$E) between the alpha and beta spin state depends on the external magnetic field strength [170].

Chemical shift

In H^1 NMR, every nucleus can experience different chemical environment and resonate at slightly different frequencies [171]. These differences in the chemical environment occur when a nucleus is shielded or de-shielded from the neighboring nuclei [170]. This is called chemical shift. Protons that are symmetrical (benzene) and have the same chemical environment are called chemically equivalent protons. Thus, the signal obtained have same chemical shift on a frequency scale. However, asymmetrical protons have different chemical environment and have different chemical shift on a frequency scale. Electrons can shield a proton from the applied magnetic field causing the signal to shift right (up field) on frequency scale. On the other hand, electronegative atoms remove the shielding effect of electrons on a proton causing the signal to shift left (down field) on a frequency scale. These frequency shifts ware very small in comparison to primary NMR frequency differences (Hz as compared to MHz). Hence chemical shifts are denoted by the unit ppm on NMR spectra [171]. The chemical shift (δ) is represented by formula,

Equation 1

$$\delta = \frac{H_{ref} - H_{sub}}{H_{machine}} \times 10^6$$

Where trimethylsilane is used as a reference standard (H_{ref}), H_{sub} is the resonance frequency of a substance and $H_{machine}$ is the operating frequency of NMR spectrometer. The area under the signal is integrated to obtain the relative number of protons causing the respective signal [169, 172] .

Instrumentation

There are two NMR spectrometers, Continuous-wave (CW) and pulsed or Fourier-transform (FT) NMR. FT-NMR has largely replaced CW-NMR [173]. In CW-NMR (Figure 2-1), a sample is placed between strong magnets and from an antenna coil, radiofrequency radiation of appropriate energy is directed towards the sample. The receiver coil collects the emitted RT energy that is monitored in the computer. The spectrum is scanned by two methods, field-sweep method or frequency-sweep method. In frequency-sweep method, magnetic field is kept constant and RF signal is swept to determine the frequency at which energy is absorbed. In field-sweep method, resonance frequency is kept constant and magnetic field strength is determined by sweeping magnetic field at varying energy levels [173] .

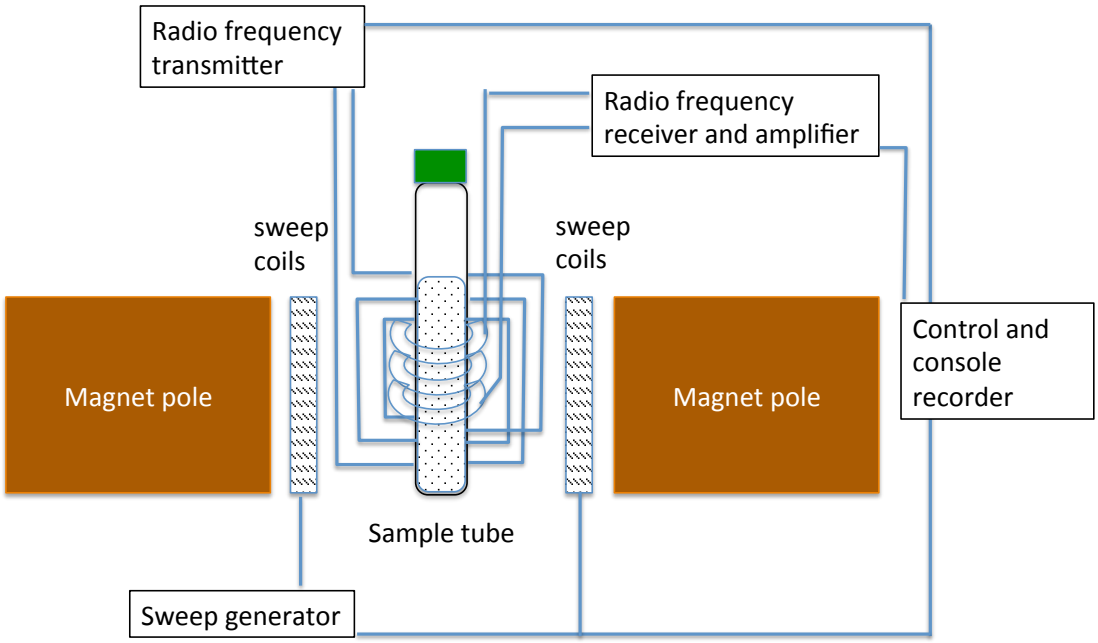

Figure 2-1 Schematic of CW-NMR Spectrometer.

In Fourier-Transform NMR spectrometer (FT-NMR), a pulse of radiofrequency radiation is applied that causes nuclei in a magnetic field to excite into the higher-energy state [173]. RF pulse lasts between 1 and 10 μs, which is sufficient to excite nuclei in all local environments. Between the pulses, the nuclei in the excited state re-emit signal at a time interval (T) (this lasts from one to several sec) called as free induction decay signal (FID). FID signals are detected by radio-receiver coil is placed perpendicular to the magnetic field. The FID signals are then processed, averaged to get signal to noise ratio. These results are converted in to a frequency-domain signal by a Fourier transformation. The output is similar to the spectrum produced by a scanning continuous-wave experiment [173] [174]. The advantage of FT-NMR over the CW-NMR is that FT-NMR saves time as all the resonance signals can be collected simultaneously. However, with CW-NMR resonance signals are collected sequentially [174].

2.2.2 Molecular weight determination by GPC-MALLS

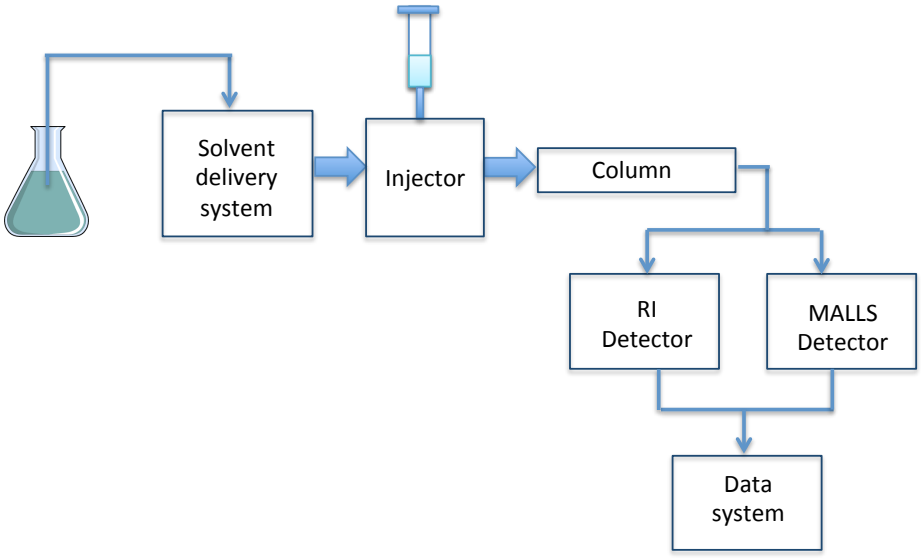

Figure 2-2 Schematic of GPC-MALLS

Gel permeation chromatography (GPC) is a type of size exclusion chromatography for the separation of molecule based on size [175, 176]. The column is packed with porous beads, which constitute the stationary phase, and sample is injected along with a suitable solvent, which constitute the mobile phase. When polymers of different sizes are injected in to the column, small sized polymers pass slowly through the pores of the beads and larger sized polymers escape the pores of the beads and pass quickly down the column. Here, the separation of polymers within the GPC column takes place with larger molecules preceding the smaller molecules and analyzed using multi angle laser light scattering (MALLS) and differential refractive index (dRI) detector [175, 176].

The scattered light intensity is measured as Rayleigh ratio (R_θ), the excess scattering of the sample and solvent over that of the sample alone. Rayleigh ratio is directly proportional to the molecular weight of the solute molecule scattering the light [177].

Equation 2

$$\frac{K^*C}{R_\theta} = \frac{1}{M_w}P_O + 2A_2C + 3A_3C + \cdots.$$

$$P_O = \left(\frac{16\pi^2}{3\lambda^2}\right) Sin^2\frac{\theta}{2}(< r > Z)^2$$

Where, P_o is scattering function; C is solute concentration; R_θ is the Rayleigh ratio; Mw, the weight-averaged molecular weight; λ, the wavelength of incident light; θ, π, the scattering angle; <r>z, the z-averaged mean radius of gyration and A_2,

the second virial coefficient, which quantifies the interaction between the macromolecule and the solvent [178].

K^* is given by the equation,

Equation 3

$$K^* = \frac{4\pi^2\eta^2}{N_O\lambda^4}\left(\frac{d\eta}{dC}\right)^2$$

Where, N_0 is the Avogadro's number; η, the refractive index and dη/dc, the change in refractive index per unit change in solute concentration. This equation simplified. For polymer and solvent combination the refractive index increment is considered a constant. Under dilute conditions, the virial expansion that relates to intermolecular interactions can be considered zero. The scattering function P_o is one if the molecule is below 10 nm [178].

Under these conditions the equation simplifies to,

Equation 4 Rayleigh's ratio

$$R_\theta = M_w K^* C$$

Where,

$$K^* = (dn/dc)^2 K$$

Therefore,

Equation 5

$$R_\theta = M_w K^* \left(\frac{dn}{dc}\right)^2 C$$

So it is clear from the equation that the response from the detector is directly proportional to the molecular weight, a constant K, and the concentration of the solute [178].

The differential refractive index detector calculates the absolute molecular weight of an analyte from the concentration used, refractive index (n) and the differential refractive index of an analyte [179]

In MALLS, monochromatic light is passed through sample and the intensity of scattered light is captured by detectors placed at multiple angles around the sample. Multi angle light scattering data are analysed using Zimm plot. A plot of K^*C/R_θ versus sin $(\theta/2)+C$ is created and double extrapolated to zero angle and zero concentration. From this plot, the intercept is used to calculate the molecular weight and from the slope the radius of gyration is obtained. [180]

2.3 Nanoparticle characterization methods

2.3.1 Transmission Electron Microscope (TEM)

Transmission electron microscopy is one of the techniques used for size and morphology characterization of nanoparticles. Unlike the light microscope, the TEM focuses an electron beam through the sample, which is placed on a TEM grid. This interaction causes amplitude and phase variation in the transmitted beam which is a function of sample thickness and sample material. The sample is coated as a thin film on the TEM grid, where it is dried and negatively stained with uranyl acetate. Uranyl acetate has a pH around 4.2 to 4.5 and only interacts with the background leaving the sample untouched. Successful imaging of the sample is obtained when a contrast is developed against the carbon background that makes up the grid [181, 182]. Samples with higher electron densities such as metals, polymeric nanoparticles [183], carbon nanotubes, quantum dots [184] and magnetic nanoparticles have smaller mean electron free path than lighter atoms. This develops, higher contrast than amorphous carbon. The electrons that pass through sample and the image are magnified and focused by an objective lens, which appears on an image screen (Figure 2-3). Size ranging from 0.1 nm to 2 μm can be measured using TEM. The major advantage is that TEM provides information on the sample's size and shape. Limitations are that TEM imaging and analysis can be time consuming. TEM also only provides qualitative results [181].

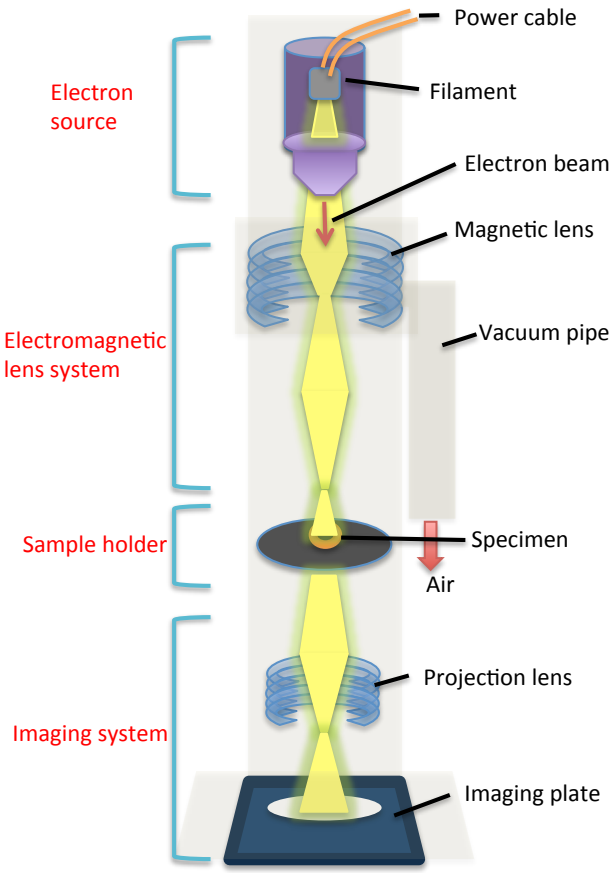

Figure 2-3 Schematic of TEM

2.3.2 Dynamic Light Scattering (DLS)

Dynamic light scattering technique is used to determine the size distribution of particles in suspension [185]. Particles in suspension exhibit Brownian motion by thermally induced collisions between the suspended particles and the solvent molecules. When the particles are illuminated with a laser (633 nm), the intensity of scattered light fluctuates as the particles move over a timescale that depends on the size of the particles (Figure 2-4). From the time dependent fluctuation, the translational diffusion coefficient and hydrodynamic diameter is determined using Stokes-Einstein equation with the assumption that particles are spherical and non interacting [185].

Equation 6- Stokes-Einstein equation

$$D = \frac{kT}{3\pi\eta D_H}$$

Where D is translational diffusion coefficient, K is Boltzmann's constant, T is absolute temperature, D_H is hydrodynamic diameter and η is viscosity.

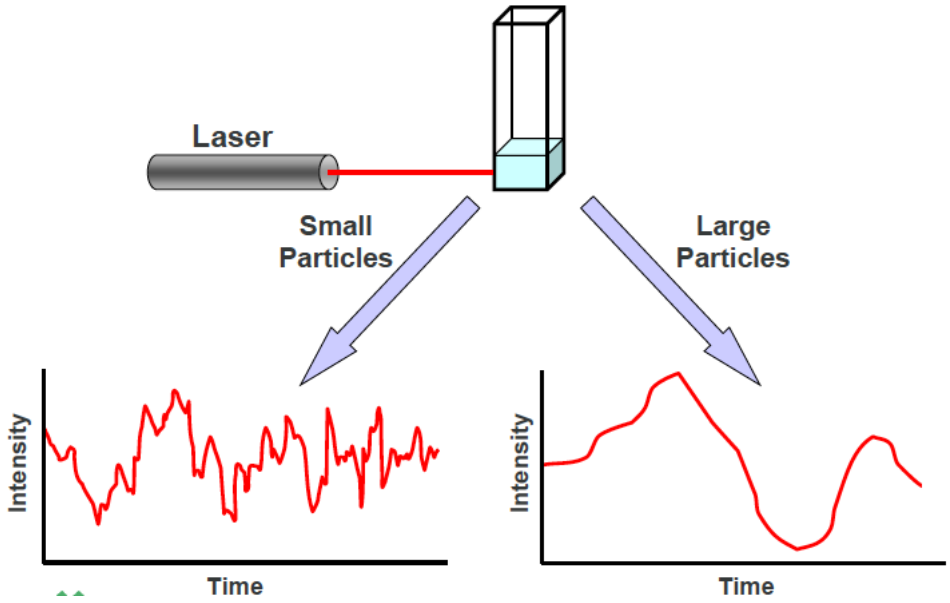

Figure 2-4 Illustration of time dependent fluctuation for small and large particles in DLS [185, 186]

The time dependent fluctuation is converted in to a correlogram to which cumulant analysis is applied to calculate intensity-based distribution using Rayleigh scattering principle [185]. The cumulant mean of intensity-based distribution gives Z-average size mean. Z-average size can only be compared to size measurements by other methods if the intensity-based distribution is monomodal (single peak). For polydisperse sample, different size populations can be analysed from volume and number based distribution. These distributions are calculated from intensity-based distribution by applying Mei theory. An Illustration showing how different distributions (intensity, number and volume) compare to one another is shown in Figure 2-5. Particle sizes of two populations, 5 and 50 nm are represented in number distribution as ratio 1:1. However the same populations are represented as ratio 1:1000 (considering volume of sphere) in volume based distribution. Further, the populations are represented as ratio 1:1,000,000 (intensity of scattering light is proportional to d^6) in intensity-based distribution [185].

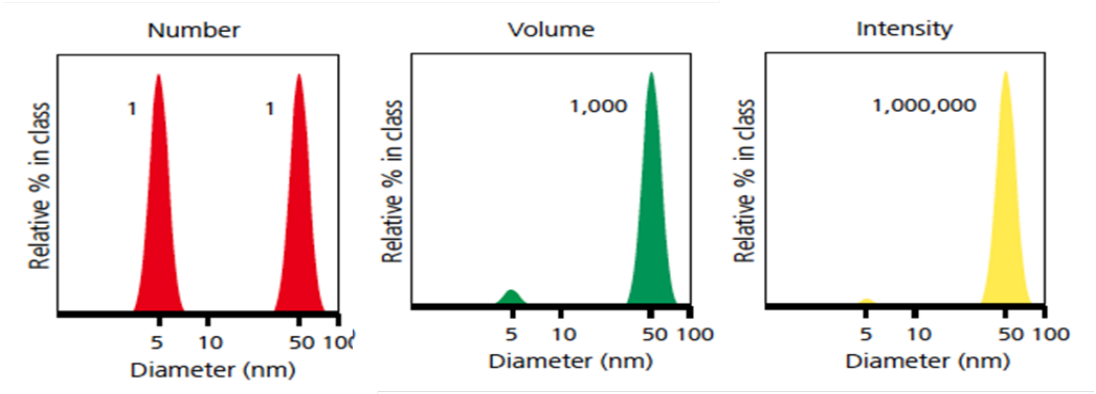

Figure 2-5 Illustration comparing particles in different weighed distribution in DLS. Number based distribution (red), volume based distribution (green) and intensity based distribution (yellow) [185].

Hydrodynamic diameter is a measure of particle diameter in diffusion. The translational diffusion coefficient also depends on the concentration, surface structure and types of ions in the medium. As a result, the size obtained in DLS is larger than observed in TEM [185, 186].

Particle sizes ranging from 0.1 nm to 6 µm can be measured using DLS. Sample measurement is fast and accurate for monomodal distribution. Limitations are that DLS measurements can be inaccurate for polydisperse samples. A small fraction of large particles within the population can obscure small particles.

2.3.3 Surface charge characterization by DLS

Surface charge of the particles can be measured by analyzing their zeta potential [187]. Particle carry net surface charge that attracts counters ions in the solution at the surface to form electrical double layer. The electric double layers surrounding the particles have two layers; stern layer that consist of those ions strongly bound to the particles and an outer diffusive layer. Ions within the diffusive layer move with the particles and those outside the diffusive layer stay with the bulk dispersant. Zeta potential is the measure of charge at the slipping plane (Figure 2-6). Physiochemical parameters like pH, conductivity and particle concentration affects the zeta potential of a sample. For the measurement, the sample is taken in a capillary cell with electrodes on either end. When a potential is applied, particles move towards the electrode and their velocity is measured from which electrophoretic mobility and zeta potential is calculated [187].

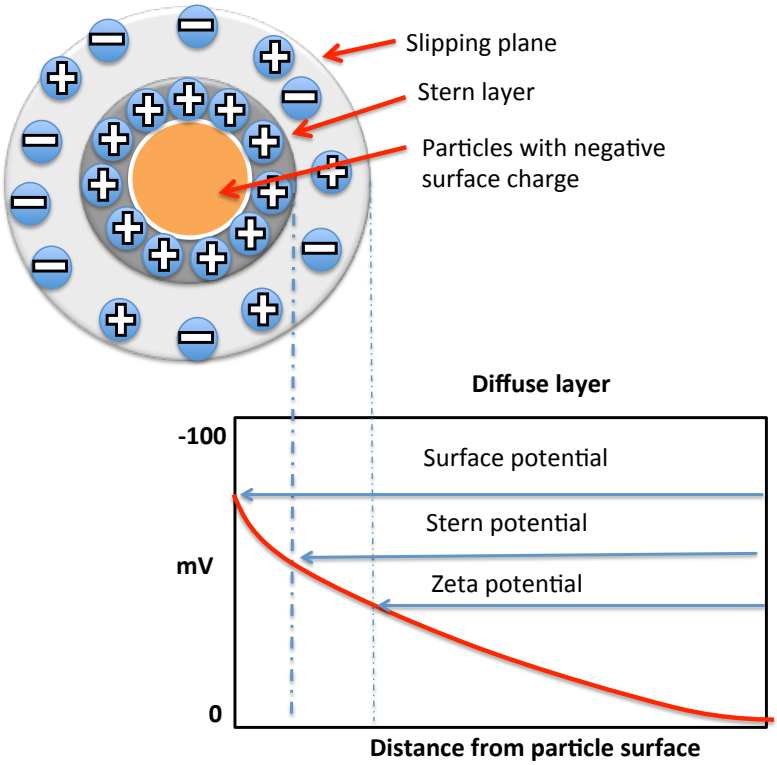

Figure 2-6 Schematic representation showing electrical double layer surrounding the particle

Colloidal stability of the particles is determined by their surface charge. The stability of colloidal particles is explained by DVLO theory. The stability of the colloidal particles is determined by the sum of van der Wall's attractive force and electrical double repulsive force that exists between particles undergoing Brownian motion. For particles to be colloidally stable, the repulsive force must be dominant. However, when the particles approach each other and if the attractive force overcomes the repulsive force between particles, flocculation takes place. Colloidal stability can be achieved by electrostatic or charge stabilization which is the effect on particle interaction due to distribution of charged species in the system [188].

2.4 Materials

Table 2-1 List of Materials Used

Chemical	Supplier
1-Methyl-2-pyrrolidone (99%)	Sigma-Aldrich (Gillingham, UK)
Amberlite IRA-96, free	Sigma-Aldrich (Gillingham, UK)
Calcium chloride	Sigma-Aldrich (Gillingham, UK)
Diethyl ether (99.5 %)	Sigma-Aldrich (Gillingham, UK)
Ethanol (absolute) (99.7 – 100 %)	UCL School of Pharmacy
Glycerol mono-oleate	Sigma-Aldrich (Gillingham, UK)
Glycol chitosan (60 %)	Sigma-Aldrich (Gillingham, UK)
Hydrochloric acid (36.5 – 38%)	VWR BDH Prolabo (Fontenay-sous-Bois, France)
Iodomethane, reagent plus (99%)	Sigma-Aldrich (Gillingham, UK)
Lecithin	Sigma-Aldrich (Gillingham, UK)
Maleic acid (99%)	Sigma-Aldrich (Gillingham, UK)
Methanol-D4 (99.80%)	Cambridge isotope laboratories, Goss Scientific Instruments Ltd. (Worleston, Nantwich, UK)
Palmitic acid N-hydroxysuccinamide ester (98%)	Sigma-Aldrich (Gillingham, UK)
Pancreatin from porcine pancreas (4X USP)	Sigma-Aldrich (Gillingham, UK)
Pepsin	Sigma-Aldrich (Gillingham, UK)
Sodium bicarbonate (99.5 %)	Sigma-Aldrich (Gillingham, UK)
Sodium chloride (99%)	Sigma-Aldrich (Gillingham, UK)
Sodium hydroxide (99.13%)	Sigma-Aldrich (Gillingham, UK)
Sodium iodide (99.5%)	Sigma-Aldrich (Gillingham, UK)
Sodium phosphate monobasic monohydrate (99%)	Sigma-Aldrich (Gillingham, UK)
Sodium oleate (99%)	Sigma-Aldrich (Gillingham, UK)
Sodium taurocholate hydrate (> 97%)	Sigma-Aldrich (Gillingham, UK)
Visking dialysis membrane with a cut-off of 3.5, 7 and 12-14 K Da	Medicell International Ltd (London, UK)
Water deionized	Millipore Elix-progaard 2
Water double deionized (18 ohm)	Millipore synergy – simpak1
Low volume disposable glass cuvette	Malvern, UK
Folded capillary Zeta cell	Malvern, UK

2.5 Methods

2.5.1 Synthesis of GCPQ (Batch 1 (B1) &Batch 2 (B2)) – old method

GCPQ synthesis steps involved acid degradation of glycol chitosan, palmitoylation of degraded chitosan and quaternization of palmitoylated glycol chitosan. The GCPQ synthesis was carried out as per protocol described in **[189]**, **[190]** and **[127]**. The protocol is summarized as follows,

2.5.1.1 Acid hydrolysis of Glycol Chitosan (GC)

Glycol chitosan (5 g) was dissolved in HCl (4 N, 380 mL) and incubated in a pre-heated water bath maintained at 50˚C for 24 h. The degraded product was dialyzed (MWCO 3500 Da) against water with six changes over 24 h. The dialysate was freeze-dried for further synthesis.

2.5.1.2 Palmitoylation of Glycol chitosan

Degraded glycol chitosan (500 mg) and sodium bicarbonate (376 mg) was dissolved in a mixture containing absolute ethanol (24 mL) and water (76 mL). Palmitic acid N-hydroxysuccinamide ester (PNS) (792 mg) was dissolved in absolute ethanol (150 mL) and added drop wise to GC mixture. The reaction was incubated for 72 h in dark condition. The palmitoylated product was rotary evaporated at 45˚C to remove residual ethanol and the remaining extract was mixed with three fold volumes of di-ethyl ether to remove free palmitic acid. This process was repeated three times and the aqueous layer collected was dialyzed (12-14 kDa) against water with six changes over 24 h. The dialysate was freeze-dried for further synthesis.

2.5.1.3 Quaternization of Palmitoyl glycol chitosan

Palmitoyl glycol chitosan (300 mg) was dispersed in 1-methyl-2-pyrrolidone (25 mL) and left overnight for 12 h at room temperature. To the above mixture, sodium hydroxide (40 mg), methyl iodide (0.44 mL) and sodium iodide (45 mg) was added and the reaction was set under the stream of nitrogen maintained at 36˚C for 3h. The quaternary ammonium product was precipitated and washed with diethyl ether. A brown hygroscopic product obtained was dissolved in a minimum volume of water and dialyzed against water with 6 changes over 24 h.

Amberlite resin (IRA-96) was packed in a separating funnel and pre-activated with HCl (150 mL, 1 M) followed by washing with distilled water (10 L) to give

neutral pH. The dialysate was passed through the resin and eluate was freeze-dried and stored in a desiccator until use.

2.5.1.4 Synthesis of GCPQ Batch 3 (B3) by new method

GCPQ polymer was also prepared by alternative method. This method allowed synthesis of GCPQ with higher palmitoylation. A summary of differences in two methods of polymer synthesis is shown in Table 2-2.

Table 2-2 GCPQ synthesis - Differences and Similarities

Synthesis steps	Old Method	New Method
Degradation of GC	Acid hydrolysis	Acid hydrolysis
Palmitoylation of dGC	**Mass ratios (DGC: PNS)** Solvent used are ethanol and water, which is polar protic. PNS soluble in ethanol but precipitates during pH adjustment. pH adjusted to > 8 to deprotonate the primary amines of GC. pH 8 is also necessary to activate the PNS. Purification done by extraction with ether. Dialysed and freeze-dried	**Molar ratios (DGC: PNS)** DMSO used as solvent. It is a polar aprotic and does not participate in the reaction. Less PNS required now as PNS is soluble in DMSO and stays soluble throughout the reaction. Triethylamine is used as the base as sodium bicarbonate bonds with DMSO. Purification done by acetone and ether wash. No dialysis, no freeze-drying.
Quaternization of PGC	**Methylation** After quaternization, the GCPQ is purified with amberlite free-base	**Methylation** GCPQ is passed through amberlite with activated chloride
Pros and cons	Cannot control palmitoylation step Molecular weight is reproducible	Can control palmitoylation step Polymer is polydisperse due to aggregation

In the old method, mass ratio of GC and palmitic acid was used to synthesis GCPQ with different degree of palmitoylation. Since it was difficult to control the degree of palmitoylation by previous method, the molar ratio of GC monomer and palmitic acid was used to synthesis PGC by new method.

2.5.1.4.a Acid hydrolysis of Glycol Chitosan

Acid hydrolysis of GC was carried out as method mentioned in section 2.5.1.1.

2.5.1.4.b Palmitoylation of Glycol Chitosan

Palmitic acid N-hydroxysuccinimide was added to GC, which was dissolved in DMSO and triethylamine. The reaction mixture was incubated for 15 h at room temperature under dark condition. The polymer was precipitated with a mixture of acetone and diethyl ether (1:2) and washed thrice with acetone (1 L). Finally, ether (1 L) was added to the precipitate and washed thrice. The precipitated product was filtered from diethyl ether under high vacuum and stored in a desiccator for drying.

2.5.1.4.c Quaternization of Palmitoylated Glycol Chitosan

Palmitoyl glycol chitosan was dispersed in N-methyl-2-pyrrolidone and stirred vigorously for 16 h until a foamy dispersion was obtained. Sodium hydroxide was added to the above mixture and stirred further for 40 min. The reaction vessel was then saturated with nitrogen gas and placed in a pre-heated oil bath maintained at 36˚C. Methyl iodide was added to the PGC suspension and the reaction was allowed to take place for 3 h. After 3 h, the product was allowed to precipitate in diethyl ether. This process was repeated twice and the precipitated product was suspended in HCl (0.1 M). The above solution was exhaustively dialyzed (MWCO 1 kDa) against NaCl (1% w/w) thrice and then with water (3X). The dialysate was freezing dried and stored in a desiccator until use.

2.5.2 Characterization of GCPQ polymer

2.5.2.1 Molecular weight analysis by GPC MALLS

Molecular weight of GCPQ was determined using gel permeation chromatography multi angle laser light scattering (GPC-MALLS). A solution of GCPQ (5 mg/mL) was prepared by dissolving the polymer in a solvent containing 35:65 ratios of acetate buffer and methanol. GCPQ solution (20 µL) was injected in to GPC column running on the same mobile phase at a flow rate of 0.7 mL/min for 20 min. The molecular weight was detected using MALLS and dRI detector. Specific refractive index increments over concentration (dη/dC) were measured by manually injecting a series of standard solutions of the GCPQ at different concentrations (0.1 to 0.6 mg/mL) prepared in mobile phase. The standards are analysed through the dRI detector set at 25°C and a wavelength of 658 nm and a pump flow rate of 0.3 mL/min.

The data obtained from both dη/dC and GPC-MALLS experiment were analysed using ASTRA software (Wyatt Technologies).

2.5.2.2 H1- Proton NMR

The degree of hydrophobicity and hydrophilicity of GCPQ was determined using ^{1}H proton NMR. GCPQ (5 mg) was dissolved in deuterated methanol (700 µL) and analysed in Bruker AMX 400 MHz spectrometer (Bruker instruments, UK). The NMR spectrum was integrated using topspin program. The palmitoylation and quaternization percentage were calculated using the following formula,

$$\%\text{Palmitoylation} = \frac{\text{Area of the } CH_3 \text{ signal} / \text{no of hydrogens } CH_3}{\text{Area of sugar chains} / \text{no of hydrogens of the sugar chain}} \times 100$$

$$\%\text{Quaternisation} = \frac{\text{Area of the } N(CH_3)_3 \text{ signal} / \text{no of hydrogens } N(CH_3)_3}{\text{Area of sugar chains} / \text{no of hydrogens of the sugar chain}} \times 100$$

2.5.3 Characterization of GCPQ nanoparticles

2.5.3.1 GCPQ nanoparticle preparation and characterization by size and charge

GCPQ B2 polymer suspensions at a concentration of 2.5 mg/mL in water and in different salt concentrations (10 mM, 20 mM, 40 mM, 80 mM, 160 mM and 300 mM) were vortexed and probe sonicated (QSonica, U.S.A) for 15 min at 25 amps and characterized for their size and polydispersity index by dynamic light scattering technique (DLS), and size alone by transmission electron microscope (TEM). The surface charge of the GCPQ nanoparticle was also measured at different values of pH and characterized by DLS.

GCPQ B2 polymer was also prepared at concentration 2.5 mg/mL in water and probe sonicated at 15 amps for 15 min. The resulting formulation was size characterized by DLS and TEM.

2.5.3.2 Transmission Electron Microscopy (TEM)

A drop of GCPQ B2 nanoparticle suspension was placed on a grid and blotted with a tissue paper. Uranyl acetate (1% w/v) was added to the grid and TEM images were taken using FEI CM129 BioTwin transmission electron microscope (Phillips, Eindoven, Netherlands) and AMI digital camera.

2.5.3.3 Size characterization using Dynamic Light Scattering (DLS)

For DLS (Malvern Zetasizer Nano ZS ZEN3600, Malvern Instruments Ltd, Worcestershire, UK) size measurement, 1 mL of GCPQ B2 nanoparticles in respective medium was dispensed into a low volume disposable cuvette and three measurements were taken per sample. The Z-average, polydispersity Index (PDI) and other weighted distributions were recorded.

2.5.3.4 Surface charge using DLS

Zeta potential of GCPQ B2 formulations were determined using DLS (Malvern Zetasizer Nano ZS ZEN3600, Malvern Instruments Ltd, Worcestershire, UK). Formulations (1 mL) were dispensed into a zeta cell and zeta distribution graphs were recorded.

2.5.3.5 Colloidal stability of GCPQ B2 nanoparticle in physiological medium

Medium mimicking physiological conditions, namely simulated intestinal fluid (SIF), SIF with pancreatin, fasted state simulated gastric fluid (FaSSGF), fasted state simulated intestinal fluid (FaSSIF) and fed state simulated intestinal fluid (FeSSIF), were prepared as per biorelevant media guidelines [191] (Table 2-3). The stability of GCPQ nanoparticle (2.5 mg/mL) in the above mentioned mediums were determined after incubation for 0, 0.5, 1, 3 and 6 h by DLS. The intensity and volume-based distributions were used to predict colloidal stability of GCPQ nanoparticle in physiological medium.

Table 2-3 Composition of GI medium

Composition for 500 ml	FaSSGF	FaSSIF-V2	FeSSIF-V2	SIF	SIF with pancreatin
Sodium taurocholate	22 mg	807 mg	2.688 g		
Lecithin	3 mg	30 mg	300 mg		
Sodium monobasic Po4				3.4 g	3.4 g
Acetic acid					
maleic acid		1.11 g	3.193 g		
HCl					
Glycerol Monooleate			891 mg		
Sodium Oleate			122 mg		
NaOH		696 mg	1.633 g	0.3 g	0.3 g
NaCL	999 mg	2.005 g	3.667 g		
Pancreatin			100U/ml		5 g
Pepsin	0.1 mg/ml				
CaCL2			277g		
pH	1.6	6.5	5.8		6.8

2.6 Results

2.6.1 GCPQ Polymer Synthesis and Characterization –

GCPQ polymer (batch 1, 2 and 3) were synthesized and characterized by proton NMR. The peaks were assigned to the respective proton in the GCPQ molecule (Figure 2-7). The area under the curve for the respective palmitoyl and quaternary ammonium group were normalized with the sugar group to calculate palmitoylation and quaternization percentage. The degree of palmitoylation and quaternization calculated for batch 1, 2 and 3 were summarized in Table 2-4.

Table 2-4 Synthesis and Characterization GCPQ polymers

GCPQ batches	Quantity of GC starting material used (g)	Quantity of GCPQ finished product Obtained (g)	Palmitoylation (%)	Quaternization (%)
GCPQ batch 1 (B1) (**Figure 2-8**)	5	3.7	16	14
GCPQ batch 2 (B2) (**Figure 2-9**)	10	6.54	19	12
GCPQ batch 3 (B3) (**Figure 2-10**)	5	3.65	22	8

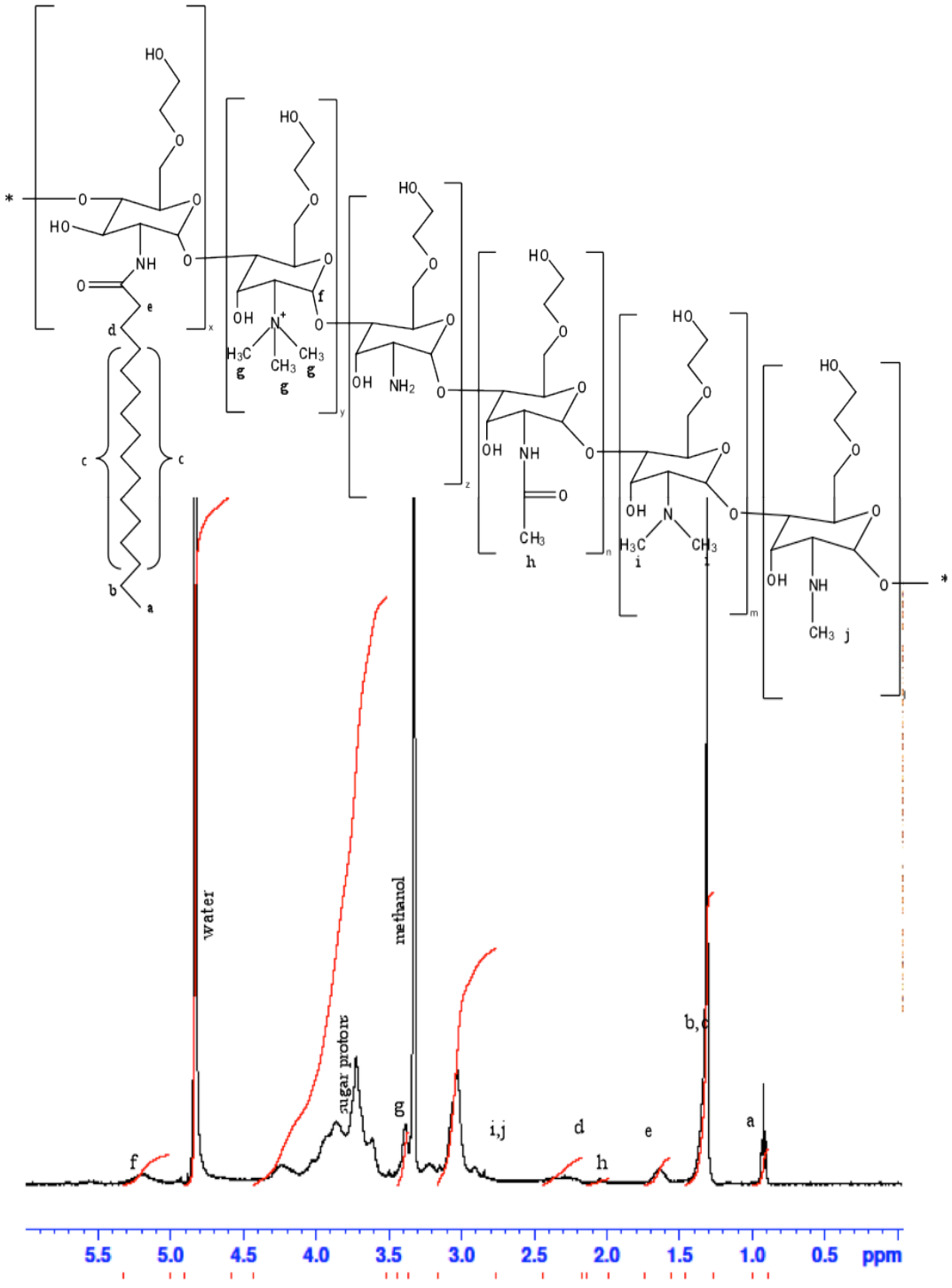

Figure 2-7 H^1 Proton NMR of GCPQ with peaks assigned

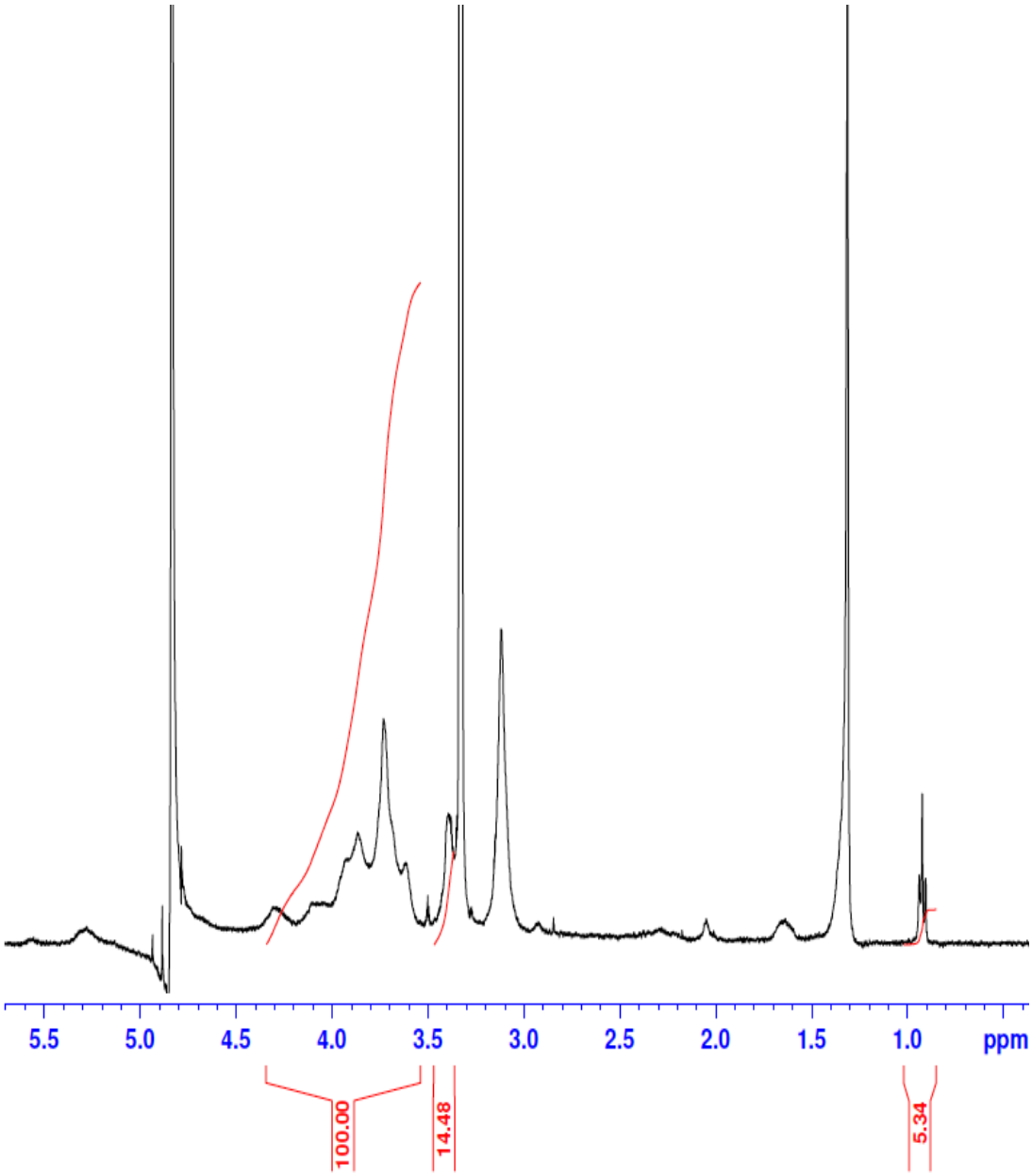

Figure 2-8 H^1 proton NMR of GCPQ batch 1. NMR peak spectrum are integrated for sugar backbone (100), palmitoyl group (5.34) and quaternary ammonium group (14.48)

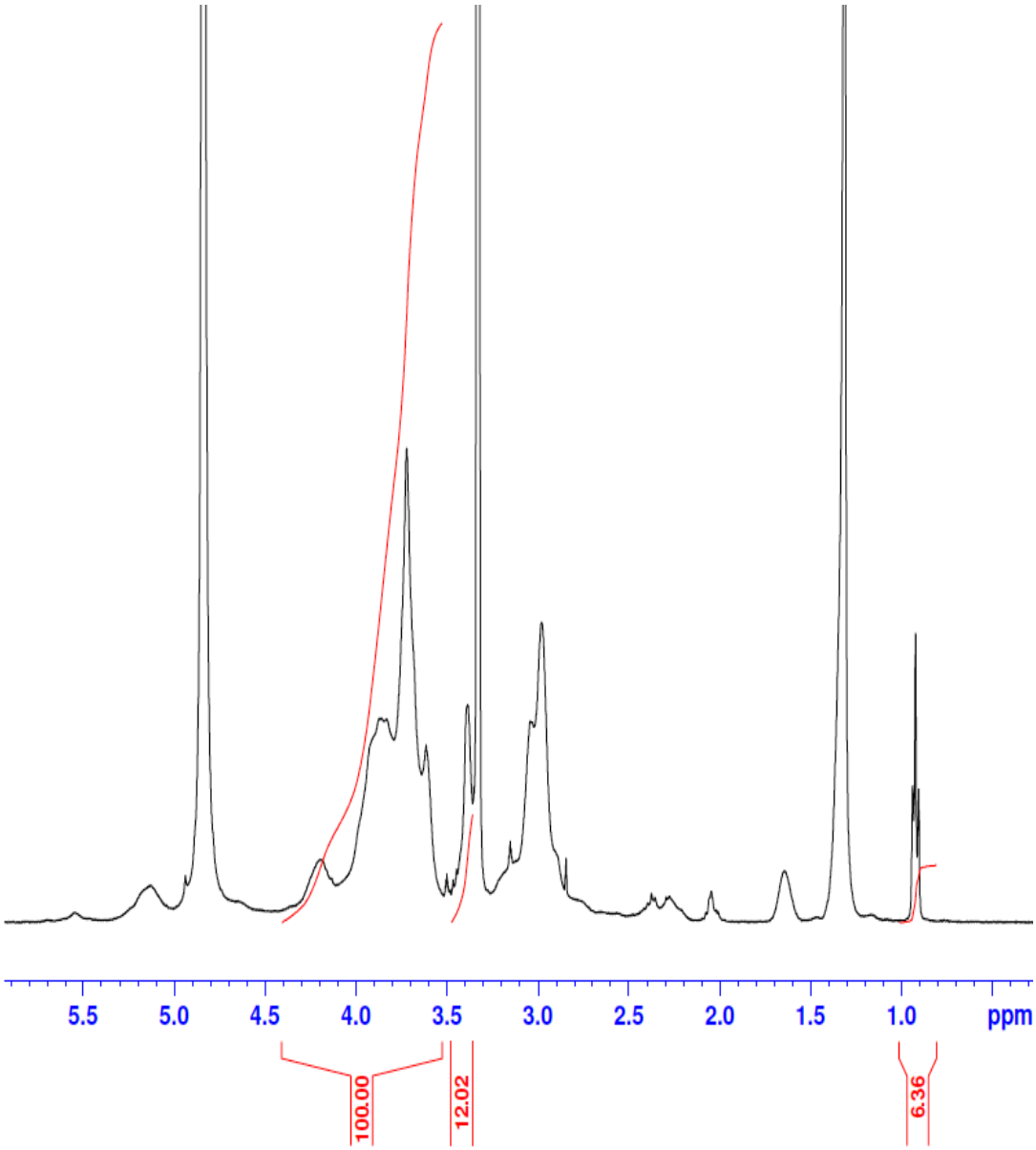

Figure 2-9 H^1 proton NMR of GCPQ batch 2. NMR peak spectrum are integrated for sugar backbone (100), palmitoyl group (6.36) and quaternary ammonium group (12.02).

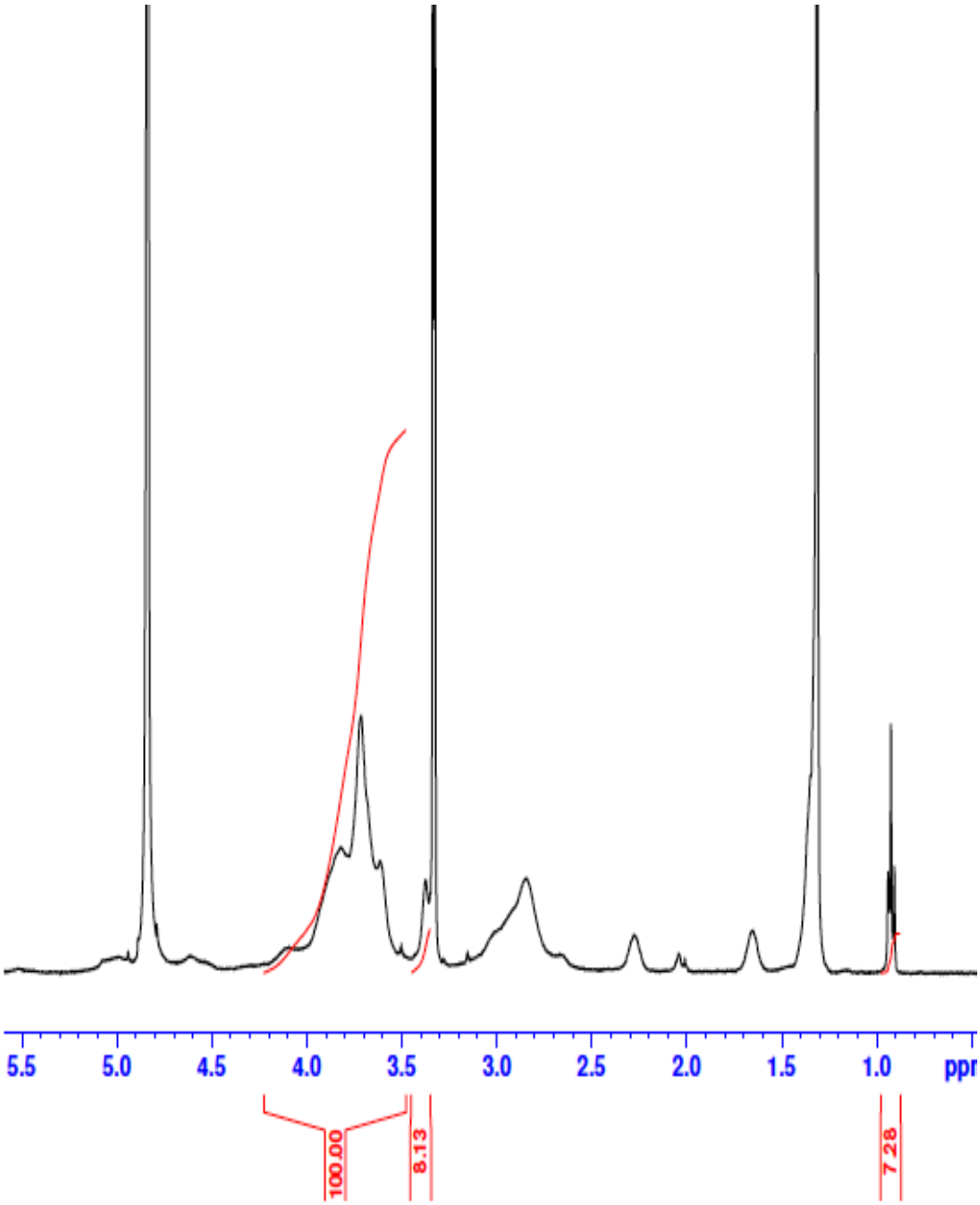

Figure 2-10 H^1 proton NMR of GCPQ batch 3. NMR peak spectrum are integrated for sugar backbone (100), palmitoyl group (8.13) and quaternary ammonium group (7.26).

2.6.2 Molecular weight determination by GPC-MALLS

The molecular weight of GCPQ batch 1, batch 2 and batch 3 determined by GPC-MALLS were 8 kDa, 13 kDa and 33 KDa with polydispersity index 1.221, 1.061 and 2.560 respectively (Table 2-5). The molecular weights of GCPQ batches 1, 2 and 3 are determined from the GPC chromatogram showing time on x-axis and relative intensity on y-axis. Earlier the peak appears on a chromatogram, larger its molecular weight and vice versa. There are three peaks on a GPC chromatogram analysed from three detectors *i.e.* light scattering, quasi-elastic light scattering and refractive index detectors. For GCPQ B1 and B2, peaks were eluted at the same time (Figure 2-11, Figure 2-13) and hence the polydispersity indices were 1.22 and 1.061 for the respective polymers. However, for GCPQ polymer B3, the peak obtained from light scattering detector eluted earlier than the peak from refractive index detector (Figure 2-15). These variations in the elution times of signals obtained from light scattering and refractive index detector can be related to the sensitivity of the detector, with the former measuring signals from multiple angles compared to the later. As a result of different elution times, the molecular weight distribution of GCPQ B3 is large and hence its polydispersity (2.56) was also larger compared to GCPQ B1 and B2. Quasi-elastic light scattering detector produced poor signal for GCPQ B3 due to detector malfunction.

Table 2-5 Molecular weight determination by GPC-MALLS

Parameters	**GCPQ batch 1 (Figure 2-11, Figure 2-12)**	**GCPQ batch 2 (Figure 2-13, Figure 2-14)**	**GCPQ batch 3 (Figure 2-15, Figure 2-16)**
Polydispersity index Mw/Mn	1.221	1.061	2.560
Number average molecular weight Mn (g/mol)	$8.804e^{+3}$	$1.328e^{+4}$	$3.389e^{+4}$
Weight average molecular weight Mw (g/mol)	$1.075e^{+4}$	$1.251e^{+4}$	$8.675e^{+4}$
dn/dc (mL/g)	0.1601 ± 0.0083	0.1735 ± 0.0060	0.1733 ± 0.192
R^2	0.989393	0.997780	0.996695

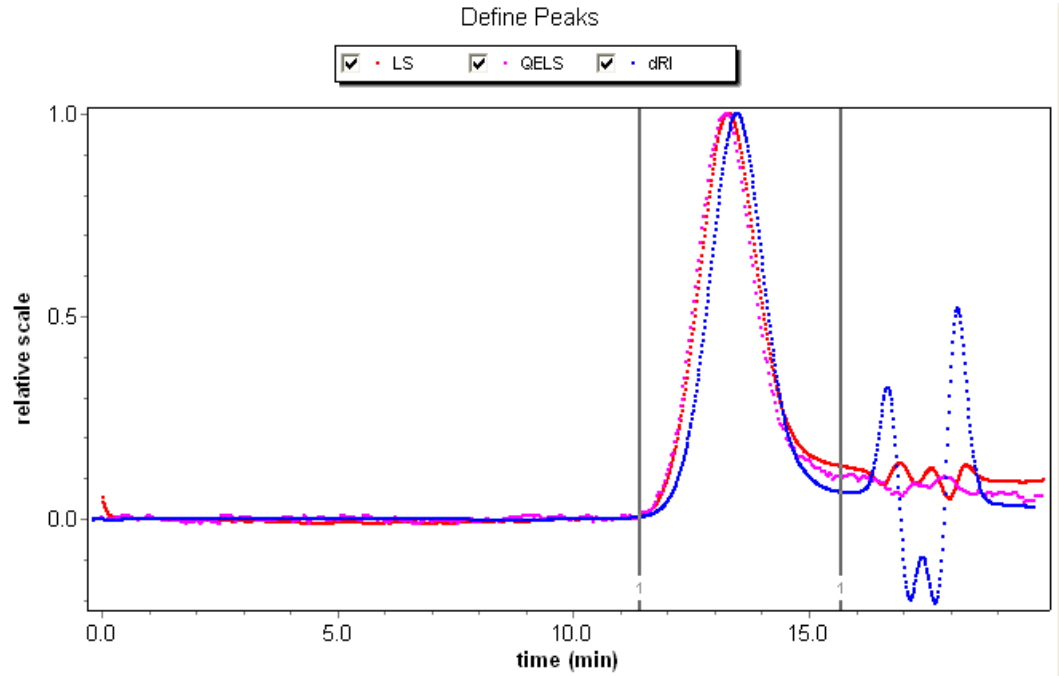

Figure 2-11 GPC chromatogram for GCPQ batch 1 analysed by different detector [Light scattering (LS) in red, Quasi elastic light scattering (QELS) in pink and dRI in blue]. Signals obtained from different detectors were eluted at the same time.

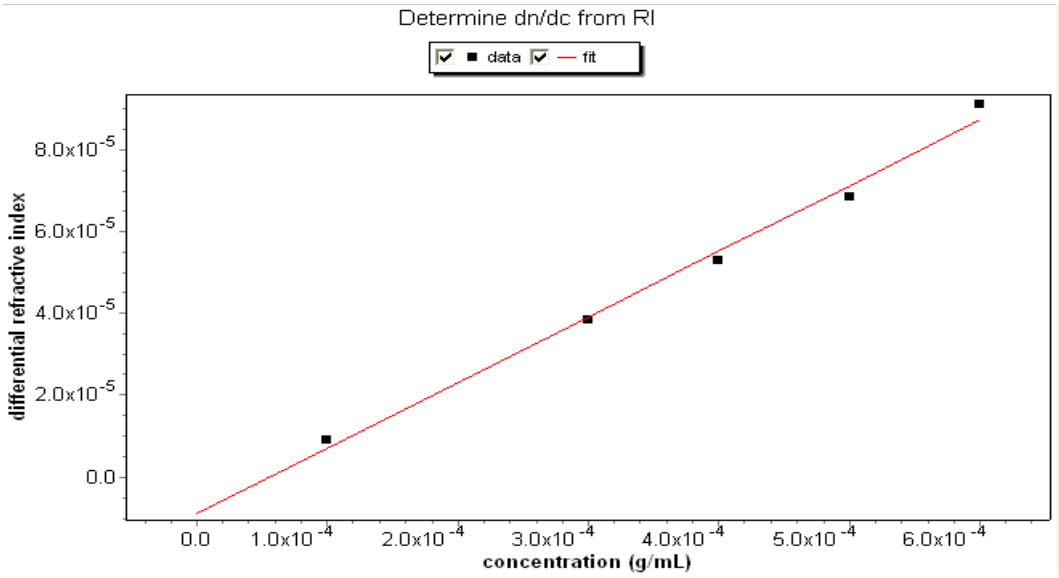

Figure 2-12 Determination of dn/dn from RI - GCPQ batch 1. Graph showing various concentrations of GCPQ (0.1 mg/mL to 0.6 mg/mL) on X-axis plotted against their respective dRI value on the Y-axis.

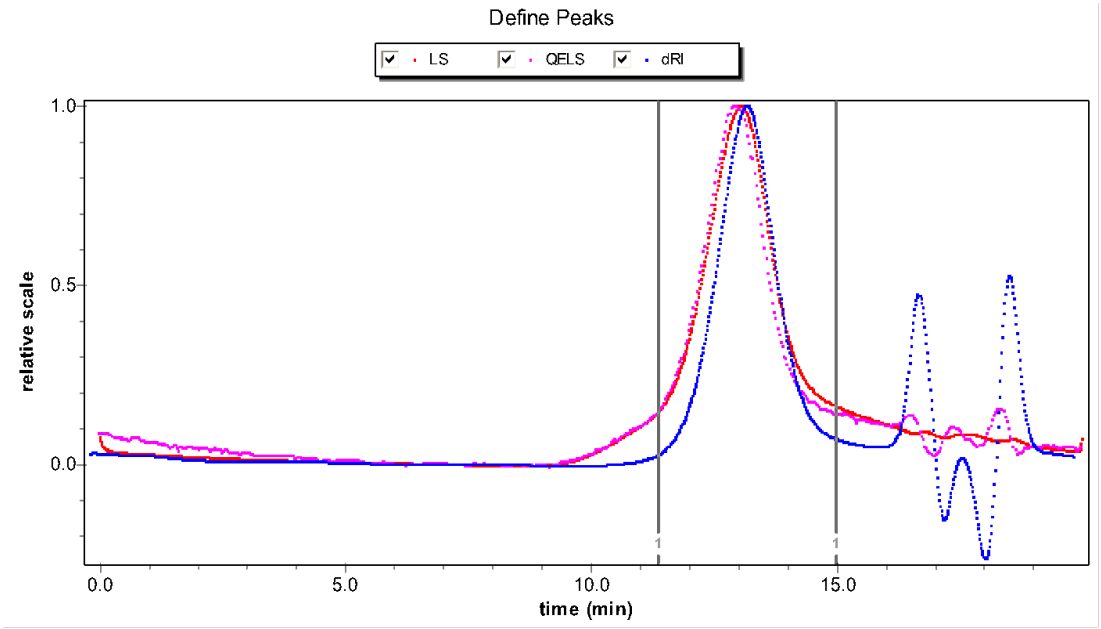

Figure 2-13 GPC chromatogram for GCPQ batch 2 analysed by different detector [Light scattering (LS) in red, quasi elastic light scattering (QELS) in pink and dRI in blue]. Signals obtained from different detectors were eluted at the same time.

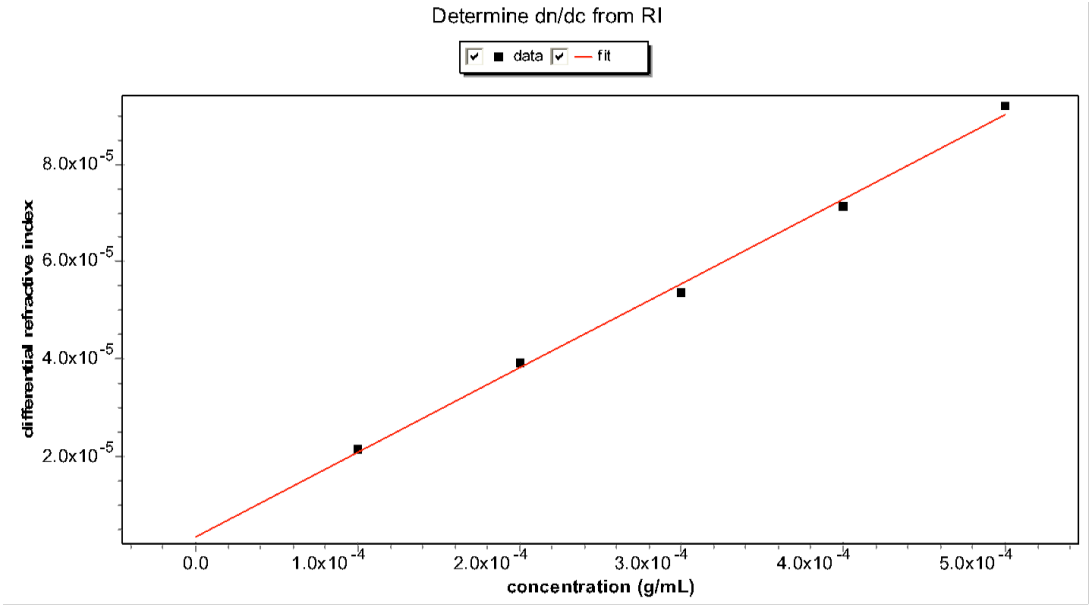

Figure 2-14 Determination of dn/dc from RI for GCPQ batch 2. Graph showing various concentrations of GCPQ (0.1 mg/mL to 0.5 mg/mL) on X-axis plotted against their respective dRI value on the Y-axis.

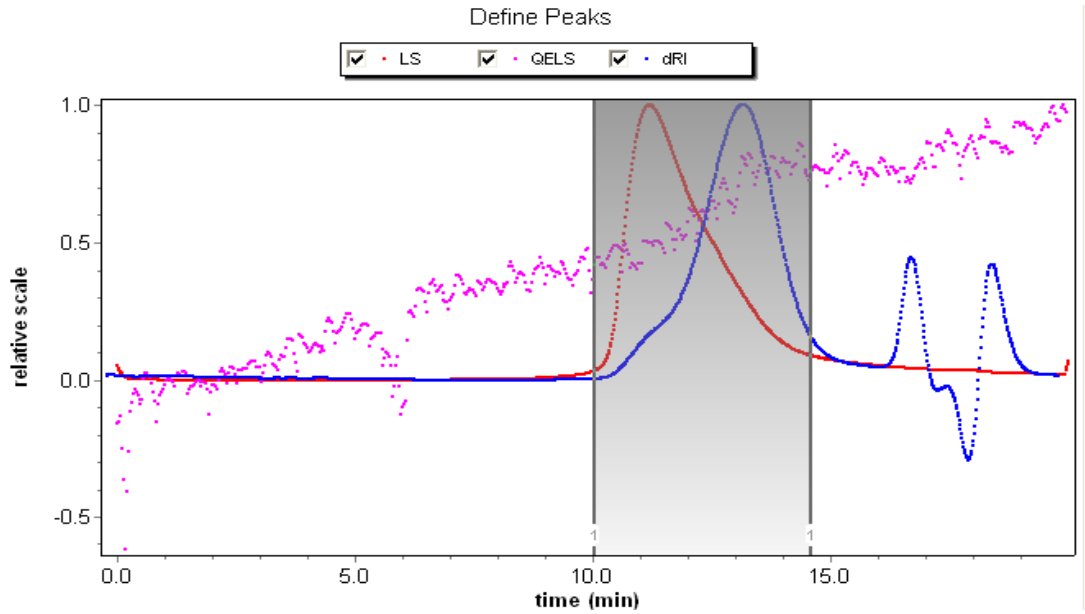

Figure 2-15 GPC chromatogram for GCPQ batch 3 analysed by different detector [Light scattering (LS) in red, Quasi elastic light scattering (QELS) in pink and dRI in blue]. Signal obtained from light scattering detector had elution time earlier than the signal obtained in dRI detector. QELS detector did not show stable peak due to detector malfunction.

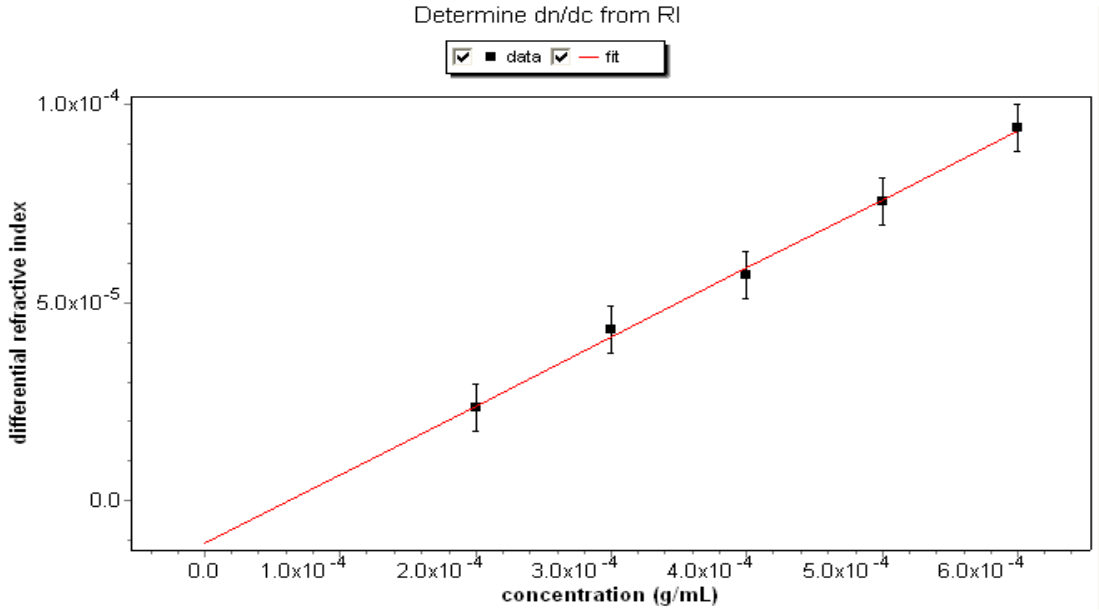

Figure 2-16 Determination of dn/dn from RI - GCPQ batch 3. Graph showing various concentrations of GCPQ (0.1 mg/mL to 0.6 mg/mL) on X-axis plotted against their respective dRI value on the Y-axis.

The effect of probe sonication on the molecular weight of GCPQ was also determined. GCPQ probe sonicated for 20 min at 15 amps did not affect the molecular weight of GCPQ. The results are shown in Figure 2-17.

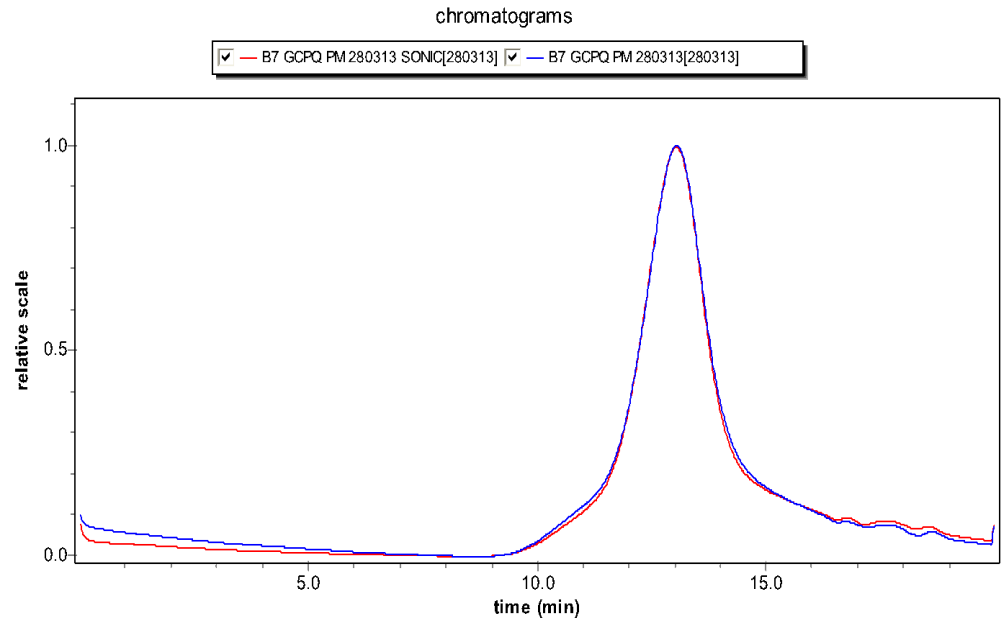

Figure 2-17 Effect of probe sonication on the molecular weight of GCPQ batch 2. Chromatogram showing GCPQ before (blue) and after probe sonication (red).

2.6.3 GCPQ B2 Nanoparticle Preparation and Characterization

GCPQ was made in to a suspension in water and different concentrations of NaCl solutions. The formulations were vortexed until homogeneous suspensions were obtained. The effects of various NaCl concentrations on the size of GCPQ particles were characterized by DLS.

2.6.3.1 Influence of salt on GCPQ B2 suspension

GCPQ polymeric micelles were prepared by dispersion of the polymer in an aqueous medium. GCPQ self-assembles to form micelles in water. The average sizes of GCPQ micelles were larger in water (406 nm) and smaller for GCPQ in NaCl concentrations from 10 mM to 300 mM (Figure 2-18). The sizes of GCPQ micelles observed were inversely proportional to the concentrations of NaCl in the GCPQ suspensions.

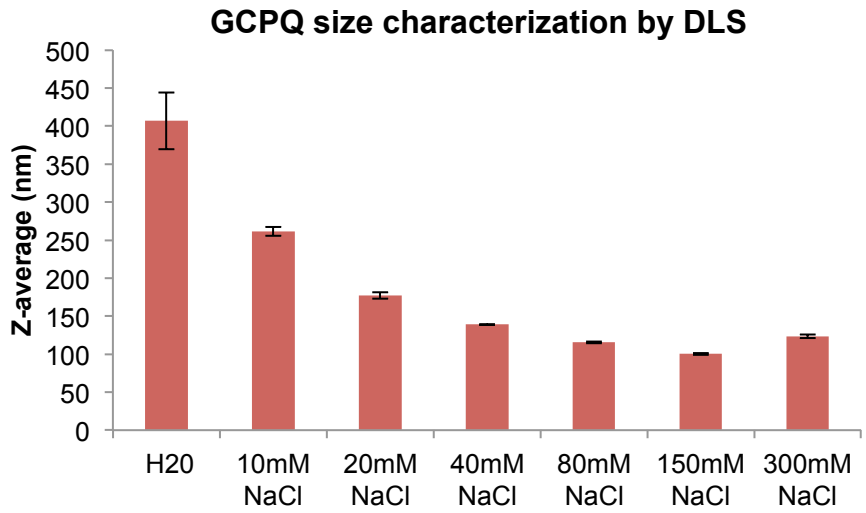

Figure 2-18 Particle size characterization of GCPQ B2 by DLS. Z-average of GCPQ (2.5 mg/mL) prepared in water and NaCl concentrations ranging from 10 mM to 300 nm

The size distribution by number (Table 2-6) suggest that GCPQ (2.5 mg/mL) in water had two populations with sizes around 303 nm and 817.9 nm that constituted 59.9% and 40.1% of the total population. However, for GCPQ in NaCl suspension (10 mM), the large sized population around size 986.9 nm constituted around 12.9% of the total population and the small sized population around size 197.8 nm constituted 87.1% of the total population. With the increase in NaCl concentration (20 mM) in GCPQ suspension, only one population of size around 72.6 nm was observed. The sizes of GCPQ micelles were smaller (12.5 nm and 11.8 nm) when prepared in NaCl solution

(40 mM and 80 mM). These results suggest that with increase in the concentration of NaCL (10 mM to 80 mM), size reduction of GCPQ micelles from 400 nm to 11.8 nm were observed. However, at NaCl concentrations 150 nm and 300 nm, the sizes of GCPQ micelles increased again to 16.7 nm and 26 nm.

Table 2-6 DLS- Peak analysis using number based distribution of GCPQ suspension in water and NaCl solution of different concentrations.

GCPQ in various suspensions	Population 1		Population 2	
	Mean size (nm)	Area (%)	Mean size (nm)	Area (%)
H_20	303.1	59.9	817.9	40.1
10 mM NaCl	197.8	87.1	986.9	12.9
20 mM NaCl	72.6	99	-	-
40 mM NaCl	12.5	99.8	-	-
80 mM NaCl	11.8	100	-	-
150 mM NaCl	16.7	100	-	-
300 mM NaCl	26	100	-	-

Polydispersity of the GCPQ formulations in water and NaCl solution (10 to 80 mM) at a concentration of 2.5 mg/mL were around one (Figure 2-19). For GCPQ in water and NaCl solution at 10 mM concentration, two population sizes can be observed (Table 2-6) and hence their PDI were 1. For GCPQ in NaCl solution (20 mM and 40 mM), although only one size population was observed (Table 2-6) the PDI was still 1. This could be due to artifacts present in the sample itself having a micellar population of area 99% (Table 2-6). However, the PDI dropped to 0.963, 0.8 and 0.78 for GCPQ in NaCl solution 80 mM, 150 mM and 300 mM. This drop in PDI was observed only for GCPQ suspensions that have single micellar population of area 100%. (Table 2-6).

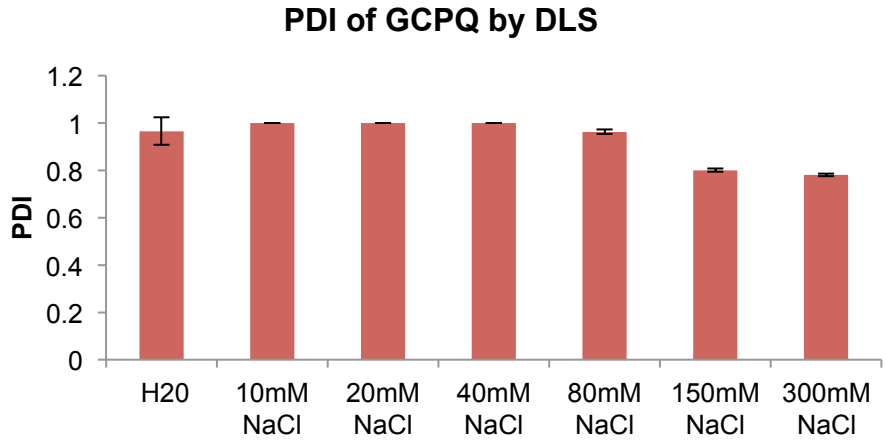

Figure 2-19 Particle size characterization of GCPQ B2 (2.5 mg/mL in water and salt concentrations) by DLS – PDI

2.6.3.2 GCPQ B2 formulation after probe sonication

GCPQ B2 formulation was prepared in water (2.5 mg/mL) and probe sonicated at 15 amps for 15 min. The sizes of micelles observed were smaller (67.7 nm) with low PDI (0.269) compared to GCPQ B2 prepared as suspension (size - 400 nm and PDI -1) without probe sonication (Figure 2-20). These small sizes were due to the disruption of large micellar clusters during sonication process yielding more homogeneous micelles with low PDI.

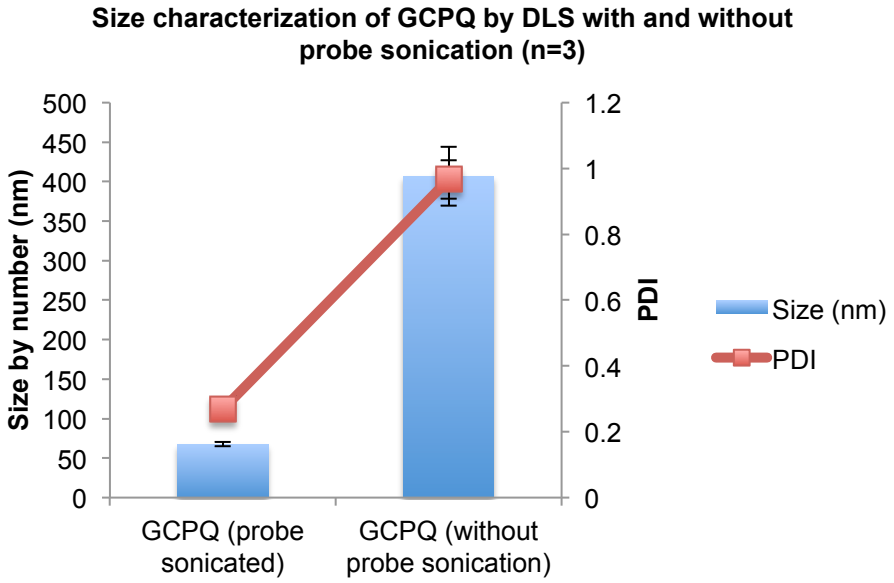

Figure 2-20 Size characterization of GCPQ B2 by DLS with and without probe sonication showing size distribution by number (blue) and PDI (red).

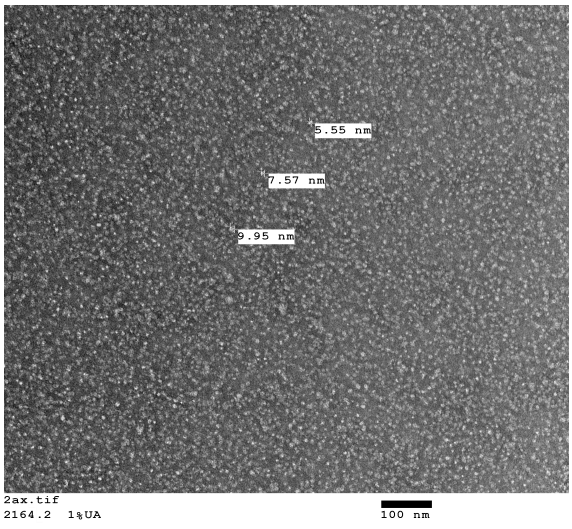

Figure 2-21 TEM of GCPQ B2 micelles (2.5 mg/mL) in water showing particles sizes around 10 nm.

Transmission electron microscopic image of GCPQ B2 micelles show sizes of approximately 10 nm (Figure 2-21). Although TEM images are not quantitative,

the majority of the size distribution was smaller than the results obtained by DLS. This could be due to two reasons:

Micelles in suspension have different surface properties than those on a dried grid (Figure 2-22).

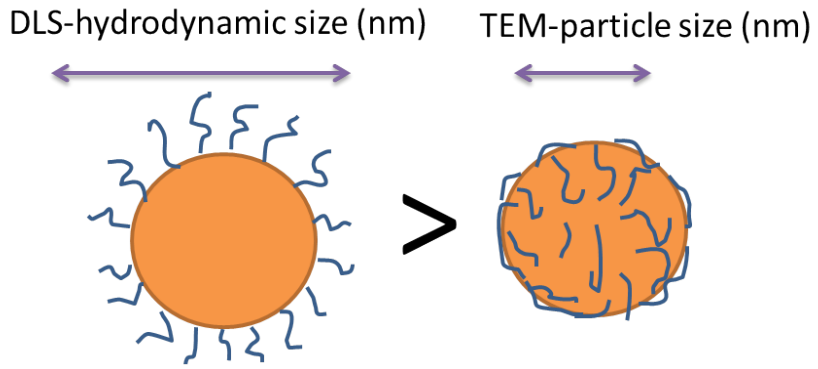

Figure 2-22 Schematic representation of possible impact of DLS and TEM on micelle image

Size obtained from intensity-based distribution could represent an over estimated value, even if a small proportion of large aggregates are present in the nanoparticle suspension.

2.6.3.3 Characterization of surface charge of GCPQ B2

The surface charge of GCPQ B2 was characterized by DLS (Figure 2-26). GCPQ at pH 4.3 has the most positive zeta potential (+50 mV) (Figure 2-23), which reduced with increase in pH to 7 and 9 to + 25.2 (Figure 2-24) and +14.5 mV (Figure 2-25). De-protonation of primary and secondary amines in the GCPQ polymer occurs at higher pH leading to decrease in the surface charge of GCPQ micelles.

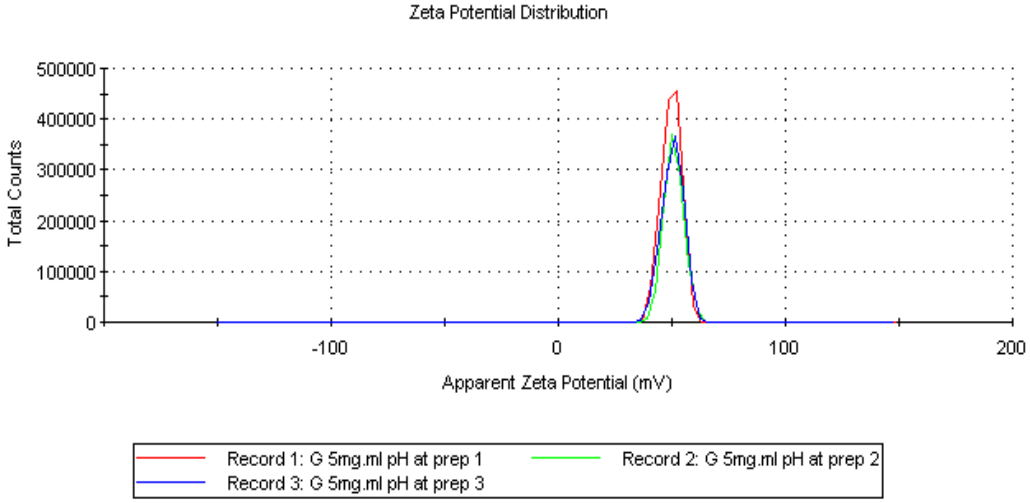

Figure 2-23 Zeta potential distribution of GCPQ B2 (2.5 mg/mL) in water at pH 4.3

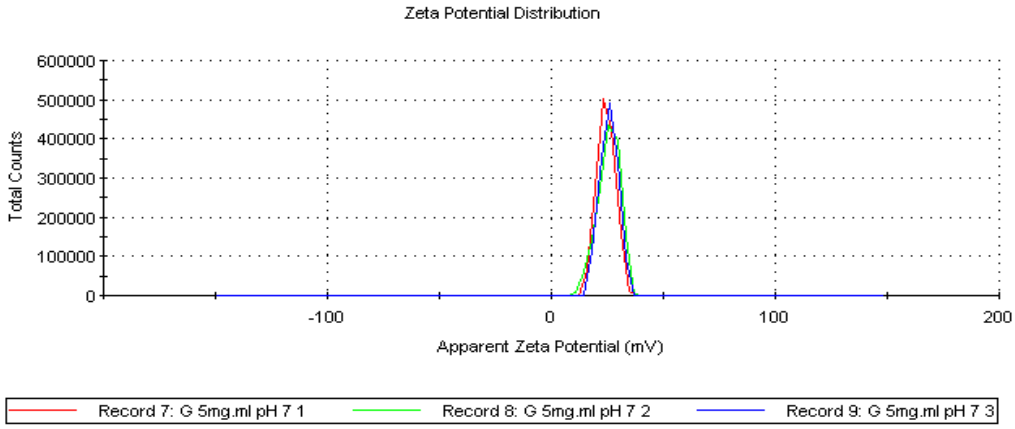

Figure 2-24 Zeta potential distribution of GCPQ B2 (2.5 mg/mL) in water at pH 7

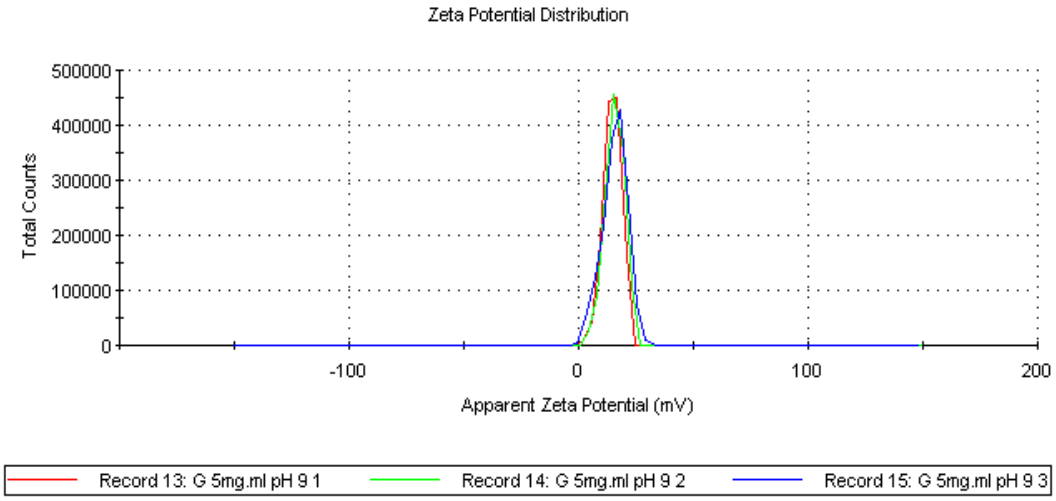

Figure 2-25 Zeta potential distribution of GCPQ B2 (2.5 mg/mL) in water at pH 9

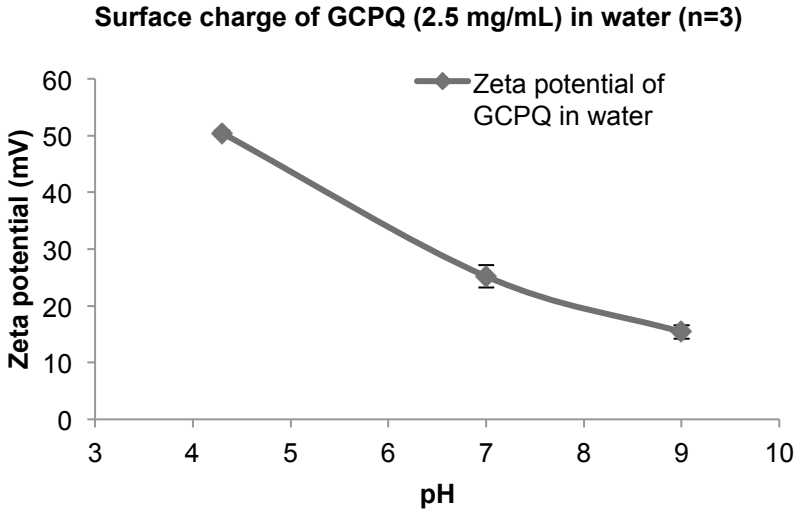

Figure 2-26 Surface charge of GCPQ B2 (2.5 mg/mL) in water analysed by DLS. Graph showing GCPQ prepared at a concentration of 2.5 mg/mL in water at different pH plotted against their zeta potential values.

2.6.4 Colloidal stability of GCPQ B2 nanoparticle in physiological medium

Determination of the colloidal stability of GCPQ B2 micelles in physiological medium is important to understand the interaction of GCPQ B2 micelles with the GI contents after oral administration.

In simple medium (Figure 2-27), SIF with and without pancreatin, the GCPQ micelles was stable at different time points indicating that pancreatin is not causing aggregation of GCPQ micelles.

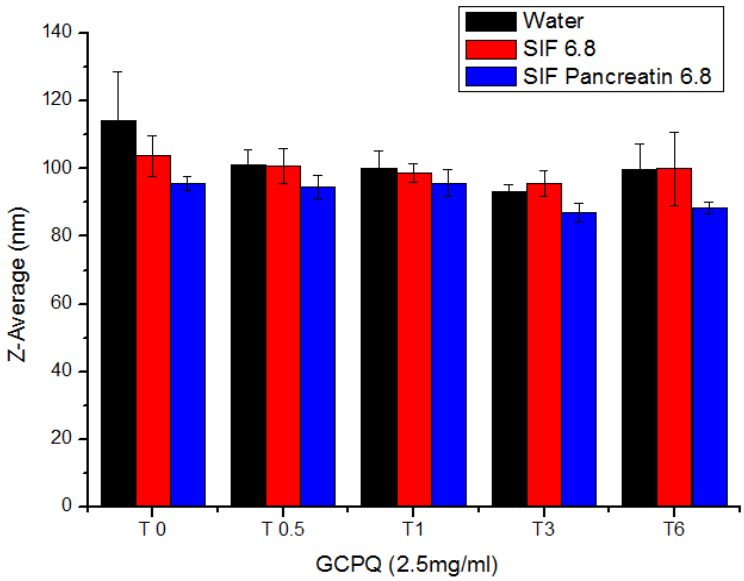

Figure 2-27 Stability of GCPQ micelles (2.5 mg/mL) in simple medium (SIF with and without pancreatin) incubated and measured at a temperature of 37˚C for time points 0, 0.5 h, 1, 3 and 6 h.

The above results were compared with more complex medium (FaSSGF, FaSSIF, FeSSIF with pancreatin) (Figure 2-28). The Z-Average result shows aggregation of GCPQ micelles over time in FaSSIF and FeSSIF. When compared with volume-based distribution (Figure 2-29), one could infer that large aggregates do exist, but that these aggregates account for less than 1% of the total population. An example comparing intensity and volume-based distribution is shown in Figure 2-29. It could also be observed that a decrease in micelle size from time 3 h to time 6 h for GCPQ incubated in FaSSIF and FeSSIF. This could be an indication that some micelles that have aggregated at time 3 h (T3) formed sediments at time 6 h (T6).

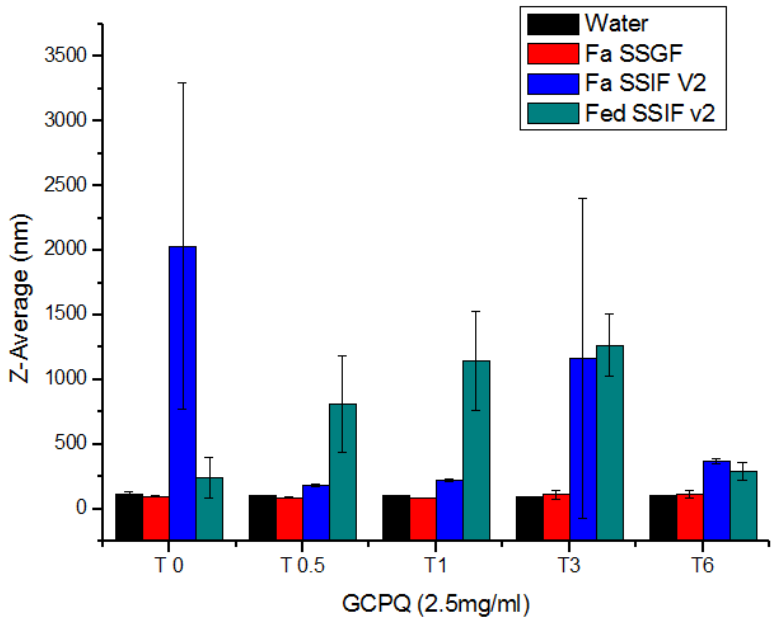

Figure 2-28 Stability of GCPQ nanoparticle in complex medium (Fa SSGF, Fa SSIF V2, Fed SSIF V2) incubated and measured at a temperature of 37˚C for time points 0, 0.5 h, 1, 3 and 6 h.

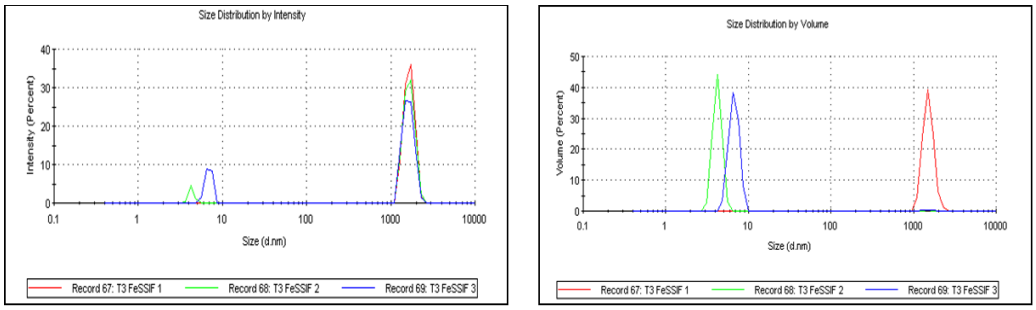

	Size (d.nm):	% Intensity:	St Dev (d.nm):
Peak 1:	1626	81.4	244.9
Peak 2:	6.890	18.6	0.6145
Peak 3:	0.000	0.0	0.000

	Size (d.nm):	% Volume:	St Dev (d.nm):
Peak 1:	1497	0.8	229.2
Peak 2:	6.752	99.2	0.9486
Peak 3:	0.000	0.0	0.000

Figure 2-29 Comparison of size distribution by intensity (left) and volume (right).

The results obtained from the colloidal stability data shows that the GCPQ micelles at pH 7 are stable for 3 h in simple and complex GI medium.

2.7 Discussion

Glycol chitosan is a water-soluble chitosan derivative used as a starting material for polymer synthesis. In this study, an amphiphilic derivative of glycol chitosan consisting of hydrophobic palmitoyl group and hydrophilic quaternary ammonium group were synthesized. Polymer modification with hydrophobic group induces self-assembly in an aqueous solution through inter and intra chain interaction. Glycol chitosan modified with hydrophobic moiety such as cholanic acid [192], fluorescein isothiocyanate (FITC)[193] , N-acetyl-histidine [194] and bile acid [180] were previously reported to have application in drug delivery. Polymer hydrophobicity has influence on particle aggregation and hence its critical micellar concentration [195]. Lower the CMC of a polymer; better its stability upon dilution in the gastro-intestinal tract. This implies that a polymer with low CMC has the tendency to retain encapsulated material at lower concentration compared to a polymer with high CMC. The CMC of GCPQ reported previously was 0.23 μg/mL for a GCPQ with palmitoylation percentage of 16% [146]. The CMC of other hydrophobically modified glycol chitosan derivatives was reported to be much high than GCPQ, with 38 - 260 μg/mL for glycol chitosan-bile acid [180] and 47 -219 μg/mL for glycol chitosan-cholanic acid [192]. The palmitoylation percentage of GCPQ reported in this study were 16% (GCPQ batch 1), 19% (GCPQ batch 2) and 22% (GCPQ batch 3) (Table 2-4).

Another key factor that affects the colloidal stability of GCPQ is its modification by quaternization. Chitosan of poor solubility was previously reported to have been quaternized to improve the solubility of a polymer at any given pH [196]. Quaternization also enhances the mucoadhesive property of chitosan-derived polymers [197]. The quaternization percentage for GCPQ polymer batch 1, 2 and 3 was 12%, 14 % and 8% (Table 2-4).

GCPQ B1 and GCPQ B2 prepared by old method had palmitoylation and quaterization of 16% and 14% and 19 % and 12%. Their molecular weight analysed by GPC-MALLS were 10 and 12 kDa with polydispersity of 1.221 and 1.061 (Table 2-4). New method of GCPQ synthesis was adopted in order to be able to control the palmitoylation reaction by using molar ratio of GC to palmitic acid N-hydroxysuccinimide. The GCPQ batch 3 produced by new method had Mw and Mn of 86.5 kDa and 34.5 kDa and PDI of 2.5 with palmitoylation and quaternization of 22% and 8 % respectively (Table 2-4).

While analyzing GCPQ in GPC-MALLS, the polymer was dissolved in a mobile phase composing of methanol and acetate buffer at ratio 65:35 due to its solubility in the respective solvent mixture [198]. It was expected that the GCPQ polymer get completely dissolved in the respectively mobile phase. However, GCPQ B3 formed aggregates (as seen from GPC results) in the respective mobile phase, as it has 22% palmitoylation that was higher than the palmitolyation of GCPQ B1 and B2 and 8% quaternization that was lower than the quaternization of GCPQ B1 and B2. Also, when using solvents such as DMSO (new method) the PGC remains soluble throughout the reaction. However, when using ethanol and water for palmitoylation reaction, the solubility of PGC reduces resulting in formation of white foam during the course of reaction. This changes the way palmitoyl chains are added on to GC polymer between the two methods of synthesis.

This could have resulted in polymer aggregation via intermolecular hydrogen bonding in methanol and acetate buffer (65:35) and hence the peak eluted from GPC column was observed at earlier time points. In order to confirm the hypothesis, the GCPQ polymer B3 could be dissolved in a mobile phase that has organic phase percentage higher than 65% methanol and analysed by GPC MALLS. Any shift in the peak could verify the hypothesis that this increase in the polydispersity index of the polymer is due to intermolecular association between polymers.

When polymers undergo intermolecular interaction in their respective solvent, the results obtained from GPC MALLS are unreliable. The GPC MALLS calculate molecular weight under an assumption that under dilute conditions intermolecular association does not exist. In this study, since there could be a possibility of intermolecular association, GPC MALLS could have resulted in an overestimated size (Mw- 86 kDa) for GCPQ B3.

GCPQ B2 was used for characterization of the polymer. The effect of sonication on the molecular weight of GCPQ was tested. Previous report has mentioned that the temperature and sonication time has effect on the molecular weight of the chitosan polymer. Azar et al previously reported that sonication time (10 to 120 min) and temperature (20˚C, 40˚C and 60˚C) decreases the molecular weight of the chitosan polymer [199]. Chitosan polymer sonicated for at least 10 min at 20˚C resulted in decrease in the molecular weight of the polymer from 3.8E+06 Da to 3.4E+06 Da. Savitri et al has used probe sonication to degrade chitosan under mild acetic acid conditions (0.2 to 1% v/v) with pH ranging from 3.2

to 4.8 at accelerated temperatures (40˚C and 60˚C) [200]. For GCPQ probe sonicated in the presence of ice for 20 min, no changes in the molecular weight was observed as compared to the molecular weight of the GCPQ polymer without probe sonication (Figure 2-17).

GCPQ oral formulations were previously made by adding the GCPQ along with drug (propofol [201] cyclosporine [146], LENK [198]) in water followed by probe sonication. GCPQ was also formulated with amphotericin by formation of polyelectrolyte complexes. The drug was prepared in basic condition and added to GCPQ, where the carboxylate salts of amphotericin interact with positively charged GCPQ to form nanoparticles [153]. For intravenous formulations, GCPQ and the drug (TP LENK - LENK ester prodrug – tyrosinyl^{1}palmitate-leucine^{5}-enkephalin) was prepared in 0.9% sodium chloride solution [162]. However, the characterization results of GCPQ without drug in water and sodium chloride solutions were not compared. In this study, GCPQ was prepared in water and sodium chloride solutions of different concentrations (10 to 300 mM) and the results were characterized using TEM and DLS. The GCPQ in water suspension was also compared before and after probe sonication.

GCPQ micelles measured to 20 nm in TEM (Figure 2-21), as the image was recorded after vacuum drying. However, the micelles in aqueous suspension measured up to 400 nm (Figure 2-18) with a polydispersity index of 0.9 (Figure 2-19).

For the first time we have reported that the sizes of the micellar clusters were found to be reducing with the increase in the NaCl concentrations in the aqueous medium (Figure 2-18). The DLS results suggest that with the introduction of NaCl in GCPQ-water suspension and with increase in the concentration of NaCL (10 mM to 80 mM), GCPQ micelle sizes reduced from 400 nm to 11.8 nm. These phenomena can be investigated in the future to understand the behavior of GCPQ in suspensions. Also, it was observed that there was a marginal increase in the GCPQ particle size at NaCl concentrations 150 nm and 300 nm. Further increase NaCl concentration is necessary to confirm this observation. These observations are contradictory to previously reported observations for the effect of salt on nanoparticles. Where, it was described that the like charged nanoparticles exhibited stability due to steric or electrostatic repulsion between the particles. However, in the presence of salt, the charges on surface of the nanoparticles were altered leading to instability and agglomeration [202-204].

GCPQ suspension prepared in water after probe sonication, resulted in a homogeneous population of micelles of 69 nm with PDI of 0.269 (Figure 2-20). This shows that probe sonication is essential for obtaining uniform sized particles.

The surface properties of GCPQ can greatly influence its interaction with proteins present in the luminal contents. The surface charge of GCPQ B2 was measured from the zeta potential obtained from DLS analysis at different values of pH. At lower pH (4.3), the zeta potential is highly positive (+50 mV) and it decreases to +25.2 mV at pH 7 and +14.5 mV at pH (9) (Figure 2-26). This trend is due to the neutralization of amines in the GCPQ polymer. This high positive surface charge is contributed by quaternary ammonium group of glycol chitosan that remains charged at alkaline pH. The surface charges of chitosan at pH 7 of different molecular weights (3.3 kDa to 29 kDa) were only between +4.10mV to +1.3mV. The surface charge becomes negative with increase in the molecular weight of chitosan above 29 kDa [205].

The colloidal stability of GCPQ was also measured in simulated gastric and intestinal medium. Incubation of GCPQ in simulated medium (simple SIF with and with out pancreatin) did not affect the stability of the micelles as analysed until 6 h (Figure 2-27). However, there was a fraction (< 1%) of GCPQ micelles that aggregated in FaSSIF and FeSSIF indicating that bile components can interact with GCPQ micelles (Figure 2-28,Figure 2-29). Previously, Garrett et al observed GCPQ in bile and gall bladder through in vivo imaging technique. From this results it was also hypothesized that GCPQ could be recirculated via bile in to the small intestine [160]. This study supports the above hypothesis that, GCPQ can interact with bile components through which micelles can recirculate between gall bladder and intestine. Previously, the role bile salts as co-surfactants has been studied to enhance the gastro intestinal residence time and oral bioavailability of drugs with carriers such as liposomes and surfactants [206-208]. Understand the role of bile components in enhancing the oral absorption of drug loaded GCPQ micelles could be investigated in the future for optimizing its oral bioavailability.

3 Delivery of Labyrinthopeptin for Chronic Pain treatment

3.1 Objective

The objective of this chapter is to,

1. Formulate Labyrinthopeptin using GCPQ (B1, B2 and B3) and glycofural formulation for oral and intranasal delivery.
2. Characterize and compare the colloidal stability of Laby GCPQ (B1, B2 and B3) formulations made from different batches of GCPQ in SGF, SIF and HBSS.
3. Evaluate the pharmacodynamics of Laby GCPQ B2 and Laby glycofural following oral and nasal formulations in CFA pain model in rats.
4. Validate method for quantification of Laby by LCMS-QQQ
5. Evaluate the pharmacokinetics of Laby GCPQ (B1 and B3) and Laby glycofural formulations.

3.2 Introduction

International Association for the Study of Pain (IASP) defines pain "as an unpleasant sensory or emotional experience resulting from actual or potential tissue damage" [209]. Chronic pain is any pain lasting for more than 12 weeks and persisting for months or longer. The nature of chronic pain can be the result of a physical injury, post surgical pain, or associated with other illness such as arthritis, cancer or diabetes. In case of arthritis, chronic pain lasts until the underlying problem of the disease, such as inflammation, persists [210]. In some cases, chronic pain is neuropathic; a condition where damage to the nerve that transmits pain can cause irreversible pain even after the condition has healed, where, there is no damage to the tissue.

Several pathophysiological and histopathological steps are involved during transition from acute to chronic pain [211]. In acute pain, noxious stimuli are transduced to the dorsal horn of the spinal cord. Here, amino acid and peptide transmitters activate second-order neurones, which then transmit signals to the brain. The pain diminishes as healing progresses followed by reduction in sensation of pain until no pain is detected. A long lasting pain can change the way in which brain and spinal cord perceives signal that results in severe pain with no or little stimulus [212]. When persistent pain occurs, secondary mechanisms are triggered [211].

These include upregulation of cyclo-oxygenase-2, interleukin-1beta sensitizing first order neurones, which further sensitize second order neurones by activation of N-methyl-D-aspartic acid channels and signaling microglia to alter neuronal cytoarchitecture. Throughout these processes, prostaglandins, endocannabinoids, ion-specific channels and scavenger cells play a role in the transformation of acute to chronic pain. These mechanisms occurring in peripheral and central nervous system causes allodynia, hyperalgesia and hyperpathia that can diminish normal functioning [211].

Chronic pain has negative implication on the quality of life. In UK alone the prevalence of severe chronic pain is 11% in adults and 8% in children [213]. The treatment plan for chronic pain is a fragmented approach as pain threshold level is subjective from patient to patient. The most commonly used medication for chronic pain management falls into one of the categories Table 3-1: a) non-steroidal anti-inflammatory drugs, b) antidepressants, c) anticonvulsants and d) opioids.

Table 3-1 Drugs for Chronic pain treatment

S.NO	Classification	Treatment	Side effects
1	Non steroidal Anti-inflammatory Drugs and Acetaminophen (NSAIDS)	**COX inhibitors** –arthritis [214]	Affects kidneys, clotting of blood and gastrointestinal system. Long-term use is associated with cardiovascular risks.
2	Antidepressants	**Tricyclic antidepressant** – peripheral neuropathic pain [215]	Sedation
3	Anticonvulsants	**Pregabalin** – postherpetic neuralgia, diabetic peripheral neuropathy and fibromyalgia [216] **Gabapentin** – Low back pain, chronic pelvic pain [217] **Carbamazepine** and **oxcarbazepine** – trigeminal neuralgia [218]	Drowsiness and weight gain
4	Opioids	**Fentanyl, morphine, oxycodone** – moderate to severe chronic pain [219]	Constipation, drowsiness and nausea

The side effects of above-mentioned drugs are due their distribution in non-target sites. Drug delivery strategies are used in pain therapy to increase drug load, reduce toxicity, increase bioavailability, prolong pharmacological effects and target delivery to specific sites. Nanomedicines provide unique approaches to these changes. Examples of nano carriers used for pain treatment and their advantages are summarised in the Table 3-2.

Table 3-2 Nanocarriers used for pain therapies

Drugs	**Nano carrier**	**Delivery route**	**Advantage**
Opioids (Endomorphin-1) **[220]**	Polysorbate 80-coated nanoparticles	IV	• Enhance penetration across blood brain barrier
Opioids (palmitoyl Leu-Enkephalin) **[53]**	GCPQ nanoparticles	Oral	• Increased stability in the gut • Penetration across blood brain barrier
Opioids (Loperamide) **[221]**	ICAM-1 targeted nanoliposomes	IV	• Sustained analgesic effect at inflammatory site • Decrease systemic toxicity
Glucocorticoids (Methylprednisolone) **[222]**	PEGylated nanoliposomes	IV	• Decrease required dosage • Improve therapeutic benefit
Local anaesthetics (Lidocaine) **[223]**	Uni/multilamellar liposomes	Topical	• Increase duration of action • Decrease required dosage

3.3 Labyrinthopeptins- Carbacyclic Lantibiotics

Lantibiotics are peptides isolated from bacteria and actinomycetes [224]. These peptides have been studied mostly for their anti infective properties [225]. They share a common unusual amino acid called lanthionine, hence the name "lantibiotics". The labyrinthopeptins are class of carbacyclic lantibiotics first isolated from *Actinomadura namibiensis [226]*. Unlike other lantibiotics, labyrinthopeptin has weak antiviral and antibacterial activity. However, its chemical structure is

similar to conotoxins [165], an ion channel blockers used to treat chronic pain [227]. Hence, labyrinthopeptins have been tested in various pain models and labyrinthopeptin A2 was found to be active [165].

Labyrinthopeptin A2 (laby) is a hydrophobic peptide consisting of 18 aminoacids [226]. The globular structure of this peptide can be divided into two nonapeptides, with each bearing a tetra (ring A) and penta (ring B) peptide that share a quaternary αC atom. The two nonapeptides are linked through C-terminal cysteine residue to form a disulphide bridge. The A/A' rings are formed by a methylene group between αC atoms of Lab1/Lab10 and Lab4/Lab13. B/B' rings are formed by thioether bridge. The rigid structure of this peptide leads to high metabolic and plasma stability [226] (Figure 3-1).

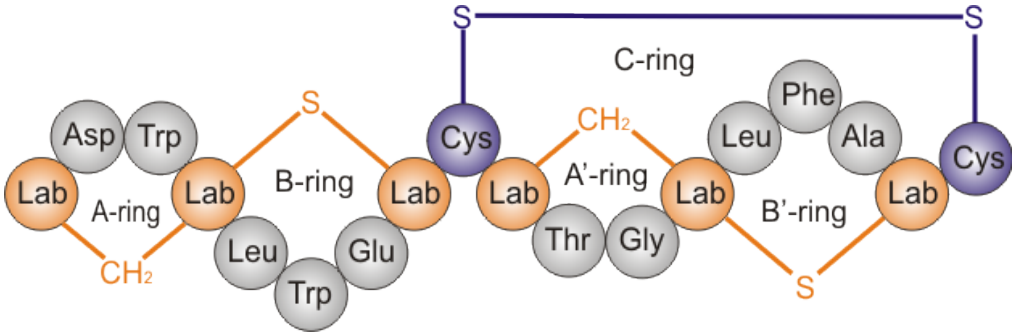

Figure 3-1 Structure of Labyrinthopeptin A2 [226]

Labyrinthopeptin has a molecular weight of 1924.18 Da and a Log D of 1.87 at pH 7.4 [165]. The solubility of this peptide in different vehicles is summarised in Table 3-3.

Table 3-3 Solubility of Labyrinthopeptin in different solvents [165]

Vehicle	Solubility (mg/ml)	Solubility (μM)
0.9% NaCl (physiological Saline)	0.6	336.8
Glucose 5%	1	505.2
PBS 10mM, NaCl 0.15M pH 7.4	3.3	1697.5
Mixture PBS/EtOH/Solutol (18/1/1)	9.6	4981.3
Glycofurol:Phosphate buffer 0.1M pH 7 50:50	150	77962.6
Glycofurol:Polysorbate 80: Phosphate buffer 0.1M pH 7 30:20:50	25	12993.8
Transcutol: Phosphate buffer 0.1M pH 7 50:50	130	67567.5
50% w/w Captisol in Phosphate Buffer 0.1M pH 7	69	35862.8
Citrate buffer 0.1M pH 3	0.1	52

Labyrinthopeptin A2 demonstrates efficacy in pre-clinical models of chronic pain [165]. Labyrinthopeptin was prepared in ethanol / solutol / phosphate buffer saline (1:1:18) and its pharmacodynamic activity was observed to be long lasting, for at least 6 h in mice (1.3 mg/kg i.v.) and rat (3mg/kg i.v.). No tolerance was observed after 5 days of treatment. At pharmacological doses, no side effects were observed as compared to gabapentin. The efficacy was also demonstrated in rats and mice via s.c. route [165].

However, labyrinthopeptin A2 at a dose of 30 mg/kg in the same diluent (ethanol / solutol / phosphate buffer saline (1:1:18)) has oral bioavailability of 0.11 % [165]. Arturrson et al. reported that drugs or peptides that are absorbed to less than 1% has a permeability coefficient less than or equal to 1×10^{-7} cm/s [228]. The permeability coefficient of labyrinthopeptin was observed to be $0.5\pm 0.3\times10^{-7}$ cm/s at pH 7.4 as tested in Caco-2 monolayer model [165]. The peptide is also not a P-gp/BCRP substrate and does not show paracellular transport. There is no evidence of protein binding and the peptide is shown to be stable in SGF (2 h), SIF and mouse plasma up to 4 h [165]. The low oral bioavailability (0.11%) of labyrinthopeptin was believed to be due to the poor permeability of the respective formulation across the gut. Hence, an alternative carrier has to be developed to improve the permeability and oral bioavailability of labyrinthopeptin.

3.4 LCMS-QQQ

Overview

LCMS-QQQ is a robust technique, which operates with four main parts (Figure 3-2). 1) Liquid chromatography column, where the extracted samples are separated and eluted in a mobile phase, 2) source, that disperses the compounds in to fine droplets and ionizes the same, triple quadrupole where compound of interest is selected and fragmented based on mass and a detector where the preselected compound is quantified [229].

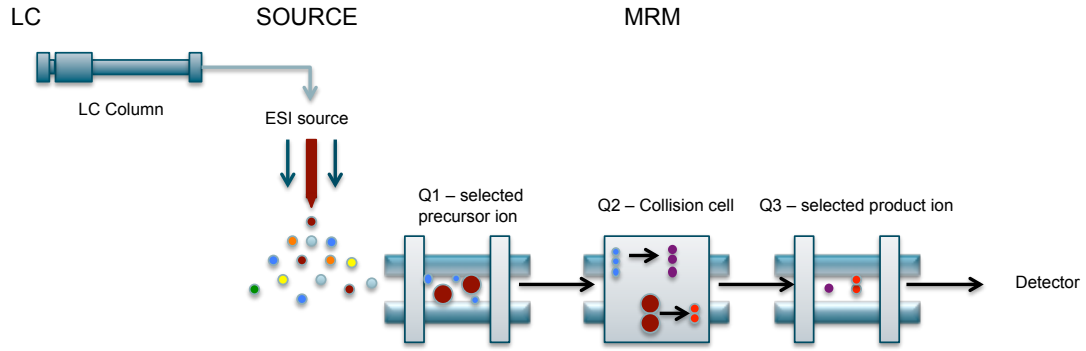

Figure 3-2 LCMS QQQ Schematic representation

Liquid chromatography

Liquid chromatography coupled with mass spectrometer generates three-dimensional data. In addition to measuring strength of the signal, the molecular weight, identity and purity of the sample can be obtained. To ensure adequate analyte concentration, liquid chromatography could be optimized to minimize co-elution of compound that can compete for ionization or suppress signal [229].

ESI source

Electron spray ionization works by generating ions in solution before the analyte reaches the mass spectrometer. LC eluent is nebulized into fine droplets, which is dried using heated drying gas in the presence of an electrostatic field. This causes reduction in the size of the droplet as well as accumulation of charge in the droplet. As the concentration of charges in the droplet increases, ions are ejected in to gas phase due to repulsive force between like charges. These ions are passed through a capillary tube in to mass analyzer [229].

Quadrupole mass analyzer

Quadrupoles are four rods arranged in square through which the ions can pass through the filter at a given time. Quadrupole analyser has same dc charge applied to opposite rods and adjacent rods carries opposite charge. Radiofrequency signal are

swept in the presence of an applied dc charge. Ions that are stable for a given frequency are directed towards the detector [230].

There are three different modes; scan mode, which monitors a range of mass to charge ratio. In selective ion monitoring (SIM) mode only monitors selected mass to charge ratio. Highly selective monitoring is carried out in multiple reaction-monitoring (MRM) modes. Here, quadrupoles screen the compound of interest by; where the first quadrapole selects the compound of interest, preselected compound is collided in to fragments in the second quadrapole and the fragment of interest is selected in the third quadrapole. This selectivity is required for quantifying therapeutic compound in the presence of biological matrices [229].

Collision induced dissociation

Collision induced dissociation fragments selected analyte by applying collision energy. The fragmentation patterns are specific for a particular analyte at that specific collision energy. The collided fragments are screened and a single fragment is selected based on sensitivity and quantified. Collision induced dissociation takes place at the second quadrupole of MRM where only a selected precursor ion is fragmented for further screening [229].

Ion detector and data acquisition

Preselected ions are drawn in to the detector and strike a detector's membrane surface causing electron to be released from the other side. The electron strikes the coated walls of the detector that will in turn release multiple electrons on each impact. The electrons are further amplified and the signals are transferred to data system [230].

3.5 Materials and Methods

3.5.1 Materials

Chemicals	Supplier
Labyrinthopeptin	Sanofi
DMSO	Sigma-Aldrich (Gillingham, UK)
Methanol (LCMS grade)	Sigma-Aldrich (Gillingham, UK)
Acetonitrile (LCMS grade)	Sigma-Aldrich (Gillingham, UK)
Water (LCMS grade)	Sigma-Aldrich (Gillingham, UK)
Acetonitrile (HPLC grade)	Sigma-Aldrich (Gillingham, UK)
Methanol (HPLC grade)	Sigma-Aldrich (Gillingham, UK)
Trifluroacetic acid (99%)	Sigma-Aldrich (Gillingham, UK)
Formic acid (≥ 95%)	Sigma-Aldrich (Gillingham, UK)
Glycofurol	Sigma-Aldrich (Gillingham, UK)
Sodium chloride	Sigma-Aldrich (Gillingham, UK)
Sodium hydroxide	Sigma-Aldrich (Gillingham, UK)
Hydrochloric acid	Fisher, UK
Monobasic potassium phosphate	Sigma-Aldrich (Gillingham, UK)
HBSS	Invitrogen, UK
Water	Sigma-Aldrich (Gillingham, UK)
Pentifylline	MP Biomedicals, CA, USA
K2 EDTA BD Vacutainer™ (3 mL)	Fisher Scientific, UK

3.5.2 Methods

3.5.2.1 Analytical method for quantification of Labyrinthopeptin

3.5.2.1.a Preparation of Stock and Working standards:

Labyrinthopeptin was quantified using high-performance liquid chromatography (HPLC). A stock solution of Labyrinthopeptin was prepared by dissolving the peptide (2 mg/mL) in DMSO. Calibration standards were prepared by diluting stock solution to working standards (S1 to S8) of concentrations ranging from 200 µg/mL to 1.56 µg/mL with equal ratios of methanol and water containing 0.1% trifluroacetic acid (TFA). The standards were analysed by HPLC. All test compounds were quantified as method mentioned above.

3.5.2.1.b HPLC Set up and analysis

HPLC chromatogram for Labyrinthopeptin were acquired using the following setup:

Table 3-4 HPLC instrument condition for the quantification of labyrinthopeptin.

HPLC Setup			
Instrument	Agilent Technologies 1200 Series HPLC system		
Column	Onyx C18 monolithic column (5 µm; 100 × 4.6 mm; Phenomenex UK) and fitted with guard cartridge (10 × 4.6 mm, 5 µm)		
Column temperature	37˚C		
Mobile phase	A: Water + 0.1 % TFA B: Acetonitrile + 0.1 % TFA		
Gradient condition	Time (min)	Mobile phase A (%)	Mobile phase B (%)
	0	95	5
	1	95	5
	5	25	75
	6	25	75
	6.5	95	5
	7	95	5
Flow rate	1.2 mL/min		
Injection volume	20 µL		
UV wavelength	220 nm		
Sample diluent	50% Methanol: 50% Water (0.1% TFA)		

Calibration curve was obtained by plotting the concentrations of standards and its respective peak area from the chromatogram. The linear equation y= mx+c was used to calculate the concentration of unknown analyte.

3.5.2.2 Preparation of Laby formulations

Laby GCPQ formulations was prepared and compared to Laby Glycofural formulation. From the solubility data, it was known that glycofural and phosphate buffer (0.1 M) prepared at ratio 1:1 has solubility of 150 mg/mL. Glycofural formulation was used as a control in this study.

3.5.2.2.a Preparation of Laby-Glycofural formulation

Laby (10 mg) was added to a solution (1mL) containing glycofurol and phosphate buffer saline (PBS - 0.1M, pH 7) prepared at a ratio 1: 1. The formulation was vortexed and allowed to dissolve completely at room temperature for 30 min.

3.5.2.2.b Preparation of Laby-GCPQ (B2) formulation

Laby (10 mg) were mixed with GCPQ (B2) as powder at different weight ratios (1:1, 1:2, 1:3, 1:4 and 1:5) and added to water (1 mL). The mixture was vortexed and allowed to rest on a table to form a suspension. The suspension was then probe sonicated in the presence of ice water at 15 amps for 15 min using a probe sonicator (Q Sonica, U.S.A).

A schematic representation of formulation preparation is shown in (Figure 3-3).

3.5.2.2.c Preparation of Laby-GCPQ (B1 & B3) formulation

Laby-GCPQ (B1 & B3) formulation at weight ratio 1:3 was prepared as method mentioned in 3.5.2.2.b.

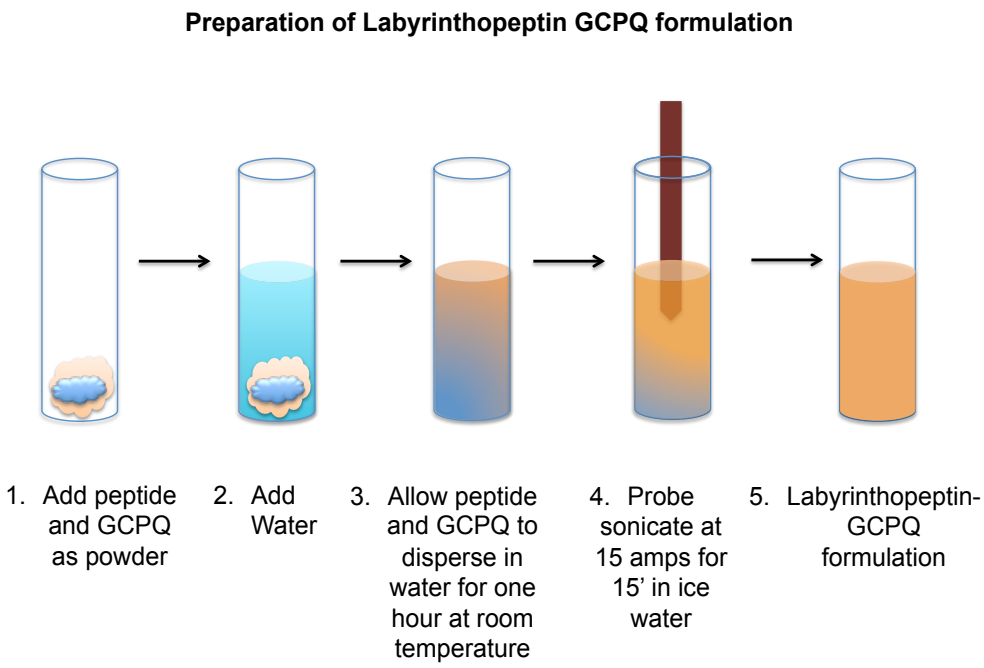

Figure 3-3 Preparation of Laby-GCPQ formulation.

3.5.2.3 Characterization of Laby formulation

3.5.2.3.a Morphology

Morphology of the Labyrinthopeptin GCPQ (B1, B2 & B3) formulations was determined using transmission electron microscope (Philips CM 120 Bio Twin Transmission electron microscope) with an AMT digital camera (5 mega pixels; AMT Deben, UK Ltd). A drop of Labyrinthopeptin GCPQ (B1, B2 & B3) formulation was placed on a grid and excess fluid was blotted with a tissue paper. A drop of uranyl acetate (1% w/v in water) or paraformaldehyde staining solution was also added to the grid and TEM images were recorded.

3.5.2.3.b Particle size

Particle sizes of Labyrinthopeptin GCPQ formulations (B1, B2 & B3) were characterized by dynamic light scattering (DLS) technique (Malvern Zetasizer Nano ZS ZEN3600, Malvern Instruments Ltd, Worcestershire, UK). Formulations (1 mL) were dispensed into a low volume disposable cuvette and size distribution graphs were recorded.

3.5.2.3.c Charge

The zeta potential of Labyrinthopeptin GCPQ formulations (B1, B2 & B3) were determined using DLS (Malvern Zetasizer Nano ZS ZEN3600, Malvern

Instruments Ltd, Worcestershire, UK). Formulations (1 mL) were dispensed into a zeta cell and zeta distribution graphs were recorded.

3.5.2.3.d Encapsulation efficiency of Labyrinthopeptin GCPQ (B1, B2 & B3) formulations.

Encapsulation efficiency of Labyrinthopeptin was determined by centrifugation method. Laby precipitates above a concentration of 0.6 mg/mL in sodium chloride (0.9%) solution. To determine the encapsulation efficiency of Laby GCPQ formulation, formulation was centrifuged to pellet out unencapsulated laby leaving Laby GCPQ nanoparticle in the supernatant. The concentration of Laby in the supernatant was normalized against the laby concentration before centrifugation from which encapsulation efficiency of the Laby formulation was determined.

A schematic representation of the separation of peptide-loaded nanoparticles from free peptide is illustrated in Figure 3-4. Labyrinthopeptin GCPQ (B1, B2 & B3) formulations were centrifuged at 5000 RPM for 10 min at room temperature. The supernatants were passed through 0.8 µm filter and reconstituted (50 µL) in sample diluent (950 µL). The solutions were vortexed and analysed by HPLC.

Encapsulation efficiency of Laby GCPQ (B1, B2 & B3) formulations were calculated using the formula,

$$\%\ \textbf{\textit{Encapsulated peptide}} = \frac{\textbf{Concentration of peptide after centrifugation and filtration}}{\textbf{Concentration of peptide before centrifugation}} \times \mathbf{100}$$

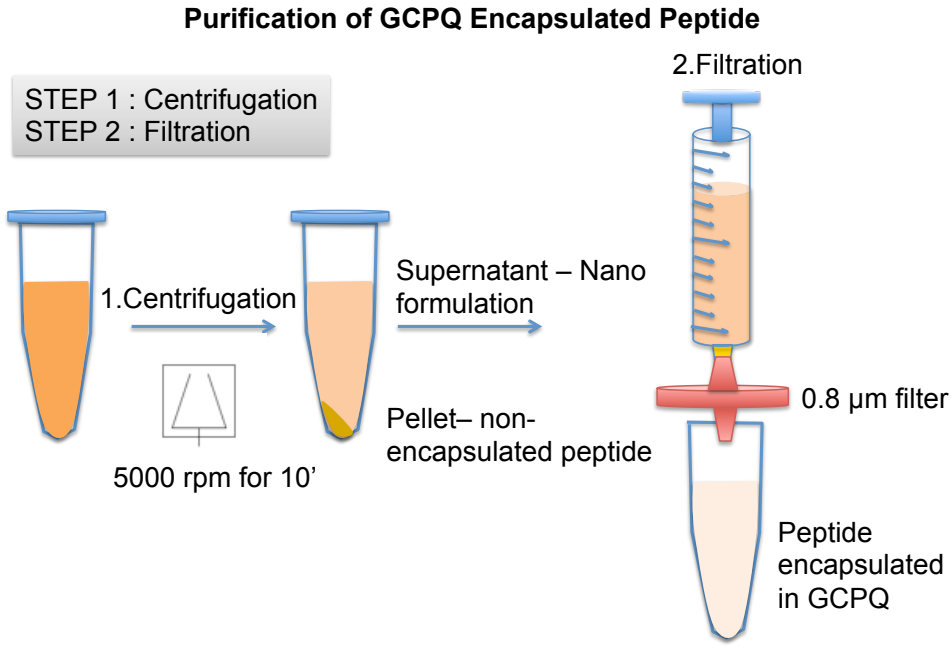

Figure 3-4: Purification of peptide loaded nanoparticles

3.5.2.4 Colloidal stability of Laby-GCPQ formulations

Labyrinthopeptin GCPQ formulations were diluted 1 in 20 times with SGF, SIF and HBSS respectively. The particle size recorded at different time points using DLS. The solutions were maintained at 37˚C throughout the experiment. The compositions of simulated fluids are as follows,

SGF and SIF were prepared by protocol described in United States Pharmacopeia 33-28NF (2010) and European Pharmacopeia 7.0 (2010).

3.5.2.4.a SGF

Sodium chloride (2 g) was dissolved in water (500 mL). The pH of the solution was adjusted to 1.2 with HCl (7 mL) and made up to 1000 ml with water.

3.5.2.4.b SIF

Monobasic potassium phosphate (6.8 g) was first dissolved in water (250 mL) and 0.2 N sodium hydroxide solution (77 mL) was added. The pH of the solution was adjusted to 6.8 with sodium hydroxide (0.2 N) or hydrochloric acid (0.2 N) and finally diluted to 1000 mL.

3.5.2.4.c HBSS

HBSS (10X) concentrated liquid (Invitrogen, U.K.) was diluted to 1X concentration with water. The HBSS (10X) solution consists of sodium chloride (80 g/L), potassium chloride (4 g/L), potassium phosphate monobasic (0.6 g/L), glucose (10 g/L) and sodium phosphate dibasic (0.479 g/L).

3.5.2.5 LCMS-QQQ detection of Laby peptide *in vivo*

Labyrinthopeptin was quantified in plasma using LCMS QQQ. The configurations are listed as follows:

3.5.2.5.a Instrument configuration

Pump	: Agilent G1312B
Autosampler	: Agilent G1367E
Column	: Agilent G1367E
Mass spectrometer	: Agilent 6460 triple quadrupole LCMS system
Software	: Agilent chem station (B.06.00)

Several parameters were optimized to get optimum Laby signal. This includes liquid chromatography optimization in order elute Laby peak from

background matrix and mass spectrometer optimization in order to enhance the sensitivity of the laby peptide signal.

3.5.2.5.b Chromatography

LC parameters for separation and identification of labyrinthopeptin is as follows:

Parameters	**Plasma**	**Brain**
Column	Onyx monolithic C18 column (100×2 mm)	Agilent Zorbax C18 column (50×2 mm)
Oven temperature	40˚C	40˚C
Injection volume	5 µL	5 µL
Mobile phase	Solvent A: 0.1% FA in water Solvent B: Acetonitrile	Solvent A: 0.1% FA in water Solvent B: Acetonitrile

Gradient program

Plasma

Time (min)	0	1	4	4.5	5.5	5.7	7
% of solvent B	20	50	74	90	20	20	20
Flow rate	0.4 mL/min						

Brain

Time (min)	0	0.5	2	2.2	2.4	3	4
% of solvent B	20	50	74	90	20	20	20
Flow rate	0.4 mL/min						

3.5.2.5.c Source Optimization

Agilent uses jet-streaming technology to maximize desolvation of ions in the source. The parameters for jet stream includes sheath gas temperature, sheath gas flow, drying gas temperature, drying gas flow, nebulizer gas and nozzle voltage. Labyrinthopeptin and internal standard (pentifylline) were optimized using a source optimizer program in LCMS. The parameter that gave the highest peak area was used to develop LCMS method.

3.5.2.5.d MS Optimization

Optimum fragmentor voltage and collision energy for the peptide and internal standard was optimized manually by running a default method with varying fragmentor voltage (50 to 300) and collision energy (10 to 200) respectively. Parameter that gave the highest peak area was used to develop LCMS method.

3.5.2.5.e Signal Optimization

EMV and MS resolution were varied to get best S/N noise ratio and optimum parameter was analyzed.

The optimum parameter from source, MS and signal optimization were listed as follows:

3.5.2.5.f Mass Spectrometry

Source Parameters	
Ionization mode	ESI jet streaming positive
Sheath gas temperature (˚C)	400
Sheath gas flow (L/min)	12
Drying gas flow (L/min)	10

Drying gas temperature (˚C)	340
Nebulizer gas (psi)	20
Nozzle voltage (V)	2000
EMV (V)	200

Test item	**Labyrinthopeptin** Quantifier	**Pentifylline** Internal standard for plasma sample	**MENK** Internal standard for brain sample
MRM transition	962.64- 159.2	265.09 – 138.2	574 - 425
Fragmentor voltage (V)	140	140	130
Collision energy (eV)	60	50	10
MS1 and MS2 resolution (nm)	Wide	Unit	Unit
Cell acceleration voltage (V)	6	6	7
Dwell time (ms)	200	200	200

3.5.2.6 Development of analytical method for Labyrinthopeptin by LCMS-QQQ

Labyrinthopeptin peptide quantification by LCMS-QQQ was validated according to the guidelines in prepared by European Medical Agency [231].

3.5.2.6.a Preparation of standards

A stock solution of labyrinthopeptin was prepared by dissolving the peptide (2 mg/mL) in DMSO. Seven calibration standards of concentrations ranging from 12800 ng/mL to 200 ng/mL were prepared by dilution of stock solution in 0.1% formic acid (FA). A stock solution of internal standard (pentifylline) was also prepared in acetonitrile (200 ng/mL) to achieve a final concentration of 20 ng/mL in plasma.

3.5.2.6.b Preparation of plasma for calibration standards

Sprague Dawley (SD) rat was culled in a CO_2 culling chamber and blood was withdrawn by cardiac puncture. Blood sample was collected in a vacutainer (BD Vacutainer™ - spray coated with anti-coagulant K2 EDTA) and centrifuged at 2000 g for 10 min at 4˚C. Plasma was carefully withdrawn and stored at – 80˚C in a freezer until LCMS analysis.

3.5.2.6.c Preparation and extraction of calibration standards from plasma matrices

Internal standard (5 µL) and calibration standards (5 µL) were spiked into each tubes containing plasma (50 µL). Blank was prepared by spiking only internal

standard (5 µL) in plasma (50 µL). For extraction, methanol (140 µL) was added to QC standards to precipitate plasma proteins followed by vortexing for 30 min. The precipitated plasma proteins were removed by centrifugation at 10000 RPM for 10 min and the supernatant was quantified by LCMS.

3.5.2.7 Validation of analytical method

3.5.2.7.a Preparation of quality control standards (QC)

Labyrinthopeptin of four different concentrations (lowest limit of quantification (LLOQ) - 20 ng/mL, low – 80 ng/mL, medium – 320 ng/mL and high – 1280 ng/mL) with IS extracted in plasma matrix were used for validation analytical method.

3.5.2.7.b Variability with-in and between days

QC standards (LLOQ, low, medium and high) prepared in triplicates ran thrice on the same day and on different days were compared to assess the intra and inter-variability of samples.

3.5.2.7.c Matrix effect

Effect of plasma matrix on sample ionization was assessed by comparing variability in concentration of QC standards (high and low) with and without plasma matrix. QC standards and IS (5 µL each) were spiked in plasma or solvent (50 µL) and extracted with methanol (140 µL). Matrix effect was calculated using the formula:

$$Matrix\ effect = \frac{\text{Concentration of peptide with matrix}}{\text{Concentration of peptide without matrix}} \times 100$$

3.5.2.8 Oral administration of labyrinthopeptin GCPQ formulation

SD rats (male) were fasted overnight and divided in to three groups (n=5) each receiving 30 mg/kg oral dose of Labyrinthopeptin GCPQ (B1 & B3) or Labyrinthopeptin glycofurol formulations. At each time point (30', 1 h, 2 h, 4 h, 6 h and 8 h) blood samples (250 µL) were withdrawn from tail vein and collected in a vacutainer (BD Vacutainer™ - spray coated with anti-coagulant K2 EDTA). Plasma samples (50 µL) were collected by centrifugation at 2000 g for 10 min and stored at – 80˚C in a freezer until LCMS analysis.

Labyrinthopeptin was extracted from plasma by a liquid-liquid extraction method. Specifically plasma samples were defrosted in ice and then at RT before extraction. An internal standard (pentifylline) of concentration 200 ng/mL in

acetonitrile was spiked (5 µL) in each plasma sample and precipitated with methanol (145 µL). The samples were vortexed for 30 min at RT followed by centrifugation at 10000 RPM for 10 min at RT. The supernatant was quantified using LCMS.

The samples were run as method mentioned in the previous section. Labyrinthopeptin and internal standard peak area were integrated and their ratios were substituted in linear equation to get the concentrations of labyrinthopeptin in the unknown plasma samples. A schematic representation of the study is presented in Figure 3-5.

Pharmacokinetics of Labyrinthopeptin-GCPQ formulation

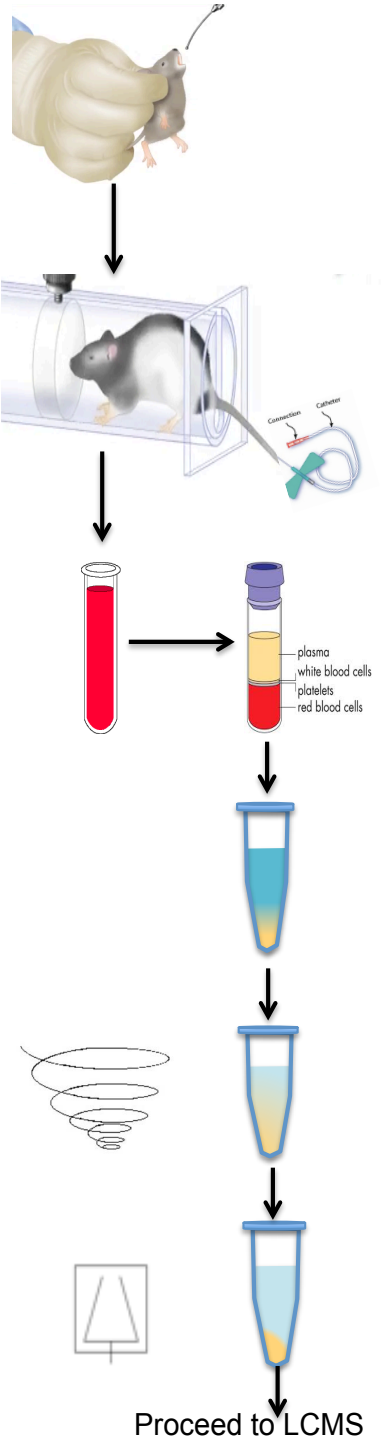

1. Oral administration of Labyrinthopeptin-GCPQ formulation
2. Withdrawal of blood at different time point
3. Separation of plasma from blood by centrifugation and spike Internal standard (200 ng/ml, 5 µl volume)
4. Extraction of analyte from plasma using methanol.
5. Vortex for 30' at RT
6. Precipitation of plasma protein by centrifugation at 10,000 RPM for 10' at RT

Figure 3-5 Schematic of pharmacokinetics of Laby formulations

3.5.2.9 Pharmacokinetics of Laby in brain sample – LCMS

Overnight fasted SD rats were administered nasally (3 mg/kg) or orally (30 mg/kg) with Laby GCPQ B3 formulation. Animals were euthanized at time point 30 min and 2 h for nasally administered formulation and at 2 h and

4 h for orally administered formulation. Brain tissues were extracted, flash frozen with liquid nitrogen and stored in -80 C until use.

Brain samples (1g/10 mL) in methanol were macerated and probe sonicated in the presence of ice to obtain a homogeneous suspension. A good internal standard must have the same solubility properties in the extraction solvent as that of the labyrinthopeptin. Since pentifylline is soluble in diethyl ether, MENK was used as an internal standard. A stock solution of MENK (4 ug/mL) was prepared in DMSO and MENK solution (10 uL) was added to brain suspension (1 mL). The sample solution was vortexed and centrifuged at 13,000 RPM for 10 min. The supernatant was transferred in to a new micro centrifuge tube and dried in a speed vac for three h at 45˚C. To the dried pellet, diethyl ether (1 mL) was added and vortexed for 5 min. The mixture was centrifuged again at 13,000 RPM for 10 min. The supernatant was decanted and the pellet was dried at room temperature. The pellet was re-suspended again in methanol (200 uL) and centrifuged again at 13,000 RPM for 10 min. The supernatant was analysed by LCMS-QQQ.

For the standards, untreated brain extracts were spiked with Laby of different concentrations (10 ng/ng to 640 ng/g) and internal standard (MENK) and processed as above. Standard curve was plotted using concentrations of Laby spiked, against area ratio of Laby to MENK. Unknown samples were substituted in the linear equation to get the concentration of Laby in the respective brain samples.

3.5.2.10 Pharmacodynamics of Laby-GCPQ B2 formulation

The anti-nociceptive effect of labyrinthopeptin in the presence and absence of GCPQ was tested in complete Freund's adjuvant (CFA) chronic pain model. Animals were habituated to Von Frey hair (VFH) grids, boxes, and procedure room before the start of experiment. The animals were then presented with 6 VFH (4, 6, 8, 10, 15, 26 g) until a withdrawal reaction was obtained. The hairs were then presented in a descending order until no response and then increased until withdrawal response was observed. The paw withdrawal was thus recorded. The animals were then injected into plantar surface either with incomplete or complete Freund's adjuvant (100 µl using 25 G needle). Inflammation was allowed to develop for 24 h. The animals were habituated to VFH boxes for 5 min tested for post CFA withdrawal (1.4, 2, 4, 6, 8, 10, 15, 26 g starting with 10 g hair and going up or down accordingly). The animals were randomized in to three groups and received nasal (15 mm PE10 tubing on

insulin syringe) or oral formulation. The paw withdrawal was assessed at 0.5 h, 1, 2 and 3 h in the same manner as the baseline. The dosing conditions and methodology are outlined in the Table 3-5 and Figure 3-6:

Table 3-5 *In vivo* dosing condition for CFA anti-noiciceptive studies

	Oral	**Nasal**
Treatment Group (no of rats)	6 per group, 3 groups	6 per group, 3 groups
Group 1: Vehicle	50% glycofurol and 50% phosphate buffer (0.1 M at pH 7)	50% glycofurol and 50% phosphate buffer (0.1 M at pH 7)
Group 2: Labyrinthopeptin	13.8 mg/mL of labyrinthopeptin in 50% glycofurol and 50% phosphate buffer (0.1 M at pH 7)	13.8 mg/mL of labyrinthopeptin in 50% glycofurol and 50% phosphate buffer (0.1 M at pH 7)
Group 3: Labyrinthopeptin GCPQ B2 (ratio 1:3)	13.8 mg/mL of labyrinthopeptin and 41.4 mg/mL of GCPQ B2 in water	13.8 mg/mL of labyrinthopeptin and 41.4 mg/mL of GCPQ B2 in water
Administration volume	250 µL	60 µL
Dosing in Rat	15 mg/kg	3 mg/kg
Time point	0, 20', 40', 1 h, 1.5 h, 2 h, 3 h, 4 h, 6 h	0, 20', 40', 1 h, 1.5 h, 2 h, 3 h, 4 h, 6 h

Pharmacodynamics of Labyrinthopeptin GCPQ formulation

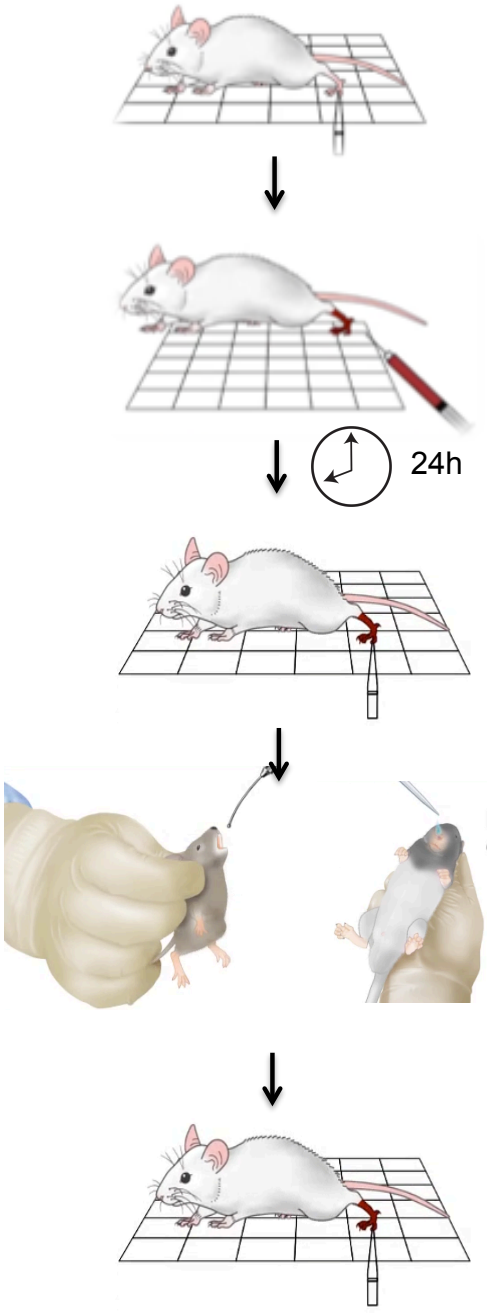

1. Baseline : Assessment of pain threshold using von frey hair
2. CFA induction in rat's hind paw.
3. Post inflammation pain threshold level using von frey hair.
4. Oral or nasal administration of Labyrinthopeptin GCPQ formulation.
5. Measurement of pain threshold level using von frey hair after treatment.

Figure 3-6 Pharmacodynamics of Laby GCPQ formulation

3.6 Results

3.6.1 Laby Glycofural formulation

From the solubility data (Table 3-3), Laby (10 mg/mL) was prepared in 1:1 ratio of glycofural and PBS (0.1 M, pH 7). This formulation is used as a control and compared with Laby GCPQ formulations for *in vivo* studies.

3.6.2 Screening and size characterization of Laby GCPQ Formulations by TEM and DLS

Laby GCPQ formulation was initially screened to know what is the minimum amount of GCPQ required to solubilize Laby in water. For this, Laby and GCPQ were added as powder at different weight ratios in water and the particles were characterized by TEM and DLS.

3.6.2.1 Morphology

The sizes of the Laby GC P(19%) Q(12%) B2 formulations prepared at different ratios were characterized by TEM and compared with Laby only formulation. Laby only formulation at a concentration 5 mg/mL in water showed thread like aggregates (Figure 3-7). With the addition of GCPQ to Laby at ratio 1:1, very large aggregates and particles were observed (Figure 3-8). However, on increasing GCPQ (10 mg/mL) concentration, only particles were observed for Laby GCPQ B2 formulation (1:2). Further increase in GCPQ concentration from 15 mg/mL up to 25 mg/mL gave particles of two sizes; around 20 nm and between 100 to 300 nm for Laby GCPQ formulation with weight ratio 1:3 (Figure 3-10), 1:4 (Figure 3-11) and 1:5 (Figure 3-12). It was also observed that the larger particles observed in Laby GCPQ (1:3) ratio reduced with increase in GCPQ concentrations at ratio 1:4 and 1:5.

TEM only gives an indication of the morphology of the particles. However, quantitative method such as DLS is required to understand what proportion of different sized particles were present in Laby GCPQ formulations prepared at different ratios.

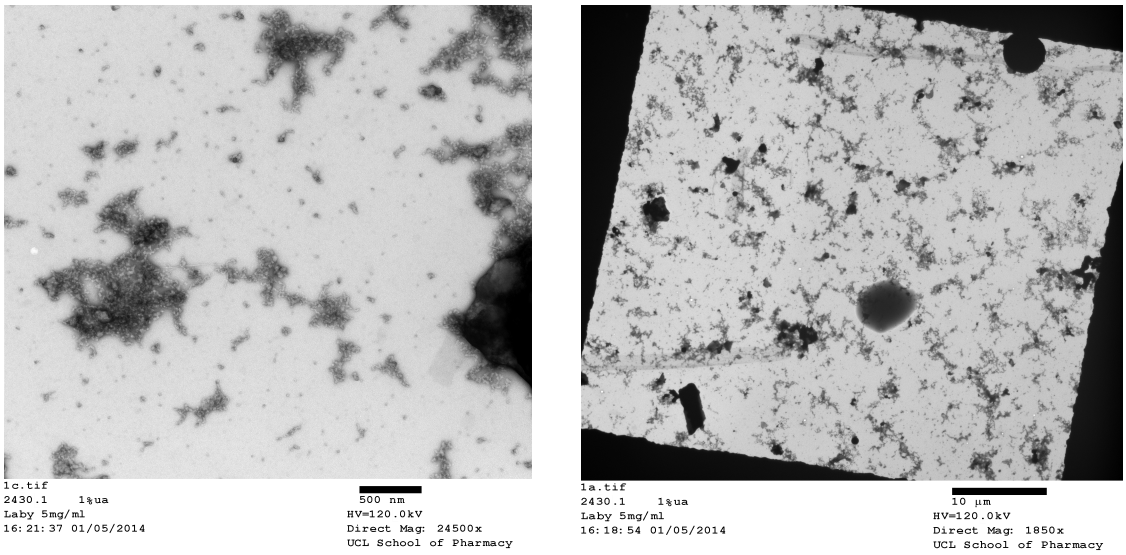

Figure 3-7 TEM images of Laby (5 mg/mL) showing precipitates in water

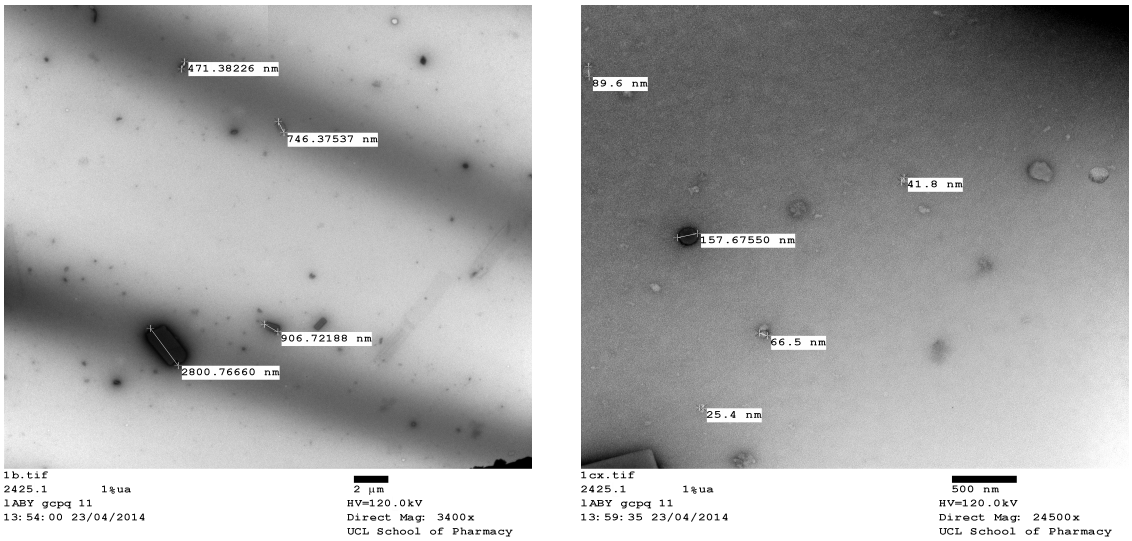

Figure 3-8 TEM images of Laby-GCPQ B2 formulation prepared at ratio 1:1. Concentration of laby and GCPQ used was 5mg/mL and 5 mg/mL. Large aggregates of sizes ranging from 740 nm to 2800 nm and particles of sizes ranging from 25 to 150 nm were observed.

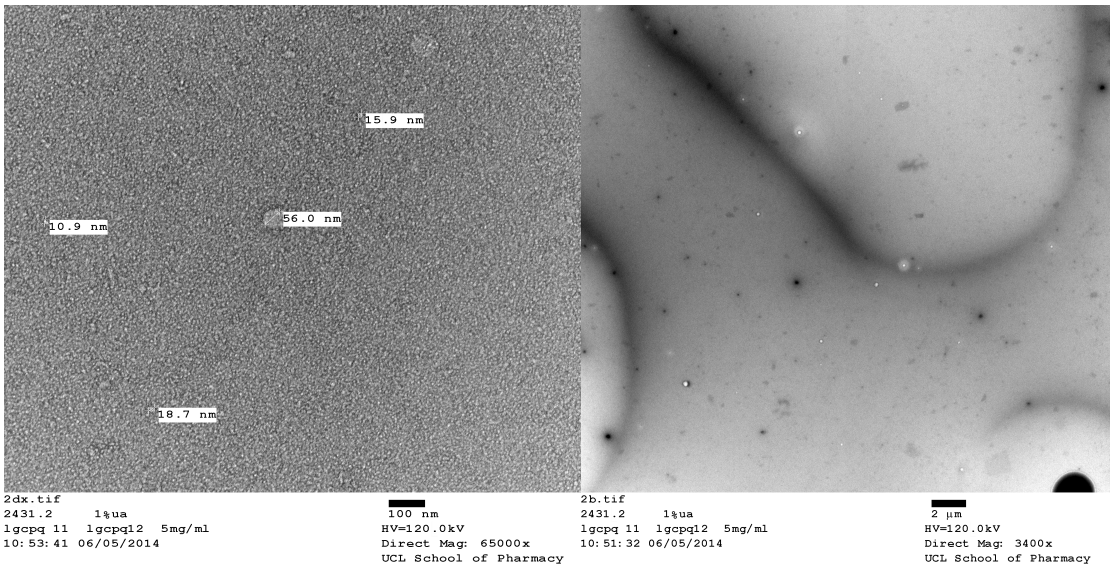

Figure 3-9 TEM images of Laby-GCPQ B2 formulation prepared at ratio 1:2. Concentration of laby and GCPQ used was 5 mg/mL and 10 mg/mL. Particles of sizes ranging from 10 to 50 nm were observed. Few large aggregates were observed.

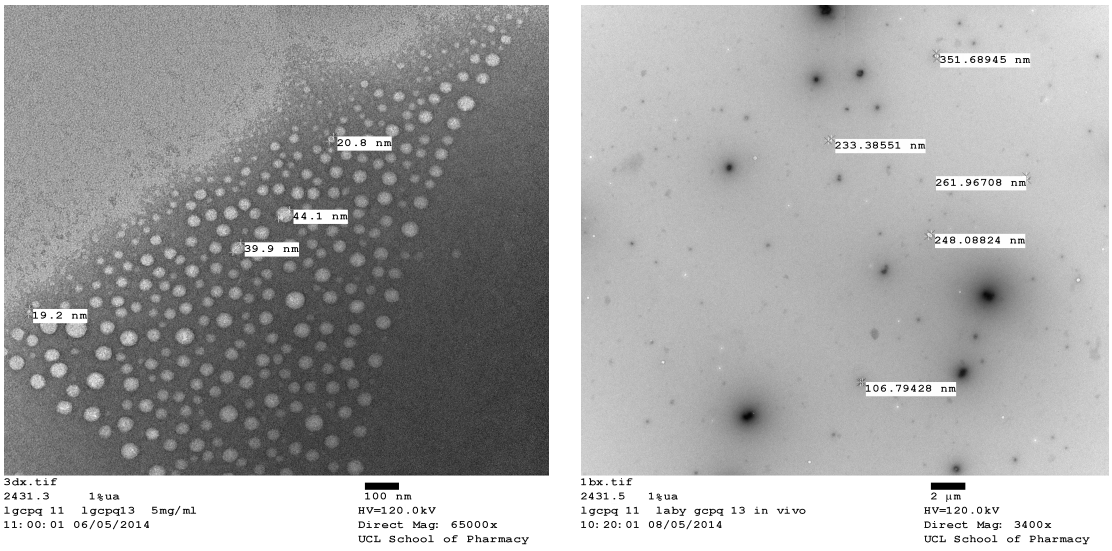

Figure 3-10 TEM images of Laby-GCPQ B2 formulation prepared at ratio 1:3. Concentration of laby and GCPQ used was 5 mg/mL and 15 mg/mL. Two size populations were observed; sizes around 20 to 40 nm and sizes around 100 to 250 nm. Large particles appear dense on TEM image.

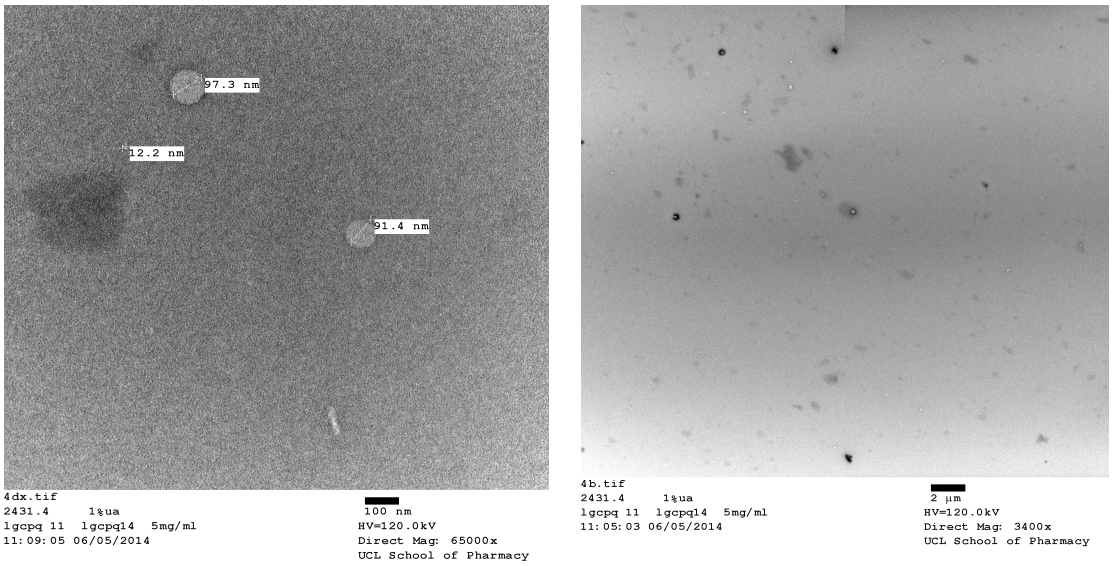

Figure 3-11 TEM images of Laby-GCPQ B2 formulation prepared at ratio 1:4. Concentration of laby and GCPQ used was 5 mg/mL and 20 mg/mL. Two size populations were observed; sizes around 20 to 40 nm and sizes around 100 to 250 nm. Very few large particles appeared on TEM image.

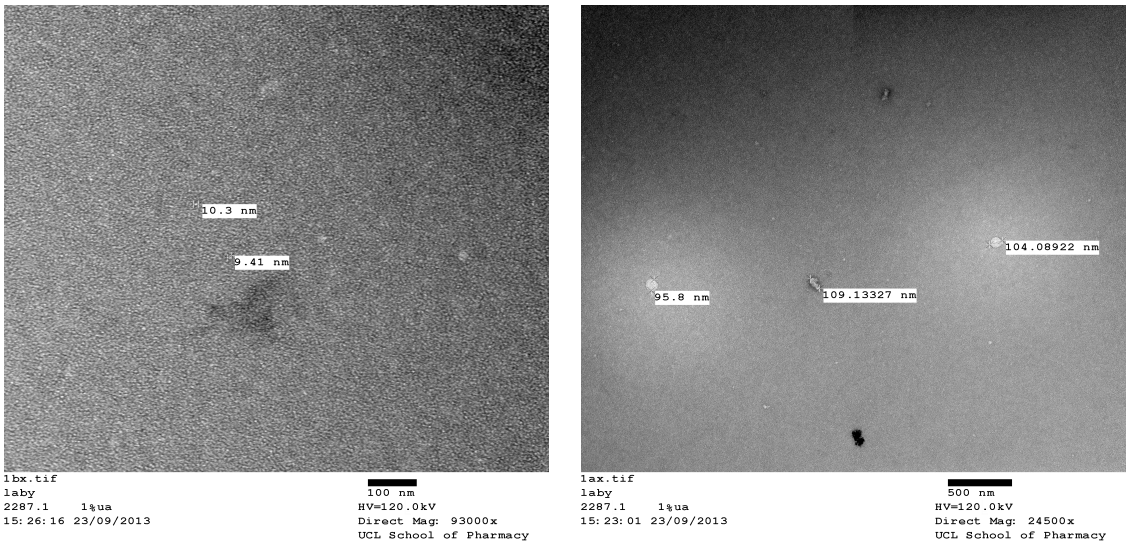

Figure 3-12 TEM images of Laby-GCPQ B2 formulation prepared at ratio 1:5. Concentration of laby and GCPQ used was 5 mg/mL and 25 mg/mL. Sizes around 10 to 100 nm appeared on TEM.

3.6.2.2 Size characterization by DLS

TEM results suggest different size populations for different ratios of Laby GCPQ B2 formulations. To confirm which size populations are predominant, Laby GCPQ B2 formulations of different weight ratios were quantified by DLS (Figure 3-13). Particle size analysis shows that Laby GCPQ B2 formulation prepared from ratio 1:1 to 1:5 formed particles around 20 nm. The polydispersity of the Laby GCPQ B2 formulations with ratio 1:1, 1:2, 1:4 and 1:5 was high (above 0.4) whereas Laby GCPQ B2 formulation of ratio 1:3 had the least PDI (0.382). From the PDI, it could be inferred that Laby GCPQ B2 formulation (1:3) has the most homogeneous population of nanoparticles compared to other ratios.

The size of GCPQ B2 micelles alone in water (2.5 mg/mL) was 67 nm with PDI 0.269 (Figure 2-20). The size of Laby GCPQ B2 particles (around 20 nm) at a given ratios (1:1 to 1:5) was observed to be smaller than the size of GCPQ B2 micelles (67 nm). However, with the introduction of Laby in GCPQ B2 formulations, the PDI was larger (ranging from 0.382 to 0.911) than GCPQ B2 micelles (0.269).

The size of Laby alone formulation was 600 nm with PDI 0.8. Very large precipitates around 2 μm were observed in TEM. This differences in the size of Laby formulation between DLS and TEM images are due to the sedimentation of large precipitates leaving only particles around 600 nm to be detected by DLS.

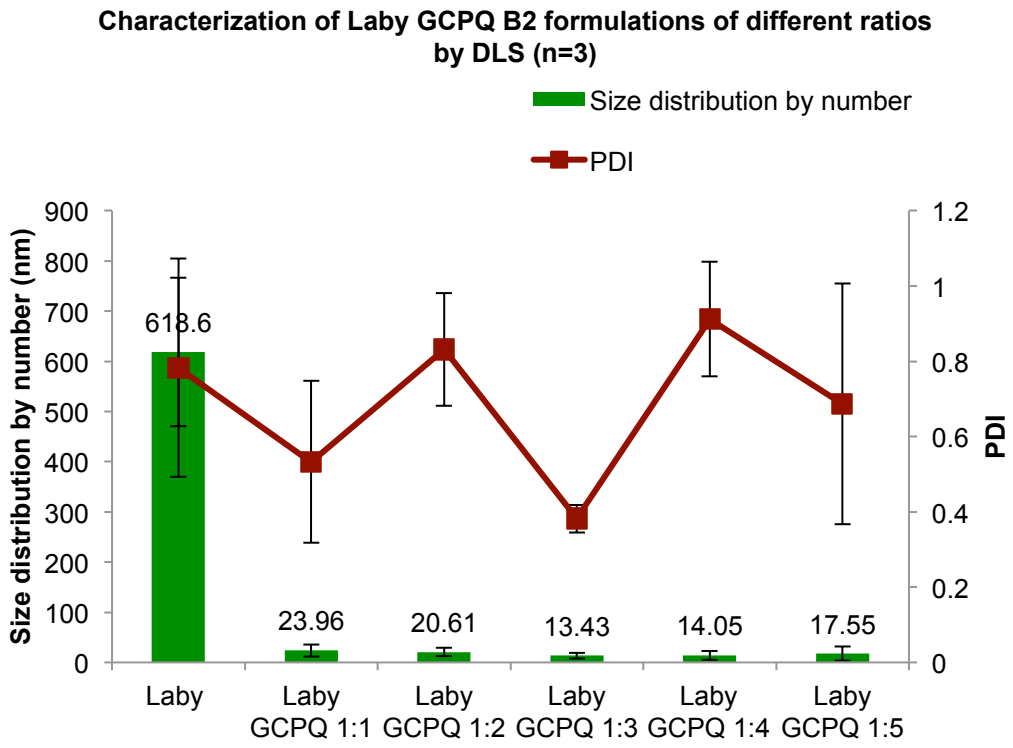

Figure 3-13 Characterization of Laby (2.5 mg/mL) GCPQ formulation at different weight ratios (1:1 to 1:5). Laby GCPQ B2 formulations compared with Laby only formulation for size distribution by number and PDI.

3.6.2.3 Size characterization of Laby GCPQ formulation at ratio 1:3 using different batches of GCPQ

Laby GCPQ B2 formulation (1:3) resulted in a clear suspension after probe sonication. An example on the appearance of Laby GCPQ at weight ratio 1:3 before and after probe sonication is shown in Figure 3-14.

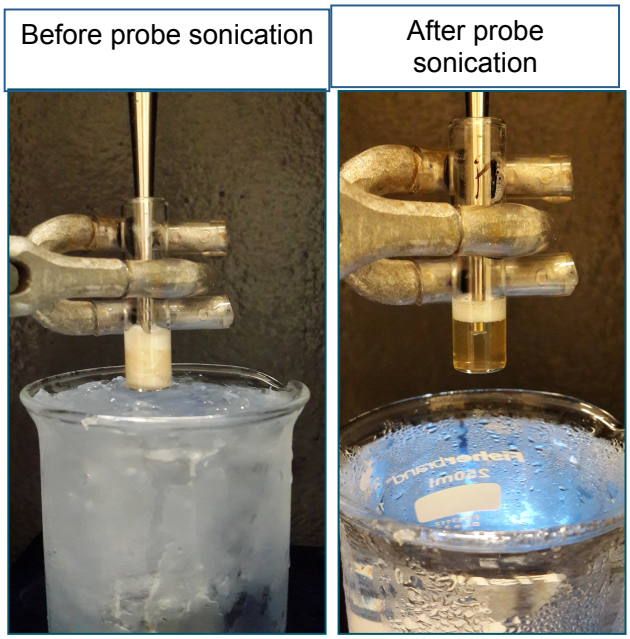

Figure 3-14 Laby GCPQ (1:3) formulation before and after probe sonication. Suspension appeared clear after probe sonication.

Laby GCPQ formulations were made at ratio 1:3 and compared between different batches of GCPQ and with Laby and Laby PGC formulations (Figure 3-15). Laby alone formed aggregates around 800 nm with PDI 0.6. Formation of Laby-PGC nanoparticles of size around 200 nm with PDI 0.672 suggests that hydrophobicity is essential for particle formation. When comparing different batches of GCPQ, one could infer that the particle sizes significantly drops with increase in the degree of palmitoylation of GCPQ. For Laby GCPQ formulation B1 with palmitolytion of 16%, the particles sizes analysed were 572 nm with PDI 0.125. However, with increase in palmitoylation of GCPQ to 19% and 22% the particle size measured were less than 100 nm. There was an increase in the size and PDI of Laby GCPQ formulation with B2 and B3. This increase in the particle size from palmitoylation 19% to 22% could be due to increase intermolecular association between the polymers.

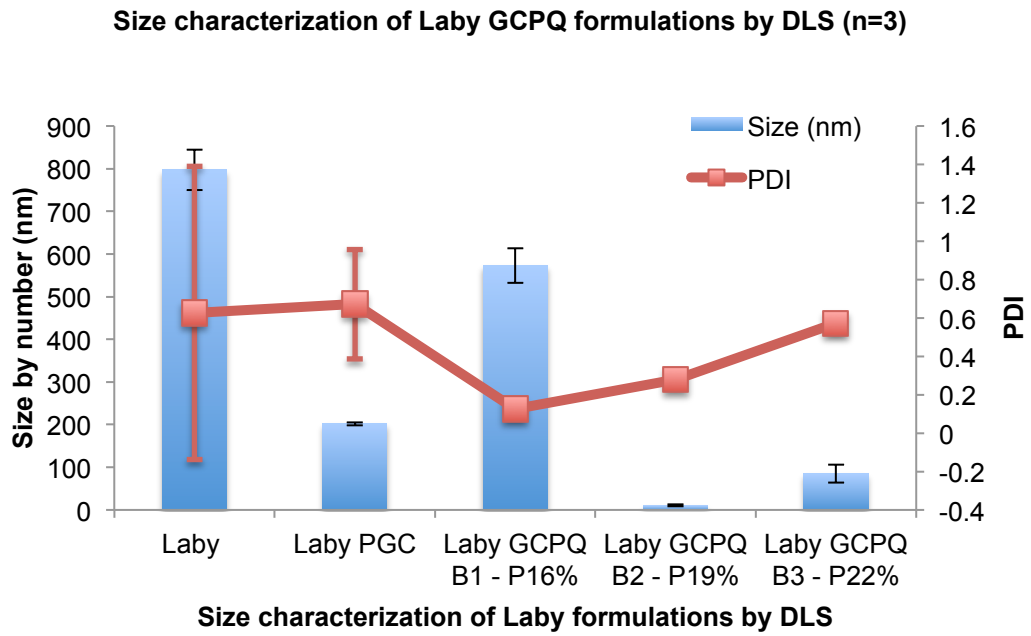

Figure 3-15 Comparison of Laby (2.5 mg/mL) GCPQ formulation at ratio 1:3 between different batches of GCPQ and with Laby (2.5 mg/mL in water) and Laby (2.5 mg/mL) PGC (7.5 mg/mL) formulation of ratio 1:3.

TEM images of Laby GCPQ formulations of different batches 1, 2 and 3 were compared. The TEM images correlated with results obtained in DLS. Aggregate of particles were observed in Laby GCPQ formulation B1 with palmitoylation of 16% (Figure 3-16). With increase in palmitoylation, homogeneous population of Laby GCPQ B2 nanoparticles of size 20 nm was observed (Figure 3-17). With further increase in palmitoylation to 22% for Laby GCPQ B3 formulation, the laby GCPQ particle aggregation was observed in TEM (Figure 3-18) and in DLS with a PDI of 0.572.

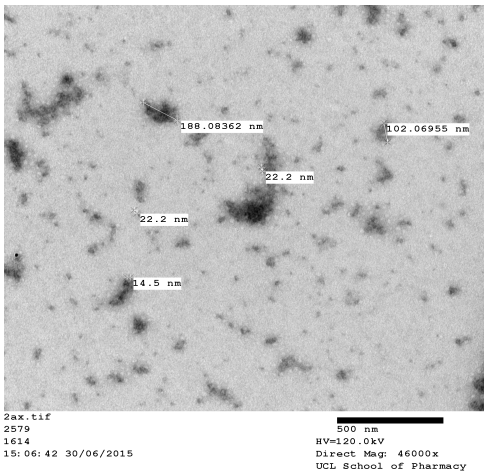

Figure 3-16 TEM image of Laby GCPQ B1 with degree of palmitoylation of 16% showing aggregates of nanoparticles of sizes ranging from 14 nm to 188 nm.

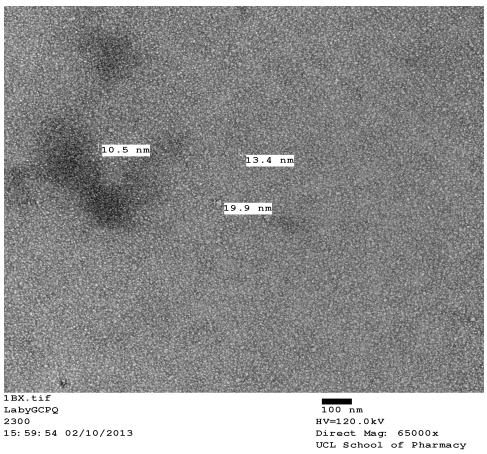

Figure 3-17 TEM image of Laby GCPQ B2 with degree of palmitoylation of 19% showing nanoparticles around 20 nm.

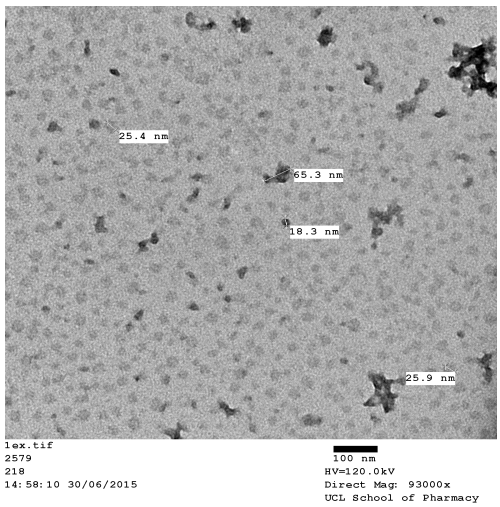

Figure 3-18 TEM of Laby GCPQ B3 formulation with degree of palmitoylation of 22% and quaternization of 8% showing small micelles around 20 nm and large particles around 200-300 nm

3.6.3 Charge and stability

Surface charge of Laby GCPQ B1, B2 & B3 formulations were assessed by measuring its zeta potential using DLS (Figure 3-19). Laby had negative zeta potential (-34.6 mV), Laby formulated with PGC had positive zeta potential around +10 mV and Laby GCPQ B1 formulation with degree of quaternization of 14 % had the most positive zeta potential (+48 mV) followed by Laby GCPQ B2 formulation (+46 mV) with quaternization percentage 12% and Laby GCPQ B3 formulation (+39.8 mV) with quaternization percentage 8%. The surface charge of Laby GCPQ formulations were observed to be increasing with increase in degree of quaternization. All measurements were carried out at pH 4.5 and temperature 25°C. The presence and absence of degree of quaternization could affect the stability of Laby formulations. TEM images show presence of precipitates in Laby-PGC formulation. This could be a result of low surface charge (+10 mV) that induced aggregation and precipitation of Laby-PGC particles. However, Laby GCPQ B1, B2 & B3 formulations were stable due to large positive zeta potential. This suggests that charge plays an important role in maintaining the stability of GCPQ formulations. From the above results, it is evident that the Laby with a negative surface charge was encapsulated in the GCPQ B1, B2 & B3 formulations resulting in positive surface charges.

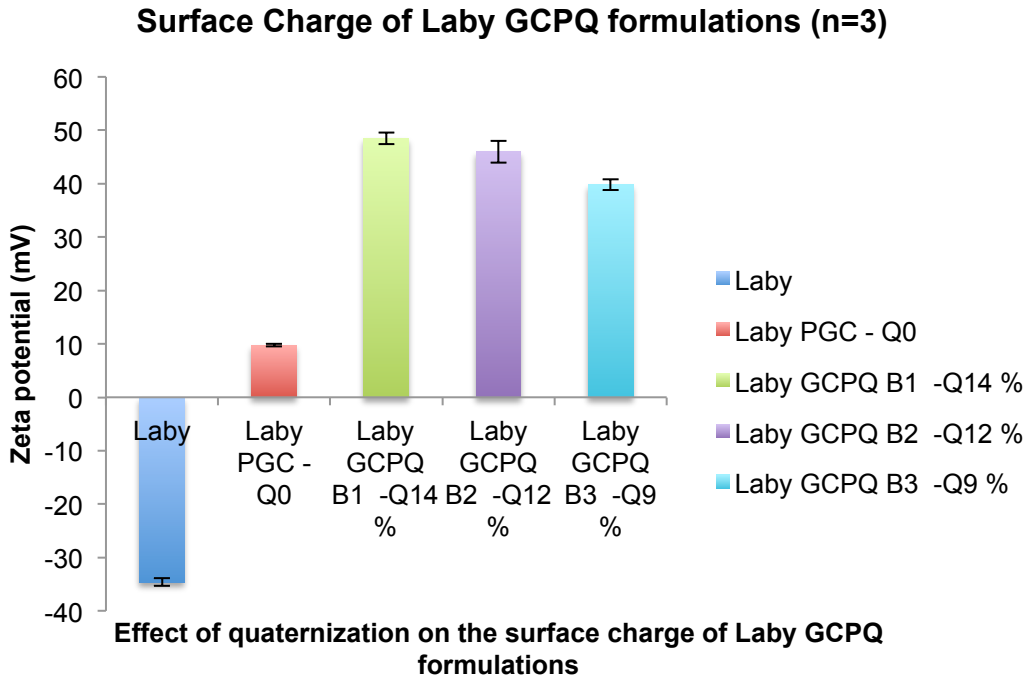

Figure 3-19 Zeta potential of Laby (2.5 mg/mL), Laby (2.5 mg/mL) with PGC formulation (1:3), Laby (2.5 mg/mL) with GCPQ formulations (B1, B2 and B3) prepared at ratio 1:3 and characterized DLS.

3.6.4 Encapsulation efficiency of Laby GCPQ Formulations

3.6.4.1 Analytical method for quantification of Laby by HPLC

Encapsulation efficiencies for Laby GCPQ formulations were analyzed using HPLC. Standard curve for laby was plotted with lowest and highest concentration being 0.79 µg/mL and 200 µg/mL. Laby was eluted at a retention time of 5.5 min (Figure 3-20) with lowest limit of detection (LLOD) and quantification (LLOQ) as 1.56 ug/mL. Along with Laby peak, trifluroacetic acid peak was also eluted at 1.5 in mobile phase (water and methanol (50:50) containing 0.1% TFA). The HPLC method was validated for variations in analysis within a day and between days.

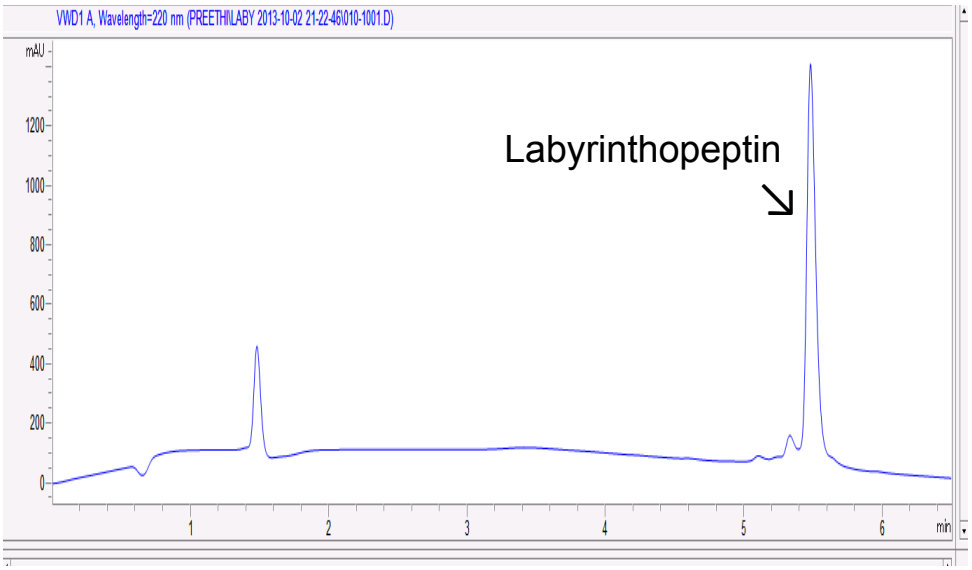

Figure 3-20 HPLC chromatogram for Laby eluted at retention time of 5.5 min and trifluroacetic acid peak eluted at time 1.5 min in 1:1 ratio of water and methanol containing 0.1% TFA. Small shoulder peak eluted with Laby peak indicates the presence of impurities in the sample.

To assess the variations within and between runs, percentage relative standard deviation was calculated by dividing standard deviation by mean area under the curve. The acceptable criteria for % RSD for standards are less than 15%. Linear equation for the calibration curve obtained from standards run on the same day was $y=40.16x+103.09$ and $r^2 = 0.99573$ (Figure 3-21). At lower concentrations (3.125 and 1.56 µg/mL), relative standard deviations (% RSD) were observed to be larger, 12% and 13% than the % RSD for higher concentrations (Table 3-6).

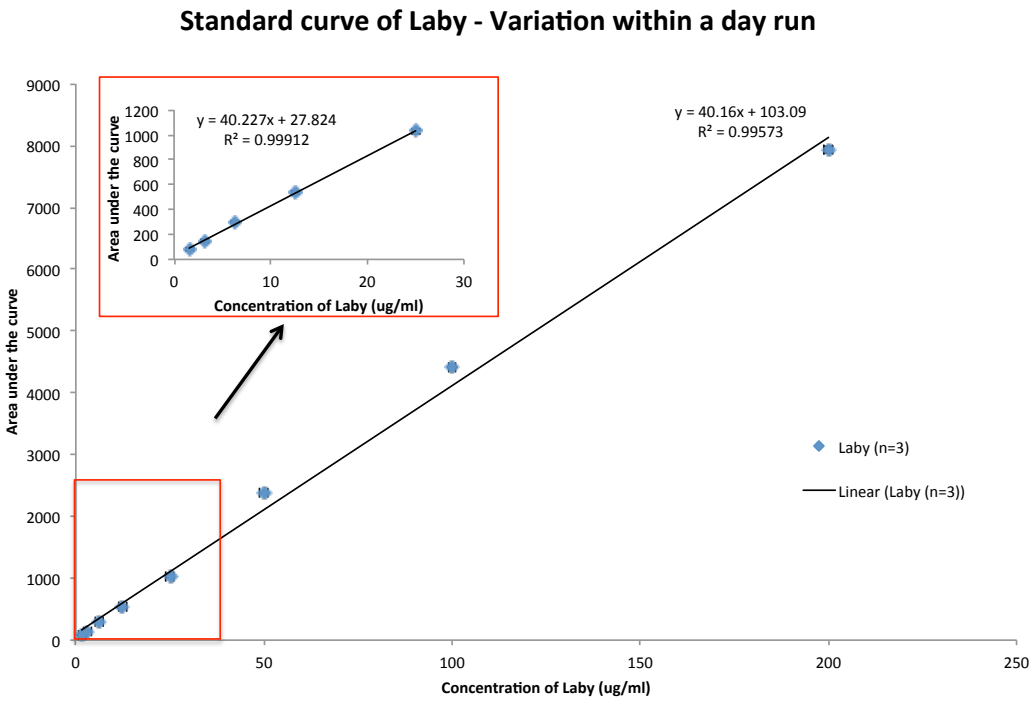

Figure 3-21: Calibration curve for laby showing concentrations of Laby ranging from 1.56 ug/mL to 200 ug/mL on x-axis plotted against area under the curve on y-axis. Three different samples sets were compared on the same day. Graph in red box showing linearity observed with lower concentrations of Laby from 1.56 ug/mL to 25 ug/mL

Similarly, linear equation for calibration curve obtained from standards run on the same day was y=35.388x+89.89 and $r^2 = 0.9989$ (Figure 3-22). For standards analysed at different days, % RSD was found to be greater than 15% at concentrations 200 µg/mL, 100 µg/mL and 50 µg/mL, 12% for the lowest concentrations 1.56 µg/mL and 3.125 µg/mL and less than 10% for remaining concentrations (Table 3-6).

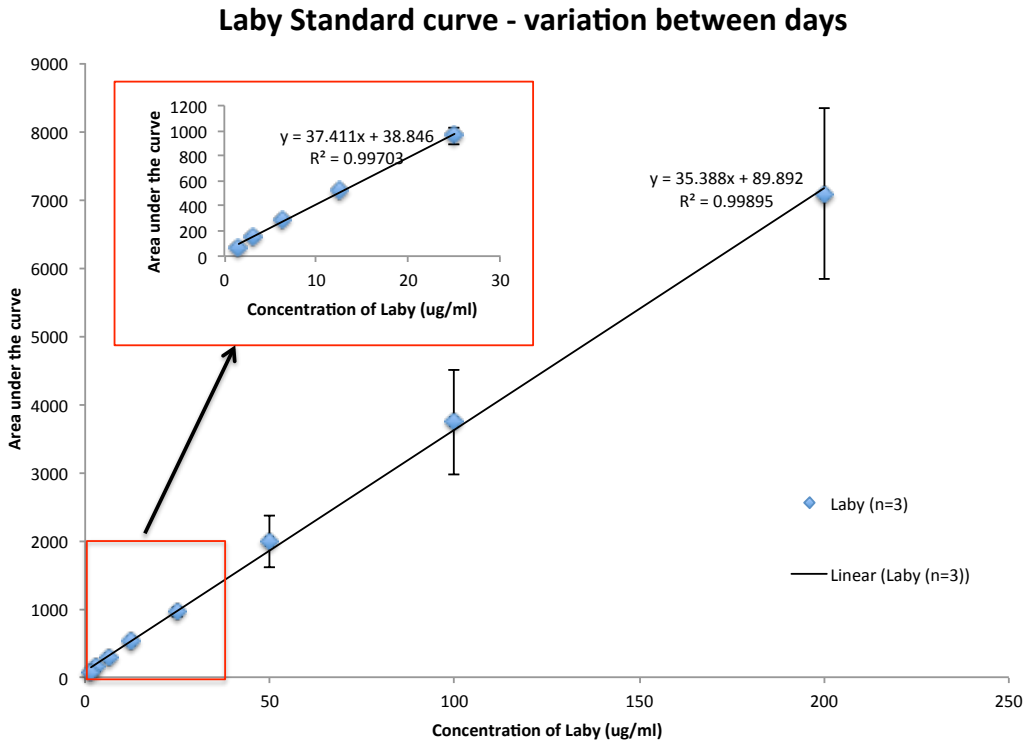

Figure 3-22 Calibration curve for laby showing concentrations of Laby ranging from 1.56 ug/mL to 200 ug/mL on x-axis plotted against area under the curve on y-axis. Three different samples sets were compared on different days. Graph in red box showing linearity observed with lower concentrations of Laby from 1.56 ug/mL to 25 ug/mL.

These results suggest that variation in analysis could be minimum (% RSD < 15%) when a standard curve is run every time along with sample analysed on the same day.

Table 3-6 RSD % of Laby at different concentrations analysed on same day and at different days

Concentration of Laby (ug/mL)	RSD% - within a day run	RSD% - between days run
200	1%	18%
100	0%	20%
50	0%	19%
25	2%	7%
12.5	2%	1%
6.25	1%	6%
3.125	12%	12%
1.56	13%	12%

3.6.4.2 Encapsulation efficiency of Laby-GCPQ B1, B2 & B3 formulations

Encapsulation efficiency of Laby (2.5 mg/mL) - GCPQ (7.5 mg/mL) formulations (1:3) were determined using HPLC. The formulations were centrifuged

to precipitate the un-encapsulated Laby peptide. The Laby GCPQ nanoparticles in the supernatant were quantified by HPLC. The encapsulation efficiency of Laby GCPQ B1, B2 & B3 formulations at ratio 1:3 had encapsulation efficiency around 89% (Figure 3-23). The same can be expressed in moles encapsulated per particle. Moles of Laby encapsulated in GCPQ of batches 1 (10.75 kDa), 2 (12.51 kDa) and 3 (86.75 kDa) were 1.88, 2.17 and 13.37 moles. This shows that laby encapsulation in GCPQ increases with increase in the molecular weights of the GCPQs.

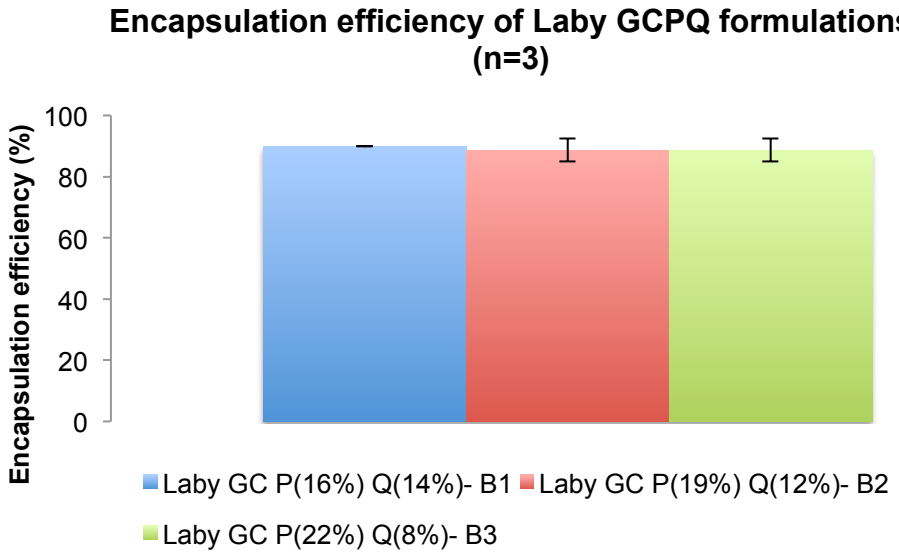

Figure 3-23 Encapsulation efficiency of Laby GCPQ formulations

3.6.5 Colloidal stability of Laby-GCPQ B1, B2 & B3 formulations in simulated medium

Colloidal stability of Laby GCPQ B1, B2 & B3 (1:3) formulations were observed *in vitro* in simulated gastric medium (SGF), simulated intestinal medium (SIF) and Hank's balanced salt solution (HBSS) by characterizing their sizes over time using DLS.

3.6.5.1 SGF

Laby GCPQ B1, B2 & B3 formulations were incubated for 2 h at 37˚C and characterized by DLS for their size and polydispersity index. The samples were measured at time point 30 min, 1 and 2 h. For Laby-GCPQ B1 formulation, the particle size reduced from 572 nm to 140 nm after dilution in SGF (Figure 3-24). The size of Laby GCPQ B2 (20 nm) remained the same after dilution in SGF (Figure 3-24). Laby GCPQ B3 formulation of size around 84 nm also reduced in size to 10 nm after dilution in SGF (Figure 3-24). This shows that larger particles reduce in size upon

dilution in SGF medium. The stability of Laby GCPQ formulations in SGF was also due to the protonation of amines present in GCPQ formulations at acidic pH that prevents particles from aggregating to each other. An increase in the polydispersity index of Laby GCPQ formulations (B2 and B3) at 2 h time point suggest that few particles may have aggregated (Figure 3-25) and a decrease in the PDI of Laby GCPQ formulation B1 at 2 h suggest that few particles may have precipitated in SGF medium (Figure 3-25).

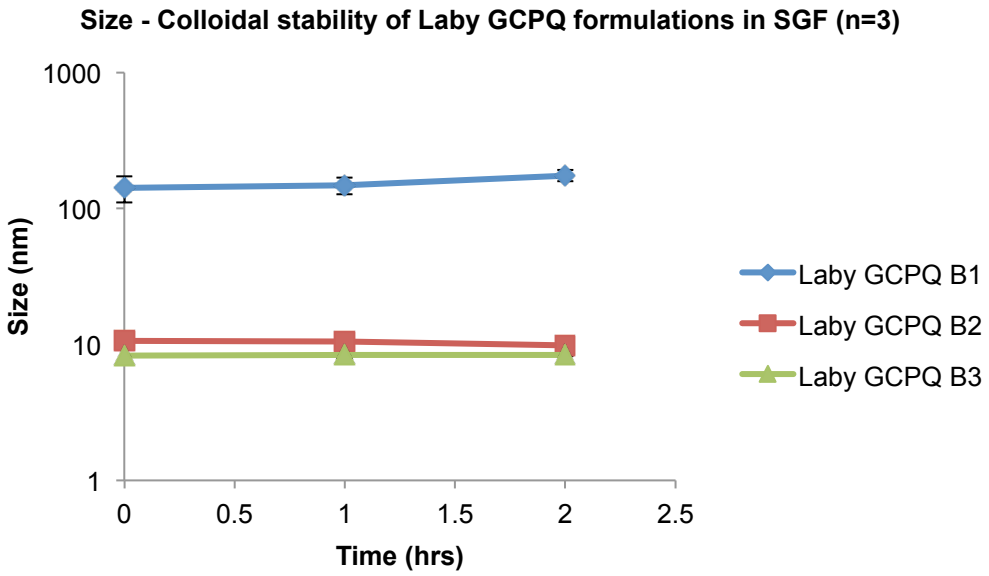

Figure 3-24 Graph showing size distribution of Laby GCPQ formulations of different batches measured using DLS as an indication of their colloidal stability in simulated gastric fluid (SGF) maintained at 37°C and measured up to 2 h.

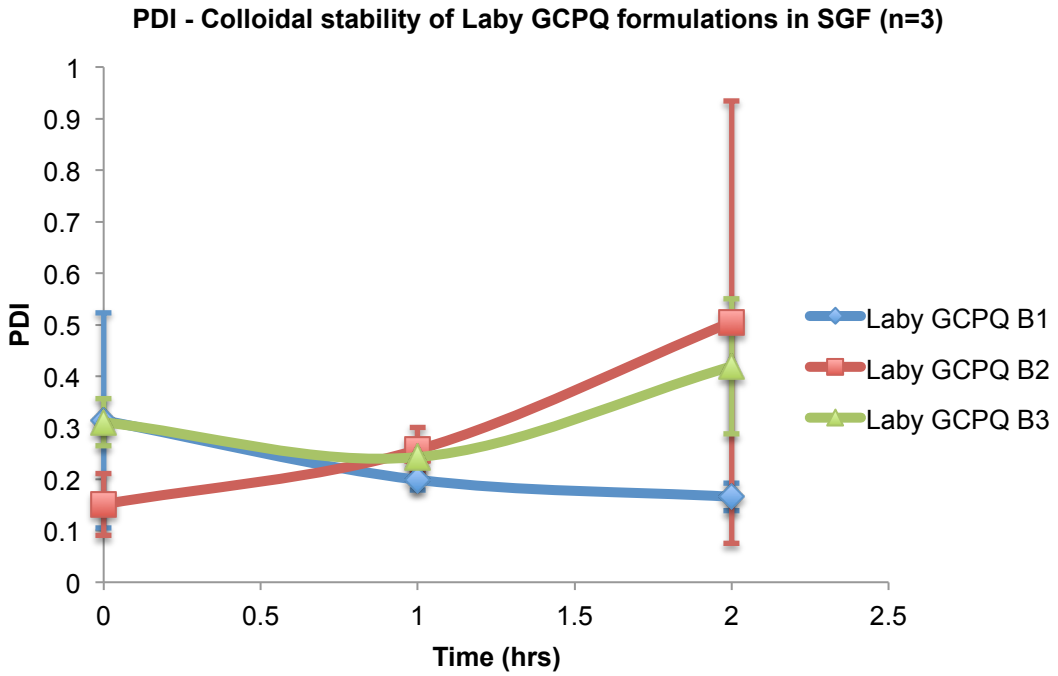

Figure 3-25 Graph showing polydispersity index of Laby GCPQ formulations of different batches measured using DLS as an indication of their colloidal stability in simulated gastric fluid (SGF) maintained at 37°C and measured up to 2 h.

3.6.5.2 SIF

Colloidal stability of Laby GCPQ B1, B2 and B3 formulation in SIF (pH 6.8) incubated at 37˚C for 4 h were characterized for size and polydispersity index by DLS. Laby GCPQ B1 and B3 formulations of size 10 and 100 nm aggregated gradually to size 33 nm and 168 nm in SIF medium (Figure 3-26). There was also an increase in the polydispersity index for both the formulations (B1 & B3) (Figure 3-27). Particle aggregation with Laby GCPQ B2 formulation was not observed (Figure 3-26). However, PDI of Laby GCPQ B2 formulation decreased indicating that few large size particles may have settled down the cuvette (Figure 3-27).

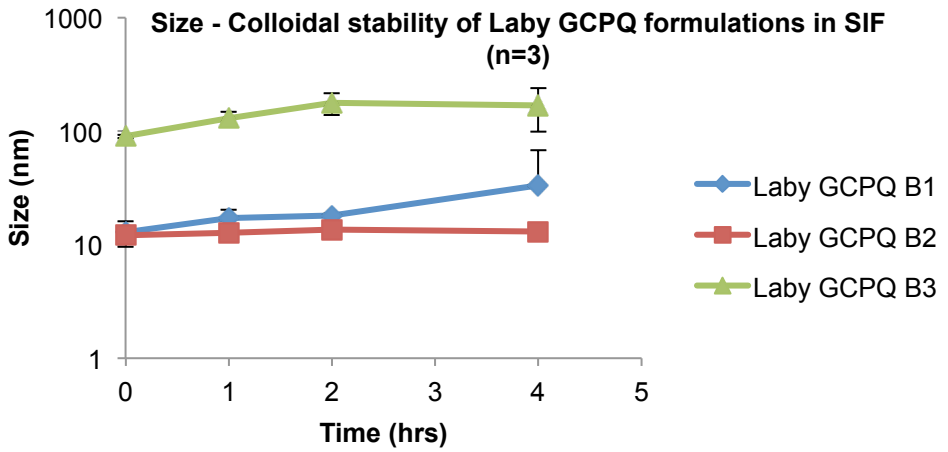

Figure 3-26 Graph showing size distribution of Laby GCPQ formulations of different batches measured using DLS as an indication of their colloidal stability in simulated intestinal fluid (SIF) maintained at 37°C and measured up to 4 h

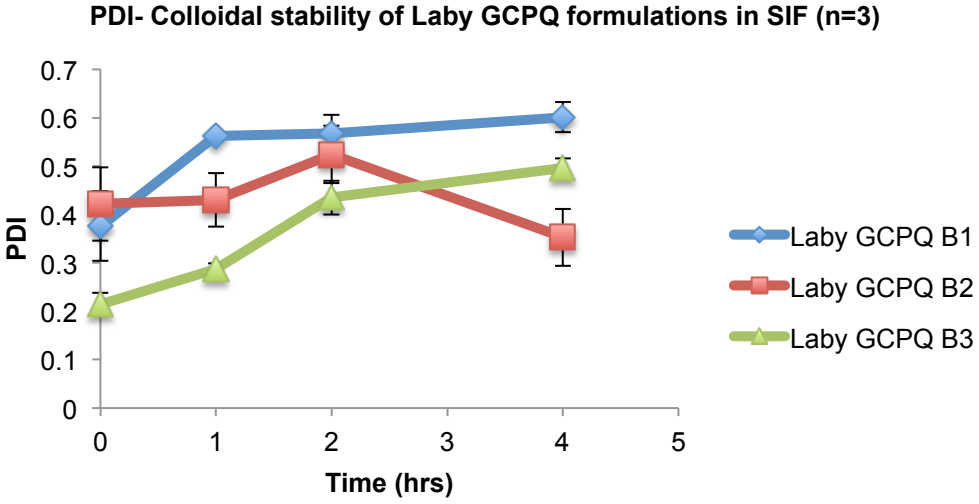

Figure 3-27 Graph showing polydispersity index of Laby GCPQ formulations of different batches measured using DLS as an indication of their colloidal stability in simulated intestinal fluid (SIF) maintained at 37°C and measured up to 4 h

3.6.5.3 HBSS

Colloidal stability of Laby GCPQ formulations B1, B2 and B3 incubated in HBSS (pH 7.4) at 37°C was characterized for size and polydispersity index by DLS. Particle aggregation was observed for all formulations in HBSS. The sizes of Laby GCPQ formulations (B1 and B2) were less than 40 nm at 4 h time point (Figure 3-28). PDI of Laby GCPQ formulation B1 had large error bar only at 4 h suggesting that the particle aggregation may have taken place at later time points (4 h) (Figure 3-29). However PDI of Laby GCPQ B2 formulation suggest that particle aggregation has initiated at earlier time points (Figure 3-29). Particle size of Laby GCPQ B3

formulation increased steadily to 1 µm over a period of 4 h (Figure 3-28). PDI of the particles also increased with increase in the size of the error bar over four h (Figure 3-29). This indicates that the particles have increased in size consistently as well sedimented over time.

Aggregation of Laby GCPQ formulations in HBSS was due to deprotonation of amines in GCPQ at alkaline pH. From the size and PDI of Laby GCPQ B1, B2 and B3 formulations, it could be inferred that the aggregation of particles takes place at different rate with Laby GCPQ B3 formulation aggregating faster in HBSS followed by Laby GCPQ B2 and Laby GCPQ B1 formulation (Figure 3-29). This trend is observed due the differences in the degree of quaternization for each batch of GCPQ (GCPQ B1- 14%, GCPQ B2- 12% and GCPQ B3 – 8%). As a result, lower the degree of quaternization of GCPQ faster their aggregation in HBSS and vice versa.

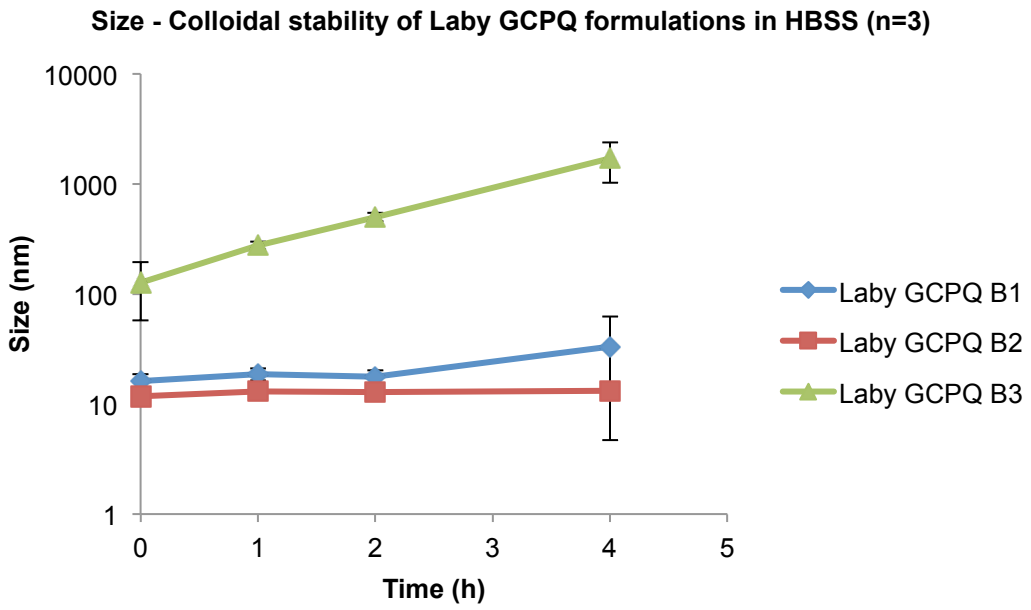

Figure 3-28 Graph showing size distribution of Laby GCPQ formulations of different batches measured using DLS as an indication of their colloidal stability in HBSS maintained at 37°C and measured up to 4 h

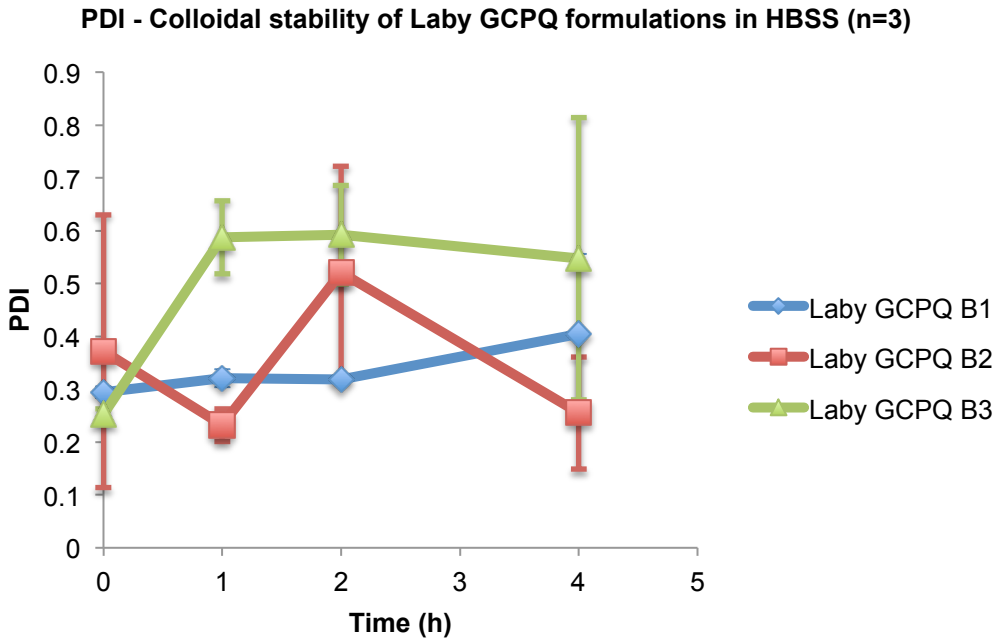

Figure 3-29 Graph showing polydispersity index of Laby GCPQ formulations of different batches measured using DLS as an indication of their colloidal stability in HBSS maintained at 37°C and measured up to 4 h.

3.6.6 Pharmacodynamics and pharmacokinetics of Laby GCPQ formulations

From the above *in vitro* results, it is evident that Laby GCPQ B3 formulation has poor colloidal stability in HBSS. For in vivo studies, Laby GCPQ B1 or B2 can be used formulations, as the formulations had colloidal stabilities in all three simulated fluids (SGF, SIF, HBSS). The pharmacodynamics study was carried out in one of the stable formulations (Laby GCPQ B2) and compared with Laby glycofural formulation.

3.6.6.1 Pharmacodynamics of Laby GCPQ B2 formulations

Pharmacodynamics of Laby formulations was tested in a Complete Freund's adjuvant (CFA) induced chronic pain rat model. As a control, Laby (10 mg/mL) was dissolved in 50:50 ratios of glycofurol and PBS (0.1M, pH 7) and glycofurol alone as vehicle. The formulations were administered orally or nasally to rats induced with inflammation on its hind paw. Rats that could withstand different pain threshold level after subjecting them to Von Frey hairs were recorded. Maximum therapeutic effects for nasally administered formulations were observed at early hours (Figure 3-30). Both Laby glycofurol and Laby GCPQ B2 nasal formulation withstand pain threshold level that was significantly higher than glycofurol (vehicle). Significantly higher therapeutic effect was observed between Laby GCPQ B2 formulation and glycofurol with maximum effect at 40 min and between Laby glycofurol formulation and vehicle with maximum effect at 40 and 60 min. No significant difference was observed between Laby GCPQ B2 and Laby glycofurol nasal formulation.

The maximum therapeutic effect of orally administered formulations were observed at later time points from 60 to 360 min after an initial lag time of around 60 min for the Laby GCPQ B2 and Laby glycofurol oral formulation (Figure 3-31). However, statistical significant difference between Laby GCPQ oral formulation and control was only observed at 240 min. No statistically significant difference was observed between Laby glycofurol and glycofurol only formulation and between Laby GCPQ B2 and Laby glycofurol formulation.

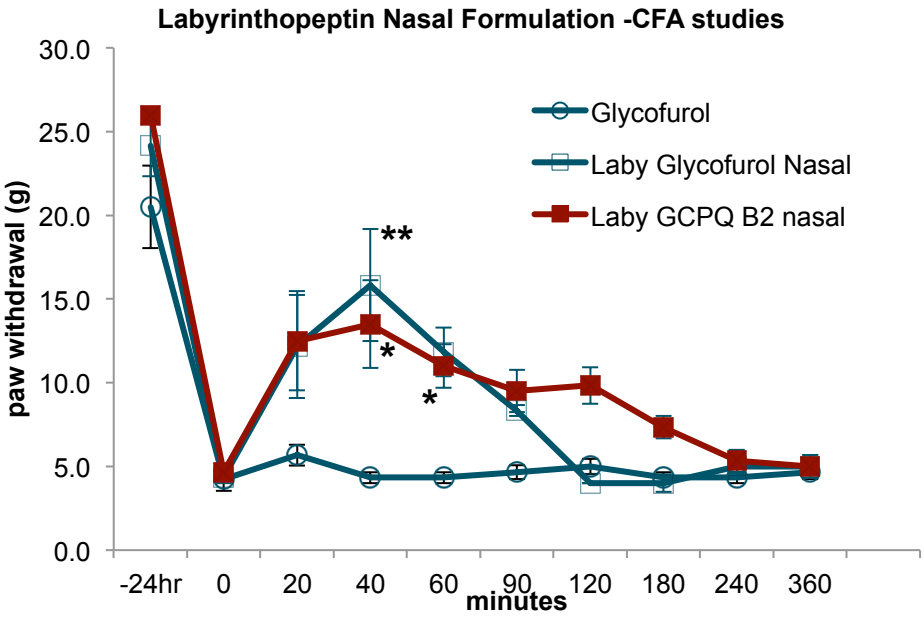

Figure 3-30 Pharmacodynamics of Laby GCPQ Nasal formulations.

(24 h indicates paw withdrawal reaction before administration of CFA. Time point from 0 to 360 min indicates paw withdrawal reaction after administration of CFA. Formulations were administered at time zero. (Subject – SD Rats, Dose – 3 mg/kg of Laby with Glycofurol or GCPQ B2, n=6. Two way repeated anova (green house geisser corrected) - Overall significant difference between Laby GCPQ B2 and glycofurol only formulation and between Laby glycofurol and glycofurol only formulation. ** Laby-GCPQ B2 formulation significantly different from control (glycofurol) at time point 40 min. * Laby-glycofurol formulation significantly different from control at time point 40 and 60 min).

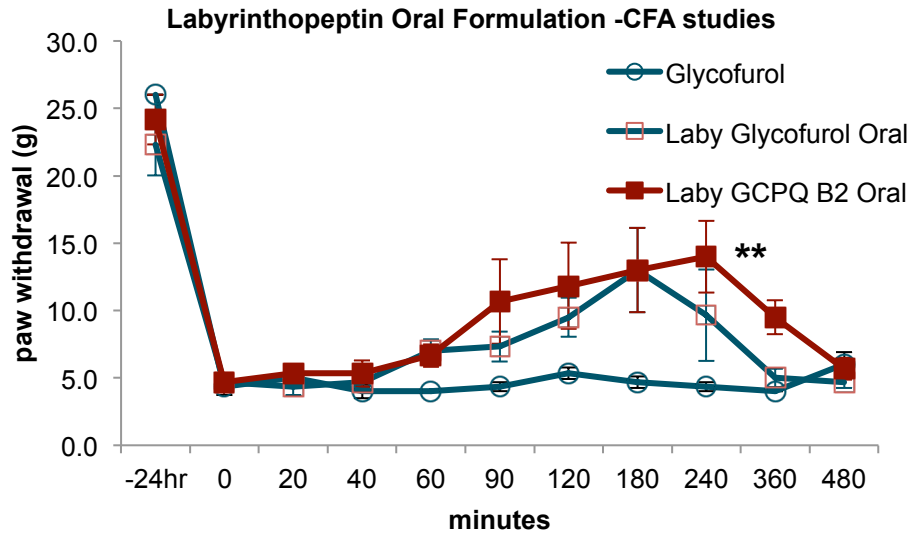

Figure 3-31 Pharmacodynamics of Laby GCPQ Oral formulation.

(24 h indicates paw withdrawal reaction before administration of CFA. Time point from 0 to 360 min indicates paw withdrawal reaction after administration of CFA. Formulations were administered at time zero. (Subject – Rats, Dose – 15 mg/kg of Laby with Glycofurol or GCPQ B2 and glycofurol only formulations, n=6. Two way repeated anova (green house geisser corrected) – Overall significant difference between Laby GCPQ B2 and glycofurol

only formulation. ** Laby-GCPQ B2 formulation significantly different from control at time point 240 min).

3.6.7 Pharmacokinetics of Laby GCPQ formulations

3.6.7.1 Analytical method for quantification of Laby *in vivo*

Mass spectrometer parameters such as source, MRM and signal parameters were optimized to selectively measure laby in plasma sample.

3.6.7.1.a Source Optimization

Source optimization enables optimum dissolvation of samples to maximize signal to noise ratio. The source parameters were optimized to maximize the signal obtained for the respective Laby and internal standard (pentifylline) fragments (Figure 3-32). Each fragment was run under different source conditions of different range. The ESI consist of parameters such as drying gas temperature, drying gas flow, nebulizer, capillary voltage, nozzle voltage, sheath gas flow and sheath gas temperature. The parameter that gives the optimum signal was used to create source method.

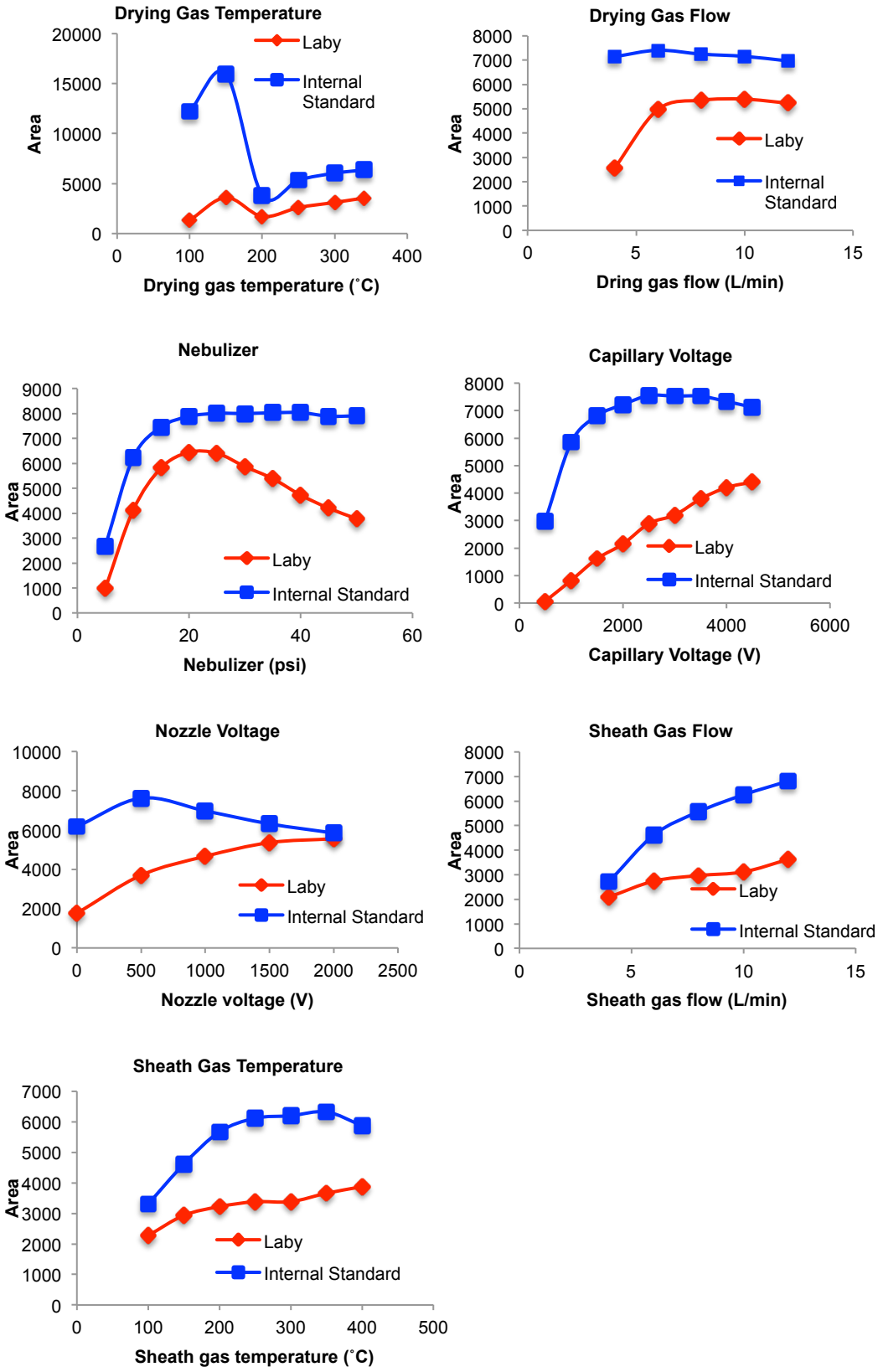

Figure 3-32 Source Optimization of Laby in plasma matrix. Peak area for Laby (blue) and internal standard (red) plotted with source parameters plotted on x-axis against area under the curve on y-axis.

3.6.7.1.b MRM Optimization

Fragmentor voltage accelerates the compounds to collision cell and collision energy fragments the compound of interest (Figure 3-33). Fragment less than a mass of 100 produces noise whereas fragments larger than 400 produces poor signal. Fragmentor voltage and collision energy optimization is necessary for producing better signal with minimum noise.

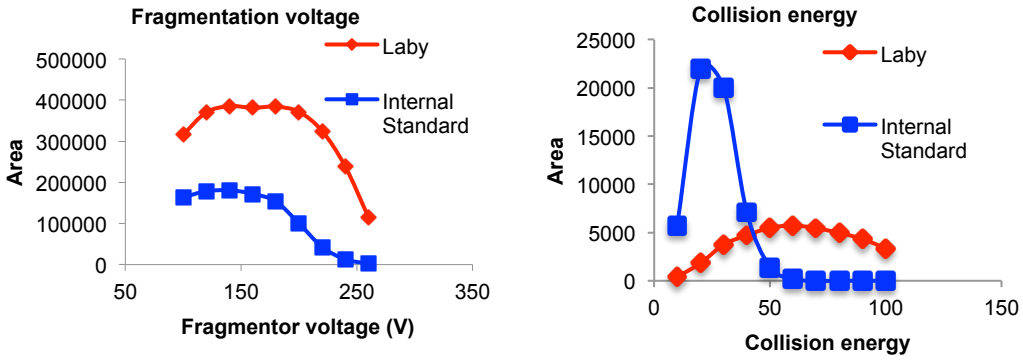

Figure 3-33 MRM Optimization of Laby in plasma matrix. Peak area for Laby (blue) and internal standard (red) plotted with MRM parameters plotted on x-axis against area under the curve on y-axis.

3.6.7.1.c Signal Optimization

Signal optimization can be further improved by optimizing cell acceleration voltage (Figure 3-34) and electron multiplier voltage (Figure 3-35). Cell acceleration voltage (CAV) accelerates the fragment out of the collision cell. CAV is important to avoid cross talk between analyte and internal standard when two peaks are eluting close to each other.

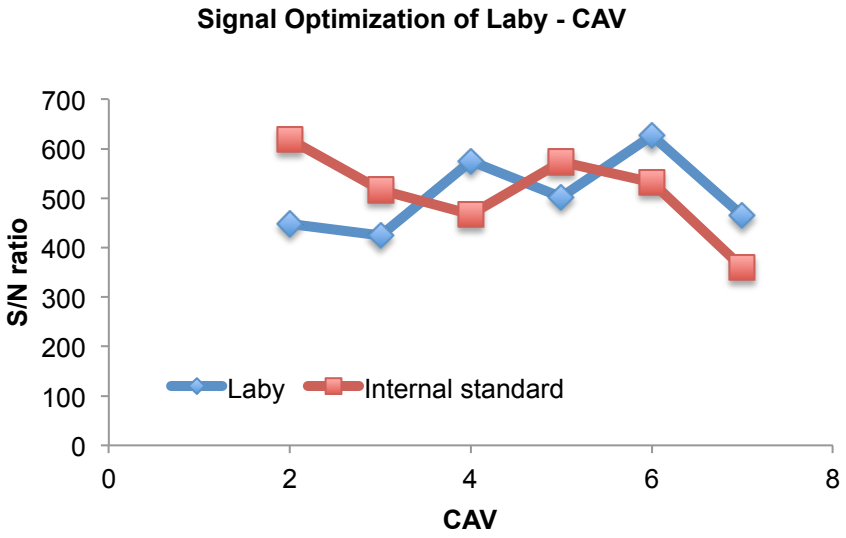

Figure 3-34 Cell acceleration voltage (CAV) for Laby in plasma showing acquisition time on x-axis and area under the curve on y-axis

Electron multiplier voltage (EMV) multiplies the signal obtained from all the parameters mentioned above. EMV can be set between 100 and 400, higher the EMV more the signal obtained and vice versa. Increasing the EMV could also increase the background noise, which can interfere with peak integration. So an optimum EMV parameter was chosen based on the peak resolution.

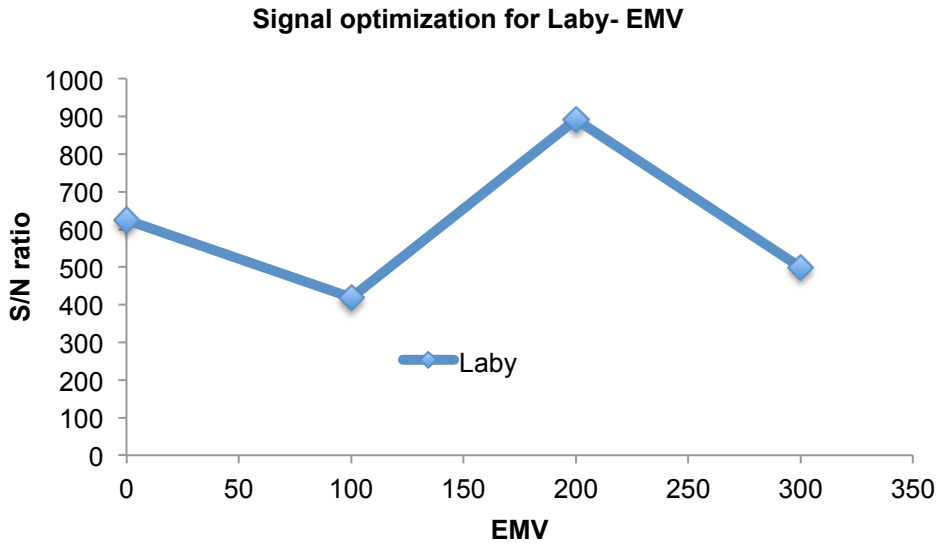

Figure 3-35 Electron multiplier voltage (EMV) for Laby in plasma showing acquisition time on x-axis and area under the curve on y-axis

3.6.7.1.d Calibration Curve for Laby in plasma

With the parameters optimized, Laby and pentifylline (internal standard) peak were obtained at elution time of 4.46 and 4.8 min (Figure 3-36). Calibration curve was plotted with standards ranging from 20 ng/mL to 1280 ng/mL (Figure 3-37). The linear equation for the calibration curve was y= 0.0041x+ 0.2111 with R^2 = 0.99496.

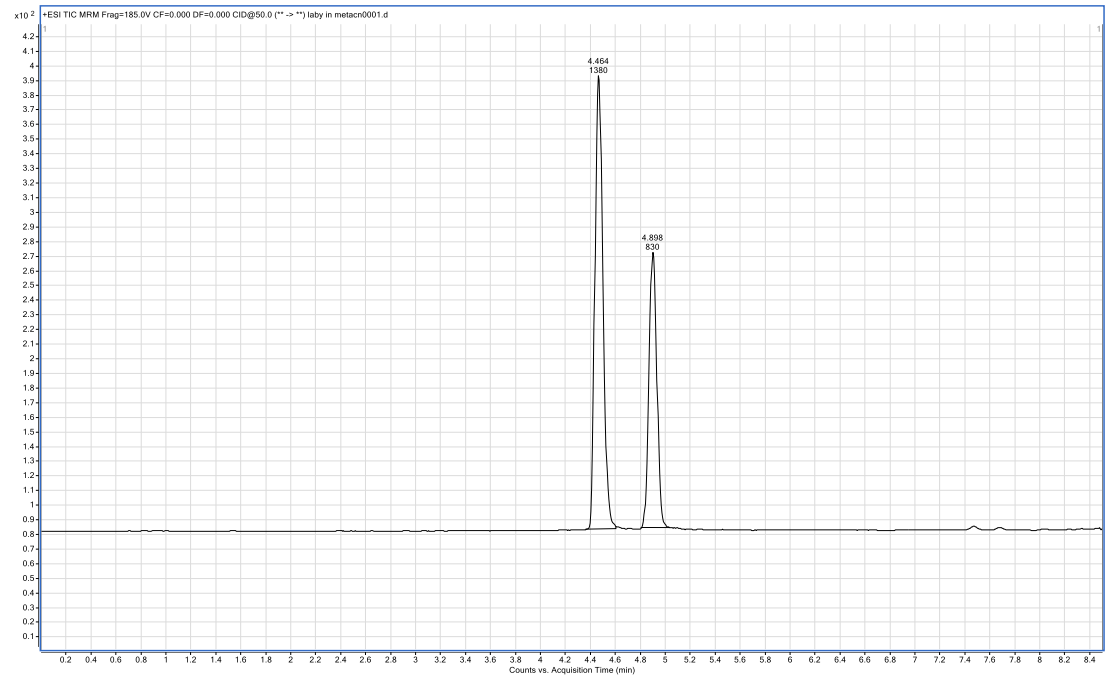

Figure 3-36 Chromatogram for Laby (4.46 min) and Pentifylline (4.8 min) in plasma plotted with time on x-ais against area under the curve on y-axis

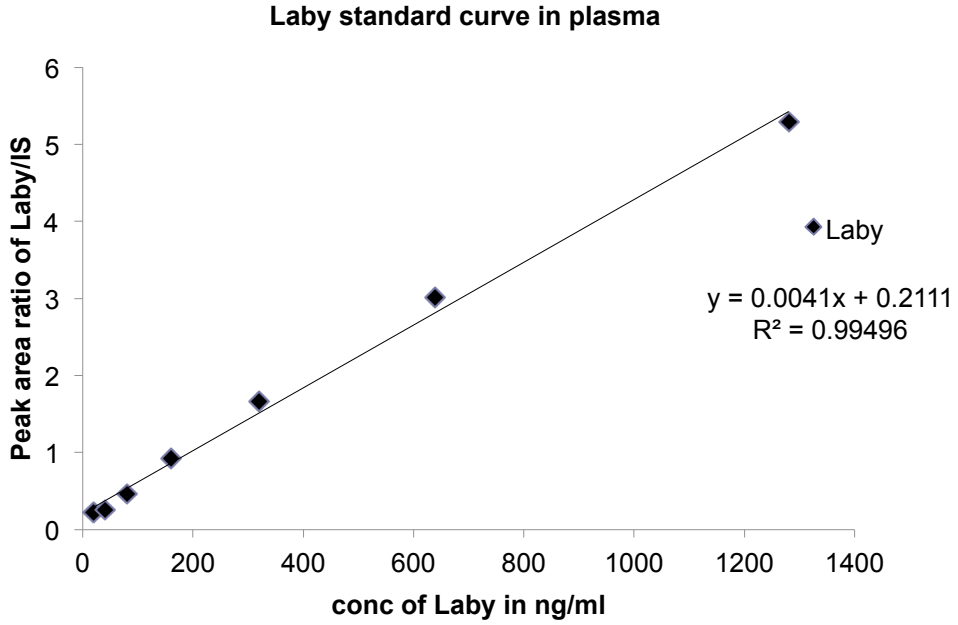

Figure 3-37 Calibration curve for Laby in plasma with concentrations (20 ng/mL to 1280 ng/mL) of Laby (ng/mL) plotted on x-axis against peak area of Laby/IS on y-axis

The LLOQ for the calibration curve was found to be 20 ng/mL with signal five times greater than blank. This method was validated to know if the samples could be compared between days and within a day. Samples run between days had higher coefficient of variation (> 20%) whereas sample run within a day had CV less than 5%. For pharmacokinetic studies, a new standard curve was run every day to

compare samples analyzed on different days (Table 3-7). Plasma matrix did not interfere with the test analyte as the matrix effect obtained by taking ratio of plasma-extracted sample to blank sample had CV around 15% (Table 3-8).

Table 3-7 Validation of Laby Standards (n=3)

Laby concentrations (ng/mL)		Same sample run on same day	Same sample run on different days	Different sample run on different days
LLOQ	**20**	4.82	27.42	13.67
Low	**80**	4.61	21.99	7.94
Medium	**320**	2.63	7.42	9.82
High	**1280**	3.34	25.86	2.88

Table 3-8 Plasma Matrix effect

Laby concentrations	Matrix effect - Laby	Matrix effect - Pentifylline
Low (80 ng/mL)	12.23	11.05
High (320 ng/mL)	8.96	12.39

3.6.7.1.e Calibration curve for Laby in Brain tissue sample

Calibration curve was plotted with standards ranging from 20 ng/g to 640 ng/g (Figure 3-38). The linear equation for the calibration curve was y= 0.0036x+ 0.0327 with R2 = 0.99767.

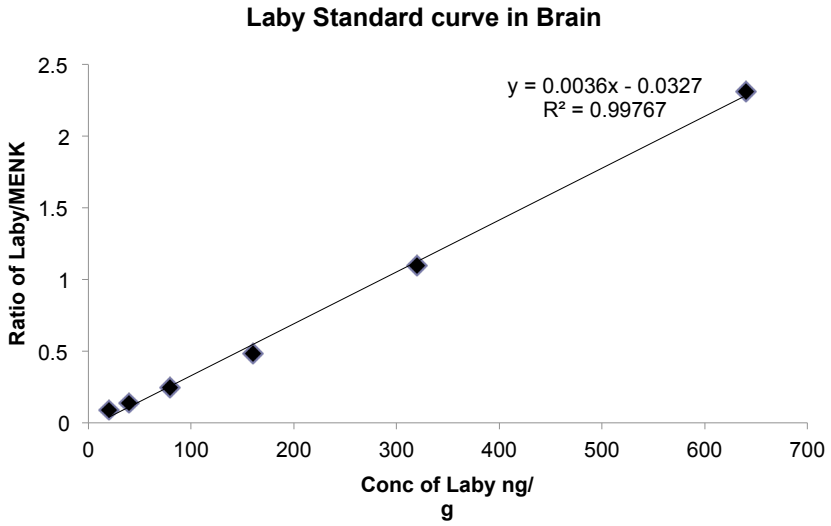

Figure 3-38 Calibration curve for Laby extracted from brain homogenate with Laby concentrations ranging from 20 ng/g to 640 ng/g plotted on x-axis against peak area of Laby/IS on y-axis

3.6.7.2 Pharmacokinetics of Laby GCP (16%)Q (14%) (B1) formulations in plasma – Comparison of oral and nasal formulation

Laby GCPQ B2 and Laby glycofural formulations exhibited anti nociceptive activity in rats. The concentrations of Laby in plasma and brain following oral and nasal delivery of Laby GCPQ and Laby glycofural formulations were tested. For pharmacokinetics studies, Laby GCPQ B1 oral formulation having similar colloidal stability was studied. This is because of the constraints in reproducing GCPQ B2 polymer of same specifications (palmitoylation -19%, quaternization -12% and molecular weight- 12.5 kDa). The pharmacokinetics results were also compared to Laby GCPQ B3 oral formulation that has poor colloidal stability in HBSS (pH 7.4). This is to understand whether the pH induced aggregation of Laby GCPQ B3 formulation has any influence on the uptake of laby compared to colloidally stable Laby GCPQ B1 formulation.

Laby GCPQ B1 formulation was compared with Laby GCPQ B3 and Laby glycofurol formulation. Concentrations of laby in plasma for Laby-GCPQ B3 formulation increased at initial time points (30 min, 60 min and 120 min) with a maximum concentration of 1042 ng/mL at 120 min time point. The laby concentrations subsided at later time points (240 min to 480 min). Next to Laby-GCPQ B3 formulation, Laby-glycofurol formulation had increasing concentrations of laby in plasma from time point 30 min to 240 min. The maximum concentration of 304 ng/mL was observed for Laby glycofurol at time point 240 min after which the concentrations subsided at later time points. Least concentrations of Laby in plasma were observed for Laby-GCPQ B1 formulation that increased only to a maximum of 117 ng/mL at 240 min. Overall significant differences were not observed between the treatments, Laby GCPQ B1 formulation and Laby glycofurol formulation (Figure 3-39). However significant differences in Laby concentrations were observed between Laby GCPQ B1 and Laby GCPQ B3 formulations at 60 min time point. Laby GCPQ B3 formulation was also significantly different from Laby GCPQ B3 and glycofurol formulation at 120 min time point.

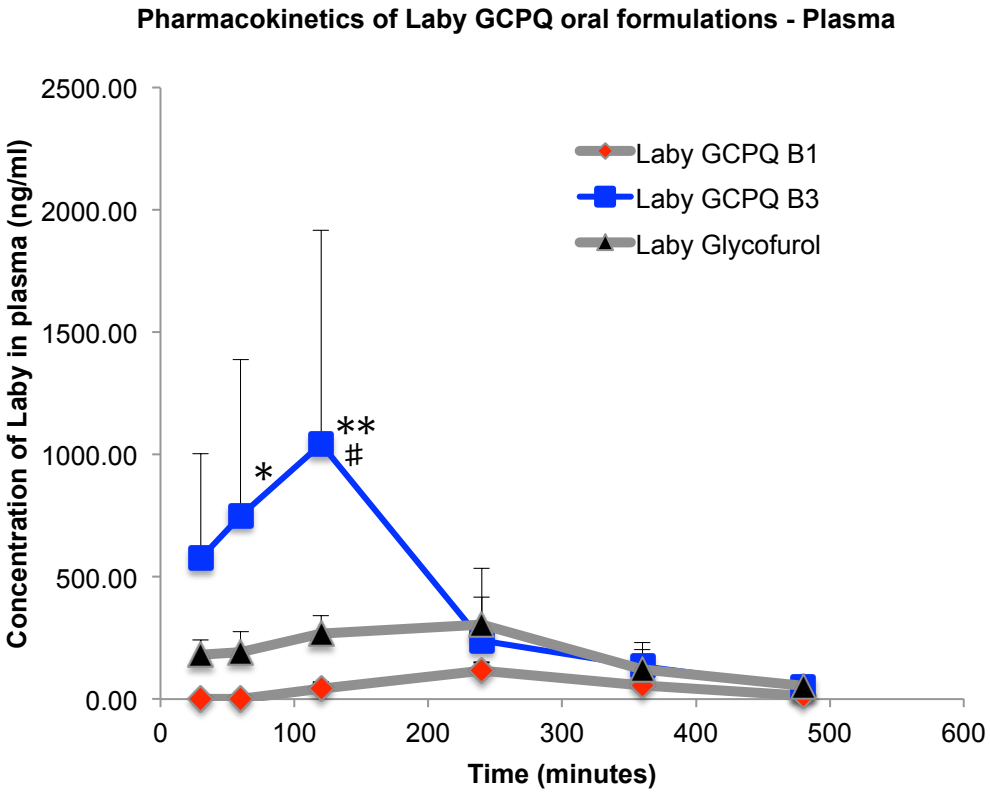

Figure 3-39 Pharmacokinetics of Laby GCPQ B1 & B3 oral formulations against Laby glycofurol oral formulation. (Subject – Rats, Dose – 30 mg/kg, repeated measure, n=5) Two-way anova - *(p = 0.0398), Laby GCPQ B3 formulation significantly different from Laby GCPQ B1 formulation at time point 60 min. ** (p= 0.0046), Laby GCPQ B3 formulation significantly different from Laby GCPQ B1 formulation at time point 120 min ♯ (p= 0.324), Laby GCPQ B3 formulation significantly different from Laby glycofurol formulation at time point 120 min.

Table 3-9 Pharmacokinetics of Laby Oral Formulations

Pharmacokinetic parameters	**Laby GCPQ B3**	**Laby Glycofurol**	**Laby GCPQ B1**
AUC (ugh/L)	3207.88 ± 5783.95	1542.18 ± 1707.10	424.34 ± 300.59
Cmax (ng/mL)	1042.99 ± 874.52	304.82 ± 230.28	117.12 ± 34.24
Tmax (min)	120	240	240

Since, Laby GCPQ B3 oral formulation had higher concentrations in the blood compared to Laby GCPQ B1 oral formulation. The pharmacokinetics of Laby GCPQ B3 nasal formulation and Laby glycofural formulation were compared.

Laby GCPQ B3 and Laby glycofurol formulation were compared after nasal administration in rats. The concentration of Laby measured from time point 30 min to 360 min after nasal administration of Laby GCPQ B3 formulations were consistently higher (677 to 396 ng/mL) than the concentrations observed for Laby glycofurol formulation (418 to 71 ng/mL). For nasal formulations, overall significant difference was observed between Laby GCPQ B3 and Laby glycofurol formulation (Figure 3-40). The area under curve (AUC), Cmax and Tmax are summarized in (Table 3-9) and (Table 3-10).

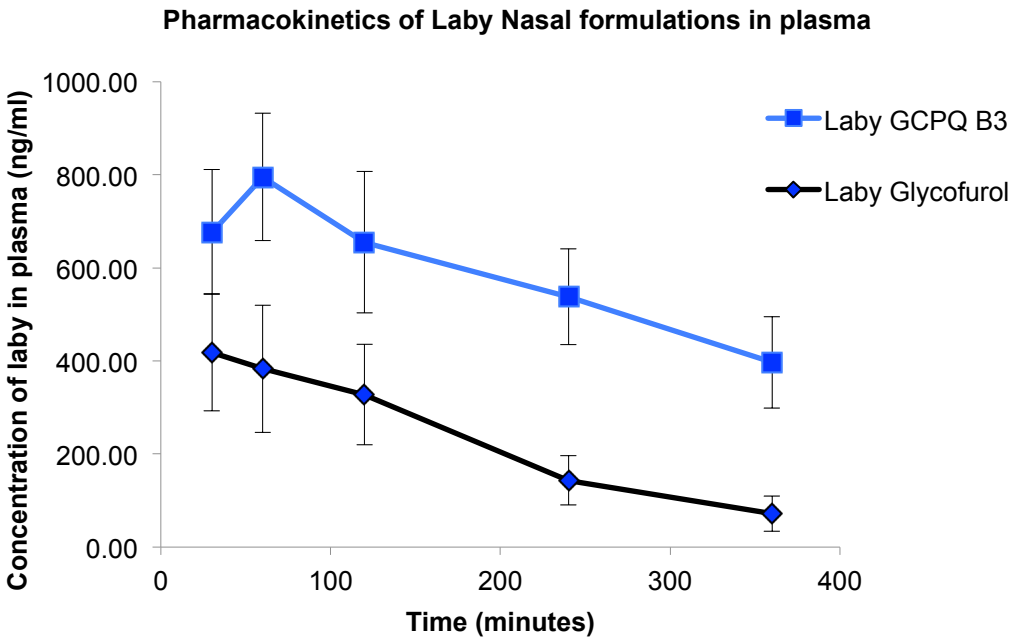

Figure 3-40 Pharmacokinetics of Laby GC P(21%) Q(8%) B3 Nasal formulation (Subject – Rats, Dose – 3 mg/kg, repeated measure, n=5). Two way anova- (p = 0.0490), Laby GCPQ B3 formulation significantly different from Laby glycofurol formulation.

Table 3-10 Pharmacokinetics of Laby Nasal Formulations

	Laby Glycofurol	Laby GC P(21%) Q(8%) B3
AUC (ugh/L)	1346.59 ± 981.56	3390.76 ± 1515.54
Cmax (ng/mL)	418.65 ± 126.23	795.38 ± 137.13
Tmax (min)	30	60

3.6.7.3 Pharmacokinetics of Laby GCPQ B3 formulations in Brain tissue sample

To understand whether Laby exhibit peripheral or central action, distribution of Laby in brain following nasal and oral administration were studied. No detectable Laby peak was observed in the brain tissue sample for Laby GCPQ formulations administered nasally or orally.

3.7 Discussion

GCPQ is an amphiphilic polymer that has been reported to solubilize hydrophobic drugs by micelle formation. Small molecular weight hydrophobic drugs and peptide such as cyclosporine [146], amphotericin B [153] and its pro drug form of leucine enkephalin (LENK) called TP-LENK [53] has been previously encapsulated with GCPQ. The resulting micelles had shown improved oral availability and therapeutic effect *in vivo* in rats and murine model.

In this study, poorly soluble labyrinthopeptin peptide was formulated with GCPQ to improve its oral bioavailability and the therapeutic effect of the peptide. GCPQ of three different batches were formulated with Laby and characterized *in vitro* and *in vivo*. Laby GCPQ B1 and Laby GCPQ B2 were prepared by old method of synthesis and GCPQ B3 was prepared by new method of synthesis. Their *in vitro* and *in vivo* results within and between the different methods of synthesis were compared.

From the solubility data, it was known that Laby has poor solubility in physiological saline (0.6 mg/mL). In order to improve the solubility of Laby in aqueous solution, Laby was formulated with GCPQ. Firstly, the minimum concentration of GCPQ that is required to solubilize Laby was evaluated by keeping the Laby concentration constant (2.5 mg/mL) and by adding different concentrations of GCPQ in water. Weight ratios of Laby to GCPQ (from Laby GCPQ of 1:1 to 1:5) was used and evaluated by TEM.

Laby GCPQ B2 formulation at different ratios was characterized. TEM analysis shows that at peptide polymer ratio 1:1, large aggregates (0.9 to 2 μm) and particles (20 to 750 nm) were formed (Figure 3-8). However, increasing the GCPQ concentration in the formulation with ratios ranging from, 1:2 to 1:5, resulted in no micron sized aggregates (Figure 3-9, Figure 3-10, Figure 3-11, Figure 3-12). In DLS, only small particles (around 20 nm) were observed at any given ratios. Laby GCPQ B2 formulation of ratio 1:3 also produced least PDI of 0.382 compared to PDI of other Laby GCPQ ratios, such as; 1:1, 1:2, 1:4 and 1:5 that were larger than 0.4 (Figure 3-13). This ratio (1:3) is observed to be lower than previous oral formulations made at 1:5 ratios [53]. For further studies Laby GCPQ formulation prepared at weight ratio 1:3 were used.

The above Laby GCP (19%) Q (12%) (B2) formulation prepared at ratio 1:3 was also compared with Laby GCPQ B1 and B3 formulation, Laby and Laby PGC

formulation (Figure 3-15). GCPQ with low palmitoylation of 16% had particle sizes analysed by DLS was observed to be significantly higher (572 nm) than the size of Laby GC P (19%) Q(12%) B2 formulation with size 13.43 nm and Laby GC P (22 %) Q(8%) B3 formulation with size 84 nm. The size characterization of different batches of GCPQ with different degree of palmitoylation follows a trend with low palmitolation GCPQ forming large particles (572 nm) and the particle size reduces down to 11 nm with GCPQ of degree of palmitoylation 19%. Further increase in palmitoylation (22%) induces aggregation of Laby GCPQ nanoparticles to size around 84 nm. TEM image also suggest that these large particles are aggregated from small particles and appears dense (Figure 3-18).

Particle sizes of Laby GCPQ formulations were also compared with Laby-PGC formulations by DLS (Figure 3-15). At any given ratio (1:3), Laby PGC formulations formed particles around 200 nm, when analysed by DLS immediately after probe sonication. However, the particles precipitated within one hour. This suggests that quaternization is important for maintaining the stability of GCPQ nanoparticles.

GCPQ has better solubility than its preceding chitosan based polymers due to the presence of quaternary ammonium group that remains charged independent of the pH of their solution. Surface charge of laby GCPQ B1, B2 & B3 formulation increased with increase in the quaternization of the GCPQ polymer. Laby GCPQ B1 formulation with the highest quaternization of 14% had zeta potential of +48mV followed by Laby GCPQ B2 (Q-12%) and B3 (Q-8%) formulation with zeta potential of +46 mV and +39.8 mV respectively (Figure 3-19). The surface charge of Laby GCPQ formulations was observed to be much higher than Laby PGC (+10 mV) or Laby only formulation (-34.6 mV). The lower surface charge of Laby PGC formulation could be the reason for aggregation and precipitation of the formulation. A change in the negative zeta potential of laby from -34.6 mV to above + 39mV with any GCPQ polymer of B1, B2 and B3 suggest that the peptide was encapsulated in the GCPQ polymer.

Laby GCPQ nanoparticles that were characterized by size and charge were also estimated to know the peptide loading efficiency of the polymer. Encapsulation efficiency of hydrophobic drug is determined by hydrophobicity of polymer. GCPQ batches B1, B2 and B3 having degree of palmityolation 16%, 19% and 22% had encapsulation efficiency of around 89% (Figure 3-23). It was previously reported

that the drug (propofol) incorporation with GCPQ nanoparticles was reported to be 1 order magnitude higher than it was seen with pluronic block copolymer [134]. Kim et al reported an encapsulation efficiency of 85% for hydrophobic RGD peptide loaded in to HGC (hydrophobic modified glycol chitosan) nanoparticles [232].

The colloidal stability of Laby GCPQ B1, B2 and B3 formulation in simulated gastric medium, simulated intestinal medium and HBSS was characterized.

Laby GCPQ B1 formulation that had particle size around 572 nm, reduced in size to 140 nm in SGF or less (20 nm) in SIF and HBSS. The size of Laby GCPQ B2 formulation remains same (20 nm) after dilution in SGF, SIF and HBSS. At a given pH, 1.2 (SGF), 6.8 (SIF) and 7.4 (HBSS), the formulations were observed to be colloidally stable (Figure 3-24, Figure 3-26, Figure 3-28). *In vitro* results suggest that Laby GCPQ B1 and B2 formulation in simulated medium has similar characteristics.

However, when the Laby GCPQ B3 formulation was dispersed in simulated medium, polymer synthesized by new method (GCPQ B3) exhibited different colloidal stability compared to polymers synthesized by old method (GCPQ B2). In SGF (Figure 3-24), Laby GCPQ formulation B3 was stable for at least 2 h. Their stability in SGF is due to the protonation of amines in acidic pH. However, Laby formulation with GCPQ B3 synthesized by new method aggregated in SIF (pH 6.8) (Figure 3-26) and precipitated in HBSS (7.4) within 4 h (Figure 3-28). The major differences between the two methods of GCPQ synthesis were that the polymer (GCPQ B3) obtained by new method was more polydisperse (2.5), which could be due to the aggregation of polymer as a result of their hydrophobic and hydrophilic characteristics. Laby GCPQ B3 formulation had degree of palmitoylation of 22% higher than the palmitoylation percentage of Laby GCPQ B1 and B2 formulation. It was previously reported that polymer hydrophobicity has influence on aggregation of GCPQ polymer [134]. This could be the cause for aggregation of Laby GCPQ (new method - B3) nanoparticles in SIF and HBSS. The degree of quaternization of Laby GCPQ B3 formulation was also observed to be lower (8%) than it was for GCPQ polymer B1 (14%) and B2 (12%) formulation. Laby GCPQ B3 formulation in SIF and HBSS resulted in aggregation due to deprotonation of GCPQ polymer at alkaline pH when the quaternization was only 8%. As the Laby GCPQ B1 and B2 formulation had similar colloidally stability at different simulated medium, pharmacodynamics was studied on one of the formulations.

Previously reported laby formulation was intravenously administered at a dose of 3 mg/kg on spared nerve injury mouse model of neuropathic pain. The efficacy was stable over a period of 6 h and disappeared completely after 24 h [226]. The dose of Laby GCPQ oral formulation (15 mg/kg) was improved by 5 folds compared to laby intravenous formulation (3 mg/kg) [226]. For *in vivo*, pharmacodynamics of Laby GCPQ B2 formulation was tested by non-invasive methods such as nasal and oral administration. Laby GCPQ B2 formulation was tested against Laby glycofurol and glycofurol formulations. Laby dissolved in glycofurol was used as a control. Laby GCPQ B2 formulation exhibited significant therapeutic effect at later time point (240 min) following oral administration (Figure 3-39). However, nasal administration of Laby GCPQ B2 and Laby glycofurol formulation exhibited significant therapeutic effect at earlier time points (40 and 60 min) (Figure 3-40). This therapeutic effect was observed to be short lived compared to previously made laby intravenous formulation, which had significant therapeutic effect lasting for 6 h from the time of administration [226]. These data suggest that prolonging the circulation time of Laby GCPQ nanoparticles during systemic circulation can improve the therapeutic effect of Laby GCPQ formulation.

It was previously reported that nasal administration of glycofurol leads to enhanced and prolonged absorption of T1 peptide [233]. The therapeutic effect observed with Laby glycofurol oral formulation could be due to the permeation enhancing characteristics of glycofurol itself. No therapeutic effect was observed for glycofurol only formulation.

Pharmacokinetics was only tested on Laby GCPQ B1 formulation due to constraints in reproducing Laby GCPQ B2 polymer with same specification. Here the comparison between two formulations i.e Laby GCPQ B2 pharmacodynamic data and Laby GCPQ B1 pharmacokinetic data were based on the *in vitro* results that, both the formulations were identical. Also the dose of Laby in glycofural or GCPQ oral formulations used in pharmacokinetics studies were twice (30 mg/kg) that of the concentrations used for oral pharmacodynamics studies (15 mg/kg). Oral dosages of Laby GCPQ B1 and Laby glycofurol were increased in order to detect measurable quantities of laby following oral administration. On the contrary, poor concentrations of Laby in blood were observed for Laby GCPQ B1 formulation (Figure 3-39). The formulation was also observed to be insignificant to Laby glycofurol formulation. It could be possible that the laby GCPQ B1 nanoparticles are

cleared faster from blood and distributed in the tissue. Bio-distribution studies for the above formulation have to be carried out in the future. Also, Laby GCPQ B1 formulation had lower palmitoylation percentage (16%) compared to Laby GCPQ B2 formulation (19%) that shows therapeutic effect in pharmacodynamic studies.

Pharmacokinetics of Laby GCPQ B3 oral formulation was also compared to Laby GCPQ B1 formulation to understand if pH induced aggregation of Laby GCPQ B3 in simulated medium has any influence on the uptake of Laby across the gut. Pharmacokinetics of Laby GCPQ B3 formulations was tested *in vivo* after oral and nasal administration. Laby GCPQ B3 oral formulations exhibited higher concentrations of Laby in plasma at earlier time points that are significantly different from laby GCPQ B1 at 1 and 2 h and from Laby glycofurol at 2 h (Figure 3-39). This was observed to be similar to pharmacokinetics of oral dose of gabapentin in rats that showed maximum concentration in plasma within 1 to 3 h after administration and eliminated between 2 to 3 h [234]. The hydrophobic nature of GCPQ B3 polymer (palmitoylation- 22%) could have resulted in enhanced absorption of laby GCPQ B3 formulation across the enterocytes. Hang et al reported that polymer hydrophobicity has positive effect on oral absorption of cyclosporine- poly(ethylenimine) nanoparticle [135]. Effect of palmitoylation on oral absorption of GCPQ nanoparticle could be studied in future.

It could also be possible that the interaction between quaternary ammonium group of GCPQ and mucus membrane had an effect on uptake of Laby GCPQ nanoparticles across the enterocytes. Chitosan and chitosan derived polymers are mucoadhesive in nature where the positively charged amines in chitosan polymers interact with negatively charged carboxyl or sulphate group of mucin proteoglycan polymer [235]. Wang et al reported that cationic nanoparticles at higher concentration could collapse mucus gel forming large channels that increases the bioavailability of target drugs [236]. This could be the reason for Laby GCPQ B3 formulation (P 21% and Q 8%) showing better concentration of Laby in plasma.

However, this was not the case with respect with Laby GCPQ B1 formulation, which has degree of quaternization of 14%. One possible hypothesis is that GCPQ B1 with high quaternization of 14% could have bound to negatively charged mucin polymers and excess positive charge could have resulted in detangling of mucin polymers due to electrostatic repulsion. This results in removal of outer mucus layer along with bound nanoparticles during gastrointestinal transit.

The effect of different quaternization of GCPQ on mucus could be studied in the future.

Since, the concentrations of Laby for Laby GCPQ B3 oral formulations were higher than Laby GCPQ B1 formulation, pharmacokinetic studies were only carried out in Laby GCPQ B3 and Laby glycofural nasal formulations. Laby GCPQ B3 nasal formulation also exhibited significantly higher laby concentration in plasma compared to Laby glycofurol formulation. No detectable Laby concentrations were observed in brain after nasal or oral administration. This suggests that Laby could have acted peripherally to exhibit analgesic effect.

3.8 Summary and future work

For the first time, an oral formulation of labyrinthopeptin was prepared using GCPQ nanoparticle. The solubility of Laby in aqueous solution was improved 10 times using GCPQ nanoparticles with better loading efficiency. Therapeutic effect of Laby GCPQ and Laby glycofurol formulation was demonstrated in rat CFA model following oral and nasal administration. High degree of palmitoylation and low quaternization GCPQ polymer could have an effect on the uptake of Laby GCPQ formulation across the enterocytes. Also anti nociceptive action of laby glycofurol formulation was observed due to penetration enhancing properties of glycofurol.

In future, it is important to understand the uptake of Laby GCPQ formulations from different palmitoylation GCPQ polymers following oral administration. Since it was observed that high palmitoylation GCPQ polymer has better concentration of Laby in plasma compared to low palmitoylation GCPQ following oral administration, it would be interesting to observe if the pharmacodynamics of Laby GCPQ B3 (P 21% and Q 8%) formulation shows better therapeutic effect compared to Laby GCPQ B2 (P 19% and Q 12%) formulation. Further, differences in the uptake mechanism of low and high palmitoylation GCPQ polymer and their respective Laby GCPQ formulations could be studied *in vitro.* Laby GCPQ B1 and B3 formulation also had different degree of quaternization of 14% and 8% respectively. It was hypothesized that the degree of quaternization has effect on interaction of Laby GCPQ nanoparticles with the mucus and hence their differences in the bioavailability of Laby. The interaction of Laby GCPQ formulation having different degree of quaternization and palmitoylation with the mucus should be studied in the future. Laby concentrations were not observed in brain. However, its concentration in spinal cord can be measured to understand if Laby has peripheral or central action. Further, tolerance to Laby GCPQ formulations could be tested against control such as morphine.

4 Oral Delivery of Methionine Enkephalin peptide for the treatment of pancreatic cancer

4.1 Objective

The objective of this chapter is to,

1. Characterize MENK peptide for size and critical micellar concentration.
2. Formulate MENK-GCPQ (B1 & B2) IV and oral formulation by various methods.
3. Characterize MENK-GCPQ (B1 & B2) IV and oral formulation for size, charge, encapsulation efficiency and colloidal stability.
4. Evaluate the pharmacokinetics of MENK-GCPQ oral and IV formulations.
5. Evaluate the pharmacodynamics of MENK-GCPQ oral and IV formulation in mice tumour xenograft model.

4.2 Met-Enkephalin (MENK)

Met-enkephalin is an endogeneous pentapeptide with amino acid sequence YGGFM (Figure 4-1). The peptide was first discovered and characterized by Hughes, Kosterlitz, et al. in 1975 [237]. Met-enkephalin has various role in physiological process as analgesic [238], as immune modulators [239] and as growth regulators [240].

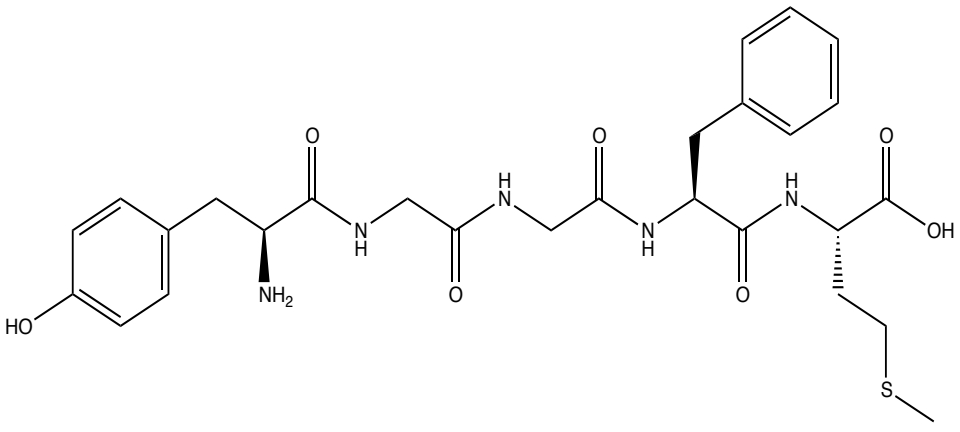

Figure 4-1 2-D structure of Methionine Enkephalin

4.2.1 Biosynthesis of MENK

MENK is produced by proteolytic cleavage of proenkephalin, a precursor peptide hormone [241]. Proenkephalin is converted to an intermediate upon action of endopeptidases. This intermediate is further cleaved by carboxypeptidases to

methionine enkephalin [242] [243]. Each proenkephalin produces four copies of Met-enkephalin, one copy of leu-enkephalin and two copies of extend Met-enkephalin [244]. The enkephalins are stored in synaptic vesicles and released into synapse where they bind to Mu (μ) and delta (δ) opioid receptor where they modulate pain [245].

4.2.2 Methionine Enkephalin as analgesic

Met-enkephalin (MENK) is an endogeneous penta-peptide distributed in adrenal medulla, central nervous system and dorsal horn of the spinal cord [246]. MENK binds to opioid receptors such as Mu (μ)-receptor and delta (δ)-receptor to exhibit analgesic effect [247]. Met-enkephalin has high affinity for δ receptor and low affinity for μ receptor [248]. The opioid receptors are G-protein coupled receptors located mostly on prejunctional neurons. The activation of opioid receptors (μ & δ) reduces intracellular cAMP formation and opens K^+ channels. These action causes neuronal hyperpolarization resulting in reduced availability of intracellular Ca^{2+} ions, which further decreases neurotransmitter release from CNS leading to analgesia [248].

4.2.3 MENK as immunomodulators

MENK also act as immunomodulators. MENK binds to delta (δ)-receptor on immune cells such as T cell [249], natural killer cells [250], dentritic cells (DCs) [251] and macrophage [252]. MENK was reported to exert positive modulation to pathway between dentritic cells (DCs) and CD4+ T cells [239]. The pathway between DCs and CD4+ T cells is important in maintaining balanced immunity in the body and its role in fighting against cancer and diseases like AIDS. MENK was reported to induce maturation of DCs by addition of surface molecules such as MHC class II, CD86 and CD40 on murine DCs, production of IL-2 and the down-regulation of ACP inside DCs. MENK alone or in combination with IL-2 or IFN- γ also reported to CD4+ T cell expansion and CD4 molecule expression [239].

4.2.4 MENK as cell growth regulator

MENK also acts on zeta (ζ)-receptor and are known to regulate cell growth and tissue regeneration. Hence MENK is also called as the opioid growth factor (OGF) and zeta (ζ)-receptor is called opioid growth factor receptor (OGFr) [253]. The action of MENK is tonic, stereospecific, reversible, non-cytotoxic and non-apoptotic. Further, MENK activity is not associated with differentiative, migratory,

and invasive or adhesive processes, anchorage-independent and occurs at physiologically relevant concentration [254].

The mechanism by which OGF exhibits anti-proliferative action on cancer cells is illustrated (Figure 4-2). OGF binds to OGFr presented on the nuclear membrane [255]. The up-regulation of OGFr induces the expression of P21 (cell cycle suppressor), a cyclin-dependant kinase inhibitor. P21 complexes with cyclin dependant kinase (CDK2) and further prevents phosphorylation of retinoblastoma protein (Rb) protein which normally interact in the presence of CDK2. The free Rb protein inhibits the dimerization of E2F transcriptional factor (E2F dimers are responsible for progression of cell cycle from G1 to S phase) leading to negative control of cell growth [255].

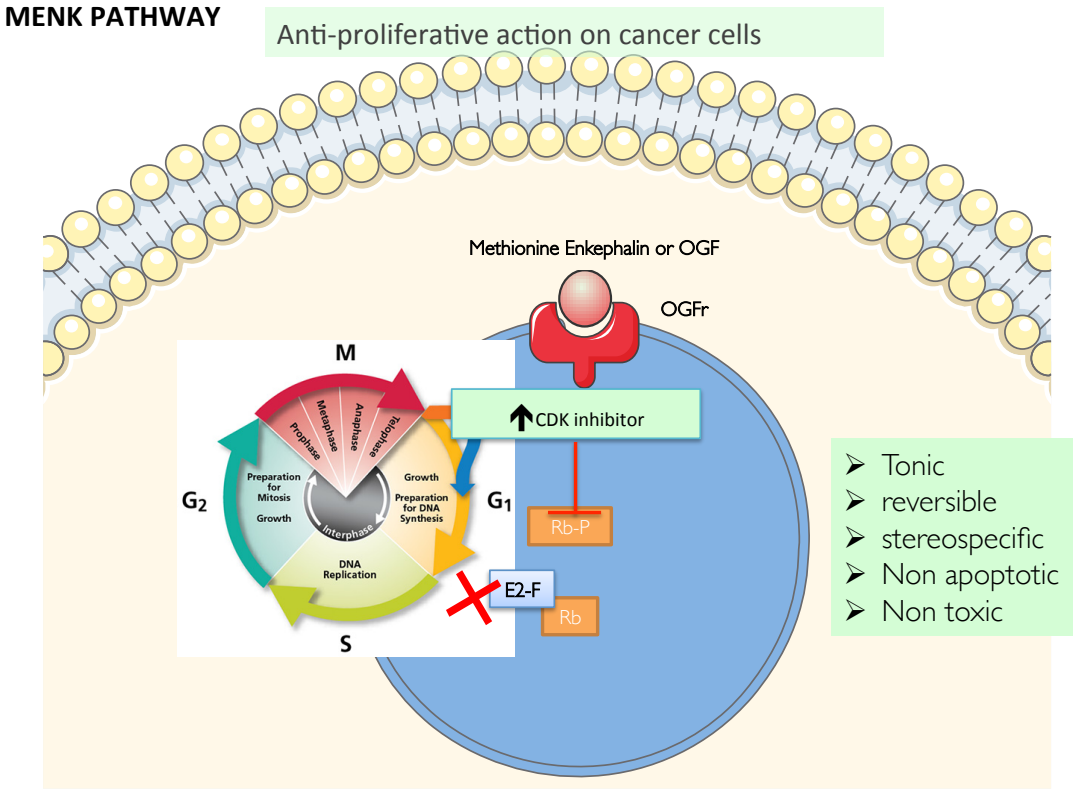

Figure 4-2 MENK Pathway

CKIs are deficient in cancer cells particularly p16ink4a and p21WAF1/CIP1. Both p16ink4a and p21WAF1/CIP1 up regulation are required for OGF inhibitory action in normal cells where as up regulation of one of the CKIs are sufficient for OGF action on cell cycle of cancer cells [256]. It has also been postulated that cancer cells that regulates cell cycle by OGF pathway have adapted by depending on only one of CKIs [255].

4.2.5 MENK for cancer therapeutics

According to Cancer Research UK, pancreatic cancer account for 3% of all new cases in the UK as of 2012 [257]. It is the tenth most common cancer in the country. Around 104,000 people in Europe and around 338,000 people worldwide were diagnosed with pancreatic cancer in 2012. The disease can be diagnosed only at its advanced stage and it is the main reason for treatment failure. Once diagnosed, around 4% of pancreatic cancer patients survive the disease for five years or more [257]. In England and Wales, during the year 2010-2011, the net survival of patients diagnosed with pancreatic cancer is 20.8% (1-year survival), 3.3% (5-year survival) and 1.1% (10-year survival) [257].

Treatment options for pancreatic cancer include surgical intervention and chemotherapy or radiation [258]. However, with the disease being diagnosed at later stage, it will not be cured with resection. Gemcitabine is the first line therapy for patient with advanced pancreatic cancer. However the survival time is only 5.65 months [259].

The anti-proliferative action of MENK was observed *in vitro* in various pancreatic cancer cell lines such as capan-1, BxPC-3, MiaPaCa-2 and Panc-1. It has also been observed that there was a marked delay in tumor appearance in the nude mouse pancreatic xenograft model [166]. A phase II clinical trial was conducted to test the efficacy of MENK in patients who had failed to respond to standard therapy for advanced pancreatic cancer. Intravenous administration of MENK, weekly twice at a dose of 250 μg/kg resulted in prolonged survival in patients by stabilizing the disease or slowing progression compared to historical controls like gemcitabine and 5-fluorouracil [260].

4.2.6 Challenges in oral delivery of MENK

Met-enkephalin is a small molecular weight pentapeptide, with molecular weight 573 Da and an isoelectric point of 5.3 [261]. As Met-enkephalin has only anti proliferative action but not cytotoxic, standard therapy requires repeated intravenous administration of the peptide, which can be patient noncompliant [262]. Moreover, met-enkephalin is degraded by enkephalinases such as aminopeptidase N, endopeptidase, dipeptidyl peptidase 3, carboxypeptidase A6 and angiotensin converting enzyme [263]. More over the half-life of MENK in plasma is 12.8 min [264]. Their poor stability results in low bioavailability making it a poor candidate

for oral delivery. The aim of this study is to enhance the oral delivery of MENK using GCPQ nanoparticles.

4.3 Materials and Methods

4.3.1 Materials

Chemical	Supplier
Methionine Enkephalin	Bachem, USA
Dalargin	Bachem, USA
Glacial acetic acid	Fisher, UK
Acetonitrile (LCMS grade)	Sigma-Aldrich (Gillingham, UK)
Acetonitrile (HPLC grade)	Sigma-Aldrich (Gillingham, UK)
Trifluoroacetic acid (99%)	Sigma-Aldrich (Gillingham, UK)
Formic acid (≥ 95%)	Sigma-Aldrich (Gillingham, UK)
Water (LCMS grade)	Sigma-Aldrich (Gillingham, UK)
Ammonium hydroxide	Fisher, UK
Sodium chloride	Sigma-Aldrich (Gillingham, UK)
Methanol (LCMS grade)	Sigma-Aldrich (Gillingham, UK)
Hydrochloric acid	Fisher, UK
Sodium hyaluronate	Lifecore Biomedicals, USA
L-Glutamine	Invitrogen, UK
Fetal bovine serum	Invitrogen, UK
Sodium hydroxide	Sigma-Aldrich (Gillingham, UK)
Monobasic potassium phosphate	Sigma-Aldrich (Gillingham, UK)
DMEM medium	Invitrogen, UK
Sephadex G-25	Fisher, UK
Matrix gel	BD Biosciences, Bedford, MA, USA

4.3.2 Methods

4.3.2.1 Characterization of MENK peptide

MENK having an isoelectric point of 5.3 can aggregate at pH close to 5.3. The aggregation behavior of MENK was characterized qualitatively and quantitatively by TEM and ITC. TEM gives an indication on the morphology of MENK aggregates and ITC suggests at what concentrations MENK forms micelles.

a) TEM

MENK acetate salt of different concentrations (5, 10 and 20 mg/mL) were prepared in water and characterized by TEM.

b) CMC of MENK peptide by Isothermal titration Calorimetry

To accurately determine the CMC of MENK free base, MENK acetate salt was purified from its acetate form by neutralization with a base. The MENK peptide (1.8 mmol) was added to ammonium hydroxide (40 mL, 1M) and incubated for 30 min at room temperature. The reaction mixture was freeze dried to remove volatile ammonium acetate.

ITC is used to understand self-association of colloids, using a demicellization experimental approach. It measures the changes in enthalpy when micelles first disassociate and re-associate above its critical micellar concentration in a diluent. The experiment involves stepwise titration of a micellar solution in a reaction cell containing diluent at a particular temperature to give the change in heat flow versus time. The reaction enthalpy is calculated by integrating the heat flow obtained during each titration. The first order derivative of reaction enthalpy versus the monomer concentration gives their CMC.

The CMC of MENK free base was determined by isothermal titration calorimetry (ITC) [265] [266] [267]. Micellar solutions of free MENK were prepared at a concentration of 10 mg/mL in water. Before analysis, MENK solution and its diluent (water) were degassed using a vacuum pump for 10 min. The reaction cell, diluent cell and the syringe were also washed with 10% decon and water. The MENK micellar solution was loaded into the syringe and inserted into the reaction cell containing water. The demicellisation experiment was carried out by titrating 50 injections of 5uL aliquots of pure MENK (17.4 mM) at temperature 25˚C with water. The heat flow during the demicellisation process was measured as a

function of time, and the peak obtained during each titration was integrated to give a sigmoid curve. The CMC was obtained by derivatization of reaction enthalpy against the MENK concentration [267]. Thermodynamics parameters such as the enthalpy of demicellisation (ΔH_{demic}), Gibbs free energy change (ΔG_{demic}) and the entropy change ($T\Delta S_{demic}$) can be derived from ITC experiment [266]. The enthalpy of demicellisation can be calculated directly from the enthalpogram by taking the difference between the enthalpy after the first and last injection of the sample (ΔH_{demic}). The Gibbs free energy change (ΔG_{demic}) is calculated from the equation,

$$\Delta G_{demic} = RT \ln (CMC)$$

Where, R = gas constant (8.3144 $Jmol^{-1}$ K^{-1}), T= temperature in K (25˚C = 298 K) and CMC in mole fraction units. The entropy change ($T\Delta S_{demic}$) can be obtained by the equation,

$$T\Delta S_{demic} = \Delta H_{demic} - \Delta G_{demic}$$

4.3.2.2 MENK GCPQ Formulation

MENK GCPQ B2 formulations were prepared and characterized by different methods.

4.3.2.2.a Solubility method

MENK and GCPQ is solubilized first and brought to the pH of the isoelectric point of MENK. It is hypothesized that MENK can aggregate at the pH of the isoelectric point and form particles with GCPQ. This hypothesis is tested at two ratios; 1:2.6 for MENK-GCPQ (B1) IV formulation and 1:5 for MENK GCPQ (B2) oral formulation. The ratios and concentrations used for IV and oral formulations were based on formulations previously made using LENK and GCPQ [53].

Preparation of MENK GCPQ B1 IV formulation: The intravenous formulation of MENK (5 mg/mL) and GCPQ (13 mg/mL) of mass ratio 1:2.6 were prepared by first dissolving MENK in 30% acetic acid and GCPQ in 0.9% NaCl. The MENK and GCPQ solutions were added together and the pH was increased to 5.6. The formulation was probe sonicated (MSE sonicator, UK) for 15 min at 15 amps in the presence of ice.

As a control, MENK IV formulation was prepared by same method without adding GCPQ.

Preparation of MENK-GCPQ oral B2 formulation: MENK-GCPQ oral formulation was prepared as method mentioned in section 4.3.2.2.a of mass ratio 1:5 using

concentrations 10 mg/mL of MENK and 50 mg/mL of GCPQ. As a control, MENK oral formulation was prepared by same method without adding GCPQ.

4.3.2.2.b Direct reconstitution without probe sonication

This method involves direct reconstitution of MENK and GCPQ B1 in water to evaluate whether the MENK-GCPQ B1 particles are formed by hydrophobic interaction.

MENK (10 mg) and GCPQ B1 (30 mg) were added to 1 mL of water and vortexed until a clear dispersion was obtained. The pH of the formulation was adjusted to 6 and characterized.

4.3.2.2.c Film method

It is hypothesized that the peptide and GCPQ B1 are at close proximity and forms particles when reconstituted in water. MENK solution was prepared by mixing MENK (10 mg) in methanol (500 µL) and glacial acetic acid (72 µL). GCPQ (50 mg) was solubilized in methanol (500 µL). The GCPQ B1 and MENK solution were mixed and dried in a rotary vacuum evaporator at 37°C until a thin film was formed. The formulation was freeze-dried to remove methanol completely.

After 48 h, the freeze-dried product was reconstituted in water and vortexed until a homogeneous formulation was obtained. The pH of the formulation was adjusted to 6 and characterized.

4.3.2.2.d Preparation of MENK-GCPQ B1 formulation by complex co-acervation method

Complex coacervation is a process where oppositely charged molecules complex due to electrostatic interaction. Since MENK and GCPQ B1 are like charged below neutral pH, MENK was first complexed with anionic polymer followed by complexation with cationic GCPQ B1 polymer. The particles thus formed were size characterized.

A stock solution of MENK (25 mg/mL) was prepared in 30% acetic acid. Hyaluronic acid (HA) at a concentration 34.8 mg/mL of different molecular weights 4.7 kDa, 16 kDa and 35 kDa was prepared in water. MENK (2.5 mg/mL) and HA complexes were mixed at molar ratios (1:0.001, 1:0.01, 1:0.1, 1:1 and 1:10). The size and PDI of MENK-HA complexes with each HA molecular weight were characterized.

After screening for desired molecular weight of HA, size, stability and zeta potential of MENK-HA (16 kDa) complexes of molar ratios ranging from 1:0.0005, 1:0.001, 1:0.002, 1:0.004, 1:0.008, 1:0.02, 1:0.04, 1:0.08 and 1: 0.1) were also characterized.

MENK-HA (16 kDa) complexes prepared at molar ratios 1:0.04 were formulated with GCPQ B1 at different mass ratios (1: 1.25, 1: 2.5, 1:5 and 1:10) and size characterized before and after probe sonication.

4.3.2.3 Characterization of MENK and MENK-GCPQ formulations

4.3.2.3.a TEM

The morphology of MENK GCPQ (B1 & B2) formulations was determined using transmission electron microscope (Philips CM 120 Bio Twin Transmission electron microscope) with an AMT digital camera (5 mega pixels; AMT Deben, UK Ltd).

A drop of MENK GCPQ (B1 & B2) formulation was placed on a grid and blotted with a tissue paper. A drop of uranyl acetate (1% w/v) staining solution was also added to the grid and TEM images were recorded.

4.3.2.3.b Particle size

The particle sizes of MENK GCPQ (B1 & B2) formulations were characterized by dynamic light scattering (DLS) technique (Malvern Zetasizer Nano ZS ZEN3600, Malvern Instruments Ltd, Worcestershire, UK). Formulations (1 mL) were dispensed into a low volume disposable cuvette and size distribution graphs were recorded.

4.3.2.3.c Charge

The zeta potential of MENK GCPQ (B1 & B2) formulations was measured using the diffusion barrier technique. MENK oxidizes on interaction with metal electrodes. Diffusion barrier technique involves isolation of small sample volume from the electrode in order to prevent denaturation of protein at the electrodes [268]. Sample diluent (NaCl -10 mM, 800 μL) was added in a zeta cell. Each MENK GCPQ formulation (200 μL) was added to the bottom of the cell and the zeta potential was characterized by DLS.

4.3.2.4 Encapsulation efficiency of MENK GCPQ (B1 & B2) formulation

Encapsulation efficiency of the MENK GCPQ (B1 & B2) formulations were determined by centrifugation and column chromatography method.

4.3.2.4.a Method 1

Encapsulation efficiency MENK GCPQ (B1 & B2) formulations were determined by centrifugation method. Sample aliquots (20 µL) were withdrawn from the formulation, before and after centrifugation and quantified by HPLC. Following centrifugation, it was expected that the MENK-GCPQ nanoparticles remains in the supernatant and the large MENK particles forms a pellet. For encapsulation efficiency, MENK GCPQ formulations were centrifuged at 5000 RPM for 10 min at room temperature. The supernatant of each formulation (20 µL) was diluted in mobile phase (980 µL) and analysed by HPLC. The encapsulation efficiency of the formulation was calculated by formula,

$$\%\ \text{Encapsulation efficiency} = \frac{\text{Concentration of MENK after centrifugation}}{\text{Concentration of MENK before centrifugation}} \times 100$$

4.3.2.4.b Method 2

Encapsulation efficiency of MENK-GCPQ B2 formulation was also determined by column chromatography method. Here, the column is packed with cross-linked dextran matrix with an exclusion limit of 5000 Da. It was hypothesized that non-encapsulated MENK with molecular weight of 573 Da passes through the pores of the matrix, whereas MENK encapsulated in GCPQ B2 with a molecular weight of 12 kDa avoid the pores of the bead and elute earlier. The differences in the elution time of unencapsulated MENK and encapsulated MENK was used to determine the encapsulation efficiency of MENK-GCPQ B2 formulation.

The sephadex G-25 was reconstituted in water (1g/5 mL) and allowed to swell for 1 h at 90˚C and was then packed in a glass column. The column was loaded with samples of MENK or MENK-GCPQ B2 formulations (100 µL, 10 mg/mL). A volume of water was gradually added without disturbing the sephadex particles and the flow-through was collected every 3 min (2 mL volume approx). The water level was maintained at a constant level throughout the experiment to achieve a consistent flow rate. Sixty fractions were collected and the MENK content quantified by HPLC was plotted against the number of fractions. Encapsulation efficiency is determined by taking the ratio of total concentrations of fractions under each peak for MENK-

GCPQ B2 formulation to the total concentrations of fractions under a single peak for MENK formulations.

4.3.2.5 Enzymatic Stability of MENK GCPQ B2 formulations

MENK-GCPQ B2 formulations were characterized to know if the GCPQ protects MENK peptide against enzymes in the gastrointestinal tract.

4.3.2.5.a SGF

SGF solution was prepared by dissolving sodium chloride (2 g) in water (500 mL). The pH of the solution was adjusted to 1.2 with HCl (7 mL) and made up to 1000 mL with water.

MENK-GCPQ B2 nanoparticles (5 mg/mL, 500 µL) and MENK peptide solution (5 mg/mL, 500 µL) was incubated in simulated gastric fluid (SGF) or rat intestinal wash (4.5 mL) at 37˚C in a water bath rotating at 125 rpm. Samples (100 µL) were withdrawn at different time points (0, 0.5, 1 and 2 h), diluted in mobile phase (900 µL) containing 16% acetonitrile: 85.98% water: 0.02% TFA and analysed by HPLC.

4.3.2.5.b SIF

SIF solution was prepared by dissolving monobasic potassium phosphate (6.8 g) and sodium hydroxide solution (0.2N, 77 mL) in water (250 mL). The pH of the solution was adjusted to 6.8 with sodium hydroxide (0.2 N) or hydrochloric acid (0.2 N) and finally diluted to 1000 mL.

MENK-GCPQ B2 nanoparticles (5 mg/mL, 500 µL) and MENK peptide solution (5 mg/mL, 500 µL) was incubated in simulated intestinal fluid (SIF) (4.5 mL) at 37˚C in water bath rotating at 125 rpm. Samples (100 µL) were withdrawn at different time points (0, 0.5, 1, 2 and 4 h), diluted in mobile phase (900 µL) containing 16% acetonitrile: 85.98% water: 0.02% TFA and analysed by HPLC.

4.3.2.6 Quantification of MENK by HPLC

4.3.2.6.a Preparation of Stock and Working standards

MENK was quantified using high-performance liquid chromatography (HPLC). A stock solution of MENK was prepared by dissolving the peptide (2 mg/mL) in acetic acid (30% v/v). Calibration standards were prepared by diluting stock solution to working standards (S1 to S8) of concentrations ranging from 200

µg/mL to 1.56 µg/mL with acetonitrile (16% v/v) containing 0.02 % trifluroacetic acid (TFA). The standards were analysed by HPLC. All test compounds were quantified as method mentioned above.

HPLC chromatogram for MENK was acquired using the following setup:

Table 4-1 HPLC instrumentation condition for analysis of MENK

	HPLC Setup
Instrument	Agilent Technologies 1200 Series HPLC system
Column	Onyx C18 monolithic column (5 µm; 100 × 4.6 mm; Phenomenex UK) fitted with guard column (5 µm; 10 × 4.6 mm)
Column temperature	37˚C
Mobile phase	16% Acetonitrile + 0.02% TFA
Flow rate	1.2 mL/min
Injection volume	20 µL
UV wavelength	220 nm
Sample diluent	16% Acetonitrile + 0.02% TFA

The calibration curve was obtained by plotting the concentrations of standards and its respective peak area from the chromatogram. The concentration of unknown analyte was calculated using linear equation y= mx+c.

4.3.2.7 Analytical method for quantification of MENK *in vivo by EIA*

EIA was used to quantify MENK in plasma sample (Figure 4-3). Briefly, the sample/standard and known concentration of biotinylated tracer competes to bind to Met-Enkephalin antiserum added on a coated immunoplates. Bt tracer binds with serum specific HRP or streptavidin conjugated horseradish peroxidase (SA-HRP). TMB (tetramethyl benzidine) in the presence of HRP enzyme reduces hydrogen peroxide to water giving a blue color. To stop the reaction, HCl (2N) was added that changes the color of the solution to yellow and measured at 650 nm. Higher the intensity of yellow colored solution lowers the quantity of peptide and vice versa.

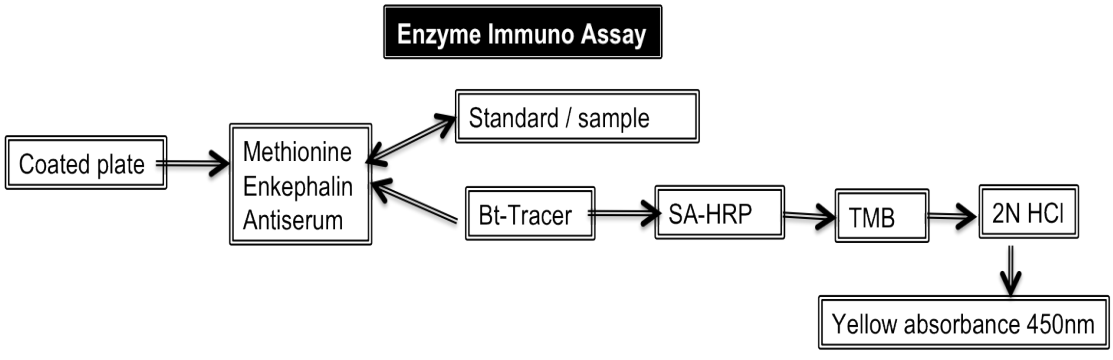

Figure 4-3 Schematics of Enzyme Immuno Assay

Enzyme immunoassay (EIA) for the quantification of methionine enkephalin in plasma was performed as per the protocol described by the manufacturer (Bachem, USA). Briefly, the standard/sample (50 µL) and anti-serum (25 µL) were

added on to an Immunoglobulin G (IgG)-coated immunoplate and incubated for 1 h. Bt tracer (25 µL) was then added to each well and incubated for 2 h. The immunoplate was washed 5 times with EIA buffer (300 µL). Streptavidin–HRP (100 µL) was added to all wells and incubated for 1 h. The immunoplates was washed 5 times followed by the addition of TMB solution (100 µL) in each well. Blue color was developed on incubation for 30-60 min. To stop the reaction, HCl (2 N, 100 µL) was added and absorbance was recorded at 650 nm.

4.3.2.8 Quantification of MENK by LCMS-QQQ

4.3.2.8.a Validation of LCMS method – Preparation of standards

A stock solution of MENK was prepared by dissolving the peptide (2 mg) in 30% acetic acid. Seven calibration standards of concentrations ranging from 10000 ng/mL to 200 ng/mL were prepared by dilution of stock solution in methanol. A stock solution of internal standard (dalargin) was also prepared in methanol (200 ng/mL). Dalargin is an analogue of leucine enkephalin with a molecular weight (725.83 Da).

4.3.2.8.b Preparation of plasma for calibration standards

A CD rat was culled in a CO_2 culling chamber and blood was withdrawn by cardiac puncture. The blood sample was collected in a vacutainer (BD Vacutainer™ - spray coated with anti-coagulant K2 EDTA) and centrifuged at 2000 g for 10 min at 4˚C. Plasma was carefully withdrawn with micropipette tips and stored at – 80˚C in a freezer until LCMS analysis.

4.3.2.8.c Preparation and extraction of calibration standards from plasma matrices

The internal standard (5 µL) and calibration standards (5 µL) were spiked into the tubes containing plasma (50 µL). Blank was prepared by spiking only internal standard (5 µL) in to plasma (50 µL). For the extraction, methanol (140 µL) was added to standards to precipitate plasma proteins followed by vortexing for 30 min. The precipitated plasma proteins were removed by centrifugation at 11000 g for 10 min and supernatant was quantified by LCMS.

4.3.2.8.d Quantification of endogenous MENK in mouse plasma

Overnight fasted CD-1® mice (n=10) were culled and the plasma was collected as method mentioned in 4.3.2.8.b. Internal standard (5 µL) was added to each plasma sample (50 µL) and the extraction was carried out with methanol (140 µL). The precipitated plasma proteins were removed by centrifugation at 11000 g for 10 min and the supernatant was quantified by LCMS.

4.3.2.8.e Quantification of MENK by LCMS-QQQ

MENK was quantified in plasma using LCMS QQQ. The configurations are listed as follows:

a) Instrument configuration

Pump : Agilent G1312B

Autosampler : Agilent G1367E

Column : Agilent G1367E

Mass spectrometer : Agilent 6460 triple quadrupole LCMS system

Software : Agilent chem station (B.06.00)

b) Chromatography

LC parameters for separation and identification of MENK is as follows:

Parameters	**Plasma**
Column	Onyx monolithic C18 column (100×2 mm)
Oven temperature	40˚C
Injection volume	10 µL
Mobile phase	Solvent A: 0.1% FA in water Solvent B: Acetonitrile

Gradient program

Plasma

Time (min)	0	4	5	6	6.10	7.5
% of solvent B	5	30	95	95	5	5
Flow rate	0.4 mL/min					

c) Source Optimization

MENK and internal standard (dalargin) were optimized using a source optimizer program in LCMS. The parameter that gave the highest signal to noise ratio was used to develop LCMS method.

d) Mass Spectrometry

Table 4-2 Source Parameters - LCMS-QQQ

Source Parameters	
Ionization mode	ESI jet streaming positive
Sheath gas temperature (˚C)	400
Sheath gas flow (L/min)	11
Drying gas flow (L/min)	12
Drying gas temperature (˚C)	290
Nebulizer gas (psi)	20
Capillary voltage (V)	3500 (positive and negative)
Nozzle voltage (V)	0
EMV (V)	200

Table 4-3 MRM parameters – LCMS-QQQ

Test item	**MENK** Quantifier	**Dalargin** Internal standard for plasma sample
MRM transition	574- 425	726 – 136.1
Fragmentor voltage (V)	255	130
Collision energy (eV)	81	10
MS1 and MS2 resolution (nm)	Unit	Unit
Cell acceleration voltage (V)	7	7
Dwell time (ms)	200	200
Polarity	Positive	Positive

4.3.2.9 Pharmacokinetics of MENK-GCPQ formulations

CD-1® mice were fasted overnight and randomized in to 5 groups (n=5 per group) each receiving the respective formulations;

Table 4-4 Dosing schedule for MENK pharmacokinetics studies

Formulation	**MENK**	**GCPQ**	**Diluent**	**Volume**	**Ratio**	**Peptide dose**
MENK GCPQ IV	5 mg/mL	13 mg/mL	0.9% NaCl	100 µL	1: 2.6	15 mg/kg
MENK IV	5 mg/mL	-	0.9% NaCl	100 µL	-	15 mg/kg
MENK GCPQ ORAL	10 mg/mL	50 mg/mL	0.9% NaCl	200 µL	1: 5	100 mg/kg
MENK ORAL	10 mg/mL	-	0.9% NaCl	200 µL	-	100 mg/kg
Control	-	-	0.9% NaCl	100 µL	-	-

At each time point (5, 15, 20, 45, 60, 90 and 180 min for IV and 30, 60, 120 and 240 min for oral formulations) mice were euthanized and blood samples were collected by cardiac puncture. Samples were processed as method mentioned in 4.3.2.8.b and analysed by LCMS.

4.3.2.10 Pharmacodynamics of MENK-GCPQ formulations

MiaPaCa-2 cells were cultured for at least two weeks *in vitro* before tumour implantation. The cells were cultured in DMEM medium supplemented with 5% FBS and 0.05% sodium pyruvate in 300 cm^2 size flask. The cells were trypsinized, centrifuged and resuspended in a mixture of DMEM medium and matrix gel (BD Bioscience, U.S.A) in the ratio 1:1 at a concentration of 1 million/100 µL. Two million cells (200 µL) were injected on the left flank of Swiss Nude mice (Charles River, U.K). The volume of the tumour was recorded using vernier calipers for 10 days before treatment. The body weights of the mice were also recorded throughout the experiment.

Five days after tumor implantation, the animals were randomized in to five groups (n = 5 per group). Every mouse in each group received 100 µL of the respective formulation:

Table 4-5 Dosing schedule for MENK pharmacodynamics studies

Formulation	MENK	GCPQ	Diluent	Volume	Ratio	Peptide dose
MENK GCPQ IV	5 mg/mL	13 mg/mL	0.9% NaCl	100 µL	1: 2.6	15 mg/kg
MENK IV	5 mg/mL	-	0.9% NaCl	100 µL	-	15 mg/kg
MENK GCPQ ORAL	10 mg/mL	50 mg/mL	0.9% NaCl	100 µL	1: 5	50 mg/kg
MENK ORAL	10 mg/mL	-	0.9% NaCl	100 µL	-	50 mg/kg
Control	-	-	0.9% NaCl	100 µL	-	-

The above formulations were given over 12 alternate days. The volumes of the tumours were recorded using vernier calipers during and after the treatment.

Tumour volume (mm^3) = Length (mm) * Width (mm^2) * 0.5

The body weight of the treated mice were also recorded and compared with mice that received no treatment.

4.4 Results

4.4.1 Morphology of MENK peptide

TEM images of MENK at different concentrations (Figure 4-4a) show that the peptide form aggregate of sizes 200 to 500 nm that are spherical in shape at 5 mg/mL concentration, the aggregates at 10 mg/mL concentration are thread like structure and at 20 mg/mL concentration, the presence of crystals can be observed. The aggregates are formed when the attractive force between the solute molecules were stronger that the forces in the solution that disrupts aggregate formation (Figure 4-4b). This acts like a nucleation site, which is the first step for crystal formation. When more solute molecules are added, crystal formation takes place (Figure 4-4c). The measured pH of MENK in water at any given concentration was 4.7.

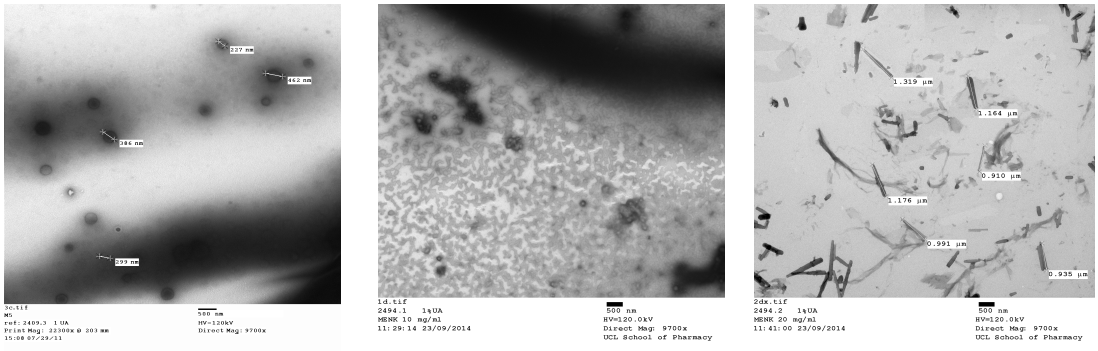

a) b) c)

Figure 4-4TEM images showing morphology of MENK at different concentrations a) MENK (5 mg/mL) in water, b) MENK (10 mg/mL) in water, c) MENK (20 mg/mL) in water.

4.4.2 CMC of MENK peptide

The aggregation of peptide is concentration dependent. It is important to know the critical micellar concentration (CMC) of MENK to understand the concentrations at or above which MENK aggregates to form nanoparticles. The dilution enthalpogram of MENK are shown in Figure 4-5. The enthalpogram can be divided into three segments; the first segment represents the disassociation of aggregate to give monomers when diluted in sample cell. As the concentration of the monomers in the sample cell increases, first aggregate was formed at the start of the transition (ST – blue line). This can be observed by a change in slope of enthalpogram that denotes the CMC of MENK. The aggregation continued until the end of transition (ET). The CMC of MENK determined by ITC is 0.32 mM (Figure 4-5). The differences between the two parallel red lines give Δ Hdemic. For MENK, Δ Hdemic is -1255 Joules/mol. Demicellisation of MENK was an exothermic

process, which required the removal heat, thus aggregation of MENK would be endothermic, having the same magnitude of enthalpy but with an opposite sign. The Gibbs free energy was -19938 J/mole denoting thermodynamically stable aggregates. The aggregation reaction of MENK is entropy driven at room temperature with TΔS calculated as 18683 J/mol.

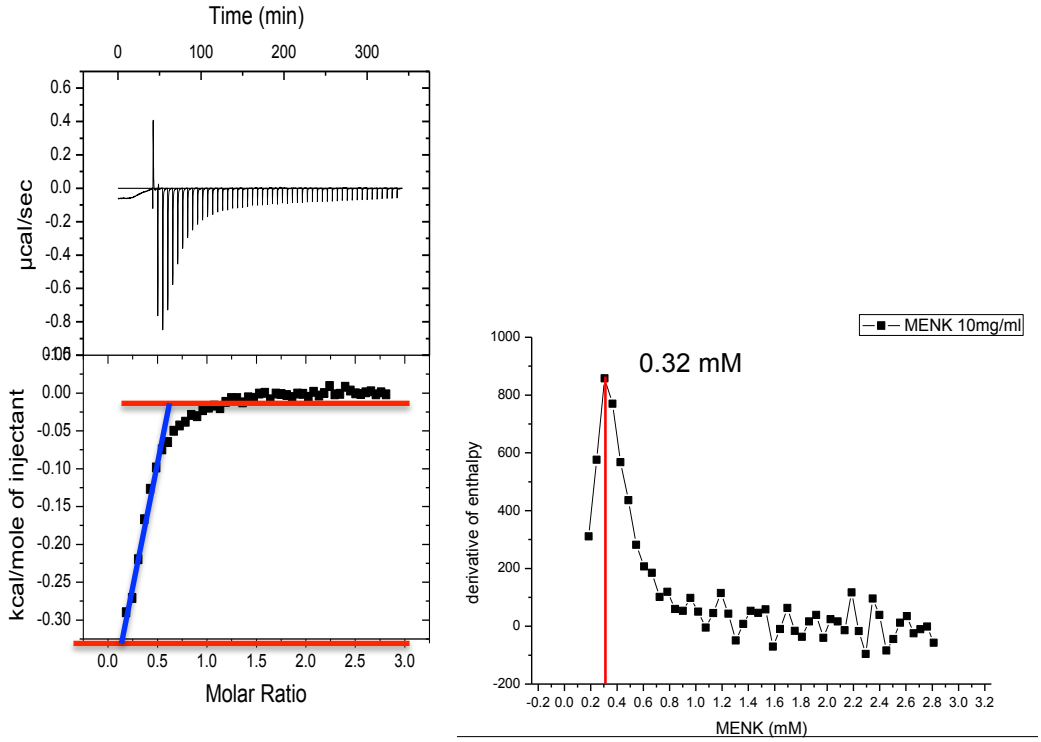

Figure 4-5 Dilution enthalpogram of demicellisation of MENK (10 mg/mL) in water at 25°C in 50 steps of 5µL injection volume.

4.4.3 *In vitro* Characterization of MENK-GCPQ IV and oral formulation by solubilization method

MENK aggregates was first solubilized by dissolving in 30% acetic acid and then added to GCPQ (B1 or B2) solution prepared with 0.9% NaCl. The pH of the solution was increased gradually with sodium hydroxide (0.1 M) and it was expected that the MENK encapsulate in GCPQ during aggregation at pH 5.3. Probe sonication was used to further enhance the encapsulation of MENK in GCPQ. The MENK-GCPQ IV and oral formulation (B1 & B2) were characterized for their size and charge and the results were compared. The ratio of MENK GCPQ formulation for IV and oral delivery were 1:2.6 and 1:5 as previously reported for LENK GCPQ formulation [53]. The concentration of the MENK (5 mg/mL) GCPQ (13 mg/mL) IV formulation and MENK (10 mg/mL) GCPQ (50 mg/mL) oral formulation were back

calculated from the MENK dose and volume to be administered *in vivo* in mice (Table 4-5).

4.4.3.1 MENK-GCPQ formulations - Morphology

MENK-GCPQ (B1) IV formulation prepared at ratio 1:2.6 had two populations; an irregular shaped particles around 60 nm and defined spherical particles around 20 nm (Figure 4-6). However, when the ratio of MENK-GCPQ (B2) formulation was increased to 1:5 only spherical particles around 20 nm was observed (Figure 4-7). An increase in the concentration of GCPQ for oral formulation could be a reason for MENK-GCPQ formulation forming homogeneous sized particles at ratio 1:5.

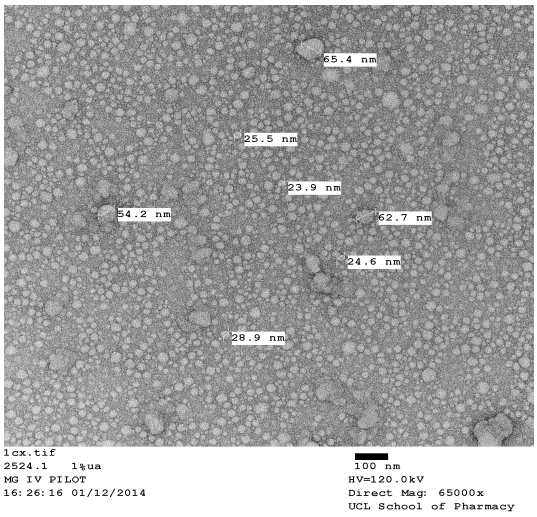

Figure 4-6 MENK-GCPQ (B1) IV formulation prepared at ratio 1:2.6 and concentrations 5 mg/mL and 13 mg/mL showing defined spherical particles around 20 nm and irregular shaped particles above 50 nm.

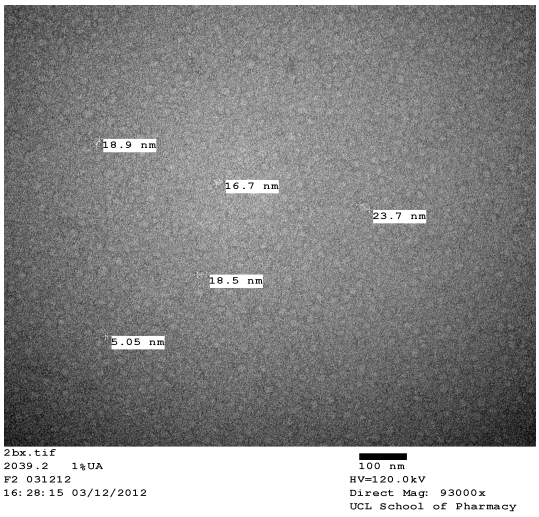

Figure 4-7 MENK-GCPQ (B2) Oral formulation prepared at ratio 1:5 and concentrations 10 mg/mL and 50 mg/mL showing defined spherical particles around 20 nm.

4.4.3.2 Size characterization of MENK GCPQ IV (B1) and oral (B2) formulations by DLS

MENK was soluble in 30 % acetic acid solution and their particle size observed was around 1 nm. MENK control was prepared by method similar to MENK-GCPQ formulation without adding GCPQ. MENK control was prepared by solubilizing in 30% acetic acid (300 uL) and reconstituted in 0.9% NaCl (700 uL). The final pH was adjusted to 5.6. The size of MENK control was around 222 nm. MENK-GCPQ (B1) IV formulation had particle size around 391 nm that was larger

than MENK-GCPQ (B2) oral formulation with particle size 16 nm (Figure 4-8). MENK-GCPQ (B1) IV formulation has lower degree of palmitoylation (16%) than MENK GCPQ (B2) oral formulation having a degree of palmitoylation of 19%. The high palmitoylation of GCPQ B2 could cause strong interaction between the GCPQ and MENK and resulted in small particle size. High concentration of GCPQ B2 used for oral formulation (ratio 1:5) could also be the reason for smaller particle size compared to IV formulation, which has lesser concentration of GCPQ B1 with ratio 1:2.6.

PDI (0.578) of MENK (30% acetic acid) shows that some aggregates of MENK do exist in the solution and the MENK control has PDI of 0.974 suggesting that the MENK aggregates are heterogeneous. MENK-GCPQ B1 IV formulation of population with two different sizes was observed in TEM and hence the PDI was higher (0.648). Although, MENK-GCPQ B2 oral formulation had uniform sized small particles in TEM, PDI by DLS measured was 0.842. However, TEM results are qualitative and the presence of very small fraction of aggregates or large sized particles could increase the PDI of the formulation.

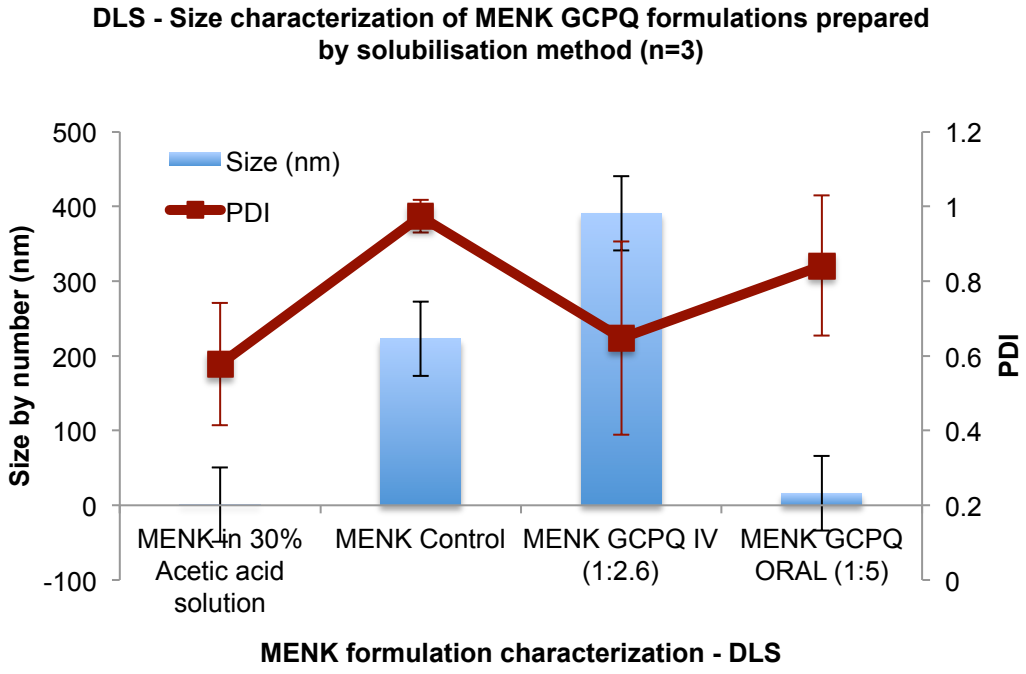

Figure 4-8 Size characterization of MENK GCPQ formulations by DLS. Formulations were characterized and compared by DLS; MENK (5 mg/mL in acetic acid solution), MENK Control (5 mg/mL in acetic acid and 0.9% NaCl, pH 5.6), MENK (5 mg/mL)-GCPQ (B1) (13 mg/mL) IV formulation at ratio 1:2.6 prepared in acetic acid and sodium chloride solution, pH 5.6 and MENK (5 mg/mL)- GCPQ (B2) (25 mg/mL) oral formulation at ratio 1:5 prepared in acetic acid and sodium chloride solution, pH 5.6.

4.4.3.3 Surface charge of MENK GCPQ formulation by DLS

The surface charge of MENK and MENK GCPQ formulations were characterized by DLS. MENK formulation has zeta potential of +18 mV whereas MENK-GCPQ (B1) IV and MENK-GCPQ (B2) oral formulation has zeta potential of +48.8 mV and +41 mV. It was previously reported that the zeta potential was found to be independent of particle concentration [157]. This can be observed in the graph, where, increase in the concentration of GCPQ used in preparing MENK-GCPQ IV (B1) and oral formulation (B2) has no effect on the zeta potential of the respective formulation. The degree of quaternization of MENK-GCPQ oral formulation (B2) was 12 % that was lower that degree of quaternization of MENK-GCPQ (B1) IV formulation B1 (14%). This could have also resulted in larger zeta potential value for MENK GCPQ (B1) IV formulation compared to MENK-GCPQ (B2) oral formulation.

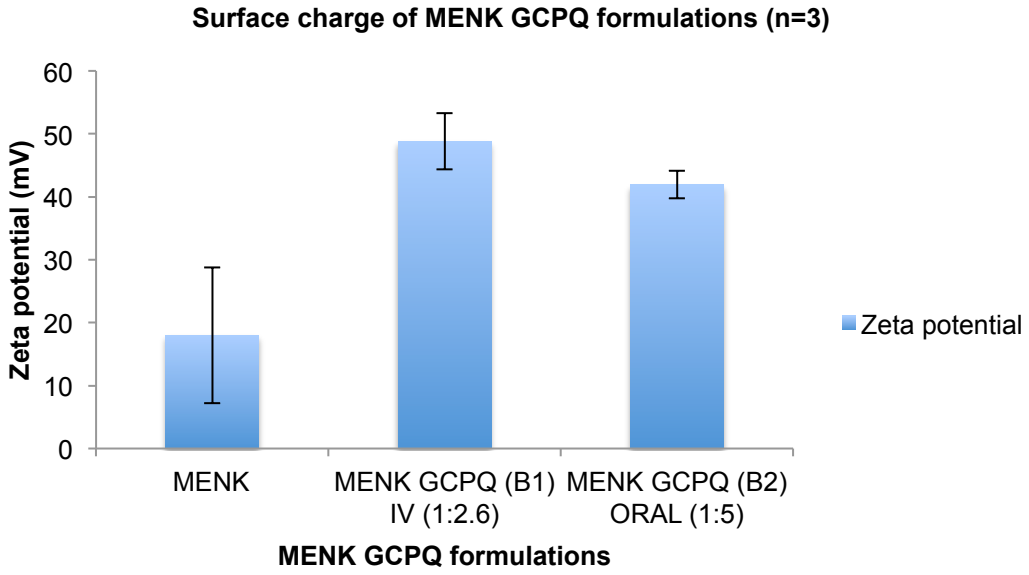

Figure 4-9 Surface charge characterization of MENK and MENK-GCPQ IV and oral formulation analysed by DLS. MENK (5 mg/mL in acetic acid and 0.9% NaCl, pH 5.6), MENK (5 mg/mL)-GCPQ (B1) (13 mg/mL) IV formulation at ratio 1:2.6 prepared in acetic acid and sodium chloride solution (pH 5.6), MENK (5 mg/mL)-GCPQ (B2) (25 mg/mL) oral formulation at ratio 1:5 prepared in acetic acid and sodium chloride solution (pH 5.6).

4.4.3.4 Analytical method for quantification of MENK in vitro by HPLC

MENK *in vitro* samples were quantified by HPLC. The HPLC chromatogram for MENK was obtained with a single peak eluting at 3.2 min (Figure 4-10). The standard curve was also plotted with concentrations of MENK ranging from 1.56 µg/mL to 20 µg/mL against their area under the curve obtained for each

concentration. The linear equation for MENK calibration curve was y=14.55X +1.6774 with R^2= 0.9999 (Figure 4-11).

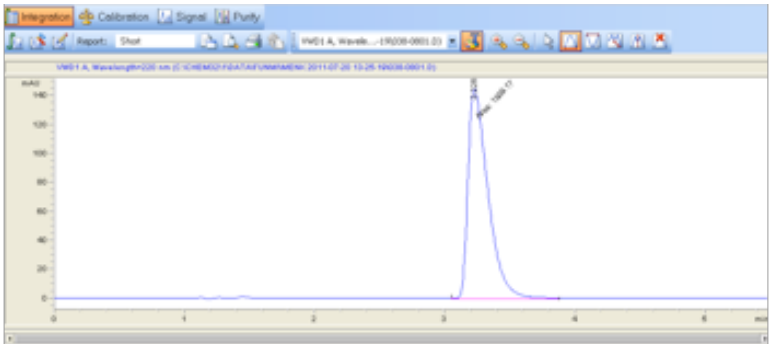

Figure 4-10 HPLC chromatogram for MENK showing time on x-axis and absorbance unit on y-axis with retention time for MENK at 3.2 min.

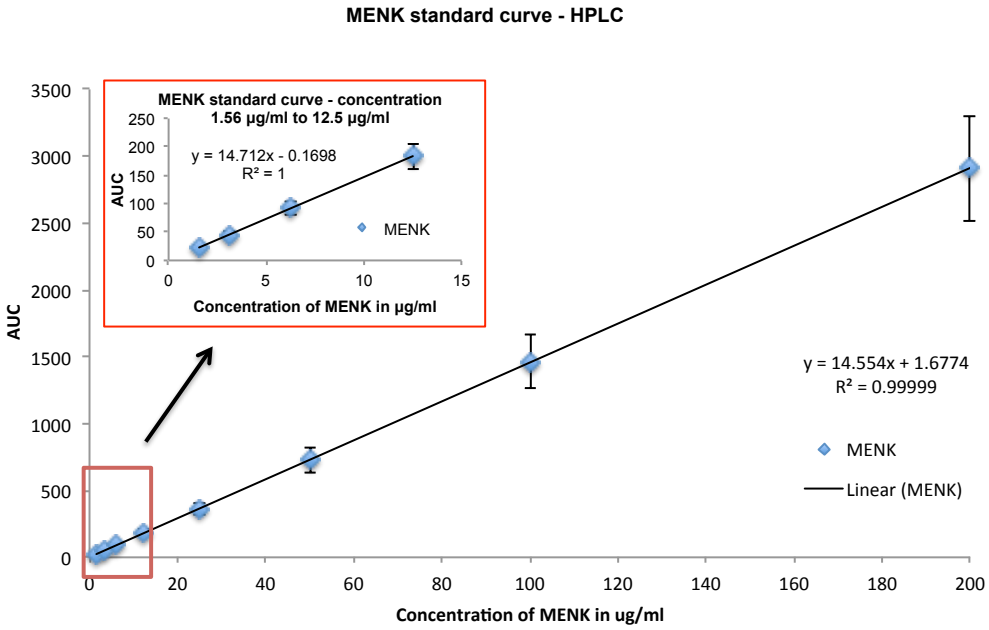

Figure 4-11 Calibration curve of MENK analyzed by HPLC with concentrations of MENK from 1.56 µg/mL to 200 µg/mL plotted on x-axis against AUC on y-axis.

4.4.3.5 Encapsulation efficiency of MENK-GCPQ formulation

4.4.3.5.a HPLC

Encapsulation efficiency of MENK-GCPQ (B1) IV formulation was 93.63% and MENK-GCPQ (B2) oral formulation was 99% (Figure 4-12). The increase in the ratio of MENK to GCPQ (1: 2.6 to 1:5) could have resulted in increased encapsulation of MENK in GCPQ B2 oral formulation.

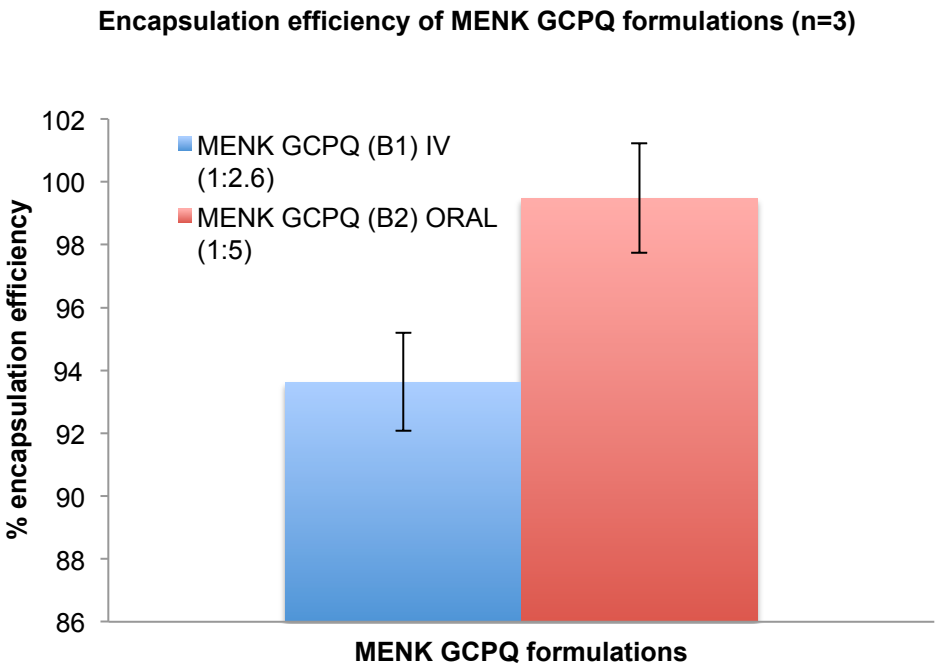

Figure 4-12 Encapsulation efficiency of MENK GCPQ (B1 & B2) formulations prepared at ratio 1:2.6 (blue) and 1:5 (red).

4.4.3.5.b Column Chromatography

Encapsulation efficiency of MENK-GCPQ B2 oral formulation was also analysed by column chromatography method. Here MENK or MENK GCPQ B2 formulations are passed through a glass column packed with sephadex G25 resin. With differences in the retention of free MENK and MENK-GCPQ B2 nanoparticles, it was expected that MENK-GCPQ B2 nanoparticles have longer retention time compared to MENK only formulation. Sixty fractions were collected for each formulation and the concentrations were quantified by HPLC. However, the result shows that the MENK and MENK GCPQ B2 formulation had similar retention time (Figure 4-13). The disassociation of MENK-GCPQ B2 formulation while passing on the column matrix could be the reason for no differences in the elution time between encapsulated and non-encapsulated MENK.

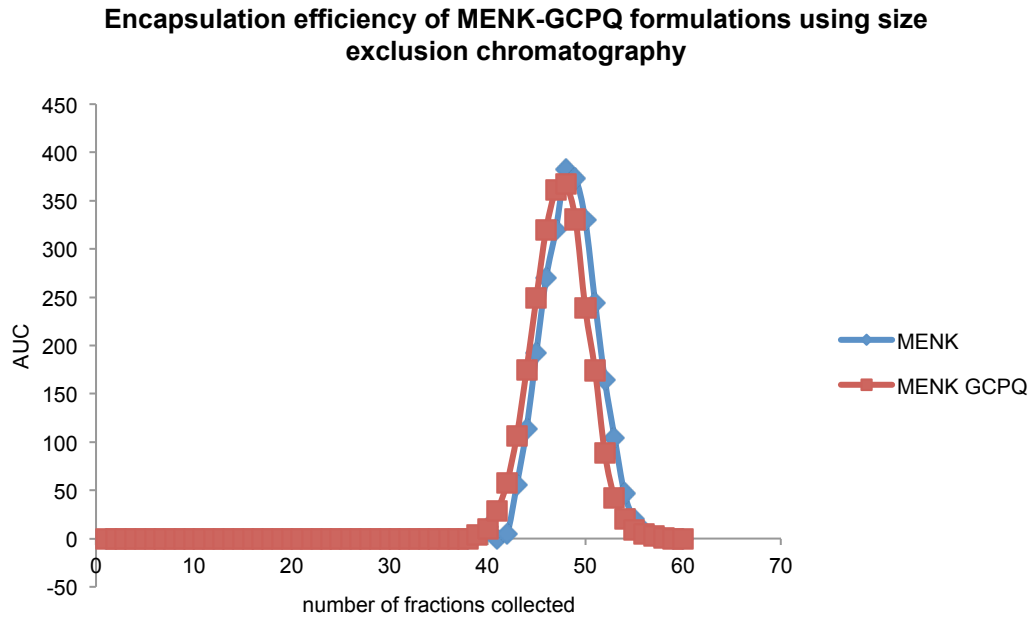

Figure 4-13 Determination of encapsulation efficiency of MENK (10mg/mL) –GCPQ B2 (50 mg/mL) (1:5) formulation by size exclusion chromatography. Each data point represents concentration of MENK in MENK (blue) or MENK GCPQ B2 formulation (red) from the fraction collected.

4.4.3.6 Colloidal Stability of MENK GCPQ B2 Oral Formulation

MENK peptide by its very nature is resistant to pepsin and hence MENK and MENK GCPQ B2 formulations were stable in SGF (Figure 4-14). However MENK peptide is susceptible to pancreatic enzymes. In SIF, MENK-GCPQ B2 oral formulation was unstable as that of MENK only formulation suggesting that GCPQ B2 does not offer stability against SIF (Figure 4-15).

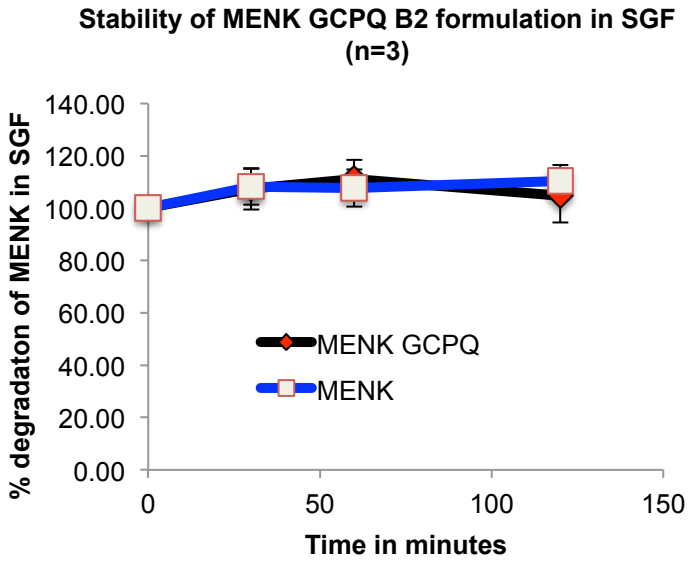

Figure 4-14 HPLC analysis of stability of MENK (5 mg/mL)-GCPQ B2 formulation (black) prepared at ratio 1:5 and MENK (5 mg/mL) (blue) in SGF maintained at pH 1.2 and temperature 37°C.

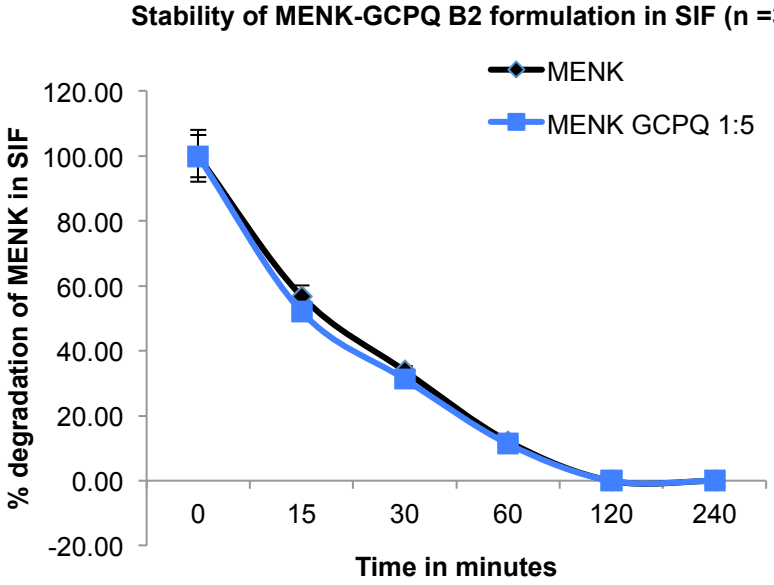

Figure 4-15 HPLC analysis of stability of MENK (5 mg/mL)-GCPQ B2 formulation (black) prepared at ratio 1:5 and MENK (5 mg/mL) (blue) in SIF maintained at pH 6.8 and temperature 37°C.

4.4.4 Other methods of preparing MENK GCPQ formulations

MENK was formulated by other methods with GCPQ B1 and their physical characteristics were evaluated.

4.4.4.1 MENK GCPQ B1 formulation by complex co-acervation method

Characterization of MENK and GCPQ B1 nanoparticle surface charge at different pH

Surface charge of MENK, GCPQ B1 and MENK-GCPQ B1 formulations were measured at different pH using DLS. MENK has positive zeta potential at its isoelectric point (5.6). GCPQ B1 and MENK GCPQ B1 formulations were also found to be more positive compared to MENK only formulation. At pH (5.6), both MENK and GCPQ B1 carried positive surface charge (Figure 4-16). So there could be electrostatic repulsion between peptide and the polymer. An alternative method to avoid charge-based repulsion is complex coacervation method.

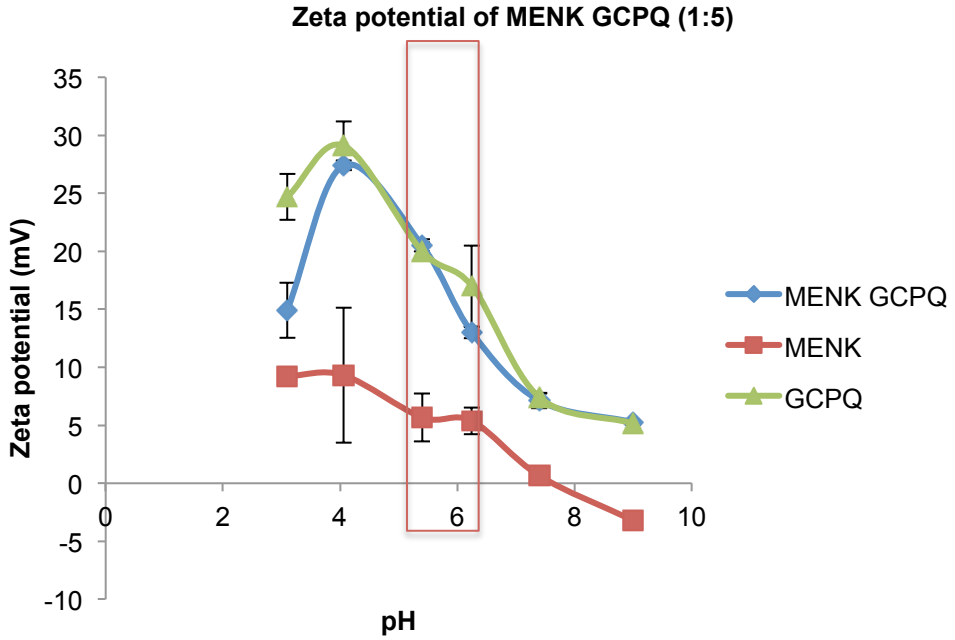

Figure 4-16 Zeta potential of MENK (2.5 mg/mL) – GCPQ B1 (12.5 mg/mL) formulation prepared in water at ratio (1:5) (blue) compared with MENK (2.5 mg/mL in water) (Red) and GCPQ B1 (12.5 mg/mL in water) (green).

MENK and GCPQ B1 have positive zeta potential between acidic and neutral pH. In order to favor interaction between MENK and GCPQ B1 polymer, MENK was first complexed with hyaluronic acid (HA), an anionic polymer to obtain negative surface charge and then complexed with positively charged GCPQ B1. The complexes were size characterized at different stages. First, the molecular weight of

HA used for coating MENK was assessed. Three different molecular weight of HA (4.7 kDa, 16 kDa and 35 kDa) were complexed with MENK using different molar ratios (Figure 4-17 & Figure 4-18). MENK complexed with small molecular weight HA (4.7 kDa) formed particles from MENK-HA ratio 1: 0.001 to 1:0.1 Above MENK-HA ratio 1:0.1, MENK was solubilized by HA. Increasing the molecular weight of HA to 16 and 35 kDa, resulted in MENK-HA solution at a ratio as low as 1:0.1. This suggests that with increase in the molecular weight and ratio of HA, MENK can be solubilized. Also the PDI of MENK HA complex increased with increase in the molecular weight and ratio of HA used. For complex coacervation, MENK should form particles with HA and hence lower ratios and molecular weight are preferred. The pH of the MENK-HA complexes was around 2.7. HA with molecular weight 16 kDa was used to complex MENK peptide.

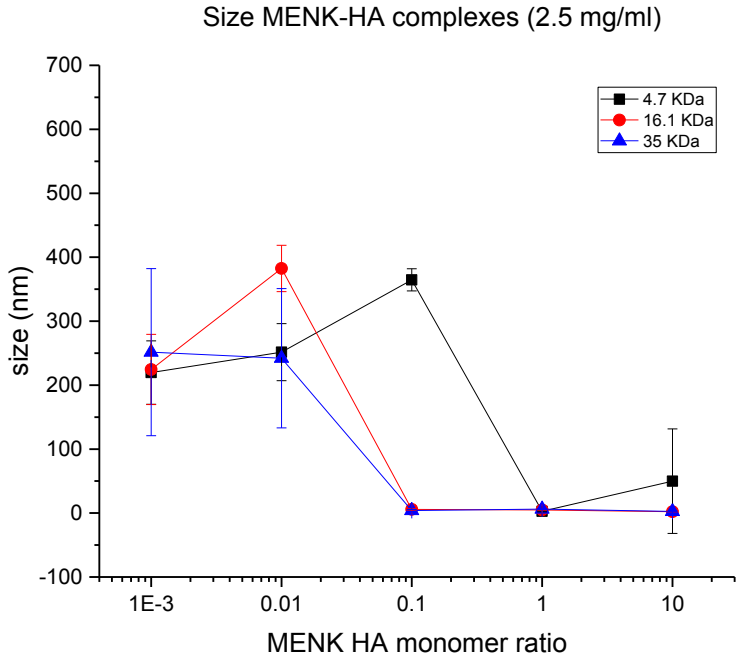

Figure 4-17 Size of MENK-HA complex analysed by DLS (n=3). Graph showing size on y-axis and MENK (2.5 mg/mL) complexed with HA of different molecular weight 4.7 kDa (black), 16.1 kDa (red) and 35 kDa (blue) prepared from ratio 1:0.001 to 1:10.

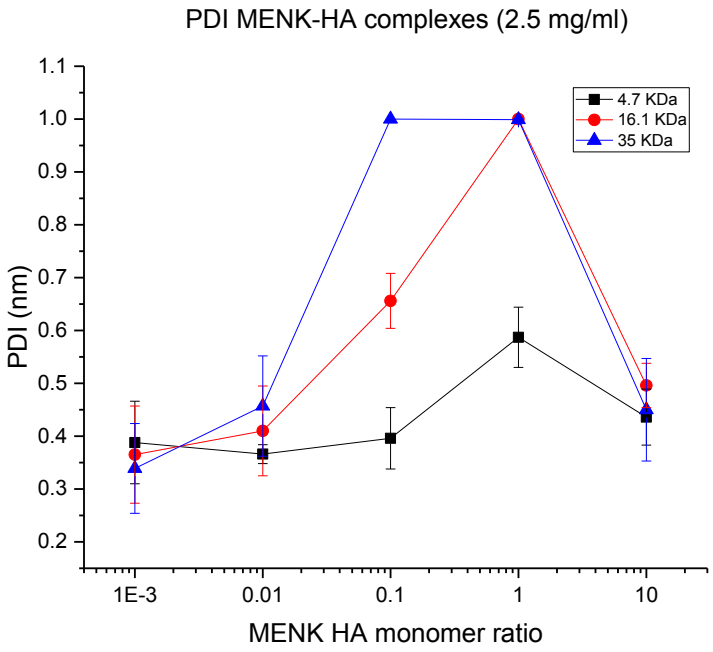

Figure 4-18 PDI of MENK-HA complex by DLS (n=3). Graph showing size on y-axis and MENK (2.5 mg/mL) complexed with HA of different molecular weight 4.7 KDa (black), 16.1 kDa (red) and 35 kDa (blue) prepared from ratio 1:0.001 to 1:10.

The minimum amount of HA (16 kDa) required to complex MENK were analysed by characterizing the stability of MENK HA complexes of different molar ratios for one day. From size and PDI results, MENK HA complexes of molar ratios 1:0.04 were found to be stable (Figure 4-19 & Figure 4-20). MENK complexed with HA at ratios less than 1:0.01 did not form stable particles on day 1 (Figure 4-19). The PDI of the complexes were also increased in one day (Figure 4-20). The negative zeta potential for MENK-HA complexes (above ratio 1:0.001) also confirm that HA was coated on MENK peptide (Figure 4-21). From the DLS size data MENK-HA complex prepared at ratio 1:0.04 was used for further studies. This ratio was preferred as it is the minimum amount of HA required to keep the complex stable for one day.

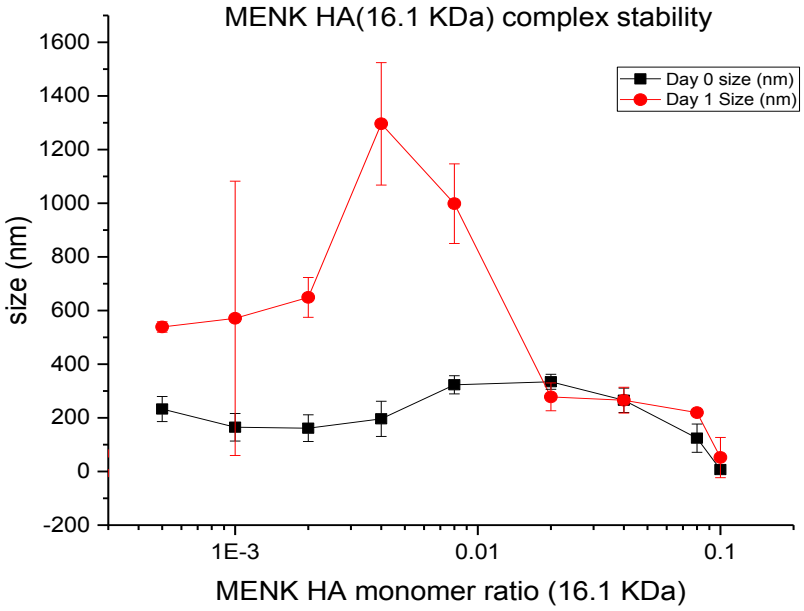

Figure 4-19 Stability of MENK-HA (16 kDa) complexes on day 0 (black) and day 1 (red) prepared at ratio from 1: 0.0005 to 1: 0.1 and characterized by DLS – Size (n=3)

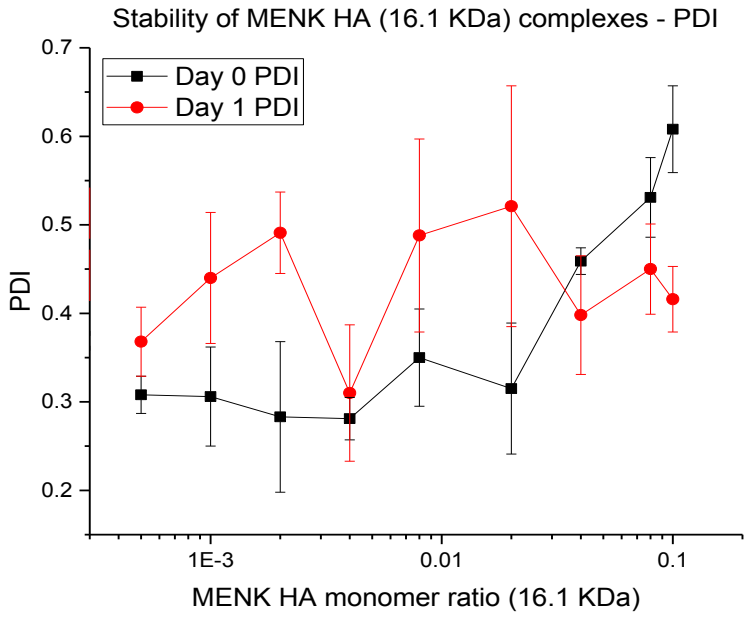

Figure 4-20 Stability of MENK-HA (16 kDa) prepared at ratio from 1: 0.0005 to 1: 0.1 and characterized by DLS - PDI (n=3)

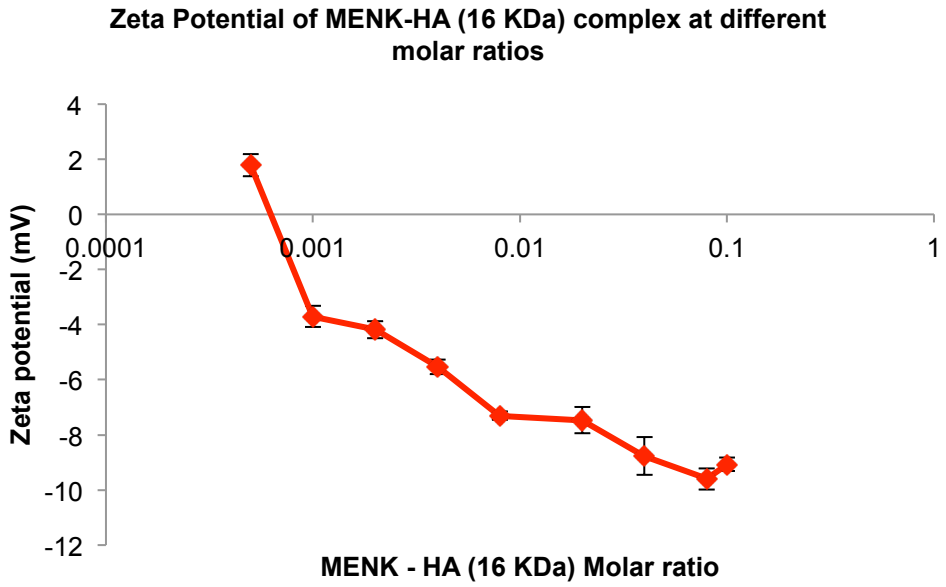

Figure 4-21 Zeta potential of MENK HA (16 kDa) complex prepared from ratio 1: 0.0005 to 1: 0.1 (n=3)

4.4.4.1.a Preparation and characterization of MENK-HA-GCPQ B1

MENK-HA complex of molar ratio 1:0.04 was complexed with GCPQ B1 at different mass ratio 1:1, 1:2.5 and 1:5 and size characterized. The pH of the resulting complexes was around 3. Particles of nanometric sizes were obtained for MENK-HA-GCPQ B1 formulations (Figure 4-22 & Figure 4-23). An increase in the positive zeta potential of MENK-HA-GCPQ B1 formulation was observed before and after probe sonication suggesting that GCPQ B1 was coated on MENK-HA complexes (Figure 4-24). However, increasing the pH of the formulations above 4, results in formation of precipitates. This suggests that the MENK-HA-GCPQ B1 formulations were not stable over pH 4. Precipitation could be a result of uncoated MENK-HA complexes at higher pH. The concentrations and molecular weight of GCPQ B1 used should be optimized for further studies.

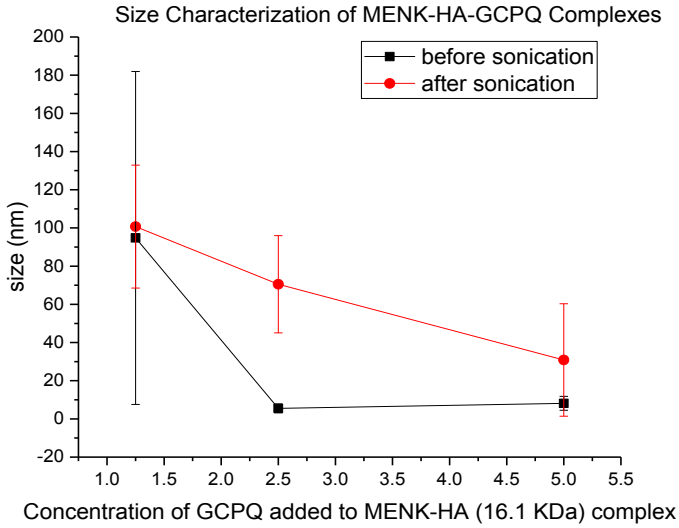

Figure 4-22 Size characteristics of MENK-HA-GCPQ B1 complex prepared at ratio [1: (0.04): 1 to 1: (0.04): 5] and characterized by DLS (n=3)

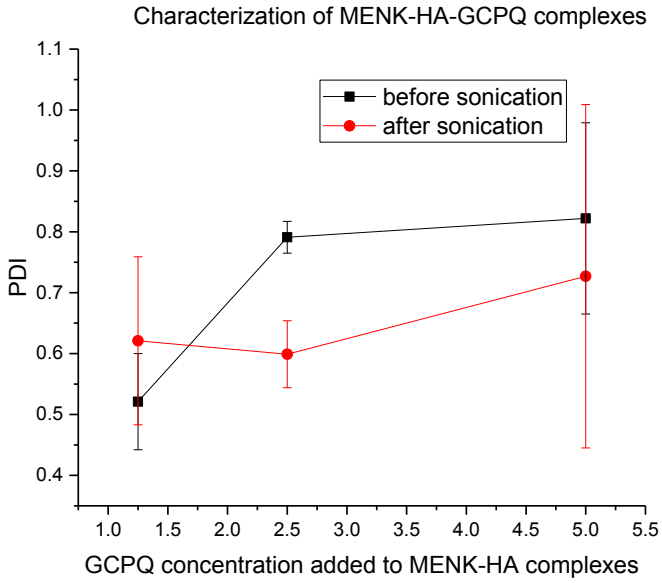

Figure 4-23 PDI of MENK-HA-GCPQ B1 complex prepared at ratio [1: (0.04): 1 to 1: (0.04): 5] and characterized by DLS (n=3)

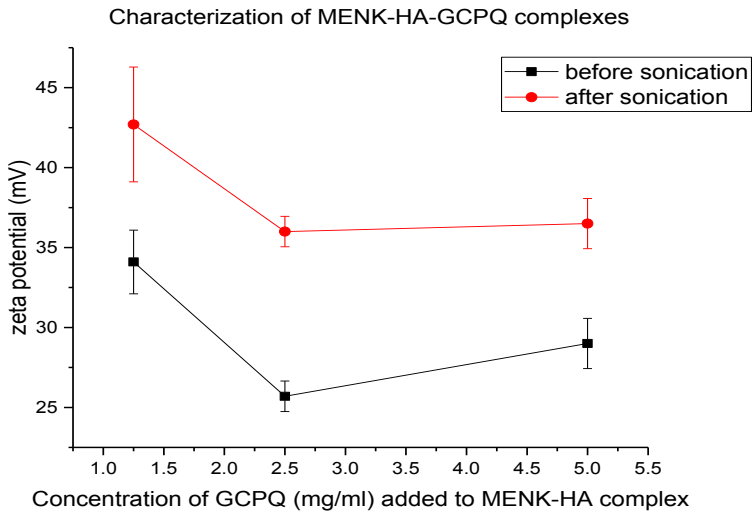

Figure 4-24 Zeta potential of MENK-HA-GCPQ B1 complex prepared at ratio [1: (0.04): 1 to 1: (0.04): 5] and characterized by DLS (n=3)

4.4.4.2 MENK GCPQ B1 formulations by direct reconstitution and film method

MENK was also formulated with GCPQ B1 by other methods such as direct reconstitution and film method. In direct reconstitution method, MENK and GCPQ B1 were added as powder and directly probe sonicated by suspending them in water. This was to avoid charge-based repulsion between MENK and GCPQ B1 as it was seen with other formulation prepared previously.

Film based method was also prepared by dissolving MENK and GCPQ B1 in their respective solvent, mixed and evaporated to form a thin film. The film was then reconstituted in water and probe sonicated. This method was to ensure that MENK and GCPQ B1 were at homogeneously distributed while probe sonication. Formulations prepared by above methods were size characterized and their stability in SIF were analysed.

4.4.4.2.a Size Characterization and stability of MENK GCPQ B1 formulations

The sizes of MENK GCPQ B1 formulations prepared by direct reconstitution and film method were in nanometric range of PDI ranging from 0.3 to 0.6 (Table 4-6). However, these formulations were unstable in SIF (Figure 4-25) that were similar to MENK, MENK-GCPQ IV or oral formulations.

Table 4-6 Size characterization of MENK-GCPQ formulation prepared by film and direct reconstitution method

Formulation	Size	PDI
Direct reconstitution of MENK GCPQ B1 (n=3)	156.9 ± 47.16	0.569 ± 0.238
MENK GCPQ B1 film method (speed vac) (n=3)	70.48 ± 1.707	0.384 ± 0.013

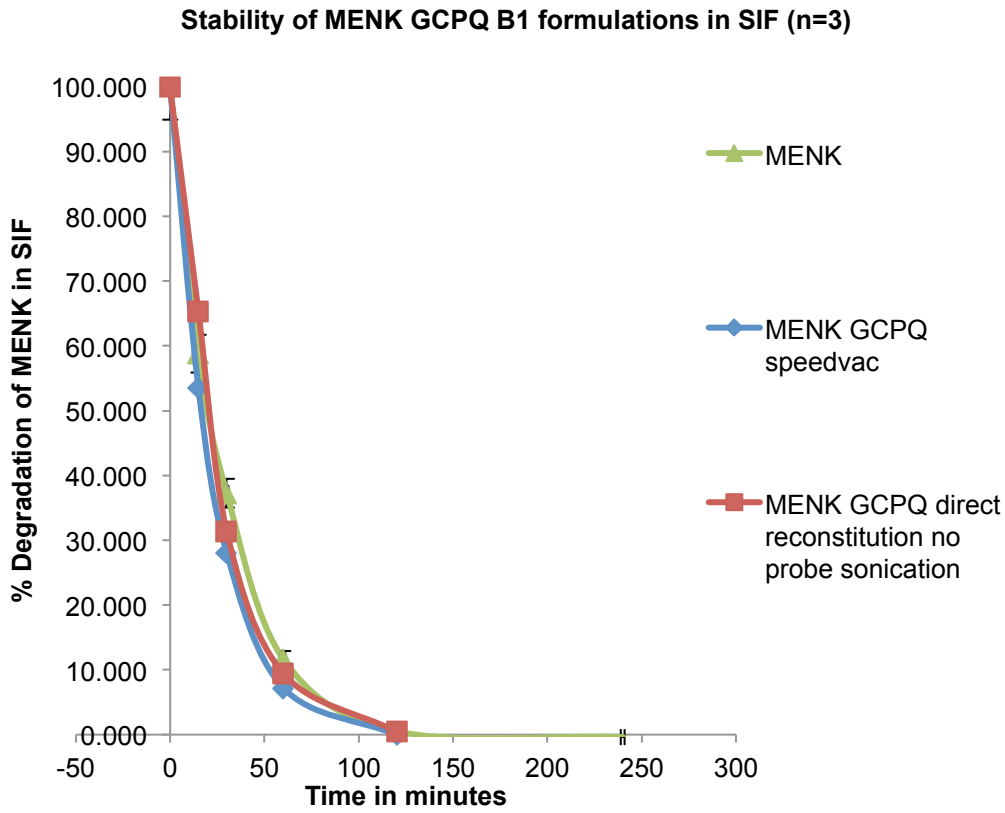

Figure 4-25 Stability of MENK-GCPQ B1 formulations prepared by film and direct reconstitution method and incubated in SIF at 37˚C for 240 min.

For *in vivo* studies, MENK GCPQ (B1 & B2) IV and oral formulation prepared by solubilisation method were used.

4.4.5 Analytic method for quantification of MENK by Enzyme Immuno Assay (EIA)

The sensitivity of EIA was first tested on MENK standards prepared in water. In the standards prepared from 500 ng/mL to 1.95 ng/mL (Figure 4-26), no signal was obtained above a concentration of 31.25 ng/mL that could be seen from the semi log plot as a flat line. At a concentration of 31.25 ng/mL, MENK binds completely to the available antiserum in the immunoplates producing no signal. Any concentration above 31.25 ng/mL will be the same due to saturation of antiserum by peptide.

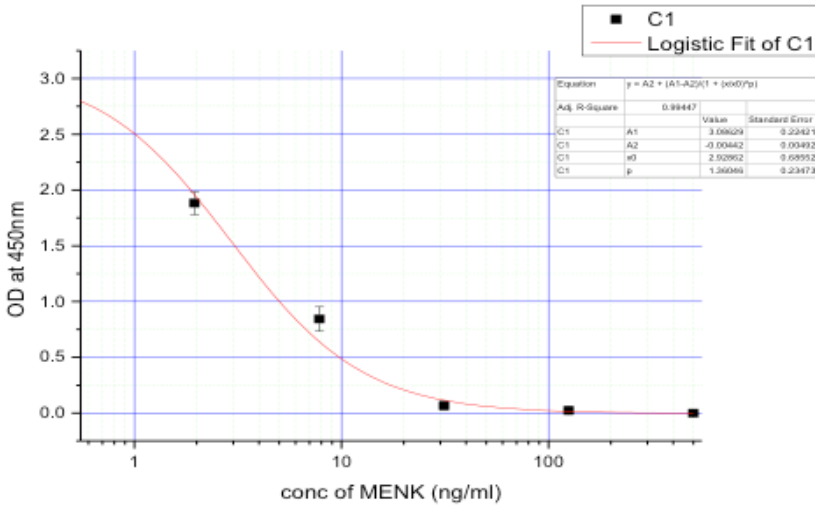

Figure 4-26 Semi log plot of Met-Enkephalin standards in water (1.95 ng/mL to 500 ng/mL)

The standards (500 ng/mL – 1.95 ng/mL) were spiked in to plasma (Figure 4-27) and the plot obtained from EIA experiment shows a similar trend in the curve. Here the saturation of the anti-serum binding sites was observed at a concentration of only 7.18 ng/mL. However, the absorbance above a concentration of 7.18 ng/mL was in a range within 0.3 to 0.6 absorbance units compared to MENK in water that showed absorbance of zero above 31.25 ng/mL. This shows that there were background interferences from plasma samples that produced intensity signal at 450 nm.

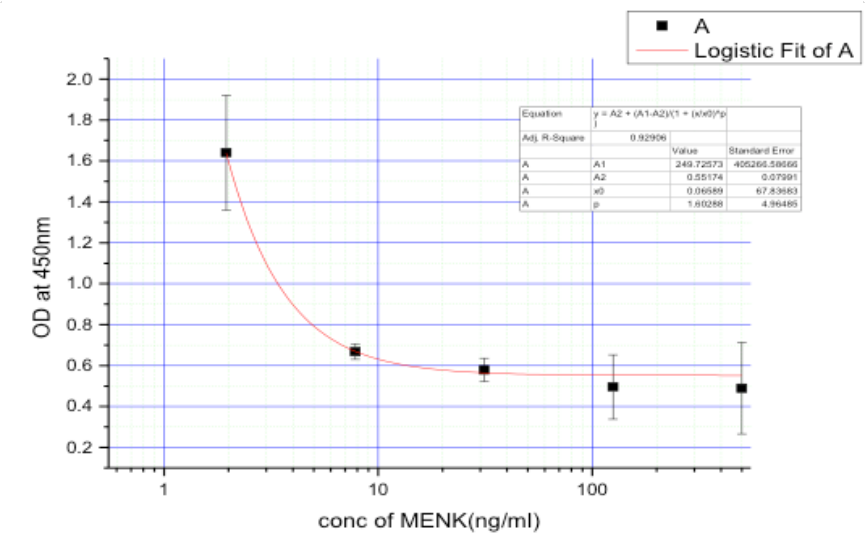

Figure 4-27 Semi log plot of Met-enkephalin standards spiked in plasma (1.95 ng/mL to 500 ng/mL)

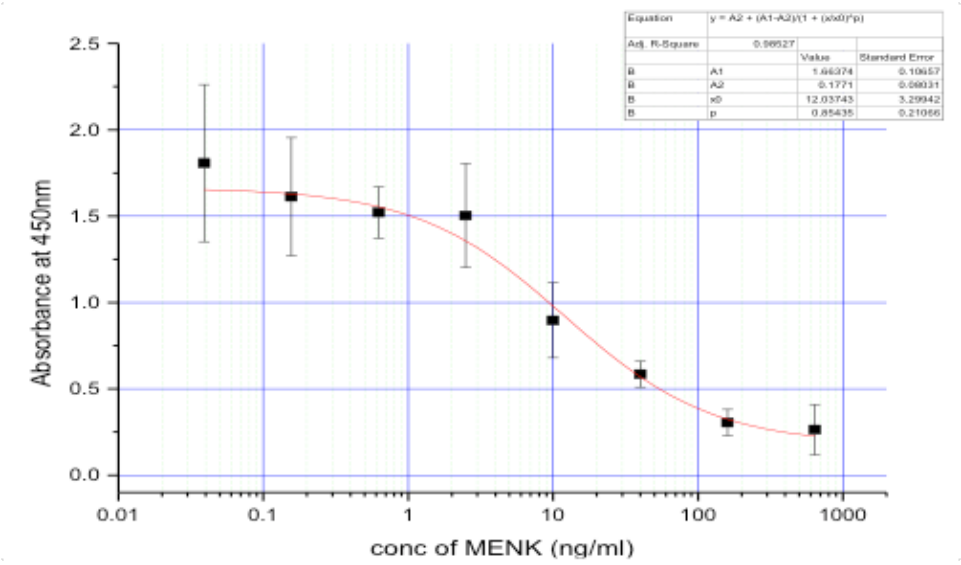

Figure 4-28 Semi log plot of Met-enkephalin spiked in 10 times diluted plasma samples

The standard curve (640 ng/mL to 0.01 ng/mL) was also repeated with MENK standards spiked in ten times diluted plasma samples (Figure 4-28). The result shows that at a concentration below 2.5 ng/mL difference in absorbance was not significant that the method is not sensitive below that concentration. The semi log plot was shallow and it would be difficult to compare between samples in vivo at different time point. *In vivo*, if the plasma samples were diluted ten times, which will eventually dilute the peptide of interest the absorbance obtained will be below the limit of detection. These constraints have limited the use of EIA for only in vitro samples than in vivo. A robust analytical method was required to measure peptide of interest in biological matrix.

4.4.6 Analytical method for quantification of MENK in vivo by LCMS

4.4.6.1 Optimization of Source parameters

Source and MRM parameters in LCMS were optimized for MENK peptide to obtained better signal. The MENK signal to noise ratio (S/N ratio) for each source parameters such as capillary voltage, nebulizer gas, drying gas flow, drying gas temperature, sheath gas flow and sheath gas temperature (Figure 4-29) were optimized and the value at which maximum S/N ratio obtained were used to create the final LCMS method. Source parameters are essential for formation of fine droplets and dessolvation of clustered ions from the LC column. Optimization of source parameters maximizes the sensitivity of the signal obtained. The optimum source parameters for MENK peptide are summarized in Table 4-7.

Table 4-7 Optimized source parameters for MENK in plasma

Source Parameters	
Ionization mode	ESI jet streaming positive
Sheath gas temperature (˚C)	400
Sheath gas flow (L/min)	11
Drying gas flow (L/min)	12
Drying gas temperature (˚C)	290
Nebulizer gas (psi)	20
Capillary voltage (V)	3500 (positive and negative)
Nozzle voltage (V)	0

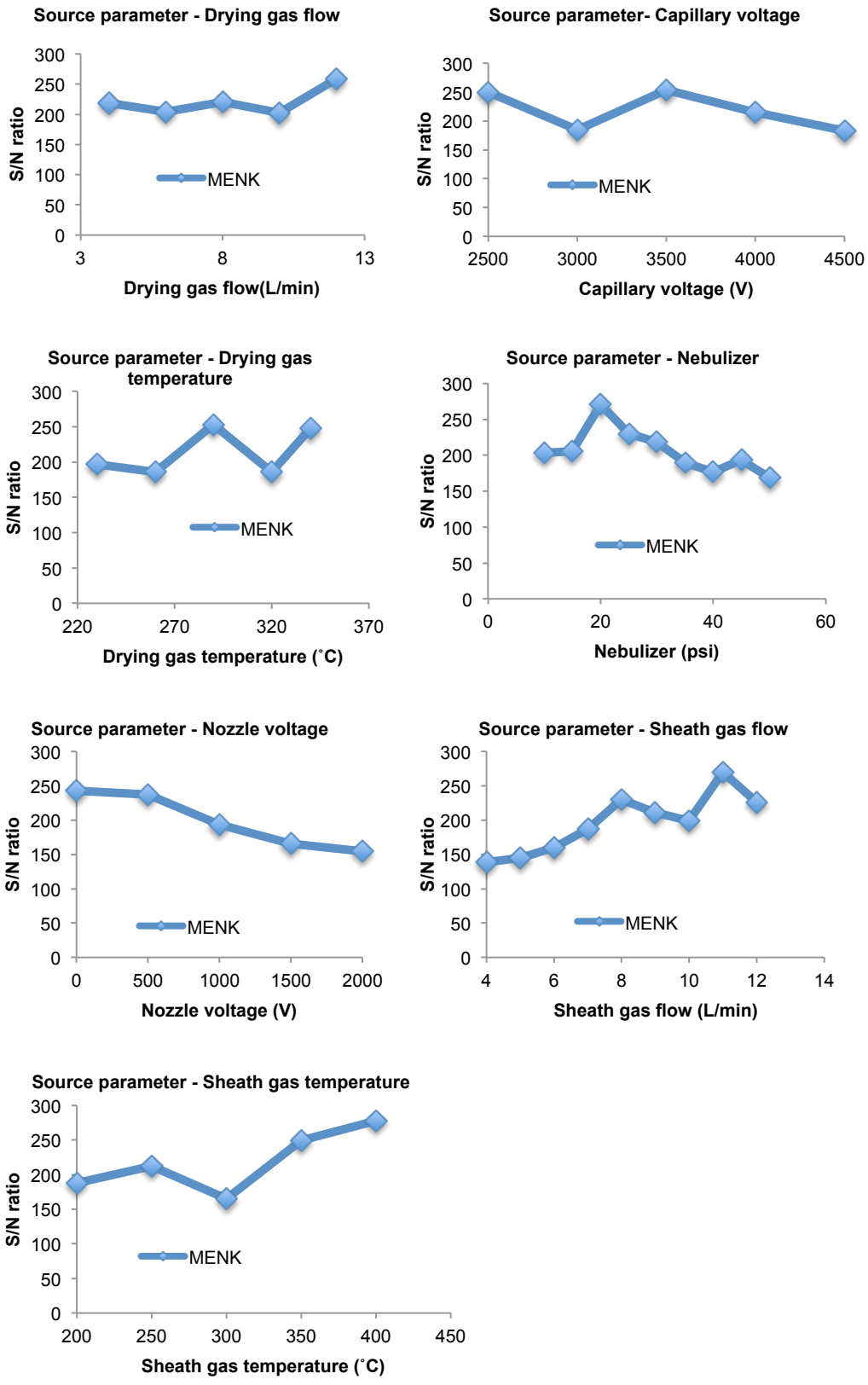

Figure 4-29 Optimization of source parameters for MENK in plasma

4.4.6.2 MENK standard curve

MENK and dalargin (internal standard) peaks were obtained at elution time of 4.9 and 4.7 min in a total run time of 7 min (Figure 4-30). Calibration curve was plotted with standards ranging from 20 ng/mL to 600 ng/mL. The linear equation for the calibration curve was y= 0.008x+0.2135 with R^2 = 0.99733 (Figure 4-31). The LLOQ for MENK was observed to be 20 ng/mL. For pharmacokinetic studies, a new standard curve was run every day and compared with the respective samples.

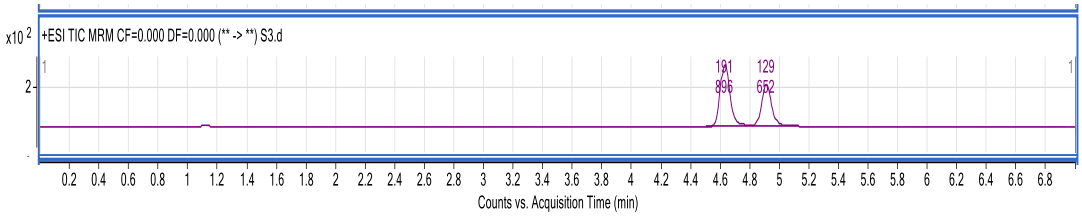

Figure 4-30 Retention times of MENK (4.9 min) and Dalargin (4.7 min)

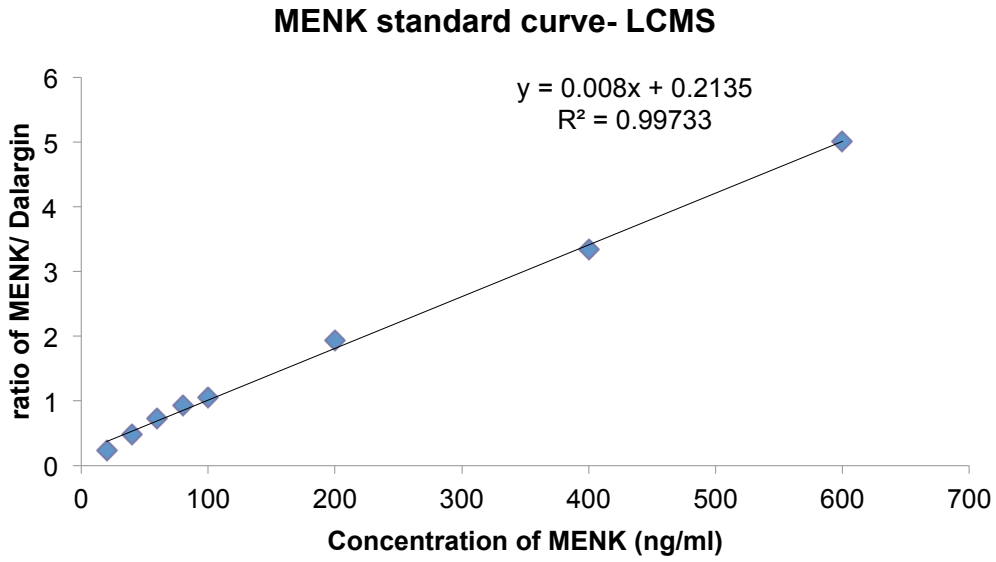

Figure 4-31 MENK standard curve in plasma

4.4.6.3 Endogenous MENK in mice plasma

The concentration of endogenous MENK in mouse plasma (n=10) was measured by LCMS-QQQ (Table 4-8). Only one in 10 mice had concentration around 22.32 ng/mL, which is close to LLOQ of MENK in plasma (20 ng/mL).

Table 4-8 Quantification of endogenous MENK in mice plasma by LCMS-QQQ

Mice	Concentration of endogeneous MENK (ng/mL)
S1	Below LLOQ
S2	Below LLOQ
S3	Below LLOQ
S4	Below LLOQ
S5	Below LLOQ
S6	Below LLOQ
S7	Below LLOQ
S8	22.32
S9	Below LLOQ
S10	Below LLOQ

4.4.7 *In vivo* Pharmacokinetics of MENK-GCPQ B1 IV formulation

MENK concentrations in plasma were monitored following intravenous administration of MENK or MENK GCPQ B1 formulations (MENK- 15 mg/kg) in mice (n= 5 per group). Significant differences between MENK and MENK GCPQ B1 formulations were observed at time point 15 min and above (two way anova, $p< 0.0001$) (Figure 4-32). MENK concentrations were not detected in plasma, 15 min after administration of MENK formulation, where as, at the same time point, MENK concentrations in plasma were observed to be 298 ± 48.84 ng/mL for MENK GCPQ B1 formulation. The MENK-GCPQ B1 formulation was stable when measured until 180 min. A sharp decrease in the concentration of MENK in MENK-GCPQ B1 formulation at first time point could be result of non-encapsulated MENK in MENK-GCPQ B1 nanoparticles.

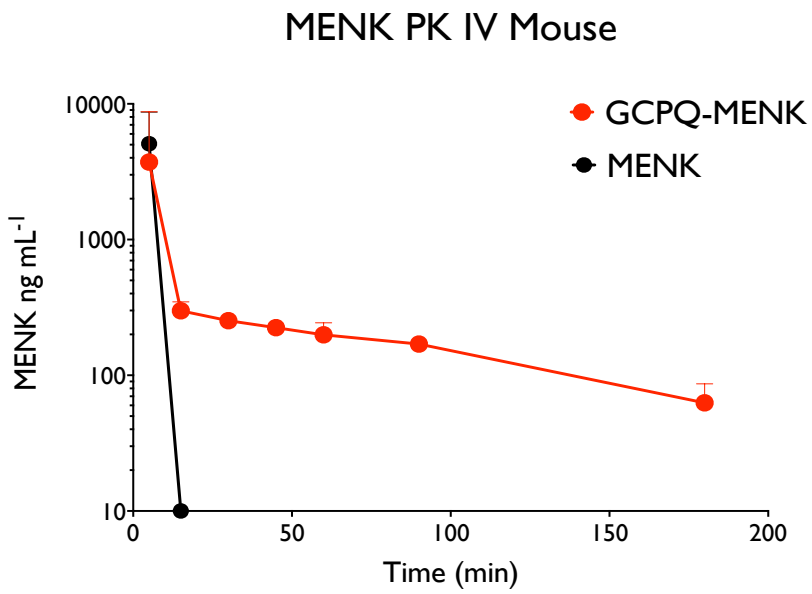

	AUC (ugh/L)	T max	C max (ng/mL)
MENK GCPQ B1	47944.9 ± 6670.89	5 min	3727.40 ± 1003.42

Figure 4-32 Pharmacokinetics of MENK (15 mg/kg) and MENK GCPQ B1 ratio 1:2.6 (15 mg/kg) formulations in plasma (n=5) Concentration of MENK dose was 15 mg/kg. Concentration of MENK in plasma quantified using LCMS-QQQ

4.4.8 *In vivo* Pharmacokinetics of MENK-GCPQ B2 Oral Formulation

CD-1 mice were administered with 100 mg/kg MENK or MENK GCPQ B2 formulation and plasma MENK concentrations at different time points were analyzed by LCMS-QQQ (Figure 4-33). MENK concentrations were not detected in plasma after 30 min and four mice have variable MENK concentrations ranging from 724.40 ng/mL to 23.51 ng/mL in mice plasma at 60 min time point. One mouse at each time point 120 and 240 min had MENK concentration in plasma around 52 and 91 ng/mL.

No concentrations of MENK in plasma were observed for mice treated with MENK alone formulation and analysed at time points ranging from 30 to 240 min.

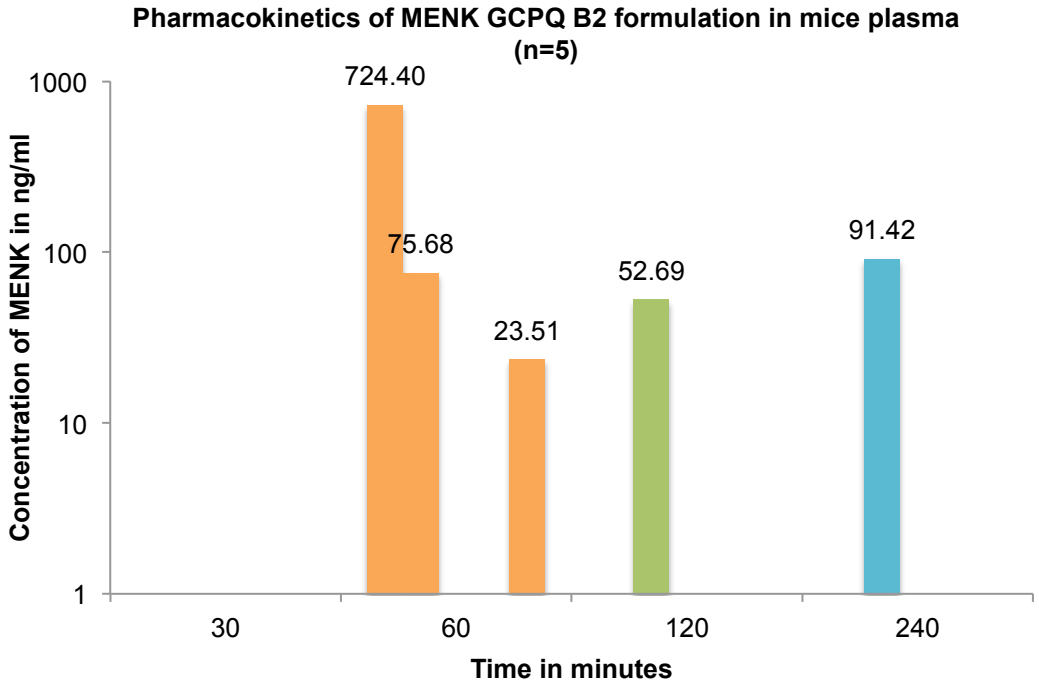

Figure 4-33 *In vivo* pharmacokinetic study of MENK (100 mg/kg)-GCPQ B2 (1:5) oral formulation (n=5). Each data point represents the concentration of MENK in mouse plasma at time points 30 (purple), 60 (orange), 120 (green) and 240 min (blue) as analysed by LCMS-QQQ.

4.4.9 *In vivo* Pharmacodynamics of MENK-GCPQ B1 IV formulation

Tumour-bearing CD1 mice (sub-cutaneous injected with MiaPaCa-2) were intravenously (15 mg/kg) administered (12 doses over a period of 29 days) with MENK or MENK-GCPQ B1 IV formulation. Tumour regression was monitored against the untreated xenografts (control) for 39 days before and after treatment. Two-tumour bearing mice treated with MENK IV formulations had to be withdrawn from the study during the course of study (11^{th} and 16^{th} day) due to tail hemorrhage. These data were not considered in tumour regression data analysis and statistical significance was analysed only for time points that has complete data sets (i.e. n=5). (Figure 4-34).

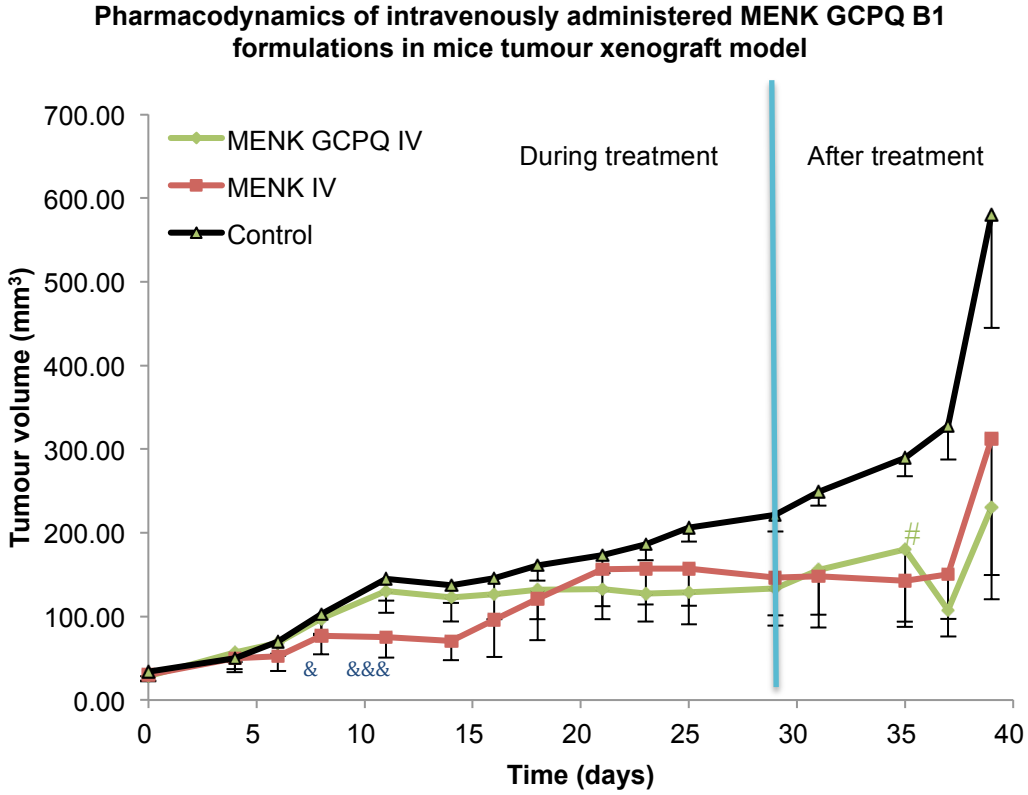

Figure 4-34 Pharmacodynamics of MENK (15 mg/kg)-GCPQ B1 formulation (n=5) in green, MENK (15 mg/kg) formulation (n=5) in red and control (0.9% NaCl) (n=5) in black intravenously administered two days once in nude mice bearing MiaPaCa-2 Xenograft. Tumour volume was measured for treatment period of 29 days and continued up to day 39. Two way anova - MENK GCPQ B1 IV formulation significantly different from control on day 35 (# $p< 0.05$) and MENK IV formulation significantly different from the MENK GCPQ B1 IV formulation on day 8 (& $p< 0.01$) and 11 (&&& $p< 0.01$). Missing data sets were excluded from statistical analysis.

An alternative method is to use Kaplan-Meier test to calculate the survival of the tumour bearing mice after treatment. The advantage of this estimator is that, this method can take in to account of censored data, particularly when a subject is withdrawn from the study before the final outcome is measured. The tumour bearing mice treated with MENK and MENK-GCPQ B1 IV formulation had mean survival time of 39 days against control, which was only 29 days (Figure 4-35).

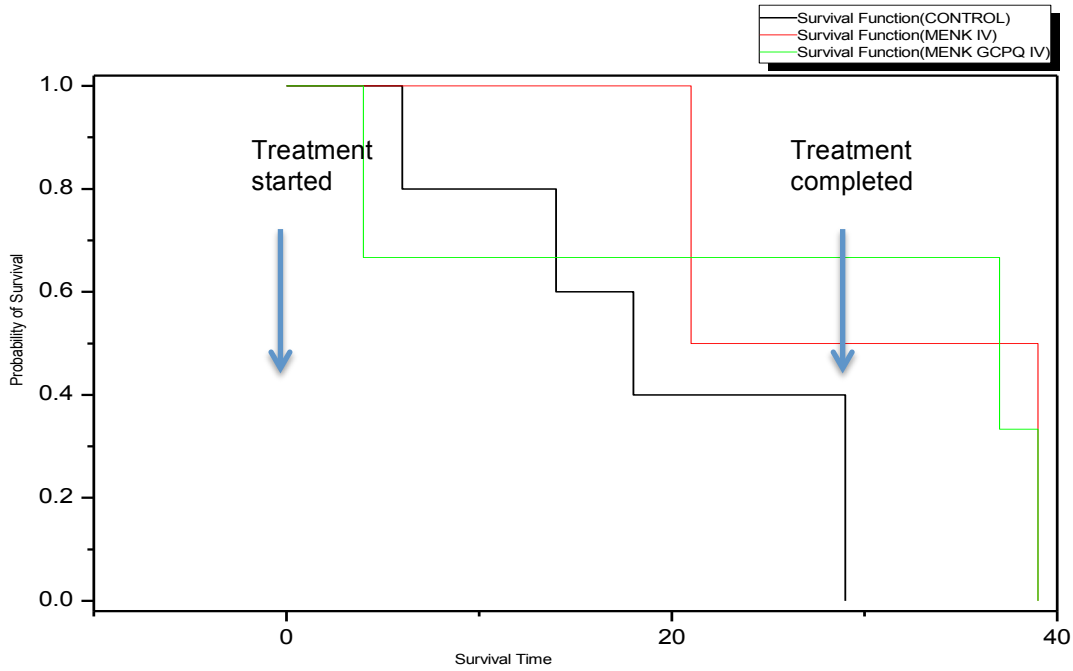

Figure 4-35 Survival analysis of MENK (15 mg/kg) IV (red), MENK (15 mg/kg)-GCPQ B1 (1:2.6) IV (green) and control (black) formulation by Kaplan Meier estimator. Survival line drops for every animal that reaches a relative tumour growth rate above 5 on the respective date.

4.4.10 *In vivo* Pharmacodynamics of MENK-GCPQ B2 Oral Formulation

The tumour regression in mice administered with MENK-GCPQ oral formulation was higher than the MENK oral formulation (Figure 4-36). This suggests that, the GCPQ B2 enhanced oral delivery of MENK peptide to the tumours resulting in delayed tumour growth. One tumour bearing mouse treated with MENK-GCPQ B2 oral or MENK formulation was withdrawn from the study (after day 16) due to poor administration. Therefore, statistically significant differences ($p < 0.05$) were only observed only at day 13 and 16.

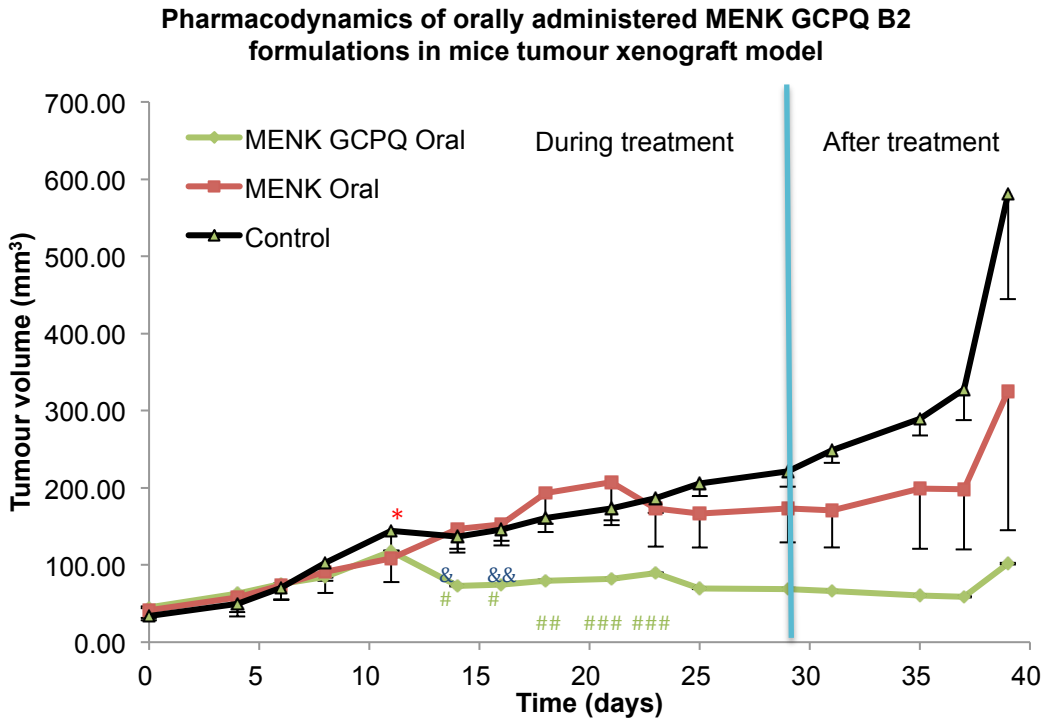

Figure 4-36 Pharmacodynamics of MENK (50 mg/kg)-GCPQ B2 formulation (n=5), MENK (50 mg/kg) formulation (n=5) and control (0.9% NaCl) (n=5) orally administered two days once in nude mice bearing MiaPaCa-2 xenograft. Tumour volume was measured for treatment period of 29 days and continued up to day 39. Two way anova - MENK oral formulation significantly different from control on day 11 (*p<0.01), MENK GCPQ B2 oral formulation significantly different from control on day 14 (# p< 0.01), 16 (# p< 0.01), 18 (## p< 0.01), 21 (### p< 0.01), and 23 (### p< 0.01) and MENK oral formulation significantly different from the MENK GCPQ B2 oral formulation on day 14 (& p< 0.01) and 16 (&& p< 0.01). Missing data sets were excluded from statistical analysis.

The survival time was calculated using Kaplan-Meier estimator. Survival analysis of tumour bearing mice with different treatment shows that the tumor bearing mice treated with MENK-GCPQ B2 oral formulation has the mean survival time of 39 days (experiments concluded at 39 days), followed by MENK oral and control with a mean survival time of 35 and 29 days respectively (Figure 4-37). This confirms the efficacy of MENK GCPQ B2 oral formulation in tumour regression over other MENK peptide alone formulations.

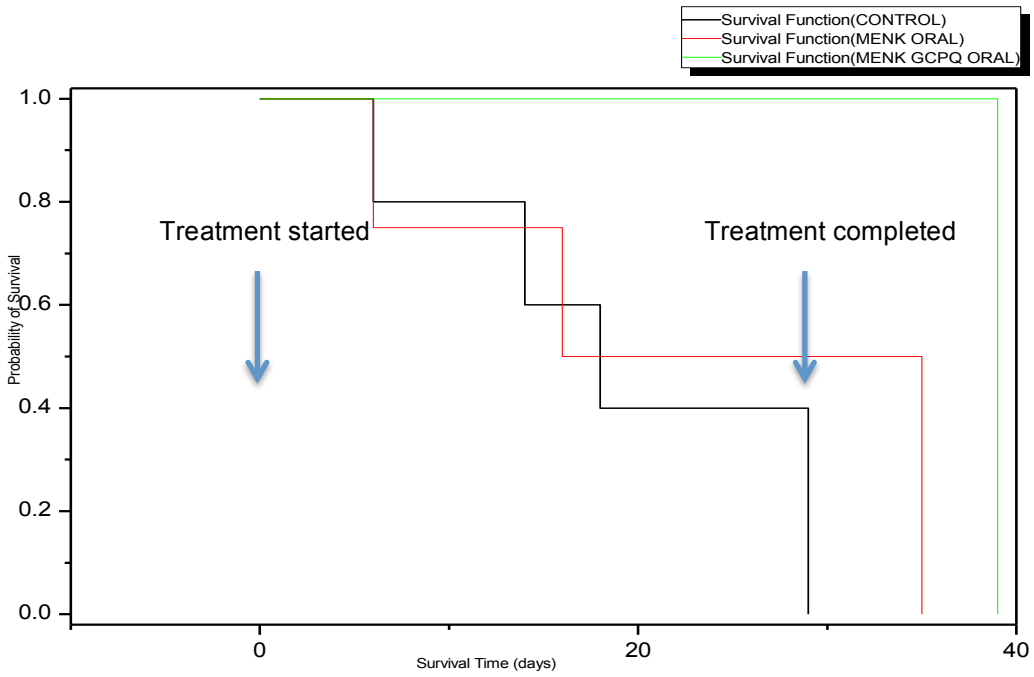

Figure 4-37 Survival analysis of MENK (50 mg/kg) oral (red), MENK (50 mg/kg)-GCPQ B2 (1:5) IV (green) and control (black) formulation by Kaplan Meier estimator. Mice having relative tumour growth rate above 5 was withdrawn from the study. Survival line drops for every animal that reaches a relative tumour growth rate above 5 on the respective date.

4.4.11 Body weight comparison

The body weight of tumour bearing mice was also measured during the course of treatment (Figure 4-38), and no significant difference between the control mice and mice that received MENK or MENK GCPQ (B1 or B2) oral/IV formulation were observed. It was also observed that the body weights of mice bearing tumour were not less than 15% of their initial body weights with or without treatment.

This suggests that the tumour burden, mode of administration and treatment did not affect the body weight of mice.

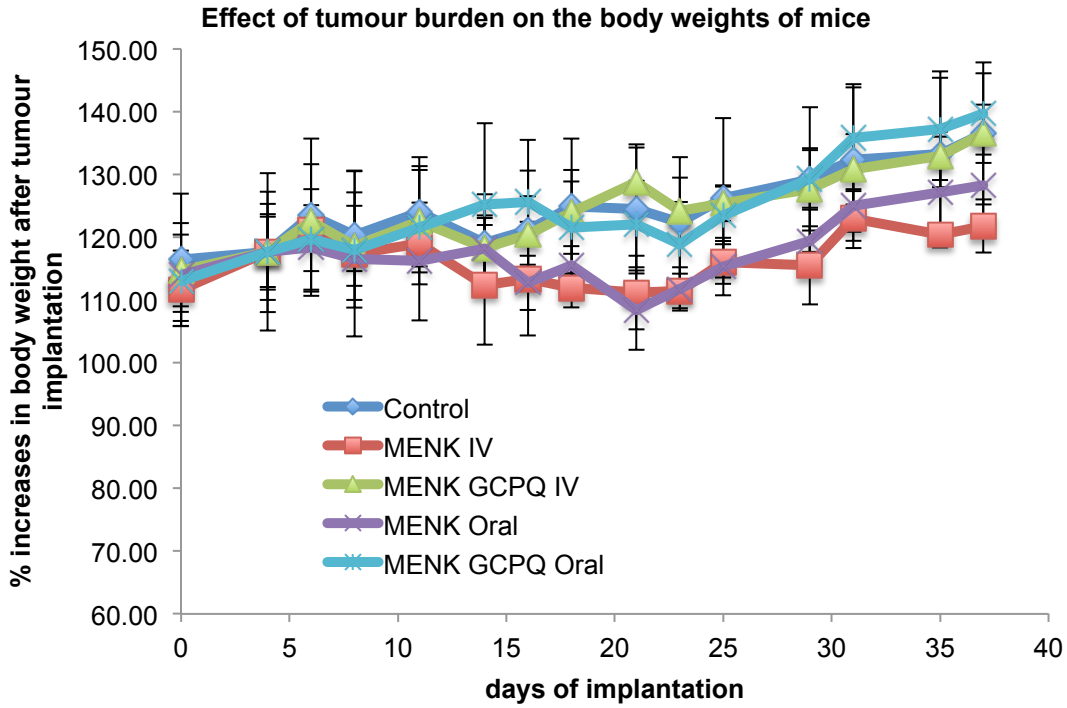

Figure 4-38 Body weight comparison between mice administered orally or intravenously with MENK/MENK GCPQ (B1 & B2) formulations (n=5) compared with control (n=5).

4.5 Discussion

MENK or opioid growth factor is an endogenous opioid peptide, reported to have shown anti-proliferative action on pancreatic cancer cells by up regulation of P21 pathway [255]. Since this action is transient, standard therapy requires repeated administration of MENK via infusion [260]. Although MENK treatment in human reported no toxic side effects [260] compared to standard chemotherapies, repeated administration via infusion can lead to medication non-compliance. An alternative approach is to use non-invasive methods such as oral delivery of Met-enkephalin. However, oral delivery of Met-enkephalin is hampered due to its poor physiochemical properties such as limited solubility and stability in the gut and plasma.

In the present study, oral delivery of MENK using GCPQ nanoparticle was demonstrated. GCPQ was previously reported to improve the oral availability of poorly soluble hydrophobic drugs [146] and peptide [53] by forming nanoparticles. Previous report suggests that MENK is sparingly soluble in water and a dose-limiting factor for intravenous delivery [269]. So the solubility characteristic of MENK was evaluated. For the first time we have reported that met-enkephalin exhibits different morphological characteristics at different concentrations. Met-enkephalin self assembles to form nanoparticles in aqueous solution at a concentration as low as 160 μg/mL (Figure 4-5) as determined by ITC and by TEM (Figure 4-4) at higher concentrations (5 mg/mL). These nanoparticles aggregates above a concentration of 10 mg/mL and forms precipitate when analyzed at 20 mg/mL. Formation of nanoparticles by methionine enkephalin was similar to observation made previously with leucine enkephalin that formed nanoparticles of size around 170 nm in aqueous solution [53]. It was also observed by DLS measurement that particle formation by MENK is pH dependent where MENK solubilizes in 30% acetic acid (pH 2.5) and forms nanoparticles at pH 5.3.

For formulation of MENK with GCPQ micelles, two batches of GCPQs were used. MENK was formulated with GCPQ B1 for IV formulation and with GCPQ B2 for oral formulation by solubilization method. MENK was also formulated with GCPQ B1 by other methods such as complex coacervation, film formation and direct reconstitution method.

GCPQ B2 of palmitolyation and quaternization of 19% and 12% was used for preparing MENK-GCPQ oral formulation. GCPQ B1 of palmitoylation and quaternization of 16% and 14% were used for preparing MENK-GCPQ IV formulation.

MENK-GCPQ (B1 & B2) nanoparticle were prepared by first solubilizing MENK in acetic acid (30% v/v) in order to prevent self-assembled micelle formation. To the solubilized MENK solution, GCPQ solution was added, followed by increase in pH of the formulation to 5.3. It was hypothesized that when MENK aggregates with increase in pH, it could favor encapsulation of MENK in GCPQ nanoparticles. The ratios (1:2.6 and 1:5) used for preparing MENK-GCPQ (B1 & B2) IV and oral formulations were same as previously reported ratios for LENK-GCPQ IV and oral formulations [53]. With increase in the concentration of GCPQ (B1 & B2) used for IV and oral formulation the size of the particles reduced from 391 nm (Figure 4-6) to 16 nm (Figure 4-7). MENK GCPQ (B1 & B2) oral and IV formulations also had positive surface charge of +41mV and +48 mV (Figure 4-9) depending on the quaternization level (12% and 14%) of GCPQs used respectively.

Stability of MENK-GCPQ B2 oral formulation was tested *in vitro* in SIF fluid. It was observed that MENK-GCPQ oral formulation did not improve its stability in SIF fluid.

MENK-GCPQ B1 formulations were also prepared by other methods. First the surface charge of MENK at different pH was monitored. It was found that MENK carries positive charge at its isoelectric point because of its self-assembling nature. There are possibilities of electrostatic repulsion between the positively charged MENK and GCPQ B1 nanoparticles at pH 5.3. So alternative strategies such as film method and complex co-acervation were used. Yuri et al first reported formation of ultrathin film by layer by layer assembly of positively charged proteins within negatively charge poly(styrene sulfonate) (PSS) polymer through electrostatic interaction [270]. This technique was further exploited in drug delivery for targeted release [271] [272]. In film method, MENK and GCPQ B1 were dissolved separately in a suitable solvent, mixed and evaporated to form a thin film. The film was reconstituted in water so that the MENK and GCPQ B1 at its proximity form nanoparticles. However the formulation prepared by film method did not improve the stability of MENK in SIF (Figure 4-25).

Complex coacervation is a pH induced complexation process prepared by electrostatic interaction between oppositely charged particles. Complex coacervation between silk fibroin/hyaluronic acid [273], chitosan/hyaluronic acid [274] and lysozyme/hyaluronic acid [275] has been previously reported to improve stability of protein formulation or as drug carrier. Complex coacervation method involves coating of MENK particles with negatively charged hyaluronic acid (HA), which was then coated with positively charged GCPQ B1 nanoparticles. MENK-HA complex were successively obtained at 0.04 molar ratios (Figure 4-19, Figure 4-20). However, when the complex were coated with GCPQ B1 (Figure 4-22) and increased its pH the complex precipitated. Precipitation could be a result of exposure of MENK-HA complexes to higher pH that were not coated by GCPQ B1 particle. Further studies needs to be conducted to justify this hypothesis.

MENK-GCPQ (B1 & B2) IV and oral formulation prepared by solubilization method were tested *in vivo*. MENK is an endogenous peptide and its basal level in plasma should be determined to quantify the MENK peptide in plasma following oral and IV administration.

EIA quantification of MENK spiked in plasma was challenging due to matrix effect (Figure 4-27). Quantification using LCMS-QQQ provided the suitable alternative for *in vivo* pharmacokinetic assay. LCMS-QQQ method is sensitive in detecting the concentration of MENK in plasma as low as 20 ng/mL. The concentration of endogenous MENK in plasma were below the LLOQ of MENK in plasma (20 ng/mL) by LCMS-QQQ (Figure 4-31). Only one in ten mice had MENK concentration of 22 ng/mL in plasma (Table 4-8). Endogenous MENK concentration reported in human as 8 pg/mL [262] and 19.64 ± 1.71 pg/mL [276]. Also concentration of endogenous MENK in nude mice was reported to be only 0.16 ± 0.03 ng/mL [277]. Several reports show quantification of MENK in plasma using radioimmunoassay (RIA) at pictogram levels [166, 278, 279]. However, there was also discrepancies MENK plasma level which was linked to differences in the RIA kit [278]. In order to achieve high sensitivity with LCMS-QQQ as that of RIA, the extraction protocol could be further optimized.

The OGF-OGFr regulation was observed to be an important determinant of pancreatic neoplasia [280]. In mice bearing pancreatic tumour xenografts the concentration of OGFr remains stable irrespective of the size and stage of tumour progression. The plasma level of OGF was observed to be 3.4 to 7.9 folds less

(~ 50 pg/mL) for nude mice bearing pancreatic tumour xenograft compared to nude mice with no tumour (~ 250 pg/mL) [278]. This suggests that MENK is down regulated in the presence of tumour. The application of exogeneous MENK was necessary for tumour growth suppression.

GCPQ improved the solubility of MENK by 3 folds for MENK-GCPQ IV formulation (15 mg/kg) and 10 folds for MENK-GCPQ oral formulation (50 mg/kg). Thus, by increasing the dose, frequency of administration was also reduced to once in two days. Previously administered MENK formulations were intravenously administered at a concentration of 5 mg/kg (thrice daily), which was three folds lower than the single dose of MENK-GCPQ formulation [166].

In vivo pharmacokinetic data for MENK-GCPQ IV formulation shows significant concentrations in plasma compared to control. The concentrations of MENK observed in plasma were at nanogram levels compared to previous pharmacokinetic data of MENK that were only in picogram level [166]. It was also observed that the concentration of MENK in plasma (Figure 4-32) for the respective formulation was 3727 ng/mL at time 0 and dropped by 100 folds (298 ng/mL) within 15 min and only a fraction of MENK concentration was stable in plasma up to 3 h (170 ng/mL). As a result, it can be concluded that the above fractions were encapsulated in GCPQ while the remaining were non-encapsulated. This is plausible as the half-life of MENK is only 4-7.5 min in mouse. The half-life of MENK in plasma is different for different organism. Studies of the *in vitro* plasma degradation of methionine enkephalin for human, mouse and rat are 10-15 min [264], 4 – 7.5 min [281], [282] and 2-4 sec [283] respectively. Studies conducted in SD rats also shows that, thirty sec after injection, the apparent volume of distribution and metabolic clearance rate of peptide were 53 mL and 10 mL/min respectively [283]. So, any un-encapsulated MENK in plasma would have been degraded or rapidly distributed or eliminated. The bio distribution of MENK and MENK-GCPQ nanoparticle in mice could be studied in the future.

Pharmacodynamics study of MENK GCPQ formulation suggested that the mean survival time of MENK-GCPQ and MENK IV formulations (39 days) were higher than that of control (29 days) (Figure 4-35). This suggests that with the concentration of MENK achieved in plasma for MENK-GCPQ B1 IV formulation (Figure 4-32), it is possible to achieve significant tumour regression compared to control (Figure 4-34). However no significant differences in tumour volume and

mean survival time were observed between MENK and MENK-GCPQ B1 IV formulations (Figure 4-34). This suggests that, though MENK level in plasma was achieved at nanogram concentration using MENK-GCPQ B1 formulation, this concentration was not sufficient enough to cause significant therapeutic effect compared to MENK formulation. It was observed previously that the concentration of MENK in plasma after intravenous administration of MENK (5mg/kg) thrice daily was in picogram level (84 pg/mL). However, this concentration was sufficient to cause tumor suppression in 62% of mice treated with MENK formulation [166]. Hence, it could be possible that with respect to MENK-GCPQ IV formulation, the OGFr was saturated by MENK and excessive concentration of MENK in plasma would have been cleared from the blood. The binding affinity of OGFr was 1.5 nM and the binding capacity of OGFr was around 20 fmol/mg of protein [278]. The binding affinity and binding capacity of OGFr in MiaPaCa-2 were not influenced by size and state of tumour differentiation [278]. It was also observed that following intravenous administration of MENK, the binding capacity of OGFr were reduced by 58% compared to control in mice bearing BxPC-3 cells [166]. Hence other routes of administration that releases MENK slowly in to the systemic circulation is preferred over intravenous administration.

The above results were contradictory to *in vitro* results on the encapsulation efficiency of MENK-GCPQ formulation suggesting that 93% of MENK was encapsulated in GCPQ (Figure 4-12). Since there were no correlations between in vitro and in vivo result, an alternative approach using size exclusion chromatography was used to determine the encapsulation efficiency of MENK GCPQ B2 nanoparticle. It was expected that free MENK and MENK encapsulated GCPQ B2 elute as different peaks. However, for MENK and MENK GCPQ B2 formulation, MENK peak eluted at the same time (Figure 4-13). Free MENK behaving as nanoparticle could be the reason for discrepancy in the result. The actual encapsulation efficiency of MENK-GCPQ B2 formulation could not be confirmed by either method.

The pilot studies were conducted to measure the concentration of MENK following oral administration of MENK-GCPQ B2 formulation. Pharmacokinetics of MENK GCPQ B2 oral formulation did show measurable concentration of MENK in plasma. However there was variability in MENK plasma concentrations between the mice. The results suggest that only three out of five mice had concentrations of

MENK in plasma around 724 ng/mL, 75 ng/mL and 23 ng/mL at 60 min time point. At other time points, (120 and 240 min) only one in five mice had concentrations of 52 and 91 ng/mL respectively (Figure 4-34). These variations could have resulted from differences in MENK-GCPQ B2 nanoparticle absorption across the enterocytes. However, in mice administered with MENK alone, no concentrations were detected in plasma.

Pharmacodynamics of MENK-GCPQ B2 oral formulation shows encouraging results. Tumor regression data shows significant therapeutic effect for MENK-GCPQ B2 oral formulation over MENK only formulation (day 14 and 16) and control (day 14 to 23) ((Figure 4-36). The mean survival time also was higher for MENK GCPQ B2 oral formulation (39 days) compared to MENK (35 days) and control (29 days) (Figure 4-37).

The MENK-GCPQ B2 formulation did not offer stability against SIF with pancreatin *in vitro*. However, the pharmacodynamic and pharmacokinetics results for the same formulation were encouraging. It could be possible that the MENK-GCPQ B2 formulation *in vivo* adheres to the mucus membrane thereby reducing the particle exposure to intestinal enzymes. Also, it was previously reported that GCPQ interacts with bile components and recirculate between liver and small intestine [160]. This explains the discrepancies between *in vitro* and *in vivo* results.

The therapeutic effect of MENK-GCPQ B2 oral formulation was promising although there was variability in the concentration of MENK detected in plasma. It should also be noted that in the previous studies, MENK level in tumour were 24 fold greater in MENK treated mice than control. However for the same treatment, the plasma MENK level were 8.6 fold lower than control [166]. For the current study, therapeutic effect was achieved for MENK GCPQ B2 oral formulation, although, significant MENK concentrations were not observed in mice plasma. The MENK level in tumor after oral administration of MENK-GCPQ B2 should be carried out and compared against the MENK formulation in the future studies.

In the above studies, only GCPQ B1 and B2 were studied. It would be interesting to know if GCPQ B3 will show improved uptake of MENK peptide as seen with Laby peptide.

4.6 Summary and future work

In this study, therapeutic effect of methionine enkephalin in mice bearing Mia-Pa-Ca-2 tumour xenograft was achieved following oral administration of MENK GCPQ B2 nanoparticles. With MENK-GCPQ B2 nanoparticle, a single daily oral dose of 50 mg/kg was sufficient to achieve therapeutic effect compared to standard therapy, which requires MENK administration at a dose of 5 mg/kg three times daily. We have also achieved significant MENK level in plasma up to 3 h following IV administration of MENK-GCPQ B1 nanoparticle. These results are encouraging, while taking in to account of its half-life, which is 4 to 7.5 min in mouse. Further, we have reported for the first time that, MENK self assembles to form nanoparticles and the challenges that it presents in forming nanoparticles with GCPQ. In future, it is necessary to understand what percentages of MENK are encapsulated in GCPQ B2 nanoparticles and what is the fate of MENK-GCPQ nanoparticle following oral administration. The pharmacokinetics of MENK-GCPQ B2 oral formulation could be studied in rats by collecting plasma aliquots for all time points from single rat. So, the variability in using individual mice for each time point can be minimized. It was not possible to relate the MENK plasma level to tumour growth suppression. The MENK basal level in plasma is subjective to change in the presence or absence of tumour xenograft and with or without treatment. Hence, it is important to measure MENK level in tumours following oral administration of MENK-GCPQ B2 formulation. It was previously reported that the combined effect of gemcitabine and MENK enhanced growth inhibition of MiaPaCa-2 transplanted in to athymic mice [167]. So, it would be interesting to study the combined effect of MENK-GCPQ nanoparticles and gemcitabine on MiaPaCa-2 cells.

5 Conclusion

5.1 Polymer architecture

Quaternary ammonium palmitoyl glycol chitosan (GCPQ) has been reported to solubilize hydrophobic drugs and peptide and thereby enhancing their oral bioavailability. GCPQ is an amphiphilic polymer that includes glycol chitosan backbone, hydrophobic palmitoyl group and hydrophilic quaternary ammonium group. GCPQ polymer of three different batches were synthesized and characterized. The molecular weight (Mn) of the different batches 1, 2 and 3 of GCPQ polymers were around 8 KDa, 13 kDa and 33 KDa. The first two batches were synthesized by old method of GCPQ synthesis as per protocol previously described by Qu et al [127]. The major disadvantage of this method is that the rate of palmitoylation reaction cannot be controlled, as the palmitoylation reactions are setup where degraded glycol chitosan and palmitic acid N hydroxysuccinimide were added as weight ratios. However, a new method of GCPQ synthesis was adopted to control the palmitoylation reaction. Here, the reactants, degraded glycol chitosan and palmitic acid N hydroxysuccinimide were used as molar ratio to get expected degree of palmitoylation. The molecular weight of GCPQ B3 polymer was observed to be higher than the molecular weight of GCPQ B1 and B2. This could be due to the hydrophobic characteristics of the polymer itself, which could have resulted from differences in the attachment of palmitoyl chain to the GC backbone between two methods of synthesis. It was hypothesized that the polymer forms intra-molecular associaton in GPC mobile phase (65:35 of methanol and acetate buffer). Increase in the composition of methanol in mobile could dissolve GCPQ B3. This could be confirmed in the future studies.

5.2 Amphiphilic characteristics of GCPQ polymer

The degree of palmitoylation and degree of quaternization for different batches of GCPQ varied with low palmitoylation (16%) and high quaternization (14%) for GCPQ B1, high palmitoylation (19%) and high quaternization (12%) for GCPQ B2 and high palmitoylation (22%) and low quaternization (8%) for GCPQ B3. The peptides were formulated with GCPQ of different batches and their *in vitro* and *in vivo* characteristics were compared. The present study shows that these characteristics had been observed to have an influence on the nature of the polymer

itself, their formulation with the peptide, *in vitro* colloidal stability and in vivo oral absorption across the enterocytes.

5.3 Characterization of GCPQ nanoparticles

Particle sizes

GCPQ B2 in water forms nanoparticles of size as large as 400 nm with a PDI greater than 0.8. However, addition of sodium chloride solution to GCPQ B2 of increasing molarity (10mM to 300mM) reduces the particle sizes to 150 nm. These results are contradictory to previous studies where the introduction of salts in the nanoparticle formulations modifies the surface charge of the particles. This results in particle aggregation due to decrease in the electrostatic repulsion between particles. Future studies need to be conducted in order to understand the interaction of salt with GCPQ nanoparticles. Probe sonication of GCPQ B2 at 15 amps for 15 min resulted in the formation of GCPQ B2 micelles of size around 20 nm and PDI 0.2 as observed with TEM and DLS. It was also observed that the probe sonication did not have any effect on the molecular weight of the GCPQ B2 polymer as characterized by GPC-MALLS.

Surface charge GCPQ micelles

The surface charge of GCPQ micelles gives information on the colloidal stability of the polymer at different pH. GCPQ has exceptional colloidal stability due to presence of quaternary ammonium group. An example of how the surface charge of GCPQ changes with different pH was recorded with GCPQ B2 having quaternization of 12%. The primary amines and the secondary amines of the GCPQ polymer remains protonated at acidic pH and hence most positive zeta potential was observed (+50.4 mV). An increase in the pH of the GCPQ B2 formulation causes deprotonation of amines at alkaline pH. This can cause aggregation of the polymer. However, due to the presence of quaternary ammonium group the formulation remains positively charged (+ 15mV) at pH as high as 9. It could be interesting to know the effect of degree of quaternization on the colloidal stability of GCPQ B2 at different pH in future studies.

Colloidal stability of GCPQ micelles in simulated gastric medium and intestinal medium

Characterization of surface charge of GCPQ B2 at different pH suggests that the colloidal stability of the GCPQ B2 polymer is pH dependent. The GCPQ B2

stock solution (25 mg/mL) was diluted 10 times in SGF and SIF fluid to final concentration of 2.5 mg/mL The dilution does not affect the colloidal stability of GCPQ B2 micelles as it known from previous studies that the CMC of GCPQ B2 micelles was only 19uM [134]. The colloidal stability was carried out to understand how does the composition of SIF or SGF fluid such as the presence of bile salts and or proteins affect the colloidal stability of GCPQ B2 in simulated gastro intestinal medium. This study helps to predict how the GCPQ B2 micelles behave in vivo after its oral administration. GCPQ B2 micellar aggregation was found to be increasing with time in fed state intestinal fluid and to a lesser extend in fasted state intestinal fluid. This shows that presence of pancreatin and oleates in fed state intestinal fluid can induce the aggregation of GCPQ B2 micelles at a faster rate compared to fasted simulated intestinal fluids. It was also observed from the number based distribution that only a fraction of GCPQ B2 (1%) aggregates resulting increased PDI and Z-average results. This results confirm the previous observation of GCPQ B2 interacting with the bile components and recirculate between liver and small intestine [160].

5.4 Peptide GCPQ nanoparticles

MENK is an anti cancer peptide of molecular weight 573 Da having poor stability in the gastrointestinal tract. The peptide requires repeated IV administration due to its anti-proliferative effect on cancer cells. Since repeated IV administration of peptide could be non-compliance to patient, an alternative non-invasive approach such as oral administration is preferred.

Labyrinthopeptin is an anti-nociceptive peptide with molecular weight 1923 Da has poor solubility in sodium chloride solution (0.9 mg/mL). The peptide has poor oral bioavailability, which sets its limitation for using it for chronic treatment.

Both the peptides of different physiochemical properties were formulated with different batches of GCPQ and the results were compared.

Influence of GCPQ polymer characteristics on GCPQ peptide formulation

Characterization of Laby GCPQ B2 formulation suggests that ratio of peptide to polymer used has effect on particle formulation. The minimum GCPQ required to formulation Laby GCPQ B2 formulation was optimized to be 1:3 which was lower than previously made peptide GCPQ formulation prepared at ratio 1:5.

The degree of palmitoylation of GCPQ (B1 & B2) polymer also affects the size of the particles formed with polymer having low palmitoylation of 16% formed large particles around 500 nm and polymer having high palmitoylation of 19% formed particles as small as 20 nm. This observation was consistent with both Laby GCPQ (B1 & B2) as well as MENK GCPQ (B1 & B2) formulation. Any increase in the palmitoylation percent (22%) causes further increase in the size of the Laby GCPQ B3 formulation to 84 nm.

The encapsulation efficiency of the Laby GCPQ (B1, B2 and B3) formulation were around 89%. It was not possible to conclude the encapsulation efficiency of MENK-GCPQ formulations as MENK itself forms aggregates with a CMC of 0.320 mM. Alternative methods of determining the encapsulation efficiency of the MENK in GCPQ formulation could be studied in the future.

Influence of GCPQ polymer characteristics on the colloidal stability of peptide GCPQ formulation

The ratio of palmitoyltion and quaternization did influence the colloidal stability of Laby GCPQ formulation. High palmitoylation (22%) and low quaternization (8%) GCPQ B3 affected the colloidal stability of Laby GCPQ B3 formulation in SIF and HBSS by forming aggregates. Whereas, Laby GCPQ formulation made with low palmitoylation (16%) and high quaternization (14%) of GCPQ B1 and high palmitoylation (19%) and high quaternization (12%) of GCPQ B2 were observed to be colloidally stable.

The proteolytic stability of MENK-GCPQ B2 formulation in SIF with pancreatin was characterized *in vitro*. The MENK-GCPQ B2 (P-19% and Q-12%) particles were not observed to be stable in SIF with pancreatin. GCPQ nanoparticles has been reported to interact with the bile components and recirculate between liver and small intestine. The constituents of *in vitro* SIF medium did differ from *in vivo* conditions, as under *in vitro* condition only the effect of pH and stability against pancreatin were studied. However, in vivo, digestive juice is composed of bile secretions, pancreatic juices that could interact with MENK-GCPQ B2 formulation before adhering to the mucus membrane.

Influence of GCPQ polymer characteristics on the oral uptake of peptide GCPQ formulation

Therapeutic effect of Laby GCPQ B2 and MENK GCPQ B2 oral formulation having palmitoylation and quaternization of 19% and 12% was tested *in vivo*. Results

suggest that for Laby GCPQ B2 oral formulation, Laby GCPQ B2 nasal formulation and MENK GCPQ B2 oral formulation significant therapeutic effects was achieved against their respective peptide alone formulation.

The concentration of MENK level in plasma for MENK-GCPQ B1 IV formulation was higher than MENK only formulation. However, no significant therapeutic effect was observed for MENK-GCPQ IV formulation against MENK only formulation. This could be due to saturation of OGFr receptor at a very low concentration and the excess MENK was cleared from the blood.

The pharmacokinetics of Laby GCPQ oral formulation prepared with GCPQ B1 P16% and Q14% resulted in poor concentration of the peptide in the blood. This result suggests that the ratio of palmitoylation and quaternization used could change the absorption of particles across the enterocytes. From the results observed with both the peptides a hypothesis could be formulated.

High quaternization of GCPQ B1 polymer carrying large positive charge could have interacted with mucin polymer and the excess positive charge on the GCPQ B1 (Q-14%) nanoparticle resulted in electrostatic repulsion leading to detangling of the mucus layer. This could be the reason for poor concentration of the peptide in plasma for Laby GCPQ B1 formulation made with GCPQ B1 having P16% and Q14%.

Also Laby GCPQ B3 formulation was observed to show high concentration of Laby in plasma after oral and nasal administration. The effect of GCPQ B3 hydrophobicity with palmitoylation of 22% on uptake across the enterocytes could be studied in the future. The *in vivo* results clearly shows that a balance between palmitoylation and quaternization of GCPQ is necessary to control oral absorption of the peptides.

6 References

1. *Cost to Develop and Win Marketing Approval for a New Drug Is $2.6 Billion*. 2014; Available from: http://csdd.tufts.edu/news/complete_story/pr_tufts_csdd_2014_cost_study.
2. *Novel Drug Summary 2015*. 2016 [cited 2016; Available from: http://www.fda.gov/Drugs/DevelopmentApprovalProcess/DrugInnovation/ucm474696.htm.
3. James R. Empfield, M.P.C., *Reducing drug attrition*. 2014: Springer.
4. Foundation, P.T., *Development Trends for Peptide Therapeutics: A Comprehensive Quantitative Analysis of Peptide Therapeutics in Clinical Development*. 2010: Peptide Therapeutics Foundation.
5. Kaspar, A.A. and J.M. Reichert, *Future directions for peptide therapeutics development.* Drug Discov Today, 2013. **18**(17-18): p. 807-17.
6. *Peptide Therapeutics Market (by Applications, by Route of Administration, and by Marketing Status) - Global Industry Analysis, Size, Share, Growth, Trends and Forecast 2014 - 2020*. 2015; Available from: http://www.transparencymarketresearch.com/peptide-therapeutics-market.html.
7. *Peptide Therapeutics Market (by Applications, by Route of Administration, and by Marketing Status) - Global Industry Analysis, Size, Share, Growth, Trends and Forecast 2014 - 2020*. 2015, Transparency Market Research.
8. Marimuthu, P. and A.G. Schätzlein, *Biological Barriers: Transdermal, Oral, Mucosal, Blood Brain Barrier, and the Blood Eye Barrier*, in *Fundamentals of Pharmaceutical Nanoscience*, F.I. Uchegbu, et al., Editors. 2013, Springer New York: New York, NY. p. 301-336.
9. Collins, L.M. and C. Dawes, *The surface area of the adult human mouth and thickness of the salivary film covering the teeth and oral mucosa.* J Dent Res, 1987. **66**(8): p. 1300-2.
10. Rathbone, J.M., I. Pather, and S. Şenel, *Overview of Oral Mucosal Delivery*, in *Oral Mucosal Drug Delivery and Therapy*, J.M. Rathbone, S. Senel, and I. Pather, Editors. 2015, Springer US: Boston, MA. p. 17-29.
11. Soybel, D.I., *Anatomy and physiology of the stomach.* Surg Clin North Am, 2005. **85**(5): p. 875-94, v.
12. Jain, R.N. and L.C. Samuelson, *Differentiation of the gastric mucosa. II. Role of gastrin in gastric epithelial cell proliferation and maturation.* Am J Physiol Gastrointest Liver Physiol, 2006. **291**(5): p. G762-5.
13. Engel, E., et al., *Barrier function of the gastric mucus gel.* Am J Physiol, 1995. **269**(6 Pt 1): p. G994-9.
14. Delgado-Aros, S., et al., *Effect of GLP-1 on gastric volume, emptying, maximum volume ingested, and postprandial symptoms in humans.* Am J Physiol Gastrointest Liver Physiol, 2002. **282**(3): p. G424-31.
15. Seeley, R.R., Stephens, T.D., Tate P.,, *Anatomy and Physiology*. 6 ed. 2003: McGraw-Hill.
16. Sherwood, L., *Fundamentals of Human Physiology*. 4th ed. 2012: Cengage Learning.
17. Guyton, J.R. and A.C. Goldberg, *CHAPTER 23 - Bile Acid Sequestrants A2 - Ballantyne, Christie M*, in *Clinical Lipidology*. 2009, W.B. Saunders: Philadelphia. p. 281-287.
18. *Servier medical art*. 2013; Available from: http://www.servier.com/Powerpoint-image-bank.

19. Gravitz, L., *Microbiome: The critters within.* Nature, 2012. **485**(7398): p. S12-3.
20. Florence TA., A.D., *Physiochemical principles of pharmacy*. 4th ed. 2006, London: Pharmaceutical Press.
21. Sangster, J., *Octanol-Water Partition Coefficients: Fundamentals and Physical Chemistry*. 1st ed. 1997, Chichester, UK John Wiley & Sons Ltd., .
22. Lipinski, C.A., et al., *Experimental and computational approaches to estimate solubility and permeability in drug discovery and development settings.* Adv Drug Deliv Rev, 2001. **46**(1-3): p. 3-26.
23. Ramasubbu, N., et al., *Structure of human salivary alpha-amylase at 1.6 A resolution: implications for its role in the oral cavity.* Acta Crystallogr D Biol Crystallogr, 1996. **52**(Pt 3): p. 435-46.
24. Code CF, H.W., *Physiology-Alimentary Canal*. Biochemistry of the pepsins., ed. T. WH. 1968, Baltimore: Williams & Wilkins.
25. Beck, I.T., *The role of pancreatic enzymes in digestion.* Am J Clin Nutr, 1973. **26**(3): p. 311-25.
26. Whitcomb, D.C. and M.E. Lowe, *Human pancreatic digestive enzymes.* Dig Dis Sci, 2007. **52**(1): p. 1-17.
27. Wieland, T. and H. Faulstich, *Amatoxins, phallotoxins, phallolysin, and antamanide: the biologically active components of poisonous Amanita mushrooms.* CRC Crit Rev Biochem, 1978. **5**(3): p. 185-260.
28. Bauer, W., et al., *SMS 201-995: a very potent and selective octapeptide analogue of somatostatin with prolonged action.* Life Sci, 1982. **31**(11): p. 1133-40.
29. Lundin, S. and H. Vilhardt, *Absorption of 1-deamino-8-D-arginine vasopressin from different regions of the gastrointestinal tract in rabbits.* Acta Endocrinol (Copenh), 1986. **112**(3): p. 457-60.
30. Webber, I.R., W.H. Peters, and D.J. Back, *Cyclosporin metabolism by human gastrointestinal mucosal microsomes.* Br J Clin Pharmacol, 1992. **33**(6): p. 661-4.
31. Bernkop-Schnurch, A., *Oral Delivery of Macromolecular Drugs- Barriers, strategies and Future Trends*. 2009: Springer.
32. Cone, R.A., *Barrier properties of mucus.* Adv Drug Deliv Rev, 2009. **61**(2): p. 75-85.
33. Atuma, C., et al., *The adherent gastrointestinal mucus gel layer: thickness and physical state in vivo.* American Journal of Physiology - Gastrointestinal and Liver Physiology, 2001. **280**(5): p. G922-G929.
34. Szentkuti, L. and K. Lorenz, *The thickness of the mucus layer in different segments of the rat intestine.* Histochem J, 1995. **27**(6): p. 466-72.
35. Strugala, V., et al., *Colonic mucin: methods of measuring mucus thickness.* Proc Nutr Soc, 2003. **62**(1): p. 237-43.
36. Lai, S.K., et al., *Micro- and macrorheology of mucus.* Adv Drug Deliv Rev, 2009. **61**(2): p. 86-100.
37. Witas, H., et al., *Lipids associated with rat small-intestinal mucus glycoprotein.* Carbohydr Res, 1983. **120**: p. 67-76.
38. Khanvilkar, K., M.D. Donovan, and D.R. Flanagan, *Drug transfer through mucus.* Adv Drug Deliv Rev, 2001. **48**(2-3): p. 173-93.
39. DeSesso, J.M. and C.F. Jacobson, *Anatomical and physiological parameters affecting gastrointestinal absorption in humans and rats.* Food Chem Toxicol, 2001. **39**(3): p. 209-28.

40. Lennernas, H., *Does fluid flow across the intestinal mucosa affect quantitative oral drug absorption? Is it time for a reevaluation?* Pharm Res, 1995. **12**(11): p. 1573-82.
41. Karlsson, J., et al., *Paracellular drug transport across intestinal epithelia: influence of charge and induced water flux.* Eur J Pharm Sci, 1999. **9**(1): p. 47-56.
42. Avdeef, A., *Physiochemical profiling (solubility, permeability and charge state).* Curr.Top.Med.Chem, 2001. **1**(4): p. 277-351.
43. Lipinski, C.A., *Drug-like properties and teh causes of poor solubility and poor permeability.* J. Pharmacol.Tox.Methods, 2000. **44**(1): p. 235-249.
44. Herrera-Ruiz, D., et al., *Spatial expression patterns of peptide transporters in the human and rat gastrointestinal tracts, Caco-2 in vitro cell culture model, and multiple human tissues.* AAPS PharmSci, 2001. **3**(1): p. E9.
45. Irie, M., et al., *Computational modelling of H+-coupled peptide transport via human PEPT1.* J Physiol, 2005. **565**(Pt 2): p. 429-39.
46. Mizuno, N., et al., *Impact of drug transporter studies on drug discovery and development.* Pharmacol Rev, 2003. **55**(3): p. 425-61.
47. Jansen, P.L., et al., *Preserved organic anion transport in mutant TR- rats with a hepatobiliary secretion defect.* Am J Physiol, 1993. **265**(3 Pt 1): p. G445-52.
48. Doyle, L. and D.D. Ross, *Multidrug resistance mediated by the breast cancer resistance protein BCRP (ABCG2).* Oncogene, 2003. **22**(47): p. 7340-58.
49. Varma, M.V., O.P. Perumal, and R. Panchagnula, *Functional role of P-glycoprotein in limiting peroral drug absorption: optimizing drug delivery.* Curr Opin Chem Biol, 2006. **10**(4): p. 367-73.
50. Werle, M., *Natural and synthetic polymers as inhibitors of drug efflux pumps.* Pharm Res, 2008. **25**(3): p. 500-11.
51. Kararli, T.T., *Comparison of the gastrointestinal anatomy, physiology, and biochemistry of humans and commonly used laboratory animals.* Biopharm Drug Dispos, 1995. **16**(5): p. 351-80.
52. Iwanaga, K., et al., *Oral delivery of insulin by using surface coating liposomes: Improvement of stability of insulin in GI tract.* International Journal of Pharmaceutics, 1997. **157**(1): p. 73-80.
53. Lalatsa, A., et al., *A prodrug nanoparticle approach for the oral delivery of a hydrophilic peptide, leucine(5)-enkephalin, to the brain.* Mol Pharm, 2012. **9**(6): p. 1665-80.
54. Leone-Bay, A., et al., *N-acylated alpha-amino acids as novel oral delivery agents for proteins.* J Med Chem, 1995. **38**(21): p. 4263-9.
55. Ferdinandi, E.S., et al., *Non-clinical pharmacology and safety evaluation of TH9507, a human growth hormone-releasing factor analogue.* Basic Clin Pharmacol Toxicol, 2007. **100**(1): p. 49-58.
56. Sharman A, L.J., *Vasopressin and its role in critical care.* Contin Educ Anaesth, Crit Care Pain, 2008. **8**(4): p. 134-7.
57. Agerso, H., et al., *Pharmacokinetics and renal excretion of desmopressin after intravenous administration to healthy subjects and renally impaired patients.* Br J Clin Pharmacol, 2004. **58**(4): p. 352-8.
58. Raun, K., et al., *Ipamorelin, the first selective growth hormone secretagogue.* Eur J Endocrinol, 1998. **139**(5): p. 552-61.

59. Gobburu, J.V., et al., *Pharmacokinetic-pharmacodynamic modeling of ipamorelin, a growth hormone releasing peptide, in human volunteers.* Pharm Res, 1999. **16**(9): p. 1412-6.
60. Grigoryev, Y., *Stapled peptide to enter human testing, but affinity questions remain.* Nat Med, 2013. **19**(2): p. 120.
61. Olson, K.A., et al., *Long-acting GHRH Analog ALRN-5281, the First Stapled Peptide Clinical Candidate, Exhibits Robust In Vitro and In Vivo Activation of the Growth Hormone Pathway*, in *GHRH, GH & IGF Biology & Signaling*. p. SAT-111-SAT-111.
62. Malm-Erjefalt, M., et al., *Metabolism and excretion of the once-daily human glucagon-like peptide-1 analog liraglutide in healthy male subjects and its in vitro degradation by dipeptidyl peptidase IV and neutral endopeptidase.* Drug Metab Dispos, 2010. **38**(11): p. 1944-53.
63. Fujii, S., et al., *Promoting effect of the new chymotrypsin inhibitor FK-448 on the intestinal absorption of insulin in rats and dogs.* J Pharm Pharmacol, 1985. **37**(8): p. 545-9.
64. Ziv, E., O. Lior, and M. Kidron, *Absorption of protein via the intestinal wall. A quantitative model.* Biochem Pharmacol, 1987. **36**(7): p. 1035-9.
65. Uchiyama, T., et al., *Effects of various protease inhibitors on the stability and permeability of [D-Ala2,D-Leu5]enkephalin in the rat intestine: comparison with leucine enkephalin.* J Pharm Sci, 1998. **87**(4): p. 448-52.
66. Hickey, R.J., *Bacitracin, its manufacture and uses.* Prog Ind Microbiol, 1964. **5**: p. 93-150.
67. Bernkop-Schnurch, A., *The use of inhibitory agents to overcome the enzymatic barrier to perorally administered therapeutic peptides and proteins.* J Control Release, 1998. **52**(1-2): p. 1-16.
68. Bernkop-Schnurch, A. and M.K. Marschutz, *Development and in vitro evaluation of systems to protect peptide drugs from aminopeptidase N.* Pharm Res, 1997. **14**(2): p. 181-5.
69. Chao, A.C., et al., *In vitro and in vivo evaluation of effects of sodium caprate on enteral peptide absorption and on mucosal morphology.* Int J Pharm, 1999. **191**(1): p. 15-24.
70. Chao, A.C., et al., *Enhancement of intestinal model compound transport by DS-1, a modified Quillaja saponin.* J Pharm Sci, 1998. **87**(11): p. 1395-9.
71. Constantinides, P.P., et al., *Water-in-oil microemulsions containing medium-chain fatty acids/salts: formulation and intestinal absorption enhancement evaluation.* Pharm Res, 1996. **13**(2): p. 210-5.
72. Maxson, W.S., J.T. Hargrove, and P.G. Meyers, *Pharmaceutical composition containing progesterone*. 1991, Google Patents.
73. Fasano, A. and S. Uzzau, *Modulation of intestinal tight junctions by Zonula occludens toxin permits enteral administration of insulin and other macromolecules in an animal model.* J Clin Invest, 1997. **99**(6): p. 1158-64.
74. Liang, J.F. and V.C. Yang, *Insulin-cell penetrating peptide hybrids with improved intestinal absorption efficiency.* Biochem Biophys Res Commun, 2005. **335**(3): p. 734-8.
75. Dawes, G.J., et al., *Size effect of PLGA spheres on drug loading efficiency and release profiles.* J Mater Sci Mater Med, 2009. **20**(5): p. 1089-94.
76. Maeda, H., G.Y. Bharate, and J. Daruwalla, *Polymeric drugs for efficient tumor-targeted drug delivery based on EPR-effect.* Eur J Pharm Biopharm, 2009. **71**(3): p. 409-19.

77. Caldorera-Moore, M., et al., *Designer nanoparticles: incorporating size, shape and triggered release into nanoscale drug carriers.* Expert Opin Drug Deliv, 2010. **7**(4): p. 479-95.
78. Cui, F.D., et al., *Preparation of insulin loaded PLGA-Hp55 nanoparticles for oral delivery.* J Pharm Sci, 2007. **96**(2): p. 421-7.
79. Reis, C.P., et al., *Polyelectrolyte biomaterial interactions provide nanoparticulate carrier for oral insulin delivery.* Drug Deliv, 2008. **15**(2): p. 127-39.
80. Damge, C., P. Maincent, and N. Ubrich, *Oral delivery of insulin associated to polymeric nanoparticles in diabetic rats.* J Control Release, 2007. **117**(2): p. 163-70.
81. Damge, C., et al., *Poly(epsilon-caprolactone)/eudragit nanoparticles for oral delivery of aspart-insulin in the treatment of diabetes.* J Pharm Sci, 2010. **99**(2): p. 879-89.
82. Clardy-James, S., et al., *Examining the effects of vitamin B12 conjugation on the biological activity of insulin: a molecular dynamic and in vivo oral uptake investigation.* MedChemComm, 2012. **3**(9): p. 1054-1058.
83. Bernkop-Schnurch, A. and M.E. Krajicek, *Mucoadhesive polymers as platforms for peroral peptide delivery and absorption: synthesis and evaluation of different chitosan-EDTA conjugates.* J Control Release, 1998. **50**(1-3): p. 215-23.
84. Roldo, M., et al., *Mucoadhesive thiolated chitosans as platforms for oral controlled drug delivery: synthesis and in vitro evaluation.* Eur J Pharm Biopharm, 2004. **57**(1): p. 115-21.
85. Hussain, N., P.U. Jani, and A.T. Florence, *Enhanced oral uptake of tomato lectin-conjugated nanoparticles in the rat.* Pharm Res, 1997. **14**(5): p. 613-8.
86. Peppas, N.A. and J.J. Sahlin, *Hydrogels as mucoadhesive and bioadhesive materials: a review.* Biomaterials, 1996. **17**(16): p. 1553-1561.
87. Gu, J.M., J.R. Robinson, and S.H. Leung, *Binding of acrylic polymers to mucin/epithelial surfaces: structure-property relationships.* Crit Rev Ther Drug Carrier Syst, 1988. **5**(1): p. 21-67.
88. Woodley, J., *Bioadhesion: new possibilities for drug administration?* Clin Pharmacokinet, 2001. **40**(2): p. 77-84.
89. Eiamtrakarn, S., et al., *Gastrointestinal mucoadhesive patch system (GI-MAPS) for oral administration of G-CSF, a model protein.* Biomaterials, 2002. **23**(1): p. 145-52.
90. Childers, N.K., et al., *Ultrastructural study of liposome uptake by M cells of rat Peyer's patch: an oral vaccine system for delivery of purified antigen.* Reg Immunol, 1990. **3**(1): p. 8-16.
91. Peppas, N.A., K.M. Wood, and J.O. Blanchette, *Hydrogels for oral delivery of therapeutic proteins.* Expert Opin Biol Ther, 2004. **4**(6): p. 881-7.
92. Jin, Y., et al., *Goblet cell-targeting nanoparticles for oral insulin delivery and the influence of mucus on insulin transport.* Biomaterials, 2012. **33**(5): p. 1573-82.
93. Kang, S.K., et al., *Identification of a peptide sequence that improves transport of macromolecules across the intestinal mucosal barrier targeting goblet cells.* J Biotechnol, 2008. **135**(2): p. 210-6.
94. Fan, T., et al., *Design and evaluation of solid lipid nanoparticles modified with peptide ligand for oral delivery of protein drugs.* Eur J Pharm Biopharm, 2014. **88**(2): p. 518-28.

95. Singh, B., et al., *Self-emulsifying drug delivery systems (SEDDS): formulation development, characterization, and applications.* Crit Rev Ther Drug Carrier Syst, 2009. **26**(5): p. 427-521.
96. Klyashchitsky, B.A. and A.J. Owen, *Drug delivery systems for cyclosporine: achievements and complications.* J Drug Target, 1998. **5**(6): p. 443-58.
97. Carino, G.P., J.S. Jacob, and E. Mathiowitz, *Nanosphere based oral insulin delivery.* J Control Release, 2000. **65**(1-2): p. 261-9.
98. Mathiowitz, E., et al., *Biologically erodable microspheres as potential oral drug delivery systems.* Nature, 1997. **386**(6623): p. 410-4.
99. Wu, Z.M., et al., *HP55-coated capsule containing PLGA/RS nanoparticles for oral delivery of insulin.* Int J Pharm, 2012. **425**(1-2): p. 1-8.
100. Chalasani, K.B., et al., *Effective oral delivery of insulin in animal models using vitamin B12-coated dextran nanoparticles.* J Control Release, 2007. **122**(2): p. 141-50.
101. Pridgen, E.M., et al., *Transepithelial transport of Fc-targeted nanoparticles by the neonatal fc receptor for oral delivery.* Sci Transl Med, 2013. **5**(213): p. 213ra167.
102. Hosseininasab, S., et al., *Synthesis, characterization, and in vitro studies of PLGA-PEG nanoparticles for oral insulin delivery.* Chem Biol Drug Des, 2014. **84**(3): p. 307-15.
103. Madsen, F. and N.A. Peppas, *Complexation graft copolymer networks: swelling properties, calcium binding and proteolytic enzyme inhibition.* Biomaterials, 1999. **20**(18): p. 1701-8.
104. Peppas, N., Lowman AM, *Protein delivery from novel bioadhesive complexation hydrogels*. Protein and peptide drug research, ed. C.L. Frokjaer S, Krogsgaard-Larsen P. 1998, Copenhagen: Munksgaard.
105. Ichikawa, H. and N.A. Peppas, *Novel complexation hydrogels for oral peptide delivery: in vitro evaluation of their cytocompatibility and insulin-transport enhancing effects using Caco-2 cell monolayers.* J Biomed Mater Res A, 2003. **67**(2): p. 609-17.
106. Iwanaga, K., et al., *Application of surface-coated liposomes for oral delivery of peptide: effects of coating the liposome's surface on the GI transit of insulin.* J Pharm Sci, 1999. **88**(2): p. 248-52.
107. Werle, M. and H. Takeuchi, *Chitosan-aprotinin coated liposomes for oral peptide delivery: Development, characterisation and in vivo evaluation.* Int J Pharm, 2009. **370**(1-2): p. 26-32.
108. Shah, N.M., et al., *Preparation, characterization and in vivo studies of proliposomes containing Cyclosporine A.* J Nanosci Nanotechnol, 2006. **6**(9-10): p. 2967-73.
109. Chen, C., et al., *Orally delivered salmon calcitonin-loaded solid lipid nanoparticles prepared by micelle-double emulsion method via the combined use of different solid lipids.* Nanomedicine (Lond), 2013. **8**(7): p. 1085-100.
110. Sarmento, B., et al., *Oral insulin delivery by means of solid lipid nanoparticles.* Int J Nanomedicine, 2007. **2**(4): p. 743-9.
111. Zhang, G., et al., *Oral delivery of oil-based formulation for a novel synthetic cationic peptide of GnRH (gonadotropin-releasing hormone) antagonist for prostate cancer treatment.* Int J Pharm, 2013. **450**(1-2): p. 138-44.
112. He, H., et al., *Overcoming oral insulin delivery barriers: application of cell penetrating peptide and silica-based nanoporous composites.* Frontiers of Chemical Science and Engineering, 2013. **7**(1): p. 9-19.

113. Whitehead, K., N. Karr, and S. Mitragotri, *Safe and effective permeation enhancers for oral drug delivery.* Pharm Res, 2008. **25**(8): p. 1782-8.
114. Khedkar, A., et al., *A dose range finding study of novel oral insulin (IN-105) under fed conditions in type 2 diabetes mellitus subjects.* Diabetes Obes Metab, 2010. **12**(8): p. 659-64.
115. *Biocon Announces Data from Key Studies for Insulin Tregopil*. 2016.
116. *Peptelligence*. enteris Biopharma 2013; Available from: http://enterisbiopharma.com/beta/technology-services/peptelligence/.
117. Binkley, N., et al., *A phase 3 trial of the efficacy and safety of oral recombinant calcitonin: the Oral Calcitonin in Postmenopausal Osteoporosis (ORACAL) trial.* J Bone Miner Res, 2012. **27**(8): p. 1821-9.
118. Therapeutics, T. *Tarsa Therapeutics' NDA for TBRIA(TM), the First Oral Calcitonin for the Treatment of Postmenopausal Osteoporosis, Accepted for Filing*. 2015; Available from: http://tarsatherapeutics.com/tarsa-therapeutics-nda-for-tbriatm-the-first-oral-calcitonin-for-the-treatment-of-postmenopausal-osteoporosis-accepted-for-filing/.
119. Chiasma, I., *Chiasma Reviews 2015 Accomplishments and Outlines Core Objectives for 2016*. 2016: Newton, Mass.,.
120. *Generex Oral - lynTM Delivered by Rapid - MistTM Spray System* 2015; Available from: http://www.generex.com/UserFiles/File/Generex Oral-lyn White Paper Aug 2015.pdf.
121. Bernstein, G. *Drug delivery in diabetes: oral-lyn needle-free buccal delivery of insulin.* 2006; Available from: http://www.ondrugdelivery.com/publications/diabetes.pdf.
122. *Axcess Oral Delivery System*. Available from: http://www.diabetology.co.uk/platforms.htm.
123. Luzio, S.D., et al., *The glucose lowering effect of an oral insulin (Capsulin) during an isoglycaemic clamp study in persons with type 2 diabetes.* Diabetes Obes Metab, 2010. **12**(1): p. 82-7.
124. Geho, W.B., et al., *Hepatic-directed vesicle insulin: a review of formulation development and preclinical evaluation.* J Diabetes Sci Technol, 2009. **3**(6): p. 1451-9.
125. Eldor, R., et al., *Glucose-reducing effect of the ORMD-0801 oral insulin preparation in patients with uncontrolled type 1 diabetes: a pilot study.* PLoS One, 2013. **8**(4): p. e59524.
126. Park, K., I.C. Kwon, and K. Park, *Oral protein delivery: Current status and future prospect.* Reactive and Functional Polymers, 2011. **71**(3): p. 280-287.
127. Uchegbu, I.F., et al., *Quaternary ammonium palmitoyl glycol chitosan--a new polysoap for drug delivery.* Int J Pharm, 2001. **224**(1-2): p. 185-99.
128. Jin, Q., S. Maji, and S. Agarwal, *Novel amphiphilic, biodegradable, biocompatible, cross-linkable copolymers: synthesis, characterization and drug delivery applications.* Polymer Chemistry, 2012. **3**(10): p. 2785-2793.
129. Chen, S., et al., *Functionalized amphiphilic hyperbranched polymers for targeted drug delivery.* Biomacromolecules, 2008. **9**(10): p. 2578-85.
130. Wang, W., et al., *Controls on Polymer Molecular Weight May Be Used To Control the Size of Palmitoyl Glycol Chitosan Polymeric Vesicles.* Langmuir, 2001. **17**(3): p. 631-636.
131. Song, X., et al., *PLGA nanoparticles simultaneously loaded with vincristine sulfate and verapamil hydrochloride: systematic study of particle size and drug entrapment efficiency.* Int J Pharm, 2008. **350**(1-2): p. 320-9.

132. Wang, W., L. Tetley, and I.F. Uchegbu, *The Level of Hydrophobic Substitution and the Molecular Weight of Amphiphilic Poly-L-lysine-Based Polymers Strongly Affects Their Assembly into Polymeric Bilayer Vesicles.* J Colloid Interface Sci, 2001. **237**(2): p. 200-207.
133. Wang, W., et al., *Self-Assembly of Cetyl Linear Polyethylenimine To Give Micelles, Vesicles, and Dense Nanoparticles.* Macromolecules, 2004. **37**(24): p. 9114-9122.
134. Qu, X., et al., *Carbohydrate-based micelle clusters which enhance hydrophobic drug bioavailability by up to 1 order of magnitude.* Biomacromolecules, 2006. **7**(12): p. 3452-9.
135. Thi Bich Le, H., A. G. Schatzlein, and I. F. Uchegbu, *Polymer Hydrophobicity Has a Positive Effect on the Oral Absorption of Cyclosporine A from Poly(ethylenimine) Based Nanomedicines.* Pharmaceutical Nanotechnology, 2013. **1**(1): p. 15-25.
136. Alexandridis, P., J.F. Holzwarth, and T.A. Hatton, *Micellization of Poly(ethylene oxide)-Poly(propylene oxide)-Poly(ethylene oxide) Triblock Copolymers in Aqueous Solutions: Thermodynamics of Copolymer Association.* Macromolecules, 1994. **27**(9): p. 2414-2425.
137. Win, K.Y. and S.S. Feng, *In vitro and in vivo studies on vitamin E TPGS-emulsified poly(D,L-lactic-co-glycolic acid) nanoparticles for paclitaxel formulation.* Biomaterials, 2006. **27**(10): p. 2285-91.
138. Dyer, A.M., et al., *Nasal delivery of insulin using novel chitosan based formulations: a comparative study in two animal models between simple chitosan formulations and chitosan nanoparticles.* Pharm Res, 2002. **19**(7): p. 998-1008.
139. Trapani, A., et al., *Systemic heparin delivery by the pulmonary route using chitosan and glycol chitosan nanoparticles.* Int J Pharm, 2013. **447**(1-2): p. 115-23.
140. Govender, T., et al., *PLGA nanoparticles prepared by nanoprecipitation: drug loading and release studies of a water soluble drug.* J Control Release, 1999. **57**(2): p. 171-85.
141. Chorny, M., et al., *Lipophilic drug loaded nanospheres prepared by nanoprecipitation: effect of formulation variables on size, drug recovery and release kinetics.* J Control Release, 2002. **83**(3): p. 389-400.
142. Hrkach, J., et al., *Preclinical development and clinical translation of a PSMA-targeted docetaxel nanoparticle with a differentiated pharmacological profile.* Sci Transl Med, 2012. **4**(128): p. 128ra39.
143. Hu, Q., et al., *F3 peptide-functionalized PEG-PLA nanoparticles co-administrated with tLyp-1 peptide for anti-glioma drug delivery.* Biomaterials, 2013. **34**(4): p. 1135-45.
144. Mendoza-Munoz, N., D. Quintanar-Guerrero, and E. Allemann, *The impact of the salting-out technique on the preparation of colloidal particulate systems for pharmaceutical applications.* Recent Pat Drug Deliv Formul, 2012. **6**(3): p. 236-49.
145. Lee, J., et al., *Self-assembled glycol chitosan nanogels containing palmityl-acylated exendin-4 peptide as a long-acting anti-diabetic inhalation system.* J Control Release, 2012. **161**(3): p. 728-34.
146. Siew, A., et al., *Enhanced oral absorption of hydrophobic and hydrophilic drugs using quaternary ammonium palmitoyl glycol chitosan nanoparticles.* Mol Pharm, 2012. **9**(1): p. 14-28.

147. Cheng, W.P., et al., *In vitro and in vivo characterisation of a novel peptide delivery system: amphiphilic polyelectrolyte-salmon calcitonin nanocomplexes.* J Control Release, 2010. **147**(2): p. 289-97.
148. Cortes, J. and C. Saura, *Nanoparticle albumin-bound (nab™)-paclitaxel: improving efficacy and tolerability by targeted drug delivery in metastatic breast cancer.* European Journal of Cancer Supplements, 2010. **8**(1): p. 1-10.
149. Zou, A., et al., *In vivo studies of octreotide-modified N-octyl-O, N-carboxymethyl chitosan micelles loaded with doxorubicin for tumor-targeted delivery.* J Pharm Sci, 2013. **102**(1): p. 126-35.
150. Yoon, H.Y., et al., *Tumor-targeting hyaluronic acid nanoparticles for photodynamic imaging and therapy.* Biomaterials, 2012. **33**(15): p. 3980-9.
151. Kataoka, K., et al., *Doxorubicin-loaded poly(ethylene glycol)-poly(beta-benzyl-L-aspartate) copolymer micelles: their pharmaceutical characteristics and biological significance.* J Control Release, 2000. **64**(1-3): p. 143-53.
152. Zhang, X., et al., *Preparation and characterization of insulin-loaded bioadhesive PLGA nanoparticles for oral administration.* Eur J Pharm Sci, 2012. **45**(5): p. 632-8.
153. Torrado, J.J., D.R. Serrano, and I.F. Uchegbu, *The oral delivery of amphotericin B.* Therapeutic Delivery, 2012. **4**(1): p. 9-12.
154. Xu, Q., C.H. Wang, and D.W. Pack, *Polymeric carriers for gene delivery: chitosan and poly(amidoamine) dendrimers.* Curr Pharm Des, 2010. **16**(21): p. 2350-68.
155. Liu, W., et al., *An investigation on the physicochemical properties of chitosan/DNA polyelectrolyte complexes.* Biomaterials, 2005. **26**(15): p. 2705-11.
156. Schipper, N.G., et al., *Chitosans as absorption enhancers of poorly absorbable drugs. 3: Influence of mucus on absorption enhancement.* Eur J Pharm Sci, 1999. **8**(4): p. 335-43.
157. Chooi, K.W., et al., *Physical Characterisation and Long-Term Stability Studies on Quaternary Ammonium Palmitoyl Glycol Chitosan (GCPQ)—A New Drug Delivery Polymer.* Journal of Pharmaceutical Sciences. **103**(8): p. 2296-2306.
158. Chooi, K.W., et al., *Physical characterisation and long-term stability studies on quaternary ammonium palmitoyl glycol chitosan (GCPQ)--a new drug delivery polymer.* J Pharm Sci, 2014. **103**(8): p. 2296-306.
159. Hang T.B Le, A.G.S.a.I.F.U., *Polymer Hydrophobicity Has a Positive Effect on the Oral Absorption of Cyclosporine A from Poly(ethylenimine) Based Nanomedicines.* Pharmaceutical Nanotechnology, 2012. **1**(1): p. 15-25.
160. Garrett, N.L., et al., *Exploring uptake mechanisms of oral nanomedicines using multimodal nonlinear optical microscopy.* J Biophotonics, 2012. **5**(5-6): p. 458-68.
161. Serrano, D.R., et al., *Oral particle uptake and organ targeting drives the activity of amphotericin B nanoparticles.* Mol Pharm, 2015. **12**(2): p. 420-31.
162. Lalatsa, A., et al., *Chitosan amphiphile coating of peptide nanofibres reduces liver uptake and delivers the peptide to the brain on intravenous administration.* J Control Release, 2015. **197**: p. 87-96.
163. Uchegbu, I., et al., *Delivery of drugs*. 2015, Google Patents.
164. Uchegbu, I., A. Schatzlein, and L. CAPRETTO, *Ocular delivery of drugs*. 2016, Google Patents.

165. report, S., *Labyrinthopeptin for Chronic Pain Treatment*, Sanofi, Editor. 2014.
166. Zagon, I.S., et al., *Opioid growth factor (OGF) inhibits human pancreatic cancer transplanted into nude mice.* Cancer Lett, 1997. **112**(2): p. 167-75.
167. Zagon, I.S., et al., *Combination chemotherapy with gemcitabine and biotherapy with opioid growth factor (OGF) enhances the growth inhibition of pancreatic adenocarcinoma.* Cancer Chemother Pharmacol, 2005. **56**(5): p. 510-20.
168. Blandford, I.C.P.S.a.D.E., *NMR Spectroscopy.* Anal Chem, 1995. **67**: p. 509.
169. Gunther, H., *The Physical Basis of the Nuclear Magnetic Resonance Experiment*. 3rd ed. NMR Spectroscopy: Basic principles, Concepts and Applications in Chemistry. 2013.
170. Stepisnik, J., *Spectroscopy: NMR down to earth. News and views.* . Nature, 2006. **439**: p. 799-801.
171. Williams, D.F., I, *Spectroscopic methods in organic chemistry*. 5th ed. 1996: The McGraw-Hill Companies.
172. Williams, D.F., I, *Spectroscopic methods in organic chemistry*. 2007: McGraw-Hill Education.
173. Farra, T.C., *Pulsed and Fourier Transform NMR Spectroscopy.* Analytical Chemistry, 1970. **42**(2): p. 109A-112A.
174. Oleg Jardetzky, G.C.K.R., *NMR in Molecular Biology*. 1981: Elsevier.
175. Mori, S.B., H, *Size Exclusion Chromatography*. 1999, Berlin, Germany: Springer.
176. Wu, C.-S., *Handbook of Size Exclusion Chromatography and Related Techniques.* 2003, New York, U.S.A.: Marcel Dekker.
177. Wyatt, *ASTRA user guide for DAWN DSP and miniDAWN Light Scattering Instruments.* 2008(4).
178. *A guide to multi-detector gel permeation chromatography*. 2012.
179. Wyatt, *Light scattering with the massess: dn/dc with an optilab.* 1999.
180. Kim, K., et al., *Self-assembled nanoparticles of bile acid-modified glycol chitosans and their applications for cancer therapy.* Macromolecular Research. **13**(3): p. 167-175.
181. Harris, J.R., *The future of transmission electron microscopy (TEM) in biology and medicine.* Micron, 2000. **31**: p. 1-3.
182. Goodhew, P.J.H., F. J., *Electron Microscopy and Analysis.* 1988: Taylor & Francis.
183. Barthel, A.K., et al., *Imaging the intracellular degradation of biodegradable polymer nanoparticles.* Beilstein J Nanotechnol, 2014. **5**: p. 1905-17.
184. Scheerschmidt, K. and P. Werner, *Characterization of Structure and Composition of Quantum Dots by Transmission Electron Microscopy*, in *Nano-Optoelectronics: Concepts, Physics and Devices*, M. Grundmann, Editor. 2002, Springer Berlin Heidelberg: Berlin, Heidelberg. p. 67-98.
185. Malvern, *Dynamic Light Scattering : An introduction in 30 minutes*.
186. Malvern, *Application of Dynamic ligth scattering (DLS) to protein therapeutics formulations: Principles, Measurements and Analysis-1. Basic principles*.
187. Malvern, *Zeta potential : An introduction in 30 minutes*.
188. Horinek, D., *DLVO Theory*, in *Encyclopedia of Applied Electrochemistry*, G. Kreysa, K.-i. Ota, and R.F. Savinell, Editors. 2014, Springer New York: New York, NY. p. 343-346.

189. Wang, W., Tetley, L., Uchegbu, I. F., *Controls on Polymer Molecular Weight May Be Used To Control the Size of Palmitoyl Glycol Chitosan Polymeric Vesicles.* Langmuir, 2001. **17**(3): p. 631-636.
190. Uchegbu, I.F., et al., *Polymeric chitosan-based vesicles for drug delivery.* J Pharm Pharmacol, 1998. **50**(5): p. 453-8.
191. Klein, S., *The use of biorelevant dissolution media to forecast the in vivo performance of a drug.* AAPS J, 2010. **12**(3): p. 397-406.
192. Kwon, S., et al., *Physicochemical Characteristics of Self-Assembled Nanoparticles Based on Glycol Chitosan Bearing 5β-Cholanic Acid.* Langmuir, 2003. **19**(24): p. 10188-10193.
193. Park, J.S. and Y.W. Cho, *In vitro cellular uptake and cytotoxicity of paclitaxel-loaded glycol chitosan self-assembled nanoparticles.* Macromolecular Research. **15**(6): p. 513-519.
194. Park, J.S., et al., *N-acetyl histidine-conjugated glycol chitosan self-assembled nanoparticles for intracytoplasmic delivery of drugs: endocytosis, exocytosis and drug release.* J Control Release, 2006. **115**(1): p. 37-45.
195. Ajit S. Narang, R.I.M., *Targeted Delivery of Small and Macromolecular Drugs*. Polymer micelles for drug delivery, ed. K.P. Sungwon Kim. 2010: CRC press.
196. Domard, A., M. Rinaudo, and C. Terrassin, *New method for the quaternization of chitosan.* International Journal of Biological Macromolecules, 1986. **8**(2): p. 105-107.
197. Snyman, D., J.H. Hamman, and A.F. Kotze, *Evaluation of the mucoadhesive properties of N-trimethyl chitosan chloride.* Drug Dev Ind Pharm, 2003. **29**(1): p. 61-9.
198. Lalatsa, A., et al., *Delivery of peptides to the blood and brain after oral uptake of quaternary ammonium palmitoyl glycol chitosan nanoparticles.* Mol Pharm, 2012. **9**(6): p. 1764-74.
199. Azra , Y., and Linggar S. ,Pradeckta, and Emma , Savitri, and Anita R., Handaratri, and S, Sumarno, *The Effect of Sonication on The Characteristic of Chitosan*, in *International Conference on Chemical and Material Engineering 2012*. 2012: Semarang Indonesia.
200. Savitri, E., et al., *Degradation of chitosan by sonication in very-low-concentration acetic acid.* Polymer Degradation and Stability, 2014. **110**: p. 344-352.
201. Ahmad, S., et al., *In silico modelling of drug-polymer interactions for pharmaceutical formulations.* J R Soc Interface, 2010. **7 Suppl 4**: p. S423-33.
202. Li, X., J.J. Lenhart, and H.W. Walker, *Aggregation kinetics and dissolution of coated silver nanoparticles.* Langmuir, 2012. **28**(2): p. 1095-104.
203. Gebauer, J.S. and L. Treuel, *Influence of individual ionic components on the agglomeration kinetics of silver nanoparticles.* J Colloid Interface Sci, 2011. **354**(2): p. 546-54.
204. Debye, P., Huckel, E., *Zur Theorie der Elektrolyte.* Phys., 1923. **Z. 24**: p. 185-206.
205. Chang, S.H., et al., *pH Effects on solubility, zeta potential, and correlation between antibacterial activity and molecular weight of chitosan.* Carbohydr Polym, 2015. **134**: p. 74-81.
206. Niu, M., et al., *Enhanced oral absorption of insulin-loaded liposomes containing bile salts: a mechanistic study.* Int J Pharm, 2014. **460**(1-2): p. 119-30.

207. Tolle-Sander, S., et al., *Increased acyclovir oral bioavailability via a bile acid conjugate.* Mol Pharm, 2004. **1**(1): p. 40-8.
208. van Hasselt, P.M., et al., *The influence of bile acids on the oral bioavailability of vitamin K encapsulated in polymeric micelles.* J Control Release, 2009. **133**(2): p. 161-8.
209. Pain, I.A.f.t.S.o., *IASP Taxonomy.* 1994.
210. NIH Medline Plus, *Chronic Pain: Symptoms, Diagnosis, & Treatment.* 2011.
211. Voscopoulos, C. and M. Lema, *When does acute pain become chronic?* Br J Anaesth, 2010. **105 Suppl 1**: p. i69-85.
212. Medicine, A.S.o.R.A.a.P., *Types of Chronic Pain.*
213. The National Pain Audit. *National Pain Audit Final Report 2010-2012*. 2012; Available from: http://www.nationalpainaudit.org/background.
214. Sundy, J.S., *COX-2 inhibitors in rheumatoid arthritis.* Curr Rheumatol Rep, 2001. **3**(1): p. 86-91.
215. Vranken, J.H., *Current Approaches to the Management of Peripheral Neuropathic Pain.* J Pain Palliat Care Pharmacother, 2015. **29**(3): p. 307-10.
216. Shoji, S., et al., *Population pharmacokinetics of pregabalin in healthy subjects and patients with post-herpetic neuralgia or diabetic peripheral neuropathy.* Br J Clin Pharmacol, 2011. **72**(1): p. 63-76.
217. Strauss, A.C. and J.D. Dimitrakov, *New treatments for chronic prostatitis/chronic pelvic pain syndrome.* Nat Rev Urol, 2010. **7**(3): p. 127-35.
218. Zakrzewska, J.M. and P.N. Patsalos, *Oxcarbazepine: a new drug in the management of intractable trigeminal neuralgia.* J Neurol Neurosurg Psychiatry, 1989. **52**(4): p. 472-6.
219. Nersesyan, H. and K.V. Slavin, *Current aproach to cancer pain management: Availability and implications of different treatment options.* Ther Clin Risk Manag, 2007. **3**(3): p. 381-400.
220. Liu, H., J. Ni, and R. Wang, *In vitro release performance and analgesic activity of endomorphin-1 loaded nanoparticles.* Pharmazie, 2006. **61**(5): p. 450-2.
221. Hua, S. and P.J. Cabot, *Targeted nanoparticles that mimic immune cells in pain control inducing analgesic and anti-inflammatory actions: a potential novel treatment of acute and chronic pain condition.* Pain Physician, 2013. **16**(3): p. E199-216.
222. Hwang, J., et al., *Alpha-methylprednisolone conjugated cyclodextrin polymer-based nanoparticles for rheumatoid arthritis therapy.* Int J Nanomedicine, 2008. **3**(3): p. 359-71.
223. Franz-Montan, M., et al., *Liposomal lidocaine gel for topical use at the oral mucosa: characterization, in vitro assays and in vivo anesthetic efficacy in humans.* Journal of Liposome Research, 2015. **25**(1): p. 11-19.
224. Ferir, G., et al., *The lantibiotic peptide labyrinthopeptin A1 demonstrates broad anti-HIV and anti-HSV activity with potential for microbicidal applications.* PLoS One, 2013. **8**(5): p. e64010.
225. Seibert, G., et al., *Antibacterial and antiviral peptides from actinomadura namibiensis*. 2008, Google Patents.
226. Meindl, K., et al., *Labyrinthopeptins: a new class of carbacyclic lantibiotics.* Angew Chem Int Ed Engl, 2010. **49**(6): p. 1151-4.
227. Garber, K., *Peptide leads new class of chronic pain drugs.* Nat Biotech, 2005. **23**(4): p. 399-399.

228. Artursson, P. and J. Karlsson, *Correlation between oral drug absorption in humans and apparent drug permeability coefficients in human intestinal epithelial (Caco-2) cells.* Biochem Biophys Res Commun, 1991. **175**(3): p. 880-5.
229. *Agilent 6400 series : Triple Quadrupole LC/MS system*. 2012: U.S.A.
230. Mc Master, M.C., *LC/MS: A Practrical User's Guide*. 2005, New Jersey: Wiley Interscience.
231. Use, C.f.M.P.f.H., *Guideline on bioanalytical method validation*. 2011, European Medicines Agency: U.K.
232. Kim, J.H., et al., *Self-assembled glycol chitosan nanoparticles for the sustained and prolonged delivery of antiangiogenic small peptide drugs in cancer therapy.* Biomaterials, 2008. **29**(12): p. 1920-30.
233. Bagger, M.A., H.W. Nielsen, and E. Bechgaard, *Nasal bioavailability of peptide T in rabbits: absorption enhancement by sodium glycocholate and glycofurol.* Eur J Pharm Sci, 2001. **14**(1): p. 69-74.
234. Vollmer, K.O., A. von Hodenberg, and E.U. Kolle, *Pharmacokinetics and metabolism of gabapentin in rat, dog and man.* Arzneimittelforschung, 1986. **36**(5): p. 830-9.
235. Menchicchi, B., et al., *Structure of chitosan determines its interactions with mucin.* Biomacromolecules, 2014. **15**(10): p. 3550-8.
236. Wang, Y.Y., et al., *Mucoadhesive nanoparticles may disrupt the protective human mucus barrier by altering its microstructure.* PLoS One, 2011. **6**(6): p. e21547.
237. Moore, T.C., *Neurovascular Immunology: Vasoactive Neurotransmitters and Modulators in Cellular Immunity and Memory*. 1992: CRC Press.
238. Vaught, J.L. and A.E. Takemori, *Differential effects of leucine and methionine enkephalin on morphine-induced analgesia, acute tolerance and dependence.* J Pharmacol Exp Ther, 1979. **208**(1): p. 86-90.
239. Shan, F., et al., *Functional modulation of the pathway between dendritic cells (DCs) and CD4+T cells by the neuropeptide: methionine enkephalin (MENK).* Peptides, 2011. **32**(5): p. 929-37.
240. Zagon, I.S., et al., *Opioid growth factor regulates the cell cycle of human neoplasias.* Int J Oncol, 2000. **17**(5): p. 1053-61.
241. Dores, R.M., et al., *The molecular evolution of neuropeptides: prospects for the '90s.* Brain Behav Evol, 1990. **36**(2-3): p. 80-99.
242. Costa, E., et al., *Opioid peptide biosynthesis: enzymatic selectivity and regulatory mechanisms.* FASEB J, 1987. **1**(1): p. 16-21.
243. Krajnik, M., et al., *Enkephalin, its precursor, processing enzymes, and receptor as part of a local opioid network throughout the respiratory system of lung cancer patients.* Hum Pathol, 2010. **41**(5): p. 632-42.
244. Pfaff, D.W., *Hormones, brain, and behavior*. 2002: Elsevier.
245. Roy, B.P., I. Jamal, and J. Go, *Synaptic mechanism of methionine-enkephalin uptake.* Life Sci, 1982. **31**(20-21): p. 2307-10.
246. MD, M.C.R., *Muscle Nerve*. opioids in pain control: Basic and clinical aspects. Vol. 22. 1999: John Wiley & Sons, Inc.
247. Snyder, S.H. and G.W. Pasternak, *Historical review: Opioid receptors.* Trends Pharmacol Sci, 2003. **24**(4): p. 198-205.
248. Tripathi K.D., *Opioid Analgesics and Antagonists.* Essentials of Medical Pharmacology, 2008: p. 462-464.

249. Bajpai, K., et al., *Immunomodulation by two potent analogs of met-enkephalin.* Immunopharmacology, 1997. **35**(3): p. 213-20.
250. Biffoni, M., et al., *Effects of beta-casomorphins and met-enkephalin on human natural killer activity.* Pharmacol Res, 1992. **26 Suppl 2**: p. 164-5.
251. Esche, C., et al., *Murine dendritic cells express functional delta-type opioid receptors.* Ann N Y Acad Sci, 1999. **885**: p. 387-90.
252. Kowalski, J., et al., *Augmenting effect of methionine-enkephalin on interleukin-6 production by cytokine-stimulated murine macrophages.* Neuropeptides, 2000. **34**(3-4): p. 187-92.
253. Zagon, I.S., M.F. Verderame, and P.J. McLaughlin, *The biology of the opioid growth factor receptor (OGFr).* Brain Res Brain Res Rev, 2002. **38**(3): p. 351-76.
254. Zagon, I.S., J.P. Smith, and P.J. McLaughlin, *Human pancreatic cancer cell proliferation in tissue culture is tonically inhibited by opioid growth factor.* Int J Oncol, 1999. **14**(3): p. 577-84.
255. Cheng, F., et al., *The OGF-OGFr axis utilizes the p21 pathway to restrict progression of human pancreatic cancer.* Mol Cancer, 2008. **7**: p. 5.
256. Cheng, F., et al., *The OGF-OGFr axis utilizes the p16INK4a and p21WAF1/CIP1 pathways to restrict normal cell proliferation.* Mol Biol Cell, 2009. **20**(1): p. 319-27.
257. *Pancreatic cancer*. 2014, Cancer Research UK.
258. Board, C.N.E. *Pancreatic Cancer: Treatment Options*. 2015; Available from: http://www.cancer.net/cancer-types/pancreatic-cancer/treatment-options.
259. Burris, H.A., 3rd, et al., *Improvements in survival and clinical benefit with gemcitabine as first-line therapy for patients with advanced pancreas cancer: a randomized trial.* J Clin Oncol, 1997. **15**(6): p. 2403-13.
260. Smith, J.P., et al., *Opioid growth factor improves clinical benefit and survival in patients with advanced pancreatic cancer.* Open Access J Clin Trials, 2010. **2010**(2): p. 37-48.
261. Lang, V.B., et al., *Structure-permeation relations of met-enkephalin peptide analogues on absorption and secretion mechanisms in Caco-2 monolayers.* J Pharm Sci, 1997. **86**(7): p. 846-53.
262. Zagon, I.S. and P.J. McLaughlin, *Opioid growth factor and the treatment of human pancreatic cancer: a review.* World J Gastroenterol, 2014. **20**(9): p. 2218-23.
263. Thanawala, V., V.J. Kadam, and R. Ghosh, *Enkephalinase inhibitors: potential agents for the management of pain.* Curr Drug Targets, 2008. **9**(10): p. 887-94.
264. Mosnaim, A.D., et al., *Studies of the in vitro human plasma degradation of methionine-enkephalin.* Gen Pharmacol, 1988. **19**(5): p. 729-33.
265. Bouchemal, K., *New challenges for pharmaceutical formulations and drug delivery systems characterization using isothermal titration calorimetry.* Drug Discov Today, 2008(13): p. 960-972.
266. Garidel, P., Hildebrand, A., Blume, A.,, *Understanding the Self-Organisation of Association Colloids. Microcal: Ultrasensitive Calorimetry for the Life Sciences.*
267. *VP-ITC MicroCalorimeter, User's Manual*. 2004, MicroCal, L.L.C.: Northhampton.
268. *Malvern - Application notes*. Improving Protein Zeta Potential Measurements Utilizing A Novel Diffusion Barrier technique; Available from:

http://www.malvern.com/en/support/resource-center/application-notes/AN110708NovelDiffusionBarrierTechnique.aspx.
269. Smith, J.P., et al., *Treatment of advanced pancreatic cancer with opioid growth factor: phase I.* Anticancer Drugs, 2004. **15**(3): p. 203-9.
270. Lvov, Y., et al., *Assembly of Multicomponent Protein Films by Means of Electrostatic Layer-by-Layer Adsorption.* Journal of the American Chemical Society, 1995. **117**(22): p. 6117-6123.
271. Redolfi Riva, E., et al., *PMMA/polysaccharides nanofilm loaded with adenosine deaminase inhibitor for targeted anti-inflammatory drug delivery.* Langmuir, 2013. **29**(43): p. 13190-7.
272. Jiang, B. and B. Li, *Tunable drug loading and release from polypeptide multilayer nanofilms.* Int J Nanomedicine, 2009. **4**: p. 37-53.
273. Malay, Ö., O. Bayraktar, and A. Batıgün, *Complex coacervation of silk fibroin and hyaluronic acid.* International Journal of Biological Macromolecules, 2007. **40**(4): p. 387-393.
274. Kayitmazer, A.B., A.F. Koksal, and E. Kilic Iyilik, *Complex coacervation of hyaluronic acid and chitosan: effects of pH, ionic strength, charge density, chain length and the charge ratio.* Soft Matter, 2015. **11**(44): p. 8605-8612.
275. Water, J.J., et al., *Complex coacervates of hyaluronic acid and lysozyme: effect on protein structure and physical stability.* Eur J Pharm Biopharm, 2014. **88**(2): p. 325-31.
276. Kobari, M., N. Ishihara, and K. Yunoki, *Increase of plasma methionine-enkephalin levels in patients at the acute stage of cerebral infarction.* Neurol Res, 1988. **10**(2): p. 120-2.
277. Zagon, I.S., P.J. McLaughlin, and J.P. Smith, *Control of cancer growth through the interaction of [MET5]-enkephalin and the zeta receptor*. 2004, Google Patents.
278. Zagon, I.S. and P.J. McLaughlin, *Opioid growth factor receptor is unaltered with the progression of human pancreatic and colon cancers.* Int J Oncol, 2006. **29**(2): p. 489-94.
279. Smith, J.P., et al., *Elevated levels of opioid growth factor in the plasma of patients with pancreatic cancer.* Pancreas, 2000. **21**(2): p. 158-64.
280. Zagon, I.S., R.N. Donahue, and P.J. McLaughlin, *Opioid growth factor-opioid growth factor receptor axis is a physiological determinant of cell proliferation in diverse human cancers.* Am J Physiol Regul Integr Comp Physiol, 2009. **297**(4): p. R1154-61.
281. Shibanoki, S., et al., *Hydrolysis of [Leu]enkephalin by chick plasma in vitro.* J Pharmacol Exp Ther, 1991. **256**(2): p. 650-5.
282. Shibanoki, S., et al., *Enkephalin hydrolysis by mouse plasma in vitro.* Life Sci, 1992. **50**(10): p. 667-75.
283. Dupont, A., Cusan, L., Garon, M., Alvarado-Urbina, G., and Labrie, F.,, *Extremely rapid degradation of [3H] methionine-enkephalin by various rat tissues in vivo and in vitro.* Life Sci, 1977(21): p. 907.

7 Supplementary

7.1.1 Size Distribution of Laby GCPQ formulations

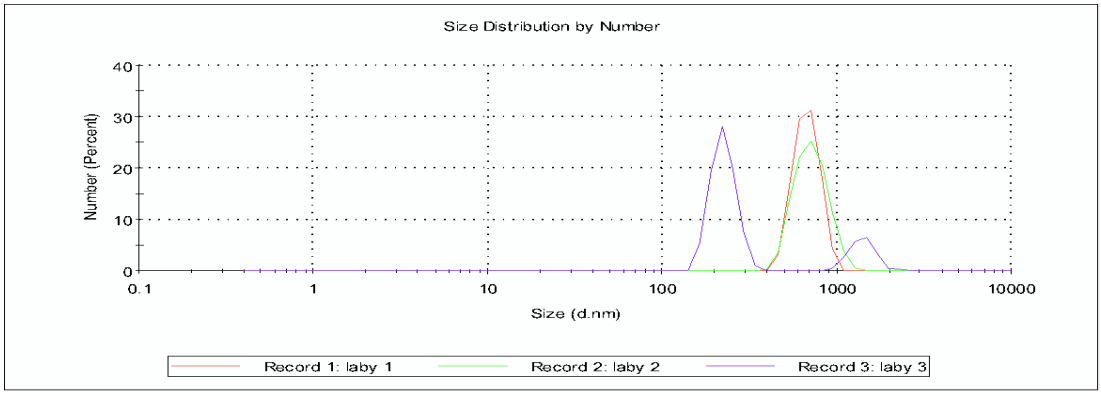

Figure 7-1 Size distribution by number for Laby formulation

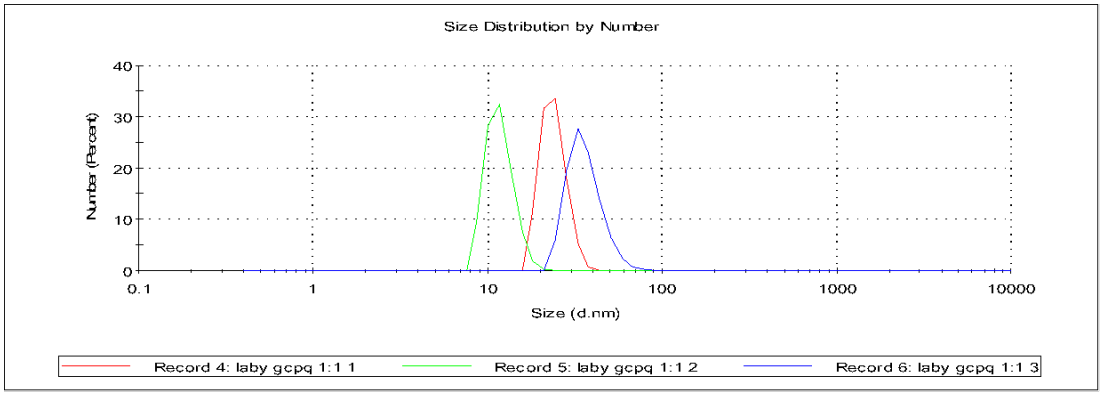

Figure 7-2 Size distribution by number for Laby GCPQ formulation (1:1)

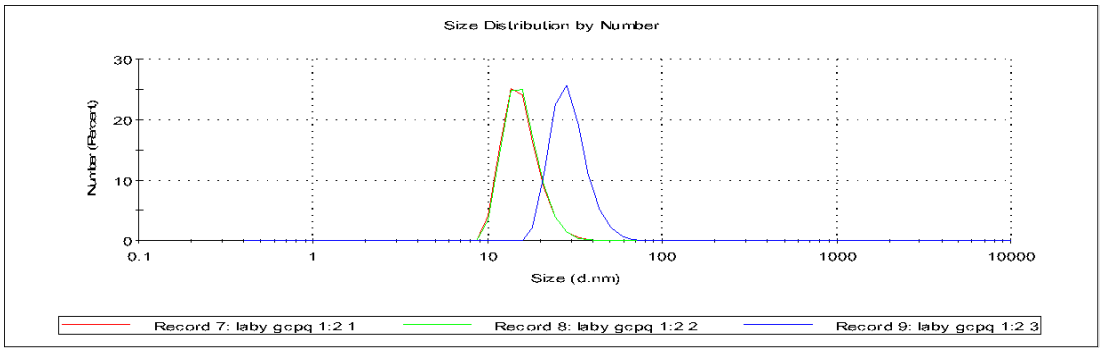

Figure 7-3 Size distribution by number for Laby GCPQ formulation (1:2)

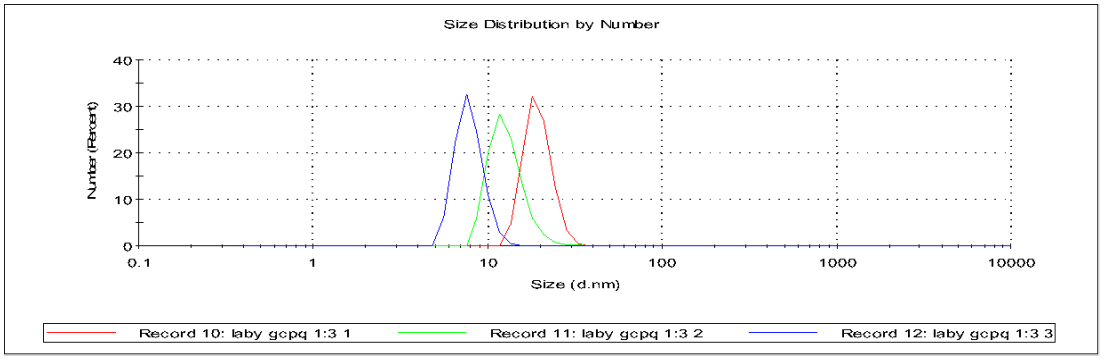

Figure 7-4 Size distribution by number for Laby GCPQ formulation (1:3)

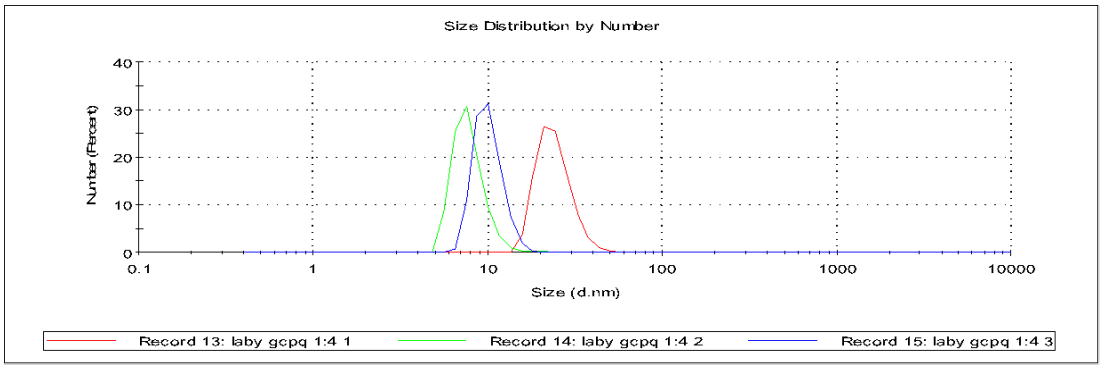

Figure 7-5 Size distribution by number for Laby GCPQ formulation (1:4)

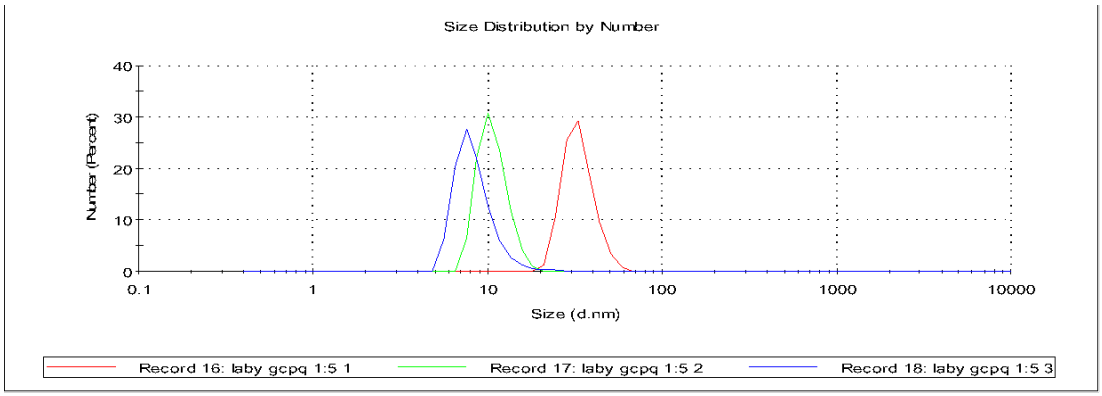

Figure 7-6 Size distribution by number for Laby GCPQ formulation (1:5)